Examining the Role of von Willebrand Factor on Breast Cancer Metastasis

AUTHOR(S)

Sean Patmore

CITATION

Patmore, Sean (2024). Examining the Role of von Willebrand Factor on Breast Cancer Metastasis. Royal College of Surgeons in Ireland. Thesis. https://doi.org/10.25419/rcsi.22699465.v1

DOI

10.25419/rcsi.22699465.v1

URL

https://repository.rcsi.com/articles/thesis/Examining_the_Role_of_von_Willebrand_Factor_on_Breast_Cancer_Metastasis/22699465/1

RCSI

Examining the role of von Willebrand Factor in breast cancer metastasis

Sean Patmore BA (Hons)

Irish centre for Vascular Biology,

School of Pharmacy and Biomolecular Sciences

A Thesis Submitted to the school of Postgraduate Studies, Faculty of Medicine and Health Sciences, Royal College of Surgeons in Ireland, in fulfilment of the degree of Doctor of Philosophy

Supervisor: Dr. Jamie O'Sullivan

January 2023

Candidate Thesis Declaration

I declare that this thesis, which I submit to RCSI for examination in consideration of the award of a higher degree is my own personal effort. Where any of the content presented is the result of input or data from a related collaborative research programme this is duly acknowledged in the text such that it is possible to ascertain how much of the work is my own. I have not already obtained a degree in RCSI or elsewhere on the basis of this work. Furthermore, I took reasonable care to ensure that the work is original, and, to the best of my knowledge, does not breach copyright law, and has not been taken from other sources except where such work has been cited and acknowledged within the text.

I declare that work herein is entirely my own, with the exception of the following figures where I worked in collaboration with other researchers.

In the case of Figures 3.4, 3.5, 3.6 and 3.7 overall survival, D-dimer, thrombin anti-thrombin, and fibrinogen levels in breast cancer patients were measured in the lab of Dr. Cliona Kirwan in Manchester.[1,2] Furthermore, subsequent measuring of VWF:Ag levels and analysis were performed with Dr. Ciara Byrne, Dr. Jamie O'Sullivan and Sean Patmore.

In the case of Figures 3.15, 3.16, 3.17, 4.15, 4.16 and 4.17 the perfusion assays were performed jointly between Dr. Sukhraj Pal Singh Dhami and Sean Patmore with data analysis conducted by Ingmar Schoen.

In the case of Figures 5.17 and 5.18 the experiment was carried out by Dr. Jamie O'Sullivan, Dr. Sukhraj Pal Singh Dhami and Sean Patmore where all members contributed to animal husbandry, surgical procedure and imaging.

Signed: Sean Patmore

Student Number: 18180221

Date: 12/01/2023

Publications arising during thesis

Published:

- S Aguila, M Lavin, N Dalton, **S Patmore**, A Chion, GD Trahan, KL Jones, C Keenan, TM Brophy, NM O'Connell, K Ryan, M Byrne, M Nolan, A Patel, RJS Preston, P James, J Di Paola, JM O'Sullivan, JS O'Donnell. Increased galactose expression and enhanced clearance in patients with low von Willebrand factor. Blood. 2019 Apr 4;133(14):1585-1596. doi: 10.1182/blood-2018-09-874636. Epub 2019 Feb 15. PMID: 30770394.
- **S Patmore**, SPS Dhami, JM O'Sullivan. Von Willebrand factor and cancer; metastasis and coagulopathies. J Thromb Haemost. 2020 Oct;18(10):2444-2456. doi: 10.1111/jth.14976. Epub 2020 Jul 23. PMID: 32573945.
- CY Goh, **S Patmore**, A Smolenski, J Howard, S Evans, JM O'Sullivan, A McCann. The role of von Willebrand factor in breast cancer metastasis. Transl Oncol. 2021 Apr;14(4):101033. doi: 10.1016/j.tranon.2021.101033. Epub 2021 Feb 8. PMID: 33571850; PMCID: PMC7876567.
- SPS Dhami, **S Patmore**, JM O'Sullivan, Advances in the management of cancer-associated thrombosis. Seminars in Thrombosis and Hemostasis 2021 Mar;47(2):139-149. doi: 10.1055/s-0041-1722863. Epub 2021 Feb 26. PMID: 33636745.
- SPS Dhami, **S Patmore**, C Comerford, B Cavanagh, J Castle, CC Kirwan, M Kenny, I Schoen, JS O'Donnell and JM O'Sullivan. Breast cancer cells mediate endothelial cell activation, promoting von Willebrand Factor release, tumour adhesion and transendothelial migration. J Thromb Haemost. 2022 Oct;20(10):2350-2365. doi: 10.1111/jth.15794. Epub 2022 Jul 10. PMID: 35722954.

Under revision for publication:

- C Comerford, SPS Dhami, P Murphy, S Patmore, N Pushkar, U Budde, E Karampini, JS. O'Donnell, S Glavey, J Quinn, JM. O'Sullivan. Elevated von Willebrand factor levels in multiple myeloma: dysregulated mechanisms of both secretion and clearance. Submitted – HemaSphere Manuscript ID [2022-0440]

Conferences

Conferences	Presentation title	Format
Haematology Association of Ireland (HAI) 2018	Von Willebrand Factor binds to breast cancer cells and modulates tumour cell migration in vitro.	Oral
RCSI Research Day 2019	Von Willebrand Factor binds to breast cancer cells and modulates tumour cell migration	Poster
Haematology Association of Ireland (HAI) 2019	Identifying the role of von Willebrand Factor in breast cancer biology	Oral
The Irish Association for Cancer Research (IACR) 2019	Coagulation-cancer crosstalk; Defining the role of Von Willebrand Factor in breast cancer progression.	Poster
RCSI Research Day 2020	Defining the metastatic role of Von Willebrand Factor in breast cancer progression.	Oral
XXIX Congress of the International Society on Thrombosis and Haemostasis (ISTH) 2021	Coagulation-cancer crosstalk; Von Willebrand Factor contributes to pro-migratory and pro-angiogenic properties in breast cancer cells.	Oral / Poster
Haematology Association of Ireland (HAI) 2021	Coagulation-cancer crosstalk; Von Willebrand Factor contributes to pro-invasive and pro-angiogenic properties in breast cancer cells.	Oral
RCSI Research Day 2022	Elevated plasma von Willebrand Factor in patients with breast cancer may contribute to the early metastatic niche, promoting endothelial adhesion and invasion of circulating breast cancer cells.	Poster
11th International conference on thrombosis and haemostasis issues in cancer (ICTHIC) 2022	Elevated plasma von Willebrand Factor in patients with breast cancer may contribute to the early metastatic niche, promoting endothelial adhesion, invasion and angiogenic properties of circulating breast cancer cells.	Oral/ Poster

Acknowledgements

Firstly, I would like to express gratitude towards my supervisor Dr. Jamie O'Sullivan, I am delighted we finally got there. I would also like to acknowledge the help provided by Professor James O'Donnell and Dr. Roger Preston. Furthermore a big thanks to the School of Postgraduate Services, Professor Steve Kerrigan and CoMPPAS for getting me across the line.

However, science is a team sport, when one player is down the rest pull together for the benefit of the team. During my times of need I could not have asked for better ~~lab~~ team mates than Sukhraj and Claire. Sukhraj for being my scientific and sometimes non-scientific sounding board with your unwaveringly calming influence I greatly appreciate your role as mentor and friend. Claire for being the embodiment of positive happy energy, your willingness to help at any moment is a true skill, especially with how difficult I made it. The two of you really made our small 'dream team' click together and I feel incredibly lucky to have worked with you both.

It would be remiss of me not to mention the vascular biology lab, many of whom have passed on, not in a RIP kind of way but in a better, higher wage type of way. Shout outs to JoJo the fireball, Judicael the master of innuendo, Sonia also known as Madame, Leila the BG G, Hannah ~~loud~~ Rushe, Orla Foxy, Jedi Martin and Clive Dr. Dre-keford. To the current lab members a special thanks to Thomas and Aisling to whom I have spent many hours chatting to while I should have been working. You only do a PhD once (thank the stars, the earth and the sea) and I feel fortunate to have you both as friends and to have relied on your support when needed. Not to mention the endless good fun on nights out, conferences and adventures long may it continue past this fearful chapter in our lives! To the rest of the Vascular Biology Lab thanks for all the help, banter and ambiance, maybe on my next PhD you'll get a direct shout out! Ok Fine… Alain, Helen, Patricia, Azaz, Dearbhla, Ciara, Dishon, Smita, Paula, Gemma!

To the technical support team, from the outside anyone else would think I had a machine break down on me on a daily basis, instead it may have just been me. You have all been very good friends and the perfect victims for my pranks, chats and whatever other mischief I had planned. I have relied on you all and the safe place you provided. Thank you Seamus, Sophie and Emma!!

The write up of this thesis has been a completely different beast with each chapter rearing its head and baring its fangs in an attempt to kill me. But there I was like a hero from mythology swiping each chapter down only to find a new one emerging like the head of a hydra while the old one grows back under the disguise of edits! Now my Greek mythology isn't great but thesis the hydra doesn't sound right… I think Theseus did something completely different, but never fear I would have been as bullishly lost as my labyrinthine compatriot without my golden strings, thanks to Raquel, Frances, Emily, Katelyn and Thomas for keeping me from going mad in the write up room and taking the plunge into the Styx. A special shout out to Raquel for all the conversations and support that got me through to the end, not to mention the plans and trips kept me looking forward. Thanks for being there when it mattered. Together you have all let me become the mythological hero everyone looks up to and I knew I could be.

Thanks are needed for my flat mates Colm and Manon, for putting up with a nearly 5 year stream of madness and providing logical solutions to my wildly illogical problems. I'm sure you enjoyed it really!

I owe a burden of debt to my hobbies, fencing for allowing me to get my anger out by stabbing my unsuspecting victims, the boardgame crew of Ed, Hannah, Leila, Thomas and Aisling for acquiescing to my need to win at something, as well as all the adventures that have shown me a world that exists outside the lab.

To Crystal, it would have been impossible to get through the PhD without your support, I am forever grateful for your being the first person I could go to during my toughest moments and being my foremost ally. I know I can always count on you being there as a friend, something I hope you know goes both ways.

Finally, to my family it has finally happened I can get a real job! To mum and dad I would never have got here if you hadn't instilled in me the importance of education and a desire to learn. It will always be taken for granted the huge support I have from you and words cannot express how grateful I truly am for all that it has taken to get me here. All the hours forcing me to do homework and pay attention has finally paid off. It is time to catch up now Casey.

P.S. Screw you Ben

Table of Contents

Table of Contents

List of Abbreviations

ADAM28	A disintegrin metalloproteinase domain 28
ADAMTS13	A disintegrin And Metalloproteinase with Thrombospondin type 1 motif, 13
AIM	Autoinhibitory module
Ang-2	Angiopoietin-2
ANOVA	Analysis of variance
ApoA-I	apoliprotein A-I
ATCC	Authenticated Cell Cultures
AUC	Area under the curve
BCA	Bicinchoninic acid assay
bPEI	Branched polyethylenimine
BSA	Bovine Serum Albumin
Ca^{2+}	Calcium ions
CAIM	C-terminal autoinhibitory module
cAMP	Cyclic adenosine monophosphate
CAT	Cancer Associated Thrombosis
CHAMPion	Cancer-induced Hypercoagulability As a Marker of Prognosis
CI	Confidence interval
CMV	Cytomegalovirus
CTCK	C-terminal cysteine knot
Cu^{2+}	Copper Ions
DCIS	Ductal carcinoma in situ
DDAVP	1-desamino-8-D-arginine vasopressin
DiOC6	3,3'-Dihexyloxacarbocyanine Iodide
DMEM	Dulbecco's modified eagles media
DTT	Dithiothreitol
ECFC	Endothelial colony-forming cells
ECM	Extracellular matrix
EGF	Epidermal growth factor
EGFR	Epidermal Growth Factor Receptor
ELISA	Enzyme Linked Immunosorbent Assay
EMT	Epithelial to mesenchymal transition
ER	Endoplasmic reticulum
ERβ1	Oestrogen receptor beta
FCS	Foetal calf serum
FDR	False discovery rate
FGF	Fibroblast growth factor
FVIII	Factor VIII
GEO	Geo expression omnibus
HBRS	HEPES-buffered ringers solution
HEK-293T	Human embryonic kidney-293T
HEPES	4-(2-hydroxyethyl)-1-piperazineethanesulfonic acid
HMEC	Human mammary epithelial cells

HMWM	High molecular weight multimers
HR	Hazards ratios
HRP	Horse radish peroxidase
HUVEC	Human endothelial cells
IDC	Invasive ductal carcinoma
IGF-1	Insulin growth factor
IGFB-3	Insulin growth factor binding protein-3
IL	Interleukins
ILC	Invasive lobular carcinoma
IQR	Interquartile range
KM	Kaplan-Meier
LLC	Lewis lung carcinoma
LLG	Leucine-Leucine-Glycine
LMWH	Low molecular weight heparin
LMWM	Low molecular weight multimers
LRP1	Lipoprotein related protein
MFI	Median fluorescence intensity
MMP-1	Matrix metalloproteinase-1
MMP-2	Matrix metalloproteinase-2
MMP-9	Matrix metalloproteinase-9
MTS tetrazolium	3-(4,5-dimethylthiazol-2-yl)-5-(3-carboxymethoxyphenyl)-2-(4-sulfophenyl)-2H-tetrazolium
NAIM	N-terminal autoinhibitory module
P/S	Penicillin streptomycin
PAR-1	Protease-activated receptor 1
PAS	Periodic acid Schiff
PBS-T	Phosphate buffered saline with 0.1% Tween
Pd-VWF	Plasma-derived Von Willebrand Factor
PDGF	Platelet-derived growth factor
Pecam-1/CD31	Platelet endothelial cell adhesion molecule-1
PFA	Paraformaldehyde
PLA	Proximity ligation assay
PMA	Phorbol 12-myristate 13-acetate
PSGL-1	P-selectin glycoprotein ligand-1
PTC	Papillary thyroid carcinoma
PVDF	Polyvinylidene difluoride
qPCR	Quantitative PCR
RAP	Receptor Associated Protein
RBC	Red blood cells
REC	Research and Ethics Committee
REMARK	Recommendations for tumour marker prognostic studies
RGD	Arginine-Glycine-Asparagine
rH	Recombinant Human
TAT	Thrombin Antithrombin III

TGF-α	Transforming growth factor alpha
TMB	3,3',5,5'-Tetramethylbenzidine
TNM	Tumour, Node, Metastasis
TuFClot	Tumour Fragments and Clotting
UL-VWF	Ultra large-VWF
V	Volts
VEGF	Vascular endothelial growth factor
VEGF-165	Vascular endothelial growth factor-165
VEGF-A	Vascular endothelial growth factor A
VEGFR2	Vascular endothelial growth factor receptor 2
VLDLR	Very low density lipoprotein receptor
VM	Vasculogenic mimicry
VM	Vasculogenic mimicry
VTE	Venous Thromboembolism
VWD	Von Willebrand disorder
VWF	Von Willebrand Factor
VWF:Ag	VWF plasma antigen
VWF:pp	VWF propeptide
WPB	Weibel-palade bodies

Table of Figures

Chapter 1:

Chapter 2:

Chapter 3:

Chapter 4:

Chapter 5:

Appendices:

Table of Tables

Chapter 1:

Chapter 2:

Chapter 3:

Chapter 4:

Appendices:

Summary

Significant crosstalk exists between tumour cells and the haemostatic system, as metastatic tumour cells undergo blood-borne migration they are exposed to a milieu of coagulation proteins that can contribute to metastatic advancement. Interestingly, the extra-haemostatic functions of VWF may facilitate tumour development with VWF regarded as a regulator of endothelial angiogenesis, an inflammatory mediator that can mediate vascular permeability, a medium for transmigration that can tether and extravasate immune cells and finally as a coagulopathic agent, where it is an independent risk factor for venous thromboembolism. We sought to characterise how VWF could influence breast cancer advancement.

In this project VWF plasma levels were identified as a clinical biomarker in patients with breast cancer, with elevated VWF indicative of disease stage. I found that increased plasmatic VWF levels in a metastatic breast cancer cohort may be associated of increased mortality. Elevated VWF also significantly correlated with higher fibrinogen levels in both early and late stage breast cancer but only in late stage breast cancer for D-dimer levels.

Secondly, I assessed the adhesion of VWF to breast cells and revealed that VWF displayed enhanced adhesion to breast cancer cells over non-neoplastic counterparts. I determined that the D'A3 VWF-domain primarily mediated adhesion through breast cancer cell receptors GPIbα and LRP1, VWF adhesion to these receptors occurred both statically and under venous shear flow. Low molecular weight heparin ablates VWF adhesion to tumour cells as well as VWF mediated tumour cell adhesion to the endothelial layer.

Finally, the functional roles of VWF in breast cancer were characterised using migration, invasion, proliferation and angiogenic assays. I was able to deduce pro-migratory and invasive properties of VWF on breast cancer cells by inducing chemotactic cell motility. Furthermore, by addressing the angiogenic capabilities of VWF I described that VWF did not directly induce classical angiogenic regulators from breast cancer cells but could induce pseudo-vasculature structures as VWF promoted breast tumour vasculogenic mimicry. An *in vivo* study targeting VWF revealed a reduction in time to metastasis by reducing pulmonary and liver metastasis.

Collectively, these novel findings determine a pro-metastatic role for VWF in breast cancer through enhanced migration, endothelial adhesion and subsequent invasion. Additionally, for the first time VWF has been described as an inducer of vasculogenic mimicry in cancer. Finally, we determined that VWF may be a therapeutic target to reduce blood-borne cancer metastasis.

1: Introduction

1.1 VWF structure and function

The following section has been adapted from a published review

(https://doi.org/10.1111/jth.14976)[3]

1.1.1 *VWF* Gene

Located on chromosome 12 (12p13.2), the *VWF* gene spans around 180kb and is composed of 52 exons.[4–6] The VWF propeptide (VWF:pp) sequence is located on the N-terminal end of the VWF polypeptide, within the first 17 exons and is cleaved off following secretion of VWF into the plasma thus resulting mature VWF antigen and VWF:pp which circulate independently.[7] Of note, chromosome 22 (22q11) contains a large, non-processed *VWF* pseudogene displaying a duplication of exons 23-24 which exhibits 97% sequence homology with the *VWF* gene.[8] Despite this, the pseudogene does not produce a functional transcript due to the presence of nonsense mutations.

1.1.2 VWF Expression

VWF is synthesised in endothelial cells and megakaryocytes, as a pre-proVWF structure consisting of 2813 amino acids.[9] The VWF polypeptide is made up of a signal peptide, propeptide and mature subunit of 22, 741 and 2050 residues respectively. The majority of circulating VWF in plasma is derived from constitutive secretion of VWF from endothelial cells lining the vasculature. However, VWF expression is heterogeneous in distinct vessel types and different organ-specific vascular beds. For example, in mice *VWF* mRNA levels are higher in lung and brain tissues than in kidney and liver.[10] In contrast, in biopsies from human tissues reveal that VWF protein expression was highest in the venules and arteries of kidneys and lungs and significantly lower in other organs examined such as the spleen and liver.[11] Furthermore, capillaries, venules, arteries and other vessels of each organ displayed variations in VWF expression when measured through immunohistochemical staining.

1.1.3 VWF Domain Structure

Monomeric VWF is a large protein (~250kDa) that is made up of multiple sub-domains. Historically, VWF was reported to be composed of a series of domains in the order D1-D2-D'-D3-A1-A2-A3-D4-B1-B2-B3-C1-C2-CK.[12,13] However, more recent evidence of these sub-domain structure and assemblies through electron microscopy as well as sequence alignment

analysis has resulted in the re-annotation of VWF structure to D1-D2-D'-D3-A1-A2- A3-D4-C1-C2-C3-C4-C5-C6-CK (Figure 1.1).[14] Importantly, specific domains of VWF have different functions.

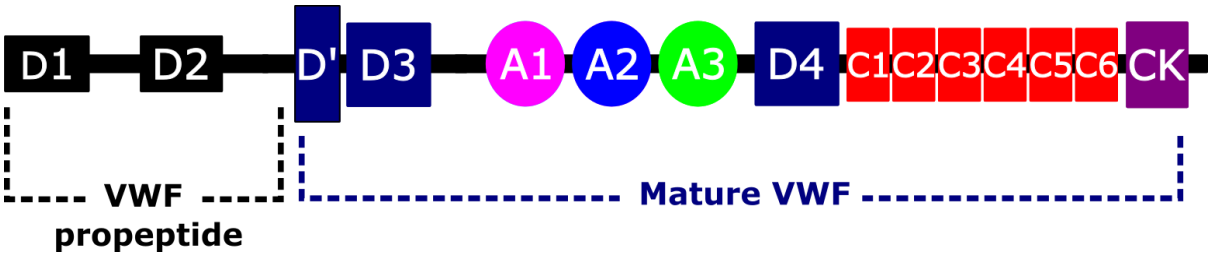

Figure 1.1 VWF domain organisation: Structural arrangement of the domains from a pro-VWF monomer

1.1.4 VWF D-Domains

The VWF D domains are comprised of D1, D2, D', D3 and D4 domains. Interestingly, the D-domains have been shown to be composed of small lobules which promote self-association.[14] Notably, the D1-D2 region makes up the propeptide unit that is cleaved away from the mature VWF structure. The D'D3 region is key in regulating VWF multimerisation intracellularly as D'D3 units self-associate through disulphide bridges resulting in the concatamerisation of dimeric VWF during tubule assembly, this is discussed in further detail below.[15] Importantly, VWF multimerisation is a key determinant of its haemostatic activity, including platelet and collagen binding. Furthermore, within the circulation, the D'D3 domains are the binding site of pro-coagulant factor VIII (FVIII), extending its circulatory half-life and preventing premature cleavage and thus key in contributing to the haemostatic role of VWF *in vivo*.[16]

1.1.5 VWF A-domains

VWF contains three A-domains, A1, A2 and A3. In contrast with other VWF domains that are cysteine rich, the A-domains only have six cysteines in total.[13] Consequently, VWF A-domains are large globular structures with hydrophobic cores.[14] Uniquely, all three A domains contain an intra-chain disulphide bond. Both A1 and A3 contain long range disulphide bridges which result in a ~186 amino acid loop. In contrast, the A2 domain contains a rare vicinal disulphide bond which is important in modulating stability.[17]

The A1 domain is the location of platelet binding site and the key ligand for platelet GPIbα receptor. Recently, it has been described that platelet-A1 domain binding is regulated by an autoinhibitory module (AIM) within the N-terminal region of the A1 domain. The AIM is a mechano-sensitive sequence that when exposed to high shear stresses undergoes a conformational shift which overcomes the inhibitory function of the AIM and permits GPIbα binding.[18–20] Interestingly, specific mutations in the A1 domain or flanking regions of the A1 domain can overcome shear dependency.[20–22] Furthermore, activating agents like ristocetin and botrocetin which bind to key regions in the A1 domain are also able to induce A1-domain exposure for GPIbα adhesion in the absence of shear stress.[23–25]

The residues Tyr1065-Met1606 within the A2 domain mark the cleavage site of ADAMTS13 (a disintegrin and metalloprotease with thrombospondin type 1 repeats, member 13). Following unfolding of VWF due to shear stresses in the circulation, the A2 domain is permissive to ADAMTS13 mediated cleavage resulting in proteolysis of high molecular weight multimers (HMWM) into less haemostatically active low molecular weight multimers (LMWM).[14,26] Finally, due to negatively charged residues within the A3 domain, it is involved in anchorage to positively charged collagens type I and III. In particular, site-directed mutagenesis has revealed a critical role for the H1786 residue in the A3 of domain of VWF in modulating collagen III binding.[27] These types of collagens are found in the sub-endothelial matrix and exposed upon vessel wall damage thus permitting circulating VWF to bind directly to the vessel wall to facilitate platelet adhesion and contribute to platelet plug formation.[28–31]

1.1.6 VWF C-domains

The VWF C-domains previously C1, C2 and C3 were re-annotated into C1, C2, C3, C4, C5 and C6 domains following observation of intervening domains.[14,32] As determined through sequence homology the original C1, C2 and C3 domains now referred to as C1, C3 and C5 are VWC domains; a protein domain found in many blood coagulation proteins. Interestingly, the intervening C-domains C2, C4 and C6 display a similar length and homology to VWC, now termed VWC-like. Electron microscopy examination of the VWF C-domains revealed that within each dimer of VWF the C-domains align into a stem-like structure, zipping up the dimer from the C-terminal tail of VWF.[14]

An integrin binding RGD (Arg-Gly-Asp) motif has been characterised in the C4 domain of VWF.[14,33] Interestingly, it was found that one or two integrins could bind per VWF dimer.[32]

Furthermore, the RGD binding motif has been found to anchor VWF to endothelial cells through integrin $\alpha_v\beta_3$ as well as mediate platelet binding through $\alpha_{iib}\beta_3$.[33,34]

1.1.7 VWF CTCK domain

At the tail end of the VWF monomer is a C-terminal cysteine knot (CTCK) domain. Arranged perpendicularly at the end of the C-domain stem the CTCK domain forms a 'T-shaped' base.[14] The VWF CTCK domain is central for the dimerization of pro-VWF monomers, with dimeric 'bouquets' formed between two CTCK domains of each monomer VWF, mediated by disulphide bridge linkages.

1.1.9 VWF synthesis and post-translational modification

VWF is synthesized in endothelial cells and megakaryocytes under normal physiological conditions.[35–37] Following gene expression and translation, VWF biosynthesis undergoes several post translational modifications while transitioning through the endoplasmic reticulum (ER), trans-Golgi network and finally storage organelles. The post-translational modifications VWF undergoes include proteolytic processing of the signal peptide, dimerisation, multimerisation, sulfation and glycosylation. These processes culminate in the secretion of highly modified mature VWF multimers and VWF pro-peptide units.[38]

Throughout its synthesis in endothelial cells and megakaryocytes VWF is significantly glycosylated with N- and O- linked glycan structures (Figure 1.2). Glycans on the VWF monomer make up to 20% of its total monomeric mass and contribute to VWF function.[39–42] Within the ER, precursory N-linked glycans are added to VWF, giving VWF a mannose rich glycan core around its asparagine residues, with N-linked glycans seen in both the mature VWF monomer and VWF:pp.[43–45] As VWF is processed in the ER a series of glycosyltransferases and glycosidase enzymes remodel the glycan structures on VWF.[46] Notably, N1515, N2223, N2290, N2400 and N2790 N-linked glycans are terminally sulphated.[45]

Furthermore, VWF O-linked glycosylation occurs at 10 sites along the VWF monomer.[47,48] While N-linked glycans are distributed across the VWF monomer, O-linked glycans are distributed in two groups of four with one at the N- and C- terminal ends of the A1 domain.[44,47–49] The remaining O-glycan chains are located at the A3 and C1 domains of VWF. O-linked glycans in VWF are simple mucins formed through sequential addition of

glycans.[47,49,50] Desialylated core 1 tetrasaccharide (or Thomas Friedenreich antigen) accounts for 70% of the total O-glycan population of VWF.[48] Interestingly, the majority of both N- and C- linked glycan chains on VWF are terminally sialylated with sialic acid.[45,48]

Finally, among its glycan groups VWF expresses ABO(H) blood group determinants.[51] These blood group determinants are observed on 13% of N-glycans and 1% of O-glycans in human VWF.[51,52] Interestingly, individuals with O-blood group have around 20% less plasma VWF:Ag than non-O counterparts. Furthermore, the lack of ABO(H) antigen as in the Bombay blood group results in much lower VWF levels.[53]

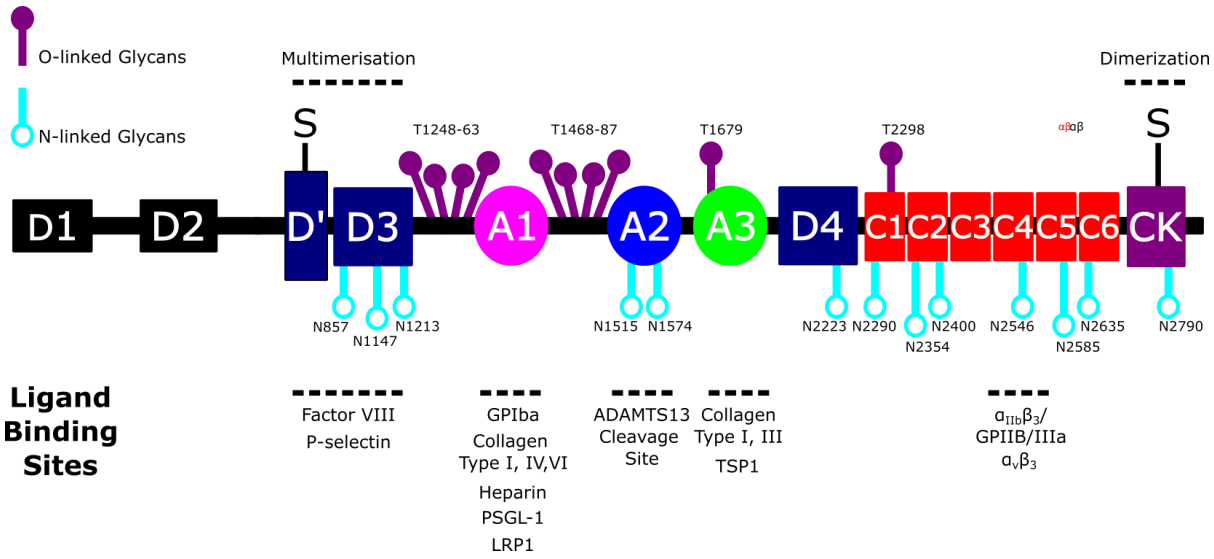

Figure 1.2 VWF domain functions: A schematic outline of VWF monomeric structure and respective ligand binding sites.

1.1.10 Dimerization and multimerisation of VWF

In addition to glycosylation and sulfation VWF undergoes a process of tail-to-tail dimerisation as two VWF monomers link together forming a 540kDa dimer, before they are multimerised into concatenated chains that can reach molecular weights of up to 20,000kDa (Figure 1.3).[13,32,54]

Within the ER, VWF forms dimeric bouquets as two VWF monomers zip up together through CTCK domain disulphide bonds.[55–58] This disulphide pairing is mediated by conserved residue Cys2010 in the pro-VWF structure.[59] Subsequently, dimerised VWF are transported through

the trans-Golgi network, where low pH (6.2) and high Ca^{2+} concentrations within the Golgi promote multimerisation.[32,60,61] Following dimeric bouquet formation via the CTCK tail, the D'D3 regions of VWF dimers can then associate through head-to-head linkage to begin multimerisation.[14] Interestingly, concatenated VWF dimers are assembled in a helix formation.[32,38,60,62] This process results in the generation of a heterogeneous population of multimers up to 60 subunits in length.

Following the multimerisation of VWF in the Golgi, the D1-D2 propeptide domains are cleaved with paired dibasic amino-acid cleaving enzyme at Ser763, next to the dibasic amino acid pair Lys761-Arg762.[63] The VWF:pp continues to non-covalently associate with mature VWF in storage organelles until its secretion.[38,64] Cleavage of the propeptide unit is critical for adhesion of procoagulant FVIII binding within the circulation.[65]

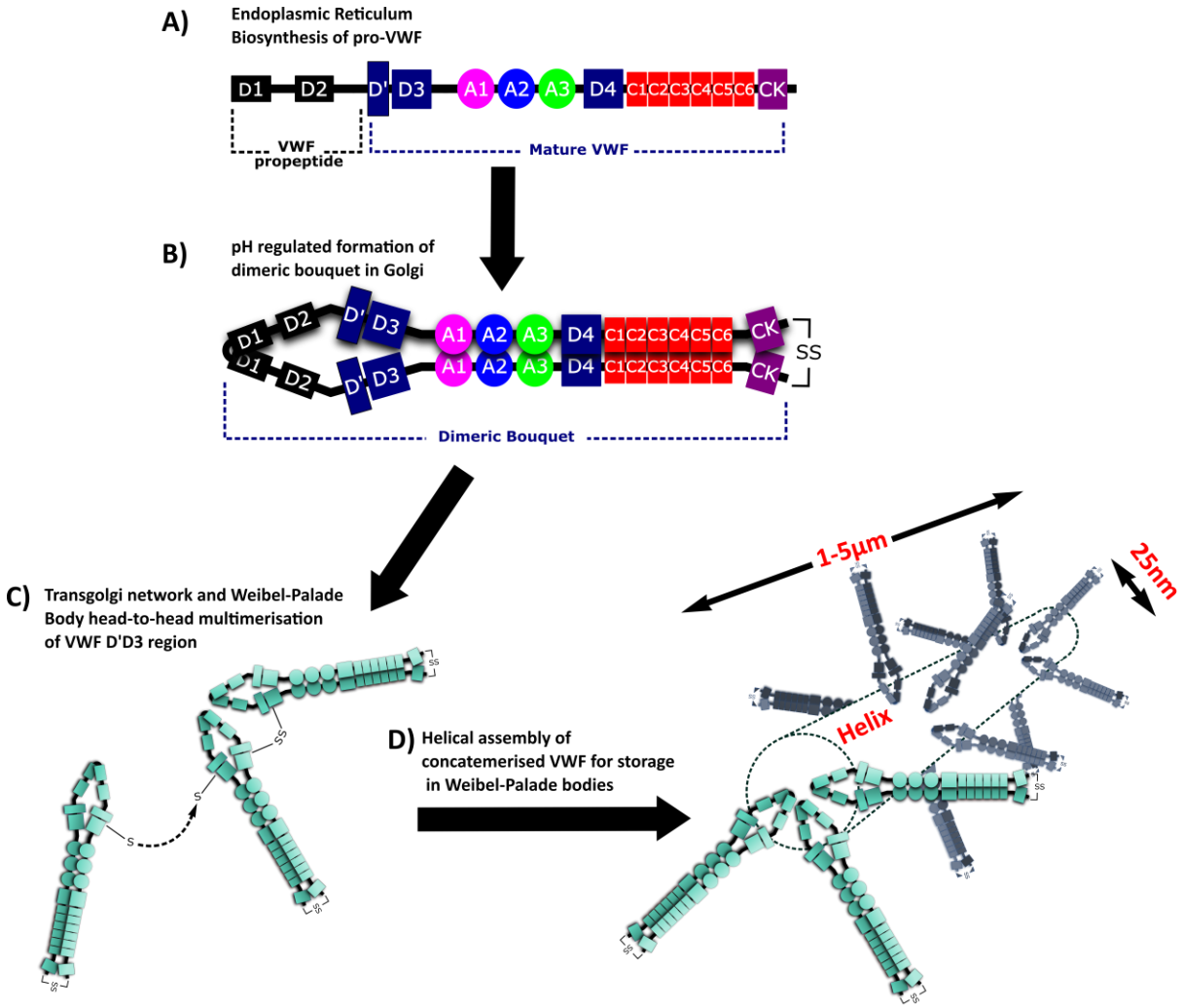

Figure 1.3 VWF dimerization and multimerisation: Dimerization and multimerisation of VWF within endothelial cells is used to form highly concatemerised chains of VWF. A) The monomeric pro-VWF form of VWF formed within the endoplasmic reticulum. B) Formation of a dimeric VWF structure within the Golgi through disulphide linkage of VWF CTCK domains. C) Dimeric bouquets are linked through Disulphide linkage of D'D3 regions within the trans-Golgi network. D) Concatenated VWF chains are assembled into helical structures to be packaged within specialised storage organelles termed Weibel-Palade bodies (WPB).

1.1.11 VWF storage

Of the VWF synthesised in endothelial cells, HMWM and ultra-large VWF (UL-VWF) are packaged within organelles called Weibel-Palade bodies (WPB).[9,66] WPB are membrane bound structures around 1-5µm in length 100-200nm in diameter forming a classic 'cigar-shape' within endothelial cells.[60,67]

The formation of WPB is dependent on VWF with many proteins packaged within WPB through VWF association. Cargo molecules within WPB include pro-inflammatory factor: interleukin-8 (IL-8), angiogenic proteins: angiopoietin-2 (Ang-2) and osteoprotegerin as well as haemostatic components like P-selectin.[68–72] The absence of VWF within endothelial cells abolishes WPB formation and dysregulates expression of the cargo molecules usually packaged within WPB, such as Ang-2.[73,74] Furthermore, both mature VWF and propeptide structures are stored within WPB.

In megakaryocytes VWF is packaged within α-granules.[75] However, while VWF synthesis is similar to endothelial cells the formation of α-granules in contrast to WPB are not dependent on VWF.

1.1.12 VWF secretion

VWF secretion from endothelial cells is released through three pathways; constitutive, basal and regulated (Figure 1.4).[76] The constitutive secretory pathway is a non-stimulated pathway that involves the basolateral release of dimeric and LMWM. In contrast to basal and regulated secretion pathways, the constitutive pathway does not undergo tubule or subsequent WPB formation, instead LMWM VWF synthesized from the trans-Golgi network are basolaterally released through small anterograde carriers.[76,77] Interestingly, the constitutive pathway is a continuous process, which leads to sub-endothelial deposits of VWF. It is proposed sub-endothelial release of VWF helps promote platelet adhesion following vascular injury.[78]

In contrast to the constitutive pathway, both basal and regulated pathways use WPB secretion mechanisms to release HMWM VWF.[76] However, these pathways are distinguished by their WPB secretion profiles, with basal secretion marked by spontaneous release of WPB without external stimulus and the regulated pathway shown to induce WPB release in response to stimuli like histamine and thrombin.[76,78] In both pathways, WPB are mostly released apically, thereby depositing VWF into the lumen. Consequently, the basal pathway is the predominant source of circulating VWF within plasma.[79,80] Of note, the formation of endothelial anchored VWF is induced by regulated release whereas basally released VWF is involved in adhering platelets and collagen at sites of vascular injury.[81–83]

In contrast to other VWF secretion pathways regulated release of VWF involves a complex signalling process instigated through endothelial activation. Activation of endothelial cells

through stimulation or trauma increases intracellular calcium (Ca^{2+}) concentration.[81] Following increased intracellular Ca^{2+} levels, cyclic adenosine monophosphate (cAMP) is upregulated which in turn induces WPB clustering in the perinuclear region. Together, clustering WPB fuse to form secretory pods of HMWM and UL-VWF to be released. Following endothelial injury regulated release allows the formation of VWF string structures in the lumen, which provide a platform for platelets to accumulate and begin formation of a platelet plug.[82,83] Interestingly, in clinical settings 1-desamino-8-D-arginine vasopressin (DDAVP) is used to induce cAMP activation and subsequent VWF release to artificially restore plasma VWF levels.[84]

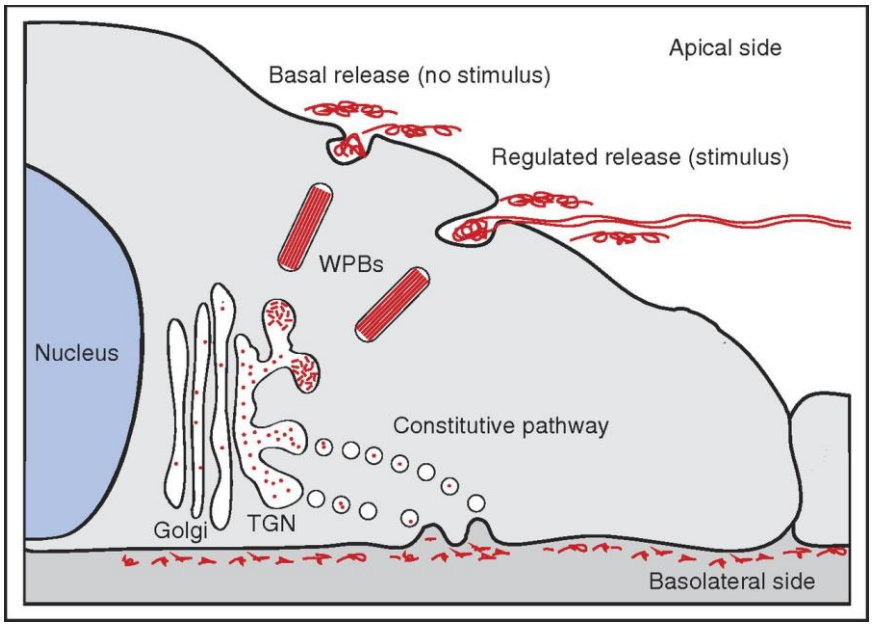

Figure 1.4 Weibel-Palade bodies secretory pathways: Weibel-Palade bodies are secreted from endothelial cells through 3 different pathways, constitutive, basal and regulated each pathway is depicted here. Image taken from (Bierings and Voorberg, 2016)[78]

1.1.13 VWF haemostatic function

VWF is critical in maintaining normal haemostasis where as part of primary haemostasis it mediates platelet adhesion at sites of vascular injury as well as acting as a molecular chaperone for pro-coagulant FVIII. With VWF multimer size associated with haemostatic activity (Figure 1.5). Interestingly, von Willebrand disorder (VWD) marked by qualitative and /or quantitative defects in VWF is the most common inherited bleeding disorder.[85] Furthermore VWD can result in a significant bleeding pathologies, with type 3 VWD associated

with a near-complete absence of VWF and constitutes the greatest risk of bleeding among VWD patients.

Upon injury to the blood vessel wall circulating plasma-derived VWF (pd-VWF) can adhere to exposed collagen of the sub-endothelial matrix. Circulating plasma VWF displays a dynamic nature. For example, in the absence of vessel wall damage and at low-shear conditions, circulating multimeric VWF exists in a globular or folded form, not permissible to platelet adhesion. However, at high shear rates, or tethered to the damaged endothelial wall, globular-VWF rapidly unwinds and elongates, transitioning to a highly active surface for platelet adhesion (Figure 1.6). Shear-stresses on globular-VWF result in the exposure of the A1 domain thereby enabling adhesion of platelets through GPIbα.[26,62,86,87] In addition to initial platelet tethering, platelet activation of $\alpha_{iib}\beta_3$ and subsequent fibrin crosslinking enables the recruitment of further platelets.[88] Interestingly, activation of platelets also induces the release of stored VWF from within platelet α-granules.

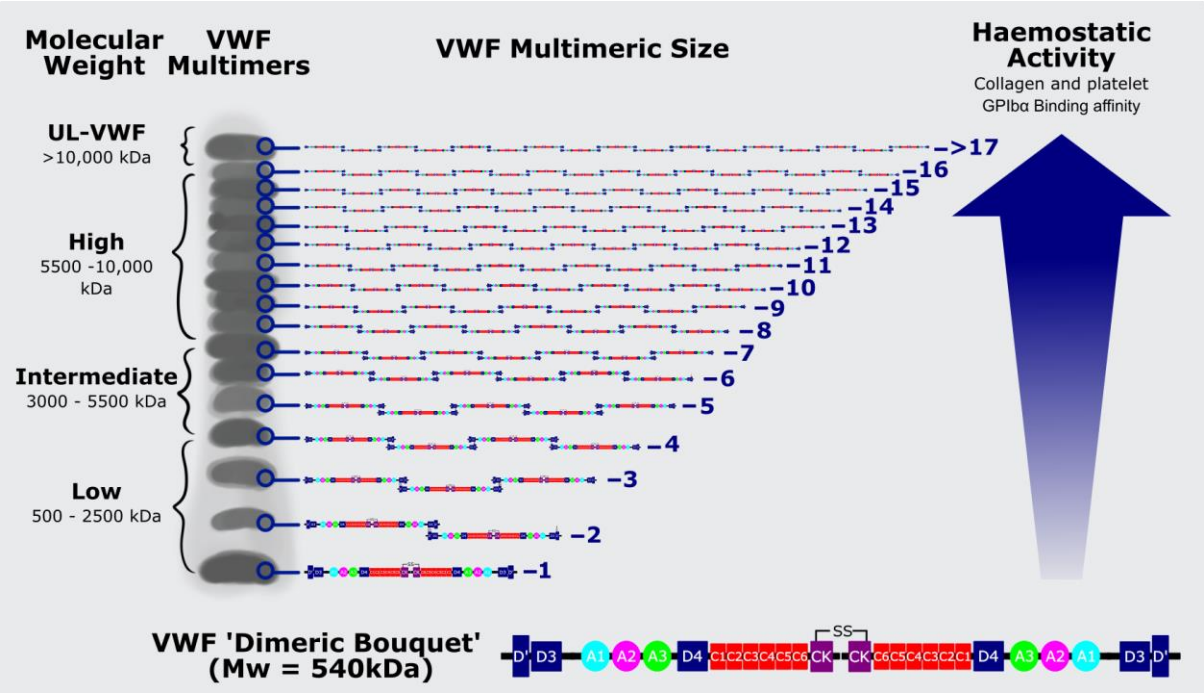

Figure 1.5 Molecular multimers of VWF: Image of the associated molecular size differences of multimeric VWF. A single dimer of VWF is 540kDa in size and multimers can reach up to 20000kDa. Increasing multimeric size is associated with increases in collagen and platelet glycoprotein binding activity and therefore corresponding haemostatic activity. Multimer sizes are broadly divided into low, intermediate, high and ultra-large, with ultra-large VWF associated with the highest haemostatic activity.

In its unfolded state, VWF serves as a substrate for ADAMTS13-mediated proteolysis thus regulating its haemostatic activity (Figure 1.6).[89] Importantly, multimeric composition is a key determinant of VWF functional activity. UL-VWF, released upon endothelial cell stimulation, is the most biologically active with higher multimers associated with greater adhesion to platelet GPIbα.[19] ADAMTS13 cleaves VWF at a unique site within the A2 domain (Tyr1605-Met1606) resulting in the proteolysis of haemostatically active UL-VWF and HMWM into LMWM forms which are less active. Levels of ADAMTS13 and VWF:Ag require balance as ADAMTS13 deficiency can cause thrombotic thrombocytopenic purpura a thrombotic microangiopathy.[90] Conversely, increased ADAMTS13 cleavage of VWF is seen in a subset of type 2A VWD and results in significant bleeding.[91]

Furthermore, VWF acts as a carrier molecule for FVIII within the circulation. VWF protects FVIII from proteolysis and being cleared from the circulation, where FVIII can then promote

clot formation at sites of vascular injury.[92–94] Interestingly, mutations to the D'D3 region of VWF that decrease FVIII adhesion as seen in VWD type 2N results in increased bleeding.[95]

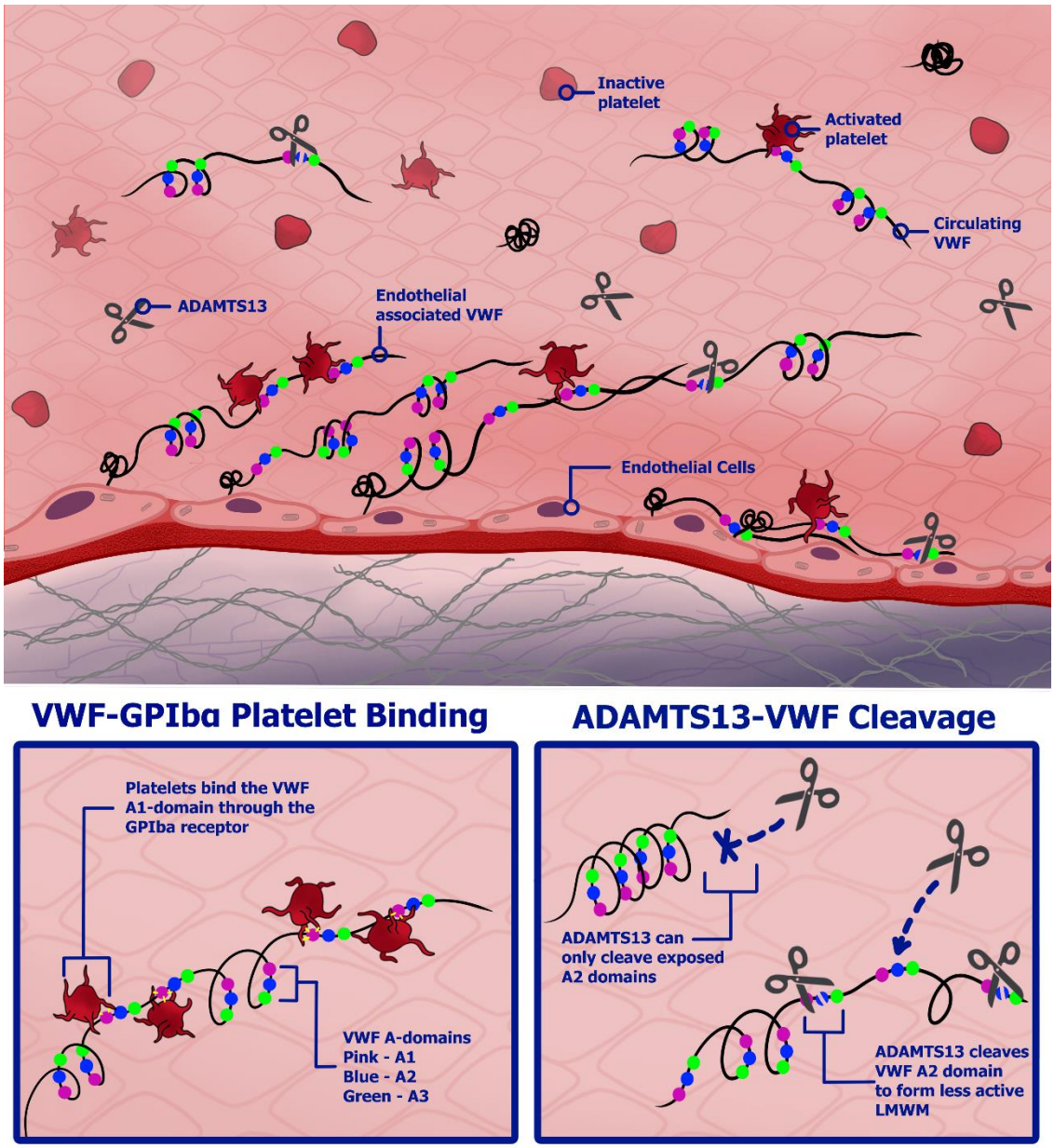

Figure 1.6 VWF as a haemostatic factor: VWF is elongated through blood-shear stresses. Elongation of the VWF structure exposes platelet binding domain A1 as well as the ADAMTS13-VWF cleavage site within the A2 domain. Platelet decorated strings form as a result of vascular injury to promote the formation of the platelet plug. ADAMTS13 circulates the blood and cleaves highly active VWF strings into less active LMWM.

1.2 VWF in cancer

Modulation of VWF plasma antigen (VWF:Ag) levels, through regulated secretion pathways and ADAMTS13-mediated proteolysis is essential in controlling VWF multimeric distribution and haemostatic activity. Increased plasma VWF:Ag levels are associated with an enhanced risk of venous thromboembolism (VTE).[96,97] More recently, VWF levels have been shown to be markedly increased in cancer cohorts (Table 1.1 and 1.2). This is perhaps not surprising, given that the association between cancer and coagulation activation has been established since 1865 when Armand Trousseau reported VTE as a common complication of cancer. In fact, VTE has been reported in up to 20% of cancer patients making it one of the leading causes of death for cancer patients.[98] Moreover, growing evidence suggests that this crosstalk between coagulation pathways and cancer is of direct clinical relevance, contributing not only to cancer associated thrombosis (CAT) but to cancer progression and metastasis (Figure 1.7). Cancer cells have been shown to directly interact with coagulation factors and platelets to promote tumour growth, survival, angiogenesis and metastasis.[99] Aside from its established role in haemostasis, the highly adhesive properties of VWF have been proposed to contribute to its involvement in other pathophysiological conditions in recent years. These include cancer metastasis and inflammation, which implicate tumour cells and leukocytes adhesion to the vessel wall. In addition, emerging data suggests VWF may modulate angiogenesis,[73] cell proliferation,[100] and apoptosis[101] all of which represent dysregulated pathways in cancer development and progression. We will provide an overview of the growing evidence base supporting the role of VWF in tumour metastasis.

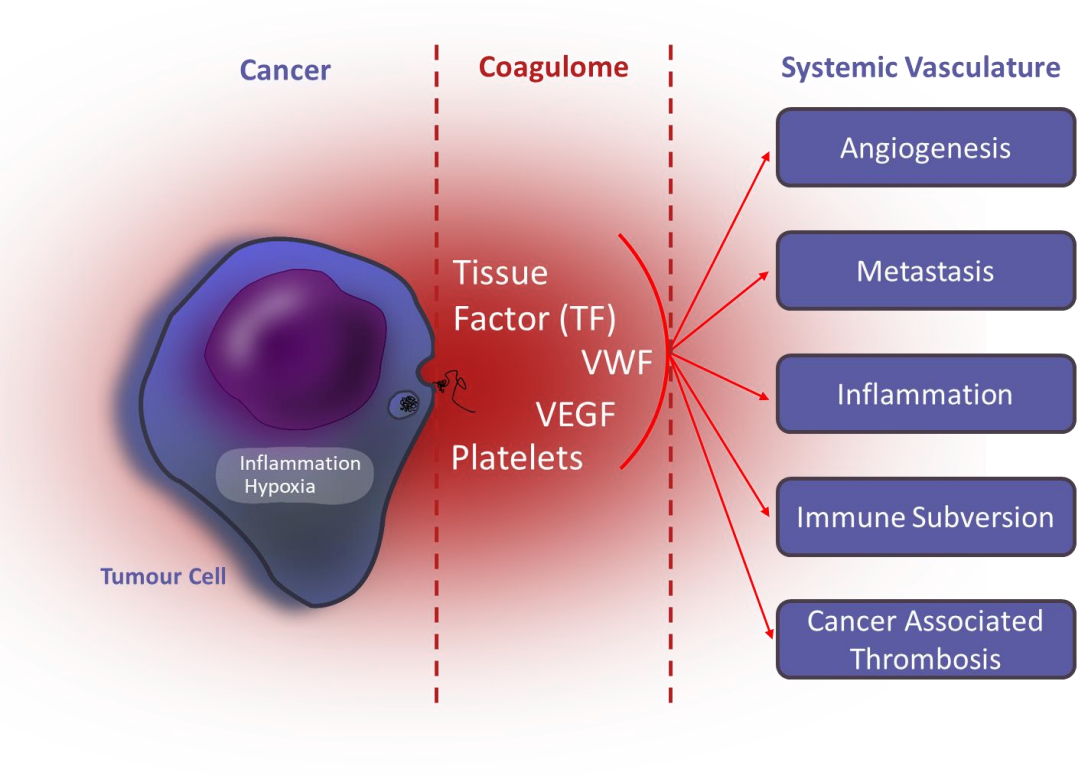

Figure 1.7 Crosstalk between cancer and the coagulome: Tumour cells can directly upregulate and activate a milieu of pro-coagulant factors, including tissue factor and platelets, interact directly with other coagulation proteins such as VWF, release cytokines and growth factors including vascular endothelial growth factor (VEGF) all of which can induce systemic changes within the vasculature promoting angiogenesis, metastasis, inflammation, immune subversion and cancer-associated thrombosis.

1.2.1 Plasma derived and tumour derived VWF

Elevated plasma VWF:Ag levels have been reported in multiple cancer patients cohorts compared to normal healthy controls (Table 1.1 and Table 1.2). Surprisingly, this increase in VWF:Ag levels is not limited to haematological malignancies but also reported across a variety of solid tumours. Interestingly, VWF:Ag levels in many of these cancer cohorts often correlate with tumour size, grade, and the presence of metastatic disease. Several studies have demonstrated the independent prognostic value of VWF:Ag, with high VWF levels correlating with poorer survival in patients with colorectal cancer, ovarian cancer, glioblastomas, oesophageal and lung cancer.[102–105] Moreover, plasma proteomic analysis reported VWF as a biomarker for the early detection of colon cancer.[106] In further support of this, multivariate analysis identified VWF:Ag/ADAMTS13 ratio as a biomarker for the early diagnosis of hepatocellular carcinoma.[107]

Table 1.1 Plasmatic VWF levels reported in cancer patient cohorts

Cancer Cohort	Healthy Controls	N	Cancer Patients	N	Metastatic Cancer Patients	N	*P*-Value	
							Cancer	Metastasis
Mixed								
Mannucci *et al* [108]	114 ± 37 %	N = 49	170 ± 103 %	N = 29	266 ± 177 %	N = 20	***P* = .002**	***P* = .03**
Pepin *et al* [109]	242 ± 158 IU mL $^{-1}$	N =140	326 ± 158 IU mL $^{-1}$	N = 20	-	-	***P* = .02**	**-**
Barrio *et al* [110]	75 – 150 %*	N/A	199.35 (45.7 – 734.5) %	N = 132	214.2 (45.7 – 734.5) %	N = 90	**N/A**	***P* < .01**
Breast								
Patmore *et al* [	89.1 (65 – 117) IU/dL	N = 11	130 (100 – 280) IU/dL	N = 130	217 (162 – 289) IU/dL	N = 44	***P* < .005**	***P* < .001**
Rohsig *et al* [111]	130.6 ± 45	N = 27	170.7 ± 78 IU/dL	N = 128	263.3 ± 113 IU/dL	N = 15	***P* < .005**	***P* < .001**
Yigit *et al* [112]	78.19 ± 43.69 %	N = 100	99.49 ± 47.27 %	N = 100	105.09 ± 48.02 %	N = 65	***P* < .01**	**-**
Blann *et al* [113]	99 ± 20 IU/dL	N = 41	121 ± 29 IU/dL	N = 41	-	-	***P* < .01**	**-**
Colorectal								
Weiss *et al* [114]	105 ± 30 IU/dL	N = 68	165 ± 40 IU/dL	N = 9	178 ± 65 IU/dL	N = 9	***P* < .0001**	**-**
Damin *et al* [115]	150.2 ± 58.1 IU/dL	N = 87	230.6 ± 96 IU/dL	N = 75	276 ± 117.2 IU/dL	N = 16	***P* < .0001**	***P* < .02**
Wang *et al* [102]	110.1 ± 27 %	N = 22	241.3 ± 68.2 %	N = 40	266.1 ± 91.3 %	N = 86	***P* < .001**	***P* = .001**
Gil-Bazo *et al* [116]	98.2 ± 46.2 IU/dL	N = 20	102.8 ± 40.7 IU/dL	N = 14	190 ± 85.3 IU/dL	N = 12	**-**	***P* = .004**
Barrio *et al* [110]	75 – 150 %*	N/A	210.7 (49.6 – 571) %	N = 43	234 (49.6 - 571) %	N = 30	**N/A**	***P* = .02**
Lung (NSCLC)								
Guo *et al* [104]	1019.9 ± 789.4 IU/L	N = 102	1583.5 ± 787.7 IU/L	N = 119	1812.3 ± 675.5 IU/L	N = 64	***P* < .001**	***P* = .018**
Martini *et al* [117]	90 ± 25 IU/dL	N = 64	79 ± 28 IU/dL	N = 64	-	-	***P* = .05**	**-**
Barrio *et al* [110]	75-150 %*	N/A	187.3 (48.8 - 734.5) %	N = 65	194.5 (48.8 - 734.5) %	N = 39	**N/A**	***P* = .16**
Gastric								
AJ YANG *et al* [118]	12.92 µg/mL	N = 67	18.84 µg/mL	N = 94	-	-	***P* < .0001**	***P* < .0001**
Xia YANG *et al* [119]	72 (21 - 115) %	N = 32	82 (8 -118) %	N = 99	101 (40 - 136) %	N = 69	***P* < .05**	***P* < .001**
Bladder Carcinoma								
Ziętek *et al* [120]	98 ± 42 %	N = 35	106 ± 51 %	N = 20	194 ± 41 %	N = 31	**NS**	***P* < .0001**
Ovarian								
Gadducci *et al* [121]	108 ± 4 IU/dL	N = 88	154 ± 13 IU/dL	N = 58	219 ± 20 IU/dL	N/A	***P* < .001**	***P* < .02**
Koh *et al* [103]	1.12 (0.89 - 1.44) IU/mL†	N = 41	1.51 (1.24 - 2.31) IU/mL	N = 55	1.75 (1.29 - 2.66) IU/mL	N = 35	***P* < .001**	***P* = .161**
Prostate								
Blann *et al* [122]	118 ± 26 IU/dL	N = 27	137 ± 20 IU/dL	N = 31	-	-	***P* = .002**	**-**
Ablin *et al* [123]	1.36 ± 0.61 IU/mL	N = 8	4.33 ± 2.34 IU/mL	N = 18	-	-	***P* < .05**	**-**
Barrio *et al* [110]	75 – 150 %*	N/A	231.0 (45.7 - 364) %	N = 32	-	-	**N/A**	**-**
Glioblastoma								
Navone *et al* [124]	121 (101-177) IU/dL†	N = 22	225 (165 – 336) IU/dL	N = 58	-	-	***P* < .001**	**-**
Marfia *et al* [105]	133 (101 – 190) IU/dL†	N = 23	175 (135 – 294) IU/dL	N = 57	-	-	***P* < .01**	**-**

Table 1.2 Plasmatic VWF levels reported in haematological cancer patient cohorts

Cancer Cohort	Healthy Controls	N	Cancer Patients	N	Metastatic Cancer Patients	N	*P*-Value	
							Cancer	Metastasis
Acute Lymphoblastic Leukaemia (ALL)								
Burley *et al* [125]	1.01 ± 0.09 IU/mL	N = 20	1.84 ± 0.11 IU/mL	N = 35	-	-	***P* < .0001**	-
Hagag *et al* [126]	119.37 ± 1.79 IU/dL	N = 20	583.85 ± 40.84 IU/dL	N = 40	-	-	***P* < .001**	-
El-Sherif *et al* [127]	56.9 ± 8 %	N = 8	102.7 ± 22.9 %	N = 24	-	-	***P* < .001**	-
Athale *et al* [128]	1.14 ± 0.48 IU/mL	N = 13	1.89 ± 0.61 IU/mL	N = 17	-	-	***P* = .001**	-
Hatzipantelis *et al* [129]	99.7 ± 9.1 %	N = 28	164.6 ± 12 %	N = 52	-	-	***P* < .005**	-
Giordano *et al* [130]	104 ± 2 %	N/A	114 ± 4 %	N = 84	-	-	**NS**	-
Multiple Myeloma								
Auwerda *et al* [131]	1.17 ± 0.5 IU/mL	N = 124	1.92 ± 1.13 IU/mL	N = 135	-	-	***P* < .0001**	-
Marion *et al* [132]	0.6 – 1.4 IU/mL*	N/A	1.95 ± 1.49 IU/mL	N = 138	-	-	***P* < .001**	-
Robak *et al* [133]	91.5 (81 – 107) %	N = 20	171.0 (54 – 420) %	N = 31	-	-	***P* < .001**	-
Tiong *et al* [134]	103 (57 – 140) IU/dL	N = 46	190 (104 – 332) IU/dL	N = 24	-	-	***P* < .001**	-

Note

VWF:Ag levels measured in a variety of cancer cohorts. *P*-values determined from healthy controls versus cancer patients VWF:Ag levels and Stage IV/Metastatic patients VWF:Ag versus total cancer patients or non-metastatic cancer patient VWF:Ag levels.

ʃ Data taken from this study

* No healthy control available, laboratory reference range used for comparison

† Patients with benign disease used as control comparison group

Importantly, as an acute phase protein increased plasma VWF:Ag levels have been reported in other disease states such as infection[135] or sepsis[136]. However, the sustained and incremental release in VWF levels observed in cancer patients is suggestive of atypical and prolonged VWF secretion from endothelial cells. Furthermore, the correlation between increased VWF:Ag levels with advanced tumour staging and poorer clinical outcome suggests that VWF may be playing a direct role in contributing to cancer progression.

The biological mechanisms underpinning elevated VWF:Ag in cancer cohorts remains poorly understood, although increased VWF synthesis and secretion from endothelial cells has been shown to be important and is discussed in further detail below. Notwithstanding that, recent studies highlight tumour-derived VWF as a novel entity which may also be important in this context.

While under normal conditions, VWF biosynthesis is limited to endothelial cells and megakaryocytes; surprisingly, some cancer cells of non-endothelial cell origin acquire *de novo* VWF gene expression. For example, osteosarcoma cells SAOS2,[137] papillary thyroid TPC-1 cells,[138] colorectal cancer cells SW480,[139] hepatocellular carcinoma cells HEPG2 and BEL7402,[140] breast cancer MCF-7 and MDA-MB-231 cells,[141] lung adenocarcinoma cells 95D and A549,[142] glioma cells M049,[143] and gastric cancer cells BGC823 and SGC7901[118,144] have all been shown to express VWF at both the gene and protein level. VWF expressing cells are outlined in Table 1.3. Moreover, expression of VWF within tumour cells induced the formation of endothelial WPB-like organelles called pseudo-Weibel-Palade bodies.[118] Despite this, no other markers of endothelial cells were found to be expressed in these tumour cells, including CD31 and vascular endothelial growth factor receptor 2 (VEGFR2), indicating that acquisition of VWF expression as unique, rather than a consequence of phenotypic shift of tumour cells towards an endothelial phenotype.[143] Furthermore, VWF expression has also been observed in a number of primary tumour biopsy samples taken from patients with osteosarcoma, hepatocellular carcinoma, glioma and gastric cancer.[118,119,137,140,143] VWF expression was associated with increasing Tumour, Node, Metastasis (TNM) stages, a global classification of malignant tumours.

Biosynthesis of a molecule as large and complex as VWF undoubtedly confers a significant cellular energy cost to the tumour cells, suggesting a potential selective advantage for tumour cells in doing so. Interestingly, *de novo* VWF expression in glioma and osteosarcoma cells has been shown to enhance tumour cell adhesion to endothelial cells as well as extravasation of the tumour cells across the endothelial barrier *in vitro*.[143] Similarly, inhibition of tumour-derived VWF, by siRNA knockdown, in hepatocellular carcinoma cells reduced tumour migration in an *in vitro* scratch wound assay.[140] Tumour-derived VWF also promotes the formation of tumour cell-platelets heteroaggregates *in vitr*o for osteosarcoma and gastric cancer cells.[118,143] Tumour-platelet heteroaggregates or platelet cloaking has been proposed as an important mechanism to protect tumour cells from shear forces with the circulation and the assault of natural killer cells thus aiding metastasis *in vivo*.

Crucially, VWF synthesised from these different cell types, tumour derived-VWF versus endothelial VWF may be structurally and functionally distinct. For example, VWF synthesised in platelets has a unique posttranslational modifications compared to endothelial derived-

VWF. In particular, platelet-VWF exists as a hyposialylated glycoform, rendering it less susceptible to ADAMTS13-mediated proteolysis.[145] Furthermore, in ischemic stroke, platelet-derived VWF contributes significantly to thrombo-inflammation whilst also being less pro-thrombotic than endothelial derived-VWF.[146] It remains to be determined whether cancer-derived VWF may also exist as a distinct VWF variant within the tumour milieu contributing to tumour progression.

Table 1. 3 VWF is synthesised by a diverse array of cell types including tumour cells

Cell type	Cellular Synthesis	Secretory pathway	Cellular packaging	Multimeric Structure	Function
Endothelial cell	**Yes**	Regulated	WPB	High molecular weight	Primary haemostasis
		Basal	WPB	High molecular weight	Primary haemostasis
		Constitutive	none	Low molecular weight	Unknown
Megakaryocyte	**Yes**	Regulated	α-granules	High molecular weight	Primary haemostasis
Platelet	**No**	Regulated	α-granules	High molecular weight	Primary haemostasis
Tumour cells	**Yes**	Unknown	Proposed pseudo-WPB	Unknown	Cancer metastasis, tumour apoptosis

1.2.2 Tumour induced endothelial activation

The endothelium occupies a strategic position at the interface between the vasculature and underlying tissues and, as such, it serves as both the entry and exit point of circulating tumour cells as they metastasize. In order to navigate this pathway, tumours can induce activation of endothelial cells, promoting secretion of pro-inflammatory mediators, proangiogenic factors and adhesion receptors. Once activated, endothelial cells release the content of their storage organelles, including WPB, resulting in significant secretion of UL-VWF multimers into the lumen of the vessel. A variety of endogenous agonists stimulate endothelial activation and VWF secretion, including thrombin, interleukins (IL) i.e. IL-6 and IL-8, histamine and tumour necrosis factor-alpha under inflammatory conditions.[147] Similarly, tumour cells have also been shown to secrete soluble factors which induce WPB exocytosis. For example, tumour secretomes derived from lung (A549) cells, prostate (PC3) cells, urothelial carcinoma (RT4) cells, colon cancer (HT-29) cells, and melanoma (MV3, BLM) cells were able to promote VWF

secretion from primary human endothelial cells *in vitro*.[148–155] Furthermore, in a recent study from our group we demonstrated that MCF-7 and MDA-MB-231 breast cancer cells could mediate VWF secretion from primary human endothelial cells. VWF release occurring in both a platelet-dependent and platelet independent manner, with a key role for tumour derived VEGF-A.[156] This increased endothelial VWF secretion induced by breast cancer cells, triggered VWF string formation along the surface of the endothelium under shear stress and subsequently contributed to the recruitment and adhesion of breast cancer cells to the endothelial layer. Tumour-mediated VWF secretion from endothelial cells is likely to contribute to the elevated plasma VWF:Ag reported in several cancer patient cohorts. The biological mechanisms through which the tumour secretome induces endothelial cell activation is varied and likely tumour cell specific, but includes inflammatory cytokines (IL-6 and -8), matrix metalloproteinases (MMP-1 and MMP-2) and angiogenic mediators (VEGF-A).[148–154]

Tumour supernatant from cultured HT-29 colon carcinoma cells induced an acute activation of both macrovascular and microvascular endothelial cells resulting in the rapid secretion of VWF *in vitro* under both static and shear stress conditions.[154,157] Interestingly, tumour induced VWF secretion was equivalent to histamine, one of the most potent endothelial activators. Moreover, low metastatic colon cancer cell line Caco-2 were unable to induce VWF secretion.[157] Further analysis revealed, VWF secretion was mediated by colon cancer-derived MMP-1, within the tumour supernatant, which triggered activation of endothelial protease-activated receptor 1 (PAR1).

Work by Desch and colleagues, demonstrated that supernatant from melanoma cells can also induce acute endothelial secretion of VWF from WPB. In contrast to colon cancer cells, but similar to our findings with breast cancer cells, proteomic profiling revealed that melanoma cells mediate endothelial cell activation and VWF release through secretion of tumour-derived VEGF-A.[152] Accordingly, inhibition of VEGF-A using blocking antibody bevacizumab, markedly attenuated melanoma-induced accumulation of UL-VWF multimers from endothelial cells *in vitro*.[148] Furthermore, analysis of tumour tissues and plasma samples from melanoma patients revealed not only an increase in UL-VWF deposited along the tumour vasculature but also a reduction in ADAMTS13 activity.[148] In support of this, using a mouse model of melanoma, Bauer *et al* observed a marked decrease in local ADAMTS13 antigen and

activity within tumour microvessels compared to healthy skin microvessels *in vivo*. Collectively, these results suggest the tumour cells increase UL-VWF secretion while simultaneously downregulating ADAMTS13 activity resulting in a prolonged half-life of UL-VWF multimers along the endothelial surface. Growing evidence, reviewed below, suggests that these multimers may also be important in contributing to CAT and disease progression.

1.2.3 VWF in the tumour microenvironment

In addition to tumour-induced VWF secretion into the circulation, emerging evidence indicates that tumour cells may also contribute to the localised accumulation of VWF within the tumour stroma or tumour microenvironment directly (Figure 1.8). Ohtani *et al*, examined VWF immunolocalisation in the microvessels of colon carcinoma patient tissues and reported the frequent deposition of VWF within the sub-endothelial extracellular space of carcinoma stroma compared to the healthy colon tissue, which they hypothesised may be caused by either cancer induced basolateral secretion of VWF from endothelial cells or increased vascular permeability.[158] Similarly, more recent studies by Cahlin *et al*, examined immunohistochemical staining of colon adenocarcinoma biopsies from patients and reported a marked increase in VWF staining within the stroma of the colon cancer tumours.[159] Moreover, regression analysis revealed that this stromal VWF staining was predictive for reduced survival in this colon cancer cohort. Furthermore, immunohistochemistry of tumour tissues taken from patients with gastric cancer and lung adenocarcinoma detected remarkably higher levels of VWF protein expression concentrated in the tumour stroma compared to adjacent non-tumour parenchyma which correlated with disease progression.[118,149]

These studies begin to suggest the potential of the tumour microenvironment in contributing to localised VWF deposition within the tumour stroma. How tumours mediate this accumulation of VWF is poorly understood. Work by Xu *et al*, has shown that the secretome from lung adenocarcinoma promote increased endothelial VWF gene expression within tumour vasculature through enhanced binding of GATA3 transcription factor to the VWF promotor region.[149] These studies suggest tumour cells not only contribute to VWF secretion through WPB exocytosis of intracellular stored VWF, but also enhance VWF expression at a genetic level within the tumour microenvironment. Intriguingly tumours may also sequester circulating VWF from plasma into the tumour stroma. A recent study suggests the collagen

binding motif within the A3 domain of VWF may facilitate targeted accumulation of VWF within tumour tissues, due to the high density of exposed collagen and vessel leakiness associated with solid tumours.[160] The biological function of VWF accumulation within the tumour microenvironment is not understood but may contribute to immune cell recruitment, enhanced angiogenic potential and localised inflammation as discussed below. Notably, co-culture of osteosarcoma cells with endothelial cells induced VWF secretion which directly contributed to tumour cell epithelial mesenchymal transitioning (EMT), an essential first step for tumour cell migration and metastasis.[161]

1.2.4 Pro-inflammatory role for VWF in cancer

In recent years it has become widely accepted that inflammation and innate immunity are key components of tumour progression.[162] For example, the tumour microenvironment contains a significant number of inflammatory cells, including tumour associated macrophages and infiltrating leukocytes, which not only contribute to immunothrombosis but are also indispensable for neoplastic proliferation, immunosuppression, and tumour dissemination.[163] In addition, many of the hallmark steps for leukocyte recruitment and trafficking within innate immunity are also fostered by tumour cells as they metastasize.[164] These steps include: migration in response to chemokines, as well as activation of selectin adhesion molecules and leukocyte integrins which facilitate tumour cell interaction with the vascular endothelium and extravasation.

Interestingly, growing evidence highlights the mechanistic involvement of VWF in inflammation and immunothrombosis, including contribution to leukocyte adhesion, and extravasation as well as proinflammatory cytokine secretion and vascular permeability (Figure 1.8).[165] For example, a number of independent studies have reported that leukocytes bind directly to VWF through β2-integrins and P-selectin glycoprotein ligand-1 (PSGL-1) under conditions of shear stress. Work by Popa *et al* and Bernardo *et al* revealed that platelet-decorated UL-VWF multimers, secreted from activated endothelial cells, facilitate the adhesion and transendothelial migration of leukocytes under high shear stress.[166,167] Taken together these results clearly demonstrate that VWF serves as an adhesive surface on activated endothelial cells to tether and sequester leukocytes. Given that tumour cells can adopt similar trafficking pathways as leukocytes it is perhaps not surprising that VWF can also tether tumour cells. Morganti *et al* demonstrates the adhesion of colon carcinoma cell line

HRT-18 to endothelial cells occurs in a VWF-dependent manner.[168] Moreover, shear stress induced release of VWF from endothelial cells enhanced breast tumour cell adhesion to the endothelium *in vitro*.[169] Interestingly, cancer cells which acquire *de novo* expression of VWF, including osteosarcoma and glioma cells, also demonstrate an enhanced ability to interact with endothelial cells and undergo extravasation across the endothelium compared to non-VWF expressing tumour cells.[143] Consequently, VWF, either endothelial- or tumour-derived may represent a novel pathway through which tumour cells mediate interaction with the vascular endothelium, in a manner similar to leukocytes. This interaction may facilitate cancer cell dissemination within the circulation.

Within the tumour microenvironment, infiltrating immune cells produce an array of pro-inflammatory cytokines, pro-angiogenic factors which serve to contribute to tumour growth, migration and dissemination. Interestingly, a recent study found that plasma VWF:Ag levels in breast cancer patients positively correlated with tumour infiltrating mast cells suggesting perhaps VWF may contribute to immune cell recruitment within tumour tissues.[170] Further studies are warranted to confirm these observations. Nevertheless, there is significant evidence to support a role for VWF in promoting the recruitment and transendothelial migration of immune cells. For example, studies in a model of cutaneous inflammation demonstrate that leukocyte recruitment was significantly reduced in mice administered a polyclonal anti-VWF treatment *in vivo* compared to control mice.[171] Similarly, antibody-mediated blocking of VWF in a model for thioglycollate-induced peritonitis ablated the transmigration of leukocytes into the peritoneum.[172] These effects may, at least in part, be mediated by the A1-domain of VWF since work by Aymé *et al* has shown that targeting this VWF region using a single-domain antibody markedly attenuate leukocyte recruitment and vascular permeability in both immune complex–mediated vasculitis and irritant contact dermatitis models *in vivo*.[173] Most recently, in a landmark article from Drakeford *et al* a direct role for VWF as an inflammatory molecule was demonstrated with exogenous VWF. More specifically, treatment of human and murine macrophages with VWF elicited a significant a pro-inflammatory response.[174] Direct VWF-macrophage interaction mediated downstream pro-inflammatory cytokine production, furthermore VWF triggered M1 polarisation in human macrophages as indicated through the generation of reactive oxygen species and positive expression of M1 markers CD11b and CD38. Moreover, injection of VWF in the peritoneum

of mice resulted in enhanced chemotactic accumulation of macrophages and significant upregulation of inflammatory cytokines TNF, IL-6 and IL-1β, affirming the inflammatory role of VWF.

VWF has been shown to play an important role in modulating vascular permeability which likely contributes to immune cell recruitment and infiltration into the extracellular matrix (ECM). VWF secreted basolaterally into the ECM negatively regulates expression of endothelial tight junction protein Claudin 5.[175] In keeping with this, infusion of VWF, in an intracerebral haemorrhage model, not only increased pro-inflammatory markers and neutrophil recruitment but also markedly enhanced blood-brain barrier permeability, with Evans blue extravasation increased by 79%. This effect could be attenuated by treatment with anti-VWF antibodies, highlighting the direct role of VWF in altering vessel permeability.[176] Given the evidence to date that VWF mediates the recruitment of immune cells and regulates vascular permeability, it is tempting to speculate on its contribution to tumour cells adhesion and extravasation across the endothelium in a similar manner.

1.2.5 Angiogenesis

Accessibility of blood vasculature is an important determinant in cancer progression.[177] VWF has been described as having both pro- and anti-angiogenic roles in different tissue beds and also in specific disease settings. For example, under physiological conditions, Starke *et al*, identified endothelial VWF as a negative regulator of angiogenesis. Knockdown of VWF expression in endothelial cells resulted in increased proliferation and migration in response to VEGF.[73] In keeping with this, increased vascularisation was observed in VWF-/- mice *in vivo* while blood outgrowth endothelial cells isolated from patients with VWD demonstrated a pro-angiogenic phenotype.[178] This effect appears to be, at least in part, mediated by disruption of the storage and regulated release of pro-angiogenic factors, including angiopoietin-2 (Ang-2) and galectin-3 which under normal conditions are coupled with VWF within endothelial WPB.

Paradoxically, in a hind limb ischemia model, VWF-/- mice displayed reduced arteriogenesis and angiogenesis which gives rise to impaired blood flow recovery in these animals.[179] More recently, in the context of wound healing, circulating VWF has been shown to bind directly to a number of growth factor including several pro-angiogenic factors (platelet-derived growth factor (PDGF), VEGF and fibroblast growth factor (FGF) families) and mediate their localized

delivery at sites of tissue damage to promote angiogenesis and repair.[100] Accordingly, VWF-/- mice, demonstrated impaired angiogenesis and delayed wound healing, compared to wild type mice.

While the interaction between VWF and angiogenic factors may help to promote wound healing, this interplay also has a darker side in the context of cancer progression. For example, both gastric and colon cancer secreted VEGF-A was shown to upregulate VWF expression and secretion from endothelial cells *in vitro* in a dose- and time-dependent manner.[119,180] Similarly, Bauer *et al* has reported that melanoma derived VEGF-A induced secretion of UL-VWF multimers in an *in vivo* model of malignant melanoma.[148] Importantly, intraluminal accumulation of VWF not only resulted in deposition of platelet-rich thrombi within the vasculature but also served to increase the number of metastatic foci in murine lung tissues. Moreover, in ADAMTS13-/- mice the increase in intraluminal VWF deposition induced by melanoma tumours, directly correlated with increased tumour vessel density, suggesting a pro-angiogenic role for endothelial secreted UL-VWF multimers in this melanoma model *in vivo*.[181] Further studies are needed to elucidate the complex crosstalk that exists between VWF and angiogenic factors in the setting of malignancy.

1.2.6 VWF in Metastasis

Activation of platelets and the coagulation system play an important role in promoting metastasis. Tumour metastasis is dependent, at least in part, on circulating platelets. Elevated platelet count is associated with poorer prognosis in several cancer cohorts, including colon, pancreatic, breast, lung and brain cancer.[99] Moreover, platelet deficiency or dysfunction have both been associated with significantly reduced metastasis in several animal models.[99,182] Platelets have been proposed to cloak circulating tumour cells masking them from attack by the natural killer cells.[99] Moreover, platelets have also been shown to facilitate tumour cell adhesion to the endothelium, promoting transendothelial migration and thereby facilitate tumour cell extravasation.[99] Given its involvement in platelet adhesion and aggregation along the endothelium, VWF is likely to play a role in mediating some of these effects. Indeed, treatment of immobilized platelets with a blocking VWF antibody significantly attenuated the adhesion of colon carcinoma cells *in vitro* under shear stress.[183] In keeping with this, inhibition of the VWF-platelet axis using targeted GPIbα inhibitory antibodies markedly attenuated the interaction between lung carcinoma cells and platelets *in vitro* as well as adhesion of these

tumour cells to EC.[184] Inhibition of the VWF-platelet axis *in vivo* resulted in a greater than 50% reduction in pulmonary metastasis in both an experimental lung cancer model and a spontaneous breast cancer model.[184] Furthermore, in an experimental metastasis model of murine melanoma, deficiency of GPIbα resulted in an ablation of metastatic foci in the lung. The authors also demonstrate that this effect is mediated by the extracellular domain of the α-subunit of GPIb, the major VWF binding domain.[185] Taken together these results suggest an important role for VWF-platelet interactions in mediating metastasis for an array of tumours.

However, VWF may also contribute to cancer metastasis independent of platelets. VWF can bind directly to a variety of tumour cells through a number of integrin receptors.[186] In addition, studies have shown that some cancer cells may express pseudo-GPIbα receptors for direct VWF adhesion.[187,188] In particular Suter *et al*, reported the surface expression of GPIbα on several cultured breast tumour cells as well as positive GPIbα staining in primary breast tumour tissues. Exposure of these GPIbα positive breast tumour cells to VWF results in increased tumour cell spreading, through cytoskeleton rearrangement, and tumour migration *in vitro*.[188] These data suggest a novel mechanism through which tumour cells may interact directly with VWF to promote dissemination. In keeping with this, experimental metastasis study found that anti-VWF treatment inhibited pulmonary metastasis by 64% for disseminating colon carcinoma cells as well as melanoma and Lewis-bladder cancer cell lines by 45% and 46% respectively.[189] Similarly, VWF expressing gastric cancer cells demonstrated significantly reduced lung metastasis in mice treated with anti-VWF antibody.[118]

Importantly, the contribution of VWF to cancer dissemination appears to be specific to blood-borne metastasis rather than lymphatic metastasis.[113,181] Melanoma induced accumulation of intraluminal UL-VWF multimers resulted in increased metastatic tumour burden in the lungs *in vivo*. Conversely, VWF multimers within the tumour vasculature had no significant effects on tumour dissemination via the lymph nodes.[181] The mechanism underpinning the role of VWF in contributing to tumour cell seeding at distal tissues sites remains unclear. However, Goertz *et al* reported intraluminal VWF multimers in a murine model of melanoma were present not only in the primary tumour microvasculature but, intriguingly, also in tumour-free distal organs, including liver, brains and lungs.[181] These findings suggest that even at an early disease stage, tumours can induce systemic VWF secretion from endothelial cells at sites which tumour frequency metastasize to.

In contrast to the evidence supporting a pro-metastatic role for VWF, VWF-/- mice demonstrate increased pulmonary metastatic burden compared to wild type controls in experimental murine metastasis models of Lewis-Lung carcinoma or BL6-B16 melanoma cells.[190] While VWF biosynthesis drives the formation of WPB within endothelial cells, genetic ablation of VWF in this mouse model is also characterized by a lack of these endothelial storage organelles. This gives rise to dysregulated storage and secretion of pro-metastatic factors, such as P-selectin and Ang-2. However, the authors demonstrate that the enhanced metastatic phenotype is corrected by re-infusion of VWF into VWF-/- mice, suggesting that circulating VWF may attenuate cancer dissemination. This is in direct contrast to studies reporting reduced metastasis with antibody mediated inhibition of VWF *in vivo*. While some studies hypothesise that deficiency of VWF may increase the availability of platelet GPIbα and thus promote metastasis. [184] In recent years, new evidence has come to light which may help to explain the apparent paradox. UL-VWF may be pro-apoptotic to specific cancer cells. Terraube *et al* reported that VWF reduced survival of circulating BL6-B16 murine melanoma within 24 hours following infusion into mice.[190] Indeed, work by Mochizuki and colleagues' demonstrated VWF-mediated apoptosis of several cultured tumour cell lines *in vitro*, including, breast, kidney, liver and lung.[101] However, not all cancer cells were susceptible to VWF-induced apoptosis. Specific tumour cells including lung (PC-9), breast (MDA-MB231) and renal (Caki-2) demonstrated high expression of a novel VWF cleaving protease ADAM28. Expression of ADAM28 rendered these tumour cells resistant to VWF-induced apoptosis *in vitro*. Further studies will be essential to fully define the biological mechanisms underpinning these findings.

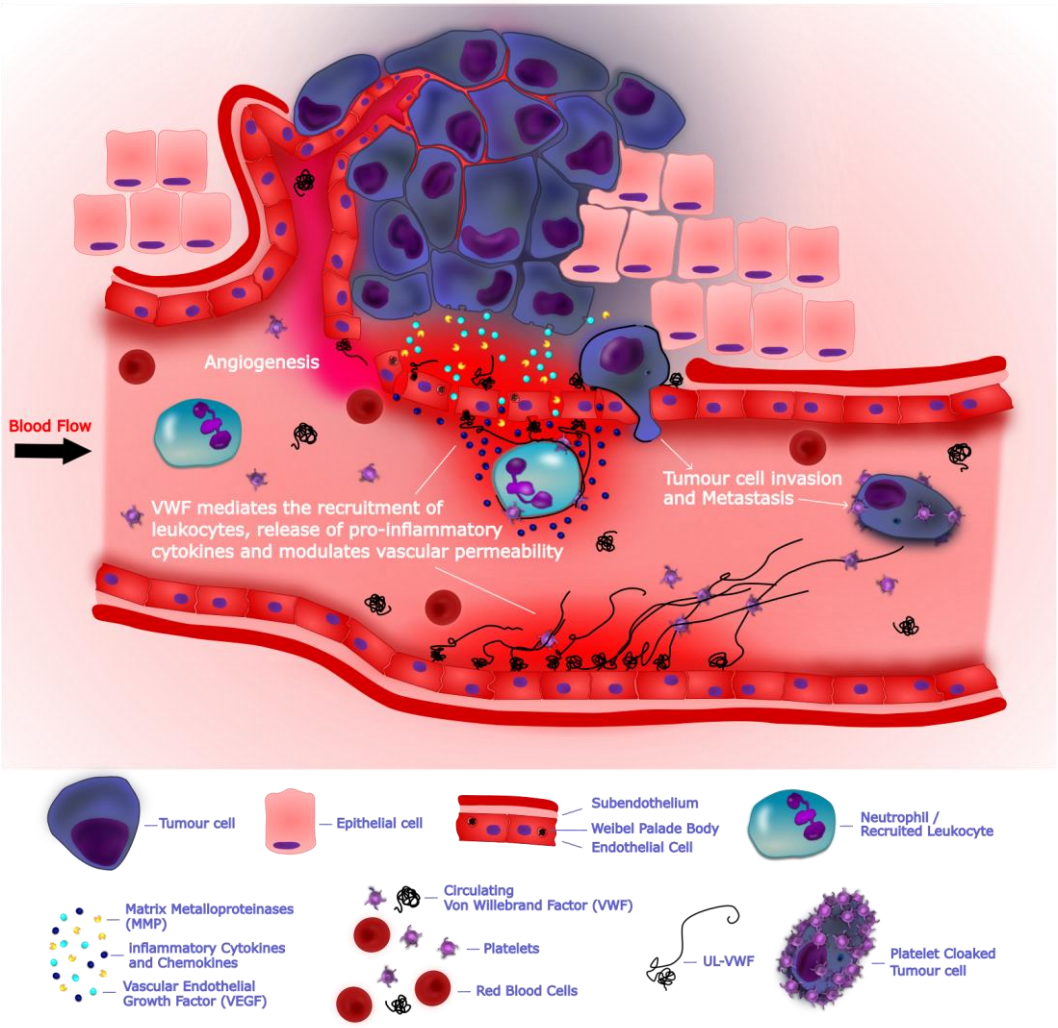

Figure 1.8 The great escape, VWF in the tumour microenvironment: Tumour-induced endothelial activation releases an array of proteases including matrix metalloproteinases that may mediate break down the sub-endothelial extracellular matrix. In addition, tumour-secreted stimulatory factors, such as VEGF, tumour necrosis factor alpha, and interleukin 8 induce activation of endothelial cells, resulting in the release of UL-VWF into the lumen, promoting the formation of platelet decorated strings within the vasculature and increasing systemic VWF plasma levels. VWF may modulate a variety of pro-metastatic processes within the tumour microenvironment. These include VWF-mediated platelet and leukocyte recruitment, contributing to pro-inflammatory cytokine signalling, enhanced angiogenesis, and altered vascular permeability. These effects may culminate in increased tumour growth and the transmigration of tumour cells across the endothelial cell wall and enhanced metastasis.

1.2.7 VWF and cancer associated coagulopathies

Cancer and its associated therapeutic strategies are established risk factors for VTE. Cancer patients have approximately a 6 fold increase risk of VTE compared to non-cancer patients. In fact, thromboembolism is the second leading cause of mortality in cancer patients.[98] The risk of VTE is also dependent on a number of factors, including tumour type, stage of disease and specific treatment regimen. For example, haematological malignancies, pancreatic, lung and brain cancers are associated with a high VTE risk, whilst prostate and subsets of breast cancer carry a lower risk of thrombosis.[191]

Critically, cancer patients with VTE have lower survival rates and poorer prognosis compared to cancer patients without VTE.[192] Sørensen *et al* reported that the 12-month survival rate was 3-fold lower in cancer patients with VTE than those without VTE. Importantly, this increased mortality rate was not solely attributed to thromboembolic events but strongly associated with advanced stage cancer.[192] These data intriguingly suggest that cancer-coagulation interplay may not only increase thrombotic risk but also accelerate tumour progression and metastasis. This is supported by the observation that adjunctive anticoagulant therapy with Low Molecular Weight Heparin (LMWH) may prolong survival in cancer patients.[193,194] However, in more recent clinical trials (FRAGMATIC, TILT and PERIOP-01) examining the survival in patients treated with LMWH it was observed that LMWH conferred no change in survival.[195–197]

Despite recent data suggesting LMWH may not increase survival in cancer several meta-analytical studies of large randomized clinical trials determined that prophylaxis with anticoagulants has been found reduce the risk of VTE in ambulatory cancer patients, with what was deemed to be an acceptable increase in major bleeding.[198] In fact, one analysis concluded that anticoagulation strategies, including LMWH, provided a measurable mortality benefit, however, this effect remains elusive when analysis is restricted to a single agent.[199] Importantly, amongst the different clinical trials assessed the duration, timing and dosages of primary thromboprohphylaxis differed.[199] As such, to reduce mortality in cancer through primary thromboprophylaxis it may be necessary to use multiple arms of anticoagulant treatment at specific times during cancer development.

Interestingly, due to the varied results in clinical trials the optimal use of LMWH in patients with cancer is not fully defined in clinical practice.[200] Furthermore, this is confounded by data

that shows patients with cancer can have recurrent VTE despite anticoagulant treatment.[200] Notably, using warfarin a conventional anticoagulant in thrombosis treatment it been shown to be inferior to LMWH in CAT as reported by the CLOT and CATCH trials.[201,202] Together, this highlights the complex underlying pathophysiology of coagulation activation in cancer and the necessity to specifically target risk factors in VTE development on top of broad spectrum anticoagulant treatment.

A diverse array of biological mechanisms underpinning VTE risk in patients with cancer have been proposed, including cancer mediated inflammation, endothelial and platelet dysfunction, microparticle secretion and tissue factor expression, however they remain poorly defined. Interestingly however, several independent studies have identified markedly increased plasma levels of VWF in a number of cancer cohorts compared to healthy individuals (Table 1.1 and 1.2). Importantly, both VWF and FVIII plasma levels correlate with risk of VTE within the general population.[97] In fact, Rietveld and colleagues suggest that VWF and FVIII levels are associated with the highest risk of VTE.[97] However, a number of studies have also reported elevated VWF levels as an independent predictor of VTE in cancer patients, even after adjustment for patient-related factors.[108,109,203,204]

Assessment of VWF propeptide, as a marker of VWF secretion, Nossent *et al* concluded that high VWF levels associated with thrombosis is largely mediated by increased VWF secretion from endothelial cells.[96] As discussed earlier, several cultured tumour cell lines stimulate endothelial cell activation and thus VWF secretion. Moreover, tumour biopsies from malignant melanoma patients has shown the presence of UL-VWF multimers within the lumen of tumour microvessels.[148] Accumulation of these adhesive UL-VWF multimers was also supported by local tumour-mediated inhibition of ADAMTS13. Collectively, these results suggest the tumour cells may induce endothelial activation to increase UL-VWF secretion while simultaneously downregulating ADAMTS13 activity. Crucially, this has been shown to contribute directly to a prothrombotic milieu, with a significant number of VWF-platelet aggregates observed in the tumour vasculature as well as fibrin deposition.[181] While the mechanism underpinning impaired ADAMTS13 activity in cancer patients is unclear, it appeared to be associated with disseminating tumours, with reduced ADAMTS13 activity reported in patients with advanced, metastatic malignancies rather than localized tumours.[108,204] Examination of therapeutic strategies to attenuate tumour-mediated release

of VWF observed that a specific LMWH, Tinzaparin, resulted in a marked reduction in intraluminal accumulation of VWF in a transgenic mouse model of melanoma.[148] This not only significantly reduced platelet aggregates *in vivo* but also reduced tumour growth, angiogenesis and metastasis. Importantly, this effect of LWMH appears to be independent of its anticoagulant properties since treatment with thrombin inhibitor, Fondaparinux, failed to reduce VWF multimer accumulation.[181] It is interesting to note that heparin directly interacts with VWF via the A1 region and impairs platelet GPIbα binding, highlighting another potential mechanism through which the anti-thrombotic and anti-metastatic role of heparin may be mediated.[205] These findings may suggest a potential dual therapeutic benefit for LMWH, not only reducing CAT but perhaps attenuate cancer metastasis in a VWF-dependent manner.

Emerging data has provided novel insights into crucial role of the vascular endothelium in mediating the cross-talk between coagulation and metastasis. As one of the largest and most abundant proteins within endothelial cells, VWF has been shown to be an important mediator. In addition to its established haemostatic function, it is fast becoming evident that VWF is multifaceted protein with roles in inflammation, angiogenesis, metastasis and cancer induced thrombotic complications (Figure 1.9). As summarised in figure 1.9, the tumour microenvironment is adept at selectively upregulating VWF expression and secretion from endothelial cells, giving rise to increased plasma VWF:Ag which appears to favour tumour cell propagation and metastasis. For example, VWF can promote pro-inflammatory signalling, regulate angiogenesis and modulate vascular permeability which has been proposed to contribute to tumour cell migration and extravasation across the endothelium. Endothelial anchored, platelet-decorated VWF multimer strings support the adhesion of circulating leukocytes under shear stress but may also contribute to the tethering of tumour cells, facilitating transendothelial migration and cancer dissemination through the circulation. In conclusion, the current findings suggest that that the VWF-endothelium axis is crucial in tumour progression. Defining the molecular pathways underpinning tumour-mediated VWF deposition within the vasculature may offer the opportunity to develop novel VWF-directed therapies to not only reduced CAT but also attenuate metastasis.

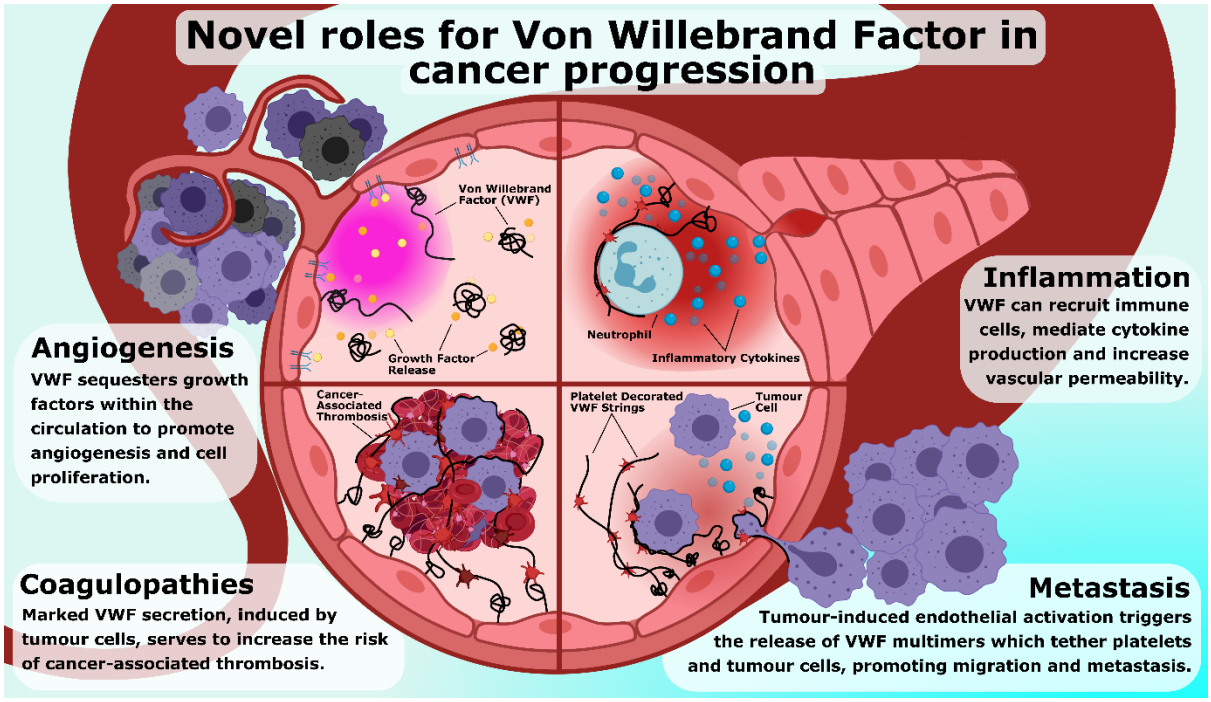

Figure 1.9 The novel roles for VWF in cancer progression: The growing evidence for novel biological functions of VWF beyond haemostasis have described. There is evidence of VWF as an angiogenic regulator and potentially proliferative factor. Moreover, VWF is associated with pro-inflammatory signalling, the recruitment of immune cells to sites of inflammation and promoting vascular permeability. Additionally, elevated plasmatic VWF levels are directly correlated with enhanced coagulopathies including venous thromboembolism. Altogether, the reports of VWF as a novel pro-metastatic factor are not surprising when many of the described functions of VWF could directly enhance cancer progression.

1.3 Project Aims

Recently novel roles for VWF have been identified in cancer metastasis. Elevated plasma VWF antigen levels have been reported in several cancer cohorts. These levels correlate with both the risk of venous thromboembolism and metastatic disease. Importantly, as breast cancer is one of the most common malignancies it is also reported to have the highest incidence of thrombotic events in malignant disease globally, as such this study aims to disentangle the distinct roles of VWF in breast cancer. To achieve this, I will examine the molecular and functional consequences of VWF breast cancer cell interactions and determine the potential for anti-VWF treatment to act as a novel anti-metastatic therapy.

The specific aims of this project include:

- Assessing VWF expression and plasma levels in patients with breast cancer and define the potential role of VWF as a clinical biomarker in breast cancer patients.

- Elucidate the molecular mechanisms through which VWF binds to breast cancer cells, mapping the specific VWF regions involved and tumour cell receptors in regulating these interactions.

- Define the role of endothelial associated VWF on breast cancer cell adhesion under shear stress.

- Examine the role of VWF in modulating key aspects of breast cancer cell biology including proliferation, apoptosis, migration and invasion.

- Investigate the effect of targeting VWF *in vivo* as a novel anti-metastatic agent.

2: Materials and Methods

2.0 Preliminary online data research

Preliminary *in silico* expression analysis was conducted through online databases to determine whether VWF may contribute to breast cancer pathology. Kaplan-Meier (KM) survival graphs were plotted through the KM-plotter online software tool (Kmplot.com/analysis/). KM plotter sources data of breast cancer patient survival from the publically available GEO expression omnibus (GEO) repository, which keeps the clinical outcomes and disease progression of patients from a variety of diseases.[206,207] In work by Balázs Győrffy the transcriptomic database was collated from 55 independent datasets with each dataset outlined in a table.[206] The dataset totalled 9423 breast cancer arrays, corresponding to 7830 unique samples with 1139 outliers and 77 biased arrays excluded from the analysis. Relapse free survival data was available for 5268 patients. The patient population was subsequently subdivided into two groups of high and low median mRNA expression and relapse free survival curves were drawn from the available clinical outcomes. Certain disease parameters, like tumour stage or grade were selected to refine the graphs to specific disease stratifications.

Furthermore, VWF protein expression in breast cancer patients was also used to generate KM survival graphs. Protein expression was quantified by liquid chromatography-mass spectrometry based proteome analysis from 65 breast tumours of all subtypes.[208] Case patients from this dataset were recruited from 1993-2003 with recruitment restricted to patients with pathologically confirmed breast cancer and no previous history of breast cancer.[209,210] Tumour specimens were collected from patients that had been diagnosed within 6 months from recruitment, demographic characteristics of the case study population is outlined by Boersma *et al*.[209] The data was then compiled and divided into high and low VWF protein expression. KM survival curves were then performed for overall survival in these patients.

2.1 Patient plasma sample collection

Plasma samples were obtained from clinical collaborators at Manchester Cancer Centre. Plasma samples from patients with early breast cancer were obtained (N=130) as part of the CHAMPion (Cancer-induced Hypercoagulability As a Marker of Prognosis).[2] The cohort was

taken from treatment naïve early breast cancer patients, ductal cancer *in situ* and invasive undergoing surgical resection, with venous blood collected prior to surgery. Exclusion criteria included previous neoadjuvant therapy, history of VTE or thrombophilia and severe immobility as part of the reporting recommendations for tumour marker prognostic studies (REMARK).[211] Of the 762 patients sampled for the case study 435 refused or did not meet inclusion criteria, resulting in 324 patients recruited as part of the study. The CHAMPion study was approved by Oldham Research Ethics Committee Study. Healthy control plasma samples were obtained as part of the CHAMPion study from patients attending with benign disease. All other healthy control plasma samples were obtained from historical age- and gender-matched control samples, as previous.[212] Furthermore, patients with metastatic breast cancer via a prospective cohort of metastatic breast cancer patients (N=44) were recruited at The Christie NHS Foundation Trust Hospital (Manchester, UK) between February 2013 and June 2015 with follow up until July 2019 as part of the TuFClot, (Tumour Fragments and Clotting) study.[1] All had either a new diagnosis of metastatic disease or new evidence of clinical or radiological disease progression, samples were taken pre-surgery. Patients were excluded if they were on any known anti-coagulation treatments or had been diagnosed with any non-breast cancer in the previous 5 years from collection again under the guidance of REMARK. The study was approved by UK National Research Ethics Service Committee North West-Greater Manchester Central Ethics Committee.

2.1.1 Patient plasma analysis; Thrombin–antithrombin III (TAT), fibrinogen and d-dimer levels

Patient blood samples were collected and processed before being measured for TAT, fibrinogen, D-dimer and circulating tumour cell levels in a previous study by our clinical collaborators as described below.[1,2] TAT levels were measured using Siemens AG (Berlin, Germany) Enzygnost® TAT micro-enzyme immunoassays (Cat: OWMG15) in the clinical and experimental pharmacology group at Manchester institute cancer biomarker centre. Fibrinogen and D-dimer levels were quantified with a Werfen (Warrington, UK) ACL TOP 500 automated haemostasis testing system in the Haematology Department at Wythenshawe Hospital. For quantification of fibrinogen levels, the HemosIL® Q.F.A. Thrombin clotting assay (Cat: 0020301700) was used. D-Dimer levels were measured with HS 500

immunoassay (Cat: 0020500100). These data were subsequently used for correlation against plasma VWF:Ag levels we measured from same patients.

2.2 Cell Culture

A complete list of the cells and their properties used in this study can be found in table 2.1. All cells used were cultured at 37°C with 95% humidity and 5% CO_2 atmosphere maintained throughout. Each cell line was regularly tested for mycoplasma during this study.

2.2.1 Breast cancer cell culture

Two breast cancer cell lines were used during this study, mesenchymal-like, highly metastatic, triple negative MDA-MB-231 cells (ATCC; Authenticated Cell Cultures, Sigma-Aldrich, UK) and epithelial-like, low metastatic, hormone receptor positive MCF-7 cells (ATCC, Sigma-Aldrich).[213–216] Both MDA-MB-231 and MCF-7 cell lines were cultured in high-glucose Dulbecco's modified eagles media (DMEM) (Cat: D6429, Sigma-Aldrich) supplemented with 10% Foetal calf serum (FCS) (Cat: 10500-064, Gibco) and 1% penicillin streptomycin (P/S) (P4333-100mL, Sigma-Aldrich). Cells were routinely cultured in T75cm^2 flasks to a confluence of 80-90% before sub-culturing.

2.2.2 Immortalised Breast cell line culture

As a control an immortalised breast epithelial cell line, MCF-10A (ATCC, Sigma-Aldrich) was used. MCF-10A cells were cultured in a high-glucose DMEM supplemented with 5% FCS, 5% horse serum (Cat: 26050088, Gibco, thermofisher), 1% P/S, 10ng/mL Cholera toxin (Cat: 9012-63-9, Sigma-Aldrich), 100µg/mL hydrocortisone (Cat: H0396-100mg, Merck Millipore) and 20ng/mL insulin (10516-5mL, Sigma-Aldrich).[217,218] These cells were grown in T75cm^2 flasks and passaged when cell confluence reached 80-90%.

2.2.3 Primary breast cell culture

A further non-tumourigenic control, primary cells from healthy human breast tissue were used, the human mammary epithelial cells (HMEC) (ATCC, Sigma-Aldrich) primary cell line.[219] HMECs were cultured in mammary epithelial cell basal medium (PCS-600-030, ATCC) and supplemented with a mammary epithelium growth kit (PCS-600-040) consisting of recombinant Human (rH) Insulin 5µg/mL, l-glutamine 6mM, adrenaline 1µM, apo-transferrin 5µg/mL, rH-TGF-α (transforming growth factor alpha) 0.5µg/mL, Extract P 0.4% and hydrocortisone 100ng/mL. HMEC cells were cultured to 80-90% confluence in T75 flasks with HMEC cells not being used beyond 10 passages.

2.2.4 Primary endothelial cell culture

Human umbilical vein endothelial cells (HUVEC) were used to represent endothelial function during the course of the study. For culturing, HUVEC were grown in endothelial cell growth medium 2 (Cat: C-22011, PromoCell) and were supplemented with 18% FCS, 1% P/S and a growth media kit (Cat: C-39216, PromoCell) consisting of, epidermal growth factor (EGF) 5ng/mL, basic fibroblast growth factor 5µg/mL, insulin-like growth factor 10ng/mL, vascular endothelial growth factor-165 (VEGF-165) 20ng/mL, ascorbic acid 0.5µg/mL, heparin 22.5µg/mL and hydrocortisone 0.2µg/mL. HUVEC were seeded onto flasks that had been pre-coated with 0.2% gelatin (G1393-100mL, Sigma-Aldrich) for 30 minutes, with the excess aspirated off. HUVEC were only used for a maximum of four passages.

2.2.5 HEK-293T Cell Culture

Human embryonic kidney-293T (HEK-293T) cells were obtained from ATCC and used to express VWF protein transiently. HEK293T cells were cultured in high-glucose DMEM supplemented with 10% FCS and 1% P/S. These cells were frequently passaged in T175cm^2 flasks at 80-90% confluency.

2.2.6 Luciferase-tagged MDA-MB-231 cell culture

The luciferase-tagged MDA-MB-231 cells are a triple negative breast cancer cell line that has been stably transfected with luciferase allowing them to bio-luminesce when exposed to luciferin salts. These cells were a kind gift from Dr. Ian Miller (RCSI) and have previously been fully characterised.[220] Cells were cultured in high-glucose DMEM supplemented with 10% FCS in the absence of P/S. The cells were grown in T75cm^2 flasks for a minimum of 3 passages to stabilise them before use in experiments *in vivo*. Cells were split when they reached 80-90% confluence.

2.2.7 Cell sub-culturing

All cells used in this study were adherent cells and underwent the same sub-culturing protocol. To passage the cells, the old media was discarded being careful not to disrupt the cell monolayer. Cells were then washed with pre-warmed PBS by applying to the non-cell coated side of the flask before gently rocking the PBS over the cell monolayer. The PBS was removed, avoiding the cell monolayer and replaced with 1mL of 1x trypsin (Cat: T4174-100mL, Sigma Aldrich) at 37°C for 5 minutes. Checking to make sure the cells had lifted through the microscope, the respective complete growth media was then added with at least a 2:1 ratio to the trypsin to prevent further trypsin catalysis. The cells were then centrifuged at 375 x g for 5 minutes before being counted via haemocytometer using trypan blue viability dye (Cat: T8154, Sigma Aldrich). Finally, the cells were sub-cultured into their respective flasks and put into the incubator to grow.

Table 2.1 Cell line properties used in this study

Cell Name	Cell Type	Type of Tissue	Tumourigenic
HUVEC 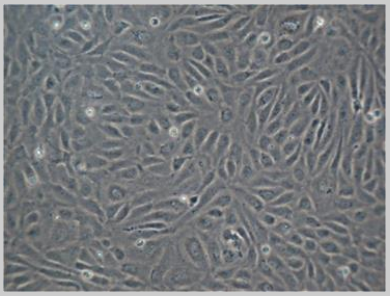	Endothelial	Human primary Umbilical Vein/ Vascular endothelium	No
HEK-293-T 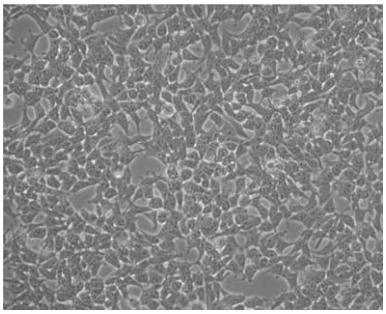	Epithelial	Human embryonic kidney tissue (Immortalised)	No

Table 2.1 Continued

Cell Name	Cell Type	Type of Tissue	Tumourigenic
MDA-MB-231 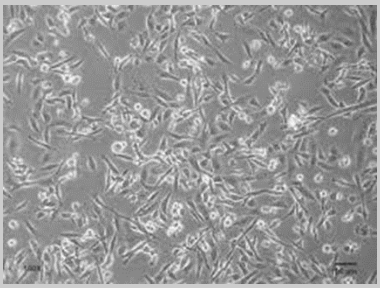	Epithelial	Mammary gland/ breast: derived from Metastatic site: pleural effusion	Yes
MCF-7 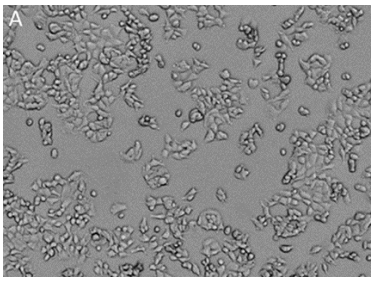	Epithelial	Mammary gland: derived from Metastatic site: pleural effusion	Yes (needs oestrogen supplement)
MCF-10A 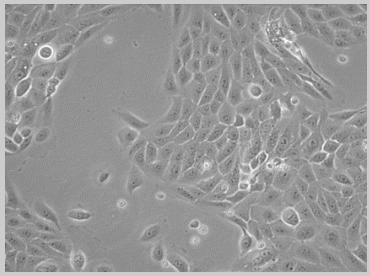	Epithelial	Mammary Gland (Immortalised)	No
HMEC 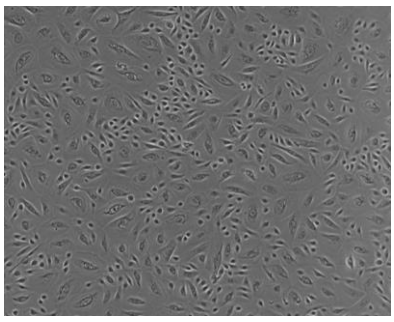	Epithelial	Primary Mammary epithelial tissue	No

2.3 VWF protein purification process

2.3.1 Recombinant VWF expression vectors

The VWF expression vector pcDNA VWF was a kind gift from Dr. McKinnon (Imperial College London, UK) and was previously described.[221] This vector encodes an ampicillin resistance gene to allow for selection in bacterial cells and a PUC origin to drive high-copy number replication in *E.coli*. For expression in mammalian cells the vector contains a cytomegalovirus (CMV) immediate-early promoter to ensure high-level gene expression. Additionally, a neomycin resistance gene facilitates selection in mammalian cells; and a SV40 origin to drive episomal replication in cells expressing the SV40 large T antigen (Figure 2.1).

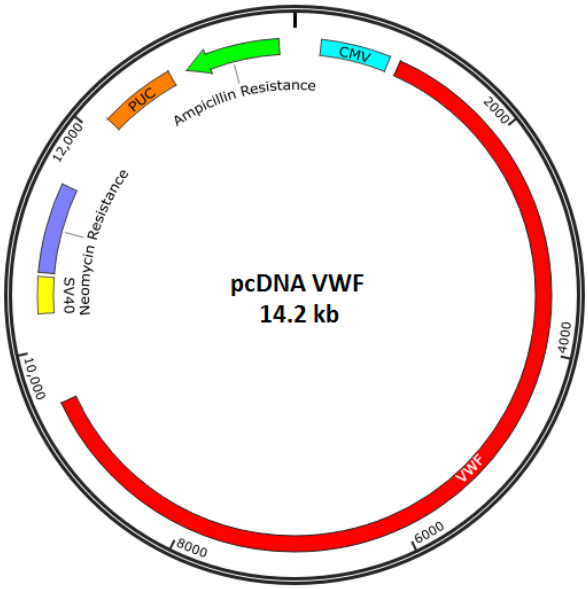

Figure 2.1 Full length VWF expression vector pcDNA VWF

2.3.2 Transient transfection of HEK 293T cells

All recombinant VWF variants were produced via transient transfection in HEK 293T cells as described previously.[222] Transient transfection of HEK 293T cells was performed in serum free medium. T175cm^2 flasks were seeded with HEK 293T and grown in supplemented DMEM until ~90% confluent. Before transfecting, cells were washed with sterile PBS and 18mL serum free opti-MEM™ (Cat: 31985070, Gibco, USA) was added to each flask. Branched polyethylenimine (bPEI; Sigma-Aldrich, Ireland) was employed as a transfection reagent. A ratio of bPEI to DNA 2:1 was used. Plasmid DNA was diluted to a final concentration of 2µg/mL in 150mM NaCl and bPEI was diluted to a final concentration of 1µg/mL in 150mM NaCl. The bPEI was then added to the diluted plasmid DNA in a drop-wise manner and incubated for 20

minutes at room temperature to allow complex formation. Subsequently 2mL of the bPEI:DNA complex was added to each flask. Flasks were incubated for 72h before conditioned media was harvested. The media was centrifuged at 3800 x g for 30 minutes and stored at -80°C until purification.

2.3.3 Anion exchange chromatography

Conditioned medium containing full length recombinant VWF protein was concentrated using anion-exchange chromatography. Conditioned medium was loaded onto a HiTrap Q HP column (packed with Q Sepharose™ High Performance; GE Healthcare, UK) in 20mM Tris, pH 7.4 at a flow rate of 1.5mL/min. The column was washed with low salt buffer, 20mM Tris, 100mM NaCl, pH 7.4, at a flow rate of 2mL/min. VWF was then eluted in high salt buffer, 20mM Tris, 500mM NaCl, pH 7.4, at a flow rate of 0.5mL/min (Figure 2.2). The VWF containing fraction (~5mL) was dialyzed against 20mM Tris, pH 7.4 at 4°C overnight with at least 2 buffer changes. Full-length recombinant VWF variants were further concentrated to final volume of ~1mL via centrifugation at 4,000g using Amicon Ultra-15 100K MWCO devices (Millipore, Ireland). VWF was then quantified by VWF ELISA and analysed by western blotting.

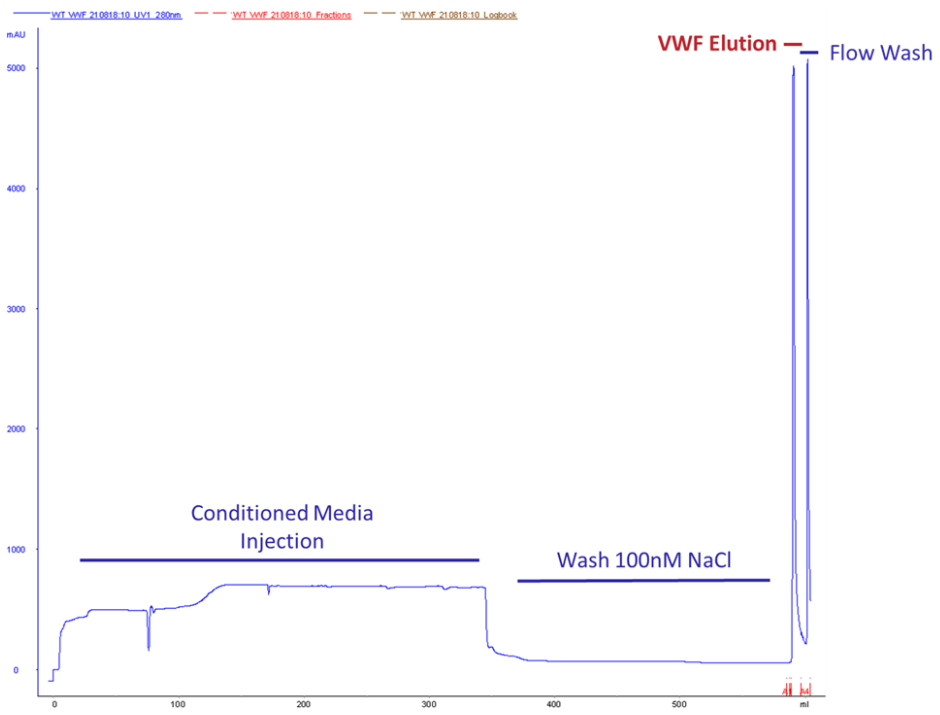

Figure 2.2 Anion exchange chromatography of full length recombinant VWF

2.3.4 Purification of truncated VWF constructs via metal affinity chromatography

Truncated VWF variants (A1A2A3, D'A3 and A3-CK) constructs were expressed with polyhistidine tags to allow for further purification. These variants were concentrated via anion exchange chromatography (as described above in section 2.3.3), and then purified via metal ion affinity chromatography. A 1mL HiTrap Chelating Column (GE Healthcare, UK) was charged with 0.1M NiCl2. The dialyzed anion exchange elute was loaded onto the column at a flow rate of 0.5mL/min in 20mM Tris, 150mM NaCl, 5mM Imidazole, pH 7.4. The column was washed at a flow rate of 1mL/min. Recombinant truncated VWF was eluted from the column with 20mM Tris, 150mM NaCl, 300mM Imidazole, pH 7.4. The ~1mL elute fraction was dialyzed against 20mM Tris, pH 7.4 at 4^{o}C overnight and VWF concentration was then quantified by bicinchoninic acid assay (BCA) as outlined in 2.3.7.

2.3.5 VWF Enzyme Linked Immunosorbent Assay (ELISA)

VWF antigen was quantified using a specific VWF ELISA. Microtiter 96 well plates (Maxisorp, Nunc) were coated with rabbit α-human VWF antibody (Cat: A0082, DAKO, Denmark) in 50nM carbonate buffer (pH 9.6) overnight at 4°C or for 1h at 37°C. After incubating, the plate was blocked with 3% Bovine Serum Albumin (BSA) (Sigma-Aldrich, Ireland) for 1h at 37°C. Following this, the plate was washed in triplicate with 0.1% PBS-T. Reference plasma (Technoclone, Austria) was used to generate a standard curve. All VWF samples were added to plate at a serially diluted gradient and incubated for 2h at 37°C. Following washing in 0.1% phosphate buffered saline with 0.1% Tween (PBS-T), 100µL of anti-VWF-HRP (horse radish peroxidase) (Cat: P0226, DAKO) diluted 1:1000 in PBS-T was added and incubated for 1h at 37°C. HRP activity was detected by adding 100µL of substrate 3,3',5,5'-Tetramethylbenzidine (TMB) (Cat: 34029, Bioscience) and the reaction was terminated with 50µL 1M H_2SO_4. Absorbance values were read at 450nm using VERSAmax microplate reader (Molecular Devices, UK). A standard curve was generated by plotting VWF concentration (µg/mL) on the x-axis against optical density (absorbance @ 450nm) on the y-axis. The curve was linearized by performing a logarithmic transformation where the slope-intercept and r^2 values were derived from the equation of the line using Microsoft Excel.

2.3.6 Protein estimation using BCA

Total cell lysates and VWF protein fragments total protein were measured using Pierce™ BCA protein assay kit (Cat 23117, Thermoscientific). The BCA is a colourimetric assay that can quantify total protein concentration in a solution, based on the reduction Cu^{2+} (Copper Ions) to Cu^{+}. The subsequent reduction of Cu^{2+} Ions is directly proportional to the number of peptide bonds in the solution. Following Cu^{2+} reduction two BCA salt molecules then chelate with the Cu^{+} ion resulting in a colourimetric change from green to purple which strongly absorbs at 562nm.[223]

Duplicates of each protein sample were made up in 50µL aliquots where they were serially diluted down in a 96 well plate leaving 25µL of solution per well. A standard curve with albumin was produced seeding 25µL of sample in duplicate starting at 2000µg/mL and ending at 20µg/mL in a series of 8 dilutions, with a diluent control at the end. Following samples and standard being added a working reagent was made up by thoroughly mixing 50 parts of BCA reagent A with 1 part BCA reagent B (50:1, Reagent A:B) before 200µL of the working reagent was added to each well on the plate. The plate was then incubated for 30 minutes at 37°C as it increases protein detection specificity before being read at 562nm. A standard curve was constructed by plotting the diluent control corrected standard values against the known concentration of albumin added (µg/mL). The protein concentration was then determined using linear regression analysis through GraphPad Prism.

2.3.7 SDS polyacrylamide gel electrophoresis of VWF for protein analysis

Purified VWF was quantified by ELISA before being analysed by western blot. 20µg of VWF was reduced in 1M Dithiothreitol (DTT) (Cat: BP172-25, Fisher scientific) and made up to a final volume of 15µL with PBS and 3µL of 4x NuPage™ loading dye (Cat: NP0008, Invitrogen) to reduce the sample. The mixture was then boiled at 90°C for 10 minutes before centrifuging at 15,000 x g for 10 seconds. A 4-12% BIS TRIS SDS-PAGE pre-cast gel (Cat: NP0321BOX, Thermofisher) was placed into a Novex gel rig system. A 20x MOPS SDS running buffer (Cat: NP0001-02, Thermofisher) solution was made into 1x solution by diluting with deionised water and placed inside the gel rig, checking to make sure there were no leaks. Each well in the pre-cast gel was pipetted up and down to remove the residual buffer within the wells. Samples were then ran on a 4-12% BIS TRIS SDS-PAGE Gel at a final volume of 15 µL per well

in parallel with Page Ruler™ plus pre-stained protein ladder (Cat: 26619, ThermoFisher Scientific) for 1h 30 minutes at 160 volts (V).

2.3.8 Western blotting

Following gel electrophoresis the gel membrane was transferred onto a methanol activated Immobilin-P Polyvinylidene difluoride (PVDF) membrane (Cat IPVH00010, Merck Millipore). To do this firstly, transfer buffer (25mM Tris, 192mM glycine, 0.2% SDS and 20% (v/v) methanol) was made up and four Whatman™ Gel blot filter papers (Cat: 10426890, GE healthcare) per gel were made to size before being immersed in the transfer buffer. The PVDF membrane was activated by immersing in methanol, where it was then washed off in deionised water before finally being added to transfer buffer with the filter paper. The gel and membrane were sandwiched between two filter papers on either side and rolled out to remove air bubbles. The gel was transferred to the activated PVDF membrane using a Thermoscientific Pierce™ Power Blotter™ (ThermoFisher Scientific) for 10 minutes on the high molecular weight setting. After the transfer of proteins to the PVDF membrane it was then blocked with 3% BSA for 1h at room temperature before adding a 1 in 5000 dilution of rabbit anti-human VWF (A0082, DAKO) antibody for 1h at room temperature. The membrane was placed on a rocker and washed with PBS-T (0.1% Tween) for 5 minutes three times. The membrane was added to 3% BSA with a secondary antibody goat anti-rabbit HRP (Cat: HAF008, R&D systems) was added as a 1 in 1000 dilution for 1h at room temperature. The blot was washed for 5 minutes in three intervals with PBS-T whilst on a rocker. When fully washed the membrane was given Pierce™ ECL Western Blotting Substrate (Cat: 32209, ThermoFisher Scientific), made up from a 1:1 dilution of substrate A and B for at least one minute. The membrane was then imaged on the Amersham imager (GE Healthcare), VWF eluate represented in Figure 2.3.

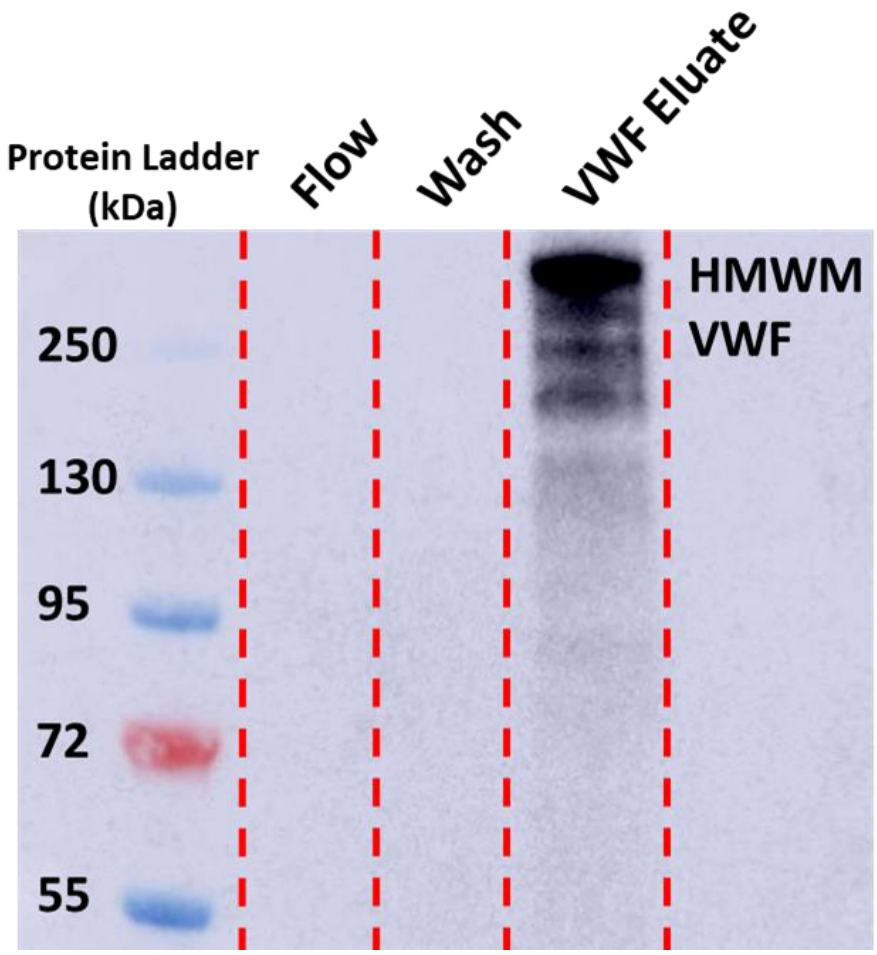

Figure 2.3 Western Blot of recombinant human VWF: Following protein purification the flow through, wash and purified eluate from HEK-293T cells with transient VWF expression were assessed for the presence of VWF through a 4-12% BIS TRIS SDS-PAGE gel. Detection of VWF with a poly-clonal anti-VWF antibody shows VWF at multiple sizes from 95 to >250kDa within the purified eluate sample.

2.3.9 Additional VWF sources

During the course of the study a number of VWF variants were used, depending on concentration and volume needed. Firstly, recombinant VWF was used to characterise tumour cell-VWF interactions. In experiments assessing static VWF adhesion to breast cells recombinant VWF was used to delineate fuctional domains where full-length recombinant VWF was used as a fair comparison between truncated forms. Plasma-derived VWF was primarily used for functional outputs, owing to high purity and sterile nature of this preparation, furthermore perfusion assays were performed with pd-VWF due to their highly multimeric composition. The different VWF variants are outlined in the Table 2.2. All additional VWF variants used were either checked for endotoxin or certified endotoxin free.

Table 2.2 Additional VWF sources

VWF name	Source	Catalogue Number
Sino Biologic VWF	Recombinant expression CHO cells	Cat: 10973-H08C, Sinobiological
Von Vendi / Vonicog alpha	Recombinant expression CHO cells	Cat: 00944-7553-02
HTI VWF	Plasma-Derived	Cat: HCVWF-0191, Haemtech
Haemate-P	Plasma-Derived	Commercial preparation from hospital clinical

2.4 Flow Cytometry

2.4.1 VWF-breast tumour binding assay

MDA-MB-231, MCF-7, MCF-10A and HMEC cells were grown to 80-90% confluence in T75 flasks as outlined in 2.2.1, 2.2.2 and 2.2.3, old media was then removed and cells were washed with PBS. All cells were detached using Accutase™ (A6964-100ML, Sigma Aldrich) to gently lift cells with minimal cleavage of cell surface receptors (Cat: A694-100mL, Sigma). Cells were given their respective complete media and centrifuged at 375 x g for 5 minutes to form a pellet. The cells were then resuspended in an experimental binding buffer composed of Phenol-Free DMEM, 1mM $CaCl_2$ and 10mM 4-(2-hydroxyethyl)-1-piperazineethanesulfonic acid (HEPES) (Cat: H0887-100mL, Sigma). The cell count was measured with a haemocytometer, and adjusted to 7.5 x 10^6cells/mL in 50µL of binding buffer.

VWF variants of interest (recombinant, pd-VWF or truncated variants) were next added to cells ± 1.5µg/mL ristocetin (Cat: 195489, MP Biomedical) to be incubated at 37°C for 30 minutes, unless they were being pre-treated with blocking agents for 15 minutes at 37°C. Following VWF binding, cells were then washed with binding buffer and centrifuged for 5 minutes at 375 x g, with the wash buffer then discarded in one fluid motion. Next, the cells were resuspended in 50µL binding buffer and 1µL of anti-Human FC receptor binding inhibitor (Cat: 14-9161-73, Invitrogen) was added for 10 minutes at room temperature. Without washing, 0.5µL of rabbit anti-human VWF antibody was added to the cell suspension and incubated at 4°C for 30 minutes on ice. Cells were then washed and centrifuged as in previous steps, and resuspended in 50µL binding buffer. Cells were then stained with 0.5µL goat anti-rabbit conjugated Alexa Fluor™ 488 antibody (Cat: A11008, Thermofisher) and 0.5µL red/APC live/dead stain (Cat: L34973, Invitrogen,) for 30 minutes at 4°C in the dark. Alternatively, binding of VWF truncated fragments were detected using Penta-HIS-PE-tagged antibody (Cat: Ab27025, Abcam). Following washing, cells were fixed with 50µL 1% paraformaldehyde (PFA) (Cat: F1635, Sigma) binding buffer mixture for 15 minutes at room temperature. Cells were washed and centrifuged again before finally resuspending the cell suspension in 200µL binding buffer. The cells were then measured using flow cytometer (BD FACSCanto System). Baseline/background fluorescence was established using stained cells which had not been treated with VWF. Dead cells were gated out using their positive APC staining as a marker.

Bound VWF was detected by FITC positive staining (Figure 2.4). Binding was quantified by fold changes in median fluorescence intensity (MFI) from baseline using FlowJo software (FlowJo & BD).

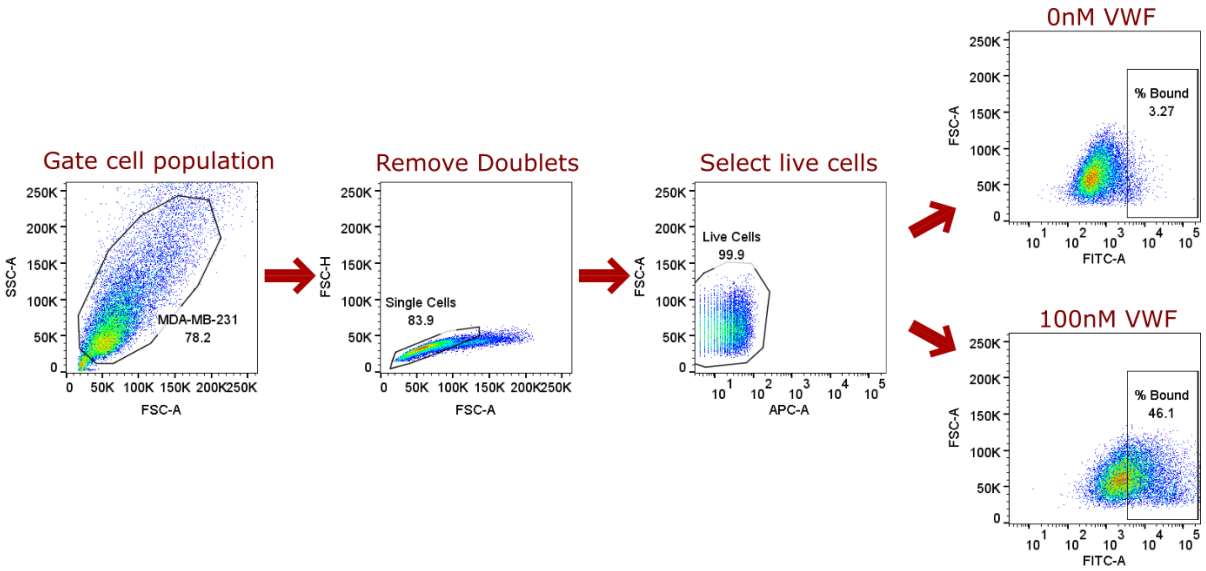

Figure 2.4 Gating strategy for VWF-breast tumour adhesion assay

Table 2. 3 Antibodies used in VWF-breast cancer adhesion assay

Component	Species	Dilution	Catalogue Number
Primary Antibodies			
anti-VWF	rabbit	1/100	A0082, DAKO
anti-pentaHIS	rabbit	1/100	Ab27025, Abcam
Secondary Antibodies			
anti-rabbit IgG (H+L)	Goat	1/100	A11008, Invitrogen

2.4.2 Endothelial adhesion of MDA-MB-231 cells

HUVEC were grown in their complete media and when confluent were uplifted using Accutase™. A 48-well plate was coated in 0.2% gelatin for 30 minutes before being aspirated off. HUVEC were then counted using a haemocytometer and seeded into the pre-coated 48-well plate at $4x10^5$ cells/mL in 200µL of complete HUVEC media. The seeded HUVEC were incubated at 37°C until fully confluent. In the meantime MDA-MB-231 cells were cultured to become confluent at the same time as the HUVEC.

Upon reaching confluence MDA-MB-231 cells were lifted using Accutase™, neutralising the process with complete media. The cell solution was centrifuged with the supernatant removed and replaced with a 5µM CellTracker™ Green CMFDA Dye (Cat: C2925, Invitrogen) solution and incubated at 37°C for 30 minutes. After labelling the live tumour cells with a green fluorescent dye, they were counted with a haemocytometer and seeded into 50µL aliquots of $2x10^6$ cells/mL. Cells were then treated with and without VWF and incubated for 30 minutes at 4°C. Following VWF treatment, cells were washed with PBS and centrifuged for 5 minutes at 375 x g, making sure to discard the supernatant. Cells were treated with Fc-blocker, to inhibit non-specific antibody binding to the cells for 30 minutes, before being washed, centrifuged and supernatant discarded. The MDA-MB-231 cells were then resuspended in 200µL in phenol-free DMEM. MDA-MB-231 cells with and without pre-bound VWF were then added to individual wells of seeded HUVEC for 2, 5, 10 or 20minutes.

Following the appropriate adhesion time, MDA-MB-231 cells not affixed to the endothelial monolayer in each well were delicately aspirated off and washed with PBS. The wells were imaged using a 10x Nikon eclipse TS100 microscope using a 470nm fluorescent filter and

images taken of MDA-MB-231 cells adhered to the HUVEC layer ± VWF treatment. Following imaging of the endothelial monolayer, all cells were delicately detached using Accutase™ to lift the co-culture off and reaction neutralised with complete media. The cell suspension was centrifuged for 5 minutes at 375 x g and supernatant discarded. The HUVEC-MDA-MB-231 co-culture suspension was stained using a specific endothelial cell marker; APC labelled CD-31 (Cat: 303116, Biolegend). The co-culture was washed and centrifuged before discarding the supernatant and resuspended in 200µL phenol-free DMEM for final flow cytometry analysis. The cellular co-culture was analysed via flow cytometry, gating to exclude CD-31 expressing HUVEC, specifically selecting for CD-31 negative, FITC positive MDA-MB-231 cells (Figure 2.5). Therefore quantifying total number of fluorescently tagged MDA-MB-231 cells which had been bound to the endothelial monolayer to correspond with the well images obtained.

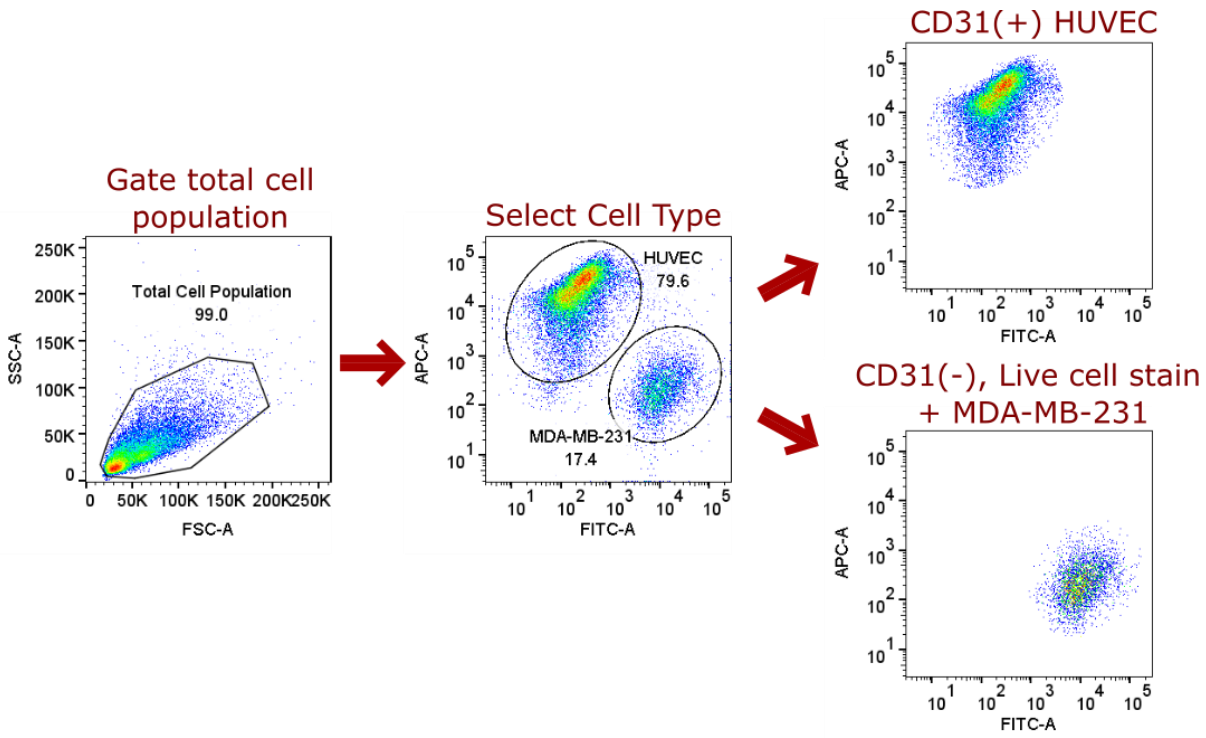

Figure 2.5 Gating strategy for endothelial adhesion of MDA-MB-231 cells

2.4.3 Breast tumour receptor expression

MDA-MB-231 and MCF-7 cells were grown and seeded as described in the VWF binding assay (section 2.4.1). The cell suspension was added to flow cytometry tubes, and cells were treated with 1/50 (1µL) dilution of Fc-Blocker for 10 minutes at room temperature. After 10 minutes of Fc-Blocking, specific antibodies for the candidate receptor of interest were added in

concentrations displayed in Table 2.4 and incubated for 30 minutes at 4°C. Following antibody adhesion the cells were washed with PBS and centrifuged for 5 minutes at 375 x g. The samples were treated with a mixture of 0.5µL live/dead APC stain and 1µL corresponding secondary antibodies outlined in Table 2.4 for 30 minutes at 4°C. Subsequently, cells were washed with PBS and centrifuged for 5 minutes at 375 x g. Finally, cells were fixed with 1% PFA:PBS for 15 minutes at room temperature. Following fixation, cells were washed again with PBS and placed in Phenol free DMEM media to be analysed by flow cytometry. Receptor expression was determined by an increase in MFI compared to an isotype antibody control, after gating away the dead cell population. All analysis was conducted with FlowJo and represented as fold change compared to an isotype stained control.

Table 2.4 Receptor Antibodies for flow cytometry detection

Component	Species	Concentration	Catalogue Number
Primary Antibodies			
anti-CD62P (P-selectin)	Mouse	40µg/mL	304911, Biolegend
anti-CD162 (PSGL-1)	Mouse	5µg/mL	328802, Biolegend
anti-$\alpha_v\beta_3$	Mouse	40µg/mL	MAB1976, Merck Millipore
anti-LRP1	Mouse	40µg/mL	L2420, Sigma-Aldrich
anti-IgG1α	Mouse	matched to sample	MAB002, RnD Systems
anti-GPIbα	Sheep	16µg/mL	AF4067, RnD Systems
anti-IgG1α	Sheep	matched to sample	5-001-A, RnD Systems
Secondary Antibodies			
anti-mouse IgG (H+L)	Goat	10µg/mL	A11001, Invitrogen
anti-sheep IgG (H+L)	Donkey	10µg/mL	A11015, Invitrogen

2.5 Immunocytochemistry

2.5.1 Preparation of cells for microscopy

MDA-MB-231 cells were grown to 80-90% confluence as described in 2.2.1 where the old media was discarded and were then washed with PBS. The cell monolayer was trypsinised for 5 minutes at 37°C. After the cells had detached, complete media was added and the

suspension centrifuged at 375 x g for 5 minutes. The cell pellet was resuspended in complete media and the cell count was measured using a haemocytometer. 250µL of MDA-MB-231 cells were seeded into a 12-well removable ibidi chamber slide (Cat: 81201, Ibidi) at $2x10^5$ cells/mL. The chamber slide was then sealed and the cells were allowed to grow at 37°C until they reached 80-90% confluence in each well.

When the MDA-MB-231 cells in the chamber slide reached the appropriate confluence they were gently washed with pre-warmed PBS. The cells were fixed using 4% PFA:PBS for 20 minutes at room temperature on a rocking platform on a gentle setting. After 20 minutes of fixation the cell layer was washed twice with PBS. Following fixation the cells were blocked with a 3% BSA:PBS solution for 1h at room temperature, gently rocking. The wells were aspirated and washed with PBS, being careful not to displace the attached cells. After washing the cells were treated ± primary antibodies in a 3% BSA solution where they were then left overnight on a rocking platform at 4°C.

2.5.2 Staining and imaging the slide

After incubating the cells with their primary antibody in a 3% BSA blocking mixture overnight the wells were then washed, cells were treated with a 200µL solution of secondary antibody diluted in PBS used at the concentrations specified in the Table 2.5. The cells and secondary antibody mixture were allowed to incubate for 1h at room temperature whilst gently rocking on a platform before being carefully washed with PBS. Following the removal of the silicon insert on the chamber slide, Fluorshield DAPI mountant (Cat: F6057-20mL, Sigma Aldrich) was applied and the slide covered with a coverslip. The mountant was allowed to dry in the dark out of direct sunlight to avoid bleaching of the fluorescent signal. Finally, the slides were imaged using Leica DM4000 microscope, DAPI was measured using a blue filter that excites at the 355-425nm range and the associated secondary antibody was measured with green filter I3 that excites at 450-490nm. The images were overlaid on one another to show expression in relation to nuclear staining.

Table 2.5 Immunocytochemistry antibody concentrations

Component	Species	Concentration	Catalogue Number
Primary Antibodies			
anti-LRP1	Mouse	10µg/mL	L2420, Sigma-Aldrich
anti-IgG1α	Mouse	matched to sample	MAB002, RnD Systems
Secondary Antibodies			
anti-mouse IgG (H+L) Alexa Fluor™ 488	Goat	10µg/mL	A11001, Invitrogen

2.6 Duolink® Proximity Ligation Assay (PLA)

2.6.1 Preparing Slide for Duolink®

MDA-MB-231 cells were grown to around 80-90% confluence as outlined in 2.2.1, cells were then washed with PBS before being lifted with trypsin. The lifted cells were given complete media to catalyse the trypsin and centrifuged, where supernatant was discarded and cells resuspended in new media. Using a haemocytometer cell numbers were counted and 250µL of the resuspended solution was seeded into 12 well removable ibidi chambers (Cat: 81201, Ibidi) at a concentration of $2x10^5$ cells/mL where they were allowed to grow at 37°C until confluent.

When the cells reached confluence in the chamber slide, the cells were washed gently with PBS before adding treatment conditions. Cells were either pre-incubated with receptor associated protein (RAP) (2ug/mL (rH-LRPAP Cat: 296-LR, RnD Systems) for 30 minutes or left in opti-MEM™ at room temperature whilst gently rocking. Subsequently, each well was either treated with or without 100nM recombinant VWF (+ 1.5µg/mL ristocetin and 1mM calcium) for 1h at room temperature on a rocking platform. After 1h each well was gently washed with PBS before being treated with anti-Hu Fc blocker 1/100 dilution for 10 minutes at room temperature. Cells were then fixed with a 4% PFA:PBS solution for 20 minutes at room temperature with gentle rocking. The PFA solution was washed off with PBS before leaving samples in PBS overnight.

2.6.2 Duolink® Protocol

Following fixation of the cells they were then set to be probed by following the protocol from the Duolink® In Situ PLA® Probe Anti-Rabbit PLUS (Cat: DUO92002-30RXN, Merck) and Duolink® In Situ PLA® Probe Anti-Mouse MINUS (Cat: DUO92004-30RXN, Merck) kits, reagent detailed in Table 2.6. Firstly, each well was blocked with 40µL of blocking solution for 1h at 37°C. Cells were then washed with PBS before primary antibodies diluted to their working concentrations in antibody diluent were added to each well α-VWF (1/100 dilution), α-LRP1 Antibody (1/100 dilution) and matched the concentrations of a-rabbit isotype and a-mouse isotype controls. Primary antibodies were incubated for 1h at 4°C on a rocker. The primary antibody was washed with PBS. PLUS and MINUS probes were diluted 1/5 in antibody diluent before being added to each well where they were incubated for 1h at 37°C. Each well was again gently washed with PBS. Using the Duolink® In Situ Detection Reagents Red (Cat: DUO92008-30RXN, Merck) Ligase was added (1/40 dilution) to the supplied ligation buffer where it was then added to each well and left to incubate for 30 minutes at 37 °C. Each well was then gently washed with PBS. Polymerase enzyme (1/80 dilution) was added to the amplification buffer where it was then applied to each well and left to incubate for 100 minutes at 37 °C. The cells were washed gently with PBS three times and excess liquid was tapped off. Finally, removing the silicon chamber divider on the slide, each well was given a drop of Fluorshield DAPI mountant and a coverslip was placed on top and allowed to fix away from the light. Each well was analysed using fluorescent microscope (Leica DM4000) from 40x to oil immersion 100x using the N21 red filter cube at excitation range 515-560nm to detect co-localisation signals as well as a blue filter cube exciting at 355-425nm to detect the nuclei of the cells. Images were processed on ImageJ software (National institute of Health, Bethesda MD, USA), where they were overlaid to give a representation of LRP1 and VWF co-localisation in relation to the nucleus.

Table 2.6 Duolink reagents

Component	Species	Concentration	Catalogue Number
Primary Antibodies			
anti-VWF	rabbit	1/100 dilution	Cat: A0082, DAKO
anti-IgG1α	rabbit	Matched to sample	Cat: X0936, DAKO
anti-LRP1	Mouse	10µg/mL	L2420, Sigma-Aldrich
anti-IgG1α	Mouse	matched to sample	MAB002, RnD Systems
Inhibitor			
RAP	rH	2µg/mL	Cat: 296-LR, RnD Systems

2.7 Perfusion Assay

To replicate the forces experienced under venous blood flow conditions, a perfusion assay system was developed. Using a live imaging microscope (Zeiss Axio Vert) and an automated Nemesys syringe pumping mechanism (Cat: NEM-B001-02C, Cetoni GmbH), breast cancer cells could be pushed from a syringe across an endothelial cell coated µ-Slide VI 0.4 (Cat: 80606, Ibidi) and interactions between breast cells and the endothelial layer could be quantified under venous shear stress. Slides were kept in a heated chamber at 37°C for the duration of the experiment to maintain physiological conditions. The system allows the analysis of binding events under dynamic conditions *in vitro* to mimic physiological environments of the circulation.

2.7.1 Perfusing breast tumour cells over an endothelial layer

Two types of cells had to be cultured prior to the experiment, with both cultured to reach 80-90% confluence on the same day. Firstly, HUVEC were grown as described in 2.2.4 where they were then trypsinised for 5 minutes at 37°C before being neutralised with complete media. HUVEC cells were centrifuged at 375 x g for 5 minutes where they were then counted via haemocytometer. A µ-Slide VI 0.4 was then coated in 0.2% gelatin for 30 minutes. After 30 minutes the excess gelatin was aspirated off and 100µL of HUVEC cell suspension was added at $5x10^5$ cells/mL. The µ-Slide VI 0.4 was incubated at 37°C in a humidified petri dish until cells reached 100% confluency. Secondly, MDA-MB-231 cells were also cultured as described in

section 2.2.2 and seeded to become 80-90% confluent at the same time as the HUVEC coated µ-Slide VI 0.4.

When both cells had reached their respective confluency, MDA-MB-231 cells were washed with PBS before being uplifted with Accutase™ for 5 minutes at 37°C. The cells were given complete media and centrifuged for 5 minutes at 375 x g. MDA-MB-231 cell numbers were calculated with a haemocytometer, and seeded at $5x10^5$ cells/mL in 5mL of HEPES-buffered ringers solution (HBRS: 140nM NaCl, 5mM KCl, 1mM $MgCl_2$, 1mM $CaCl_2$, 5mM glucose and 10mM HEPES) and kept at 37°C. Cells to be treated with inhibitors were centrifuged and resuspended in 500µL HBRS ± their treatment conditions. After inhibitor treatment, cells were washed, centrifuged as before and resuspended in 5mL of HBRS supplemented with 1mM $CaCl_2$. The cells were fluorescently stained at a final concentration of 200nM with 3,3'-Dihexyloxacarbocyanine Iodide (DiOC6) (Cat: 318426-250MG, Sigma-Aldrich), and transferred into a 10mL syringe and affixed to the Nemesys pumping mechanism. Prior to perfusion of tumour cells, the HUVEC layer was stimulated with 100nM Phorbol 12-myristate 13-acetate (PMA) (Cat: P1585-1MG, Sigma-Aldrich) for 10 minutes to activate the endothelial cells. The µ-Slide VI 0.4 and syringe system were connected, avoiding any air bubble formation. Fluorescently stained MDA-MB-231 cells were perfused across the HUVEC layer at a flow rate of 0.2 mL/min resulting in shear stress on the endothelial cell layer of 0.25 dyn/cm^2 and a venous shear rate of 35 1/s calculated as per manufacturers guidelines (Ibidi) using the fluid shear rate formulas below.

$$\tau = 176.1 \cdot \Phi$$

τ = Shear Stress (dyn/cm^2)
ϕ = Flow rate (mL/min)
176.1 = Slide variable
Shear Rate at wall of channel

$$\tau = \eta \cdot 176.1 \cdot \Phi$$

τ = Shear Stress (dyn/cm^2)
η = dynamical viscosity (dyn.s/cm^2)
ϕ = Flow rate (mL/min)
176.1 = Slide variable
Shear Stress Formula

$$\tau = \eta \cdot \gamma$$

$$\gamma = \frac{\tau}{\eta}$$

γ = Shear Rate
τ = Shear Stress (dyn/cm^2)
η = dynamical viscosity (dyn.s/cm^2)
Shear Rate Formula

Subsequently, images of circulating breast tumour cells were captured for 700 frames as they passed over the activated endothelium. The series of images were analysed and quantified using an in-house algorithm.[156] Total adhered tumour cells were measured by surface area coverage for the duration of the run. Additionally, transient adhesion ($K_{[on]}$) and respective detachment rates ($K_{[off]}$) were quantified. These transient events were used to assess differences in stable adhesion events upon the addition of inhibitors. The resulting data was plotted on GraphPad Prism.

2.7.2 Perfusion of breast tumour cells over immobilised VWF

For a specific subset of the experiment, breast tumour cells were perfused directly over immobilised VWF in a purified system. For these experiments, the μ-Slide VI 0.4 was coated with 100nM recombinant VWF or PBS overnight at 37°C. Following the protocol described in 2.7.1 MDA-MB-231 cells were cultured and perfused under fluidic stress over the immobilised VWF layer at the same venous shear rates described above.

2.8 Proteome profiler antibody array set up

MDA-MB-231 cells were cultured as normal, described in section 2.2. Upon reaching 80-90% confluence the cells were trypsinised for 5 minutes at 37°C, before the uplifting process was stopped by using complete media. Cells were centrifuged for 5 minutes at 375 x g and quantified using a haemocytometer. MDA-MB-231 cells were seeded into 12-well plates at a density of $1x10^5$ cells/mL in 1mL complete media and incubated until they reached 70-80% confluence. The MDA-MB-231 cells were then gently washed with PBS before being treated with 750μL of opti-MEM™ media ± pd-VWF treatment. Dependent on the experimental conditions, cells were stimulated for a range of 6-48h at 37°C. Following sufficient incubation, the 12-well plate supernatant was aspirated off and centrifuged at 375 x g for 5 minutes before storing at -20°C for further analysis.

2.8.1 Cytokine array

All reagents used in the human XL cytokine array kit (Cat: ARY022B, R&D Systems) were brought to room temperature before use, while the supernatant samples prepared earlier were left on ice and slowly thawed. The kit was used according to the manufactures instructions as detailed below. In the 4-well multi dish supplied, 2mL of array buffer 6 was put into each well to act as a blocking buffer. Each individual membrane was then put into a well in the 4-well multi dish with identifying number code facing upwards. Upon addition of the membrane to the blocking buffer the blue spots on the membrane faded. The membrane was allowed to block for 1h on a rocking platform at room temperature, making sure the membrane rocked from end-to-end. While the membrane was blocking, 1mL of the prepared sample supernatants were added to 500μL of the blocking buffer solution. After the 1h

incubation, the blocking solution was aspirated off of the 4-well multi dish. Subsequently, the sample supernatant/ blocking buffer mixture was applied to the membrane and left to incubate overnight at 4°C on a rocking platform, shaking the membrane from end-to-end.

Following overnight incubation the membrane was carefully removed from the samples and washed in separate containers in 1x wash buffer 3 times for 10 minutes. Meanwhile, the 4-well multi dish was washed of the sample supernatant/ blocking buffer mixture with deionised water. A mixture of 30µL detection antibody cocktail and 1.5mL of antibody diluent was made up and placed in the 4-well multi dish. Excess wash buffer was dabbed off of the membrane before adding it into the antibody cocktail mixture. The membrane was incubated in the antibody cocktail mixture for 1h on the rocking platform. Following incubation the membrane was again washed 3 times for 10 minutes each and excess wash buffer dabbed off. The membrane was put back into the 4-well multi dish with 2mL of streptavidin-HRP in each well where it was left to incubate for 30 minutes at room temperature on a rocking platform. The membrane was then washed 3 times with wash buffer for 10 minutes each.

Following streptavidin incubation the membrane was ready to be imaged. Placing the membranes in a plastic sheet with the number identifier facing upwards, 1mL of chemi-reagent was added to the membrane. The chemi-reagent was gently smoothed out, making sure no bubbles were present and the entire membrane was covered, where it was incubated for 1 minute. The membrane was then imaged using the Amersham imager and images were taken at 1 minute intervals with each exposure time saved. The data was analysed using ImageJ, the pixel density for each spot was calculated and normalised against the 3 reference spots in the corners of the membrane.

2.8.2 Angiogenesis array

All reagents used in the human angiogenesis array (Cat: ARY007, R&D Systems) were brought to room temperature before use, while the supernatant samples prepared earlier were left on ice and slowly thawed. The kit was used according to the manufacturer's instructions as detailed below. In the 4-well multi dish supplied 2mL of array buffer 7 was put into each well to act as a blocking buffer. Each individual membrane was then put into a well in the 4-well multi dish with identifying number code facing upwards. Upon addition of the membrane to

the blocking buffer the blue spots on the membrane faded. The membrane was allowed to block for 1h on a rocking platform at room temperature, making sure the membrane rocked from end-to-end. While the membrane was blocking 1mL of the prepared sample supernatants were added to 500µL of array buffer 5. The array buffer 5 / sample mixtures were then treated with 15µL of detection antibody cocktail which was then mixed and allowed to incubate for 1h at room temperature. After incubating the membrane for 1h in array buffer 7, the blocking solution was aspirated off of the 4-well multi dish. Subsequently, the sample supernatant detection antibody mixture was applied to the membrane and left to incubate overnight at 4°C on a rocking platform, shaking the membrane from end-to-end.

Following overnight incubation the membrane was carefully removed from the samples and washed in separate containers in 1x wash buffer 3 times for 10 minutes. Meanwhile, the 4-well multi dish was washed of the sample supernatant/ blocking buffer mixture with deionised water. Following the wash step the membrane was put back into the 4-well multi dish with a 2mL dilution of streptavidin-HRP and array buffer 5 in each well where it was left to incubate for 30 minutes at room temperature on a rocking platform. The membrane was then washed 3 times with wash buffer for 10 minutes each and dabbed to dry off excess wash buffer.

Following streptavidin incubation the membrane was ready to be imaged. Placing the membranes in a plastic sheet with the number identifier facing upwards, 1mL of chemi-reagent was added to the membrane. The chemi-reagent was gently smoothed out, making sure no bubbles were present and the entire membrane was covered, where it was incubated for 1 minute. The membrane was then added to the Amersham imager and images were taken at 1 minute intervals with each exposure time saved. The data was analysed using ImageJ, the pixel density for each spot was calculated and normalised against the 3 reference spots in the corners of the membrane.

2.9. Gene expression analysis

Breast tumour cells were grown as described in 2.2.1 and seeded into 6 or 12 well plates in their complete media until they reach confluence of around 80-90%. Upon reaching confluence the cells were gently washed with pre-warmed PBS and opti-MEM™ media

applied ± pd-VWF/inhibitor treatment conditions, for 24h. After 24h stimulation the supernatant was removed and cells were washed with PBS. A solution of cell lysis buffer with β-mercaptoethanol (Cat: M3148-100mL, Sigma-Aldrich) was applied to the cell monolayer and then spread across the cell monolayer until it became viscous. Cell lysates were frozen at -80°C for further analysis.

2.9.1 RNA isolation

RNA isolation was performed by following the protocol from the PureLink™ RNA Mini Kit (Cat: 12183025, Invitrogen). Lysed cells were homogenised using a centrifuge at 12,000 x *g* for 1 minute. Following homogenisation the cell lysate was added to 1.5 times its volume in 70% ethanol. In order to bind RNA to the column 700µL of ethanol-cell lysate solution was added into the collection tube and centrifuged at 12,000 x *g* for 1 minute. After centrifugation, the flow through that passed through the column was discarded. Addition of 700µL volumes of ethanol-cell lysate solution was repeated until there was no more left, discarding the flow through every time. After all the cell lysate was ran through the column it was then treated with 700µL wash buffer and spun down at 12,000 x *g* for 1 minute. The flow-through was discarded and the bottom collection tube replaced. 500µL of a second wash buffer was run through the column and centrifuged at 12,000 x *g* for 1 minute. After discarding the flow through, the previous step was repeated and flow through discarded again. The column was then dried out using another centrifugation step at 12,000 x *g* for 2 minutes. Finally, putting the RNA binding column in a recovery Eppendorf, 30µL of RNAse free water was added to the centre of the binding column and allowed to sit for 1 minute. After 1 minute the column was spun at 12,000 x *g* for 2 minutes and resultant RNA was quantified via nanodrop (ND-1000), and stored at -80°C.

2.9.2 cDNA synthesis

A reverse transcription master mix was made up using a high capacity cDNA synthesis kit (Cat: 4368814, Thermofisher scientific) according to table below Table 2.7, making sure to keep all reagents on ice. When reverse transcription master mix was made, 1000ng of total RNA was made up in 10µL of RNAse free H_2O and added to the master mix. Samples were then placed

in a thermocycler (PTC 200, Bio-Rad) following the cDNA amplification protocol in Table 2.8. Following cDNA synthesis, samples were kept at -20°C until needed.

Table 2.7 cDNA synthesis materials

Component	Volume (µL)	Catalogue Number
10x RT Buffer	2.0	4368814, Thermofisher
10x Random Primers	2.0	4368814, Thermofisher
25x DNTPs	0.8	4368814, Thermofisher
Multiscribe Reverse Transcriptase	1.0	4368814, Thermofisher
Nuclease Free H_2O	3.2	4368814, Thermofisher
RNAse Inhibitor	1.0	EO0382, Thermoscientific
Total Volume	**10µL**	
+ 1000ng RNA in 10µL RNAse free H_2O		

Table 2.8 cDNA synthesis thermocycler protocol

Settings	Stage 1	Stage 2	Stage 3	Stage 4
Temperature	25°C	37°C	85°C	4°C
Time	10 minutes	120 minutes	5 minutes	∞

2.9.3 Quantitative PCR (qPCR)

A master mix of desired forward and reverse primers and GoTaq qPCR master mix (A600A, Promega) was made up on ice at 4.2µL per well as outlined in Table 2.9 with corresponding primers defined in Table 2.10. After gently mixing the components each primer master mix was added to the bottom of their respective wells, making sure to keep the 384 well plate (Cat: 4309849, Thermofisher) on ice. Following the addition of the master mix a 1.8µL solution of cDNA and RNAse Free H_2O was added to the corresponding wells. After adding all the components, the plate was sealed using an adhesive film (Cat: 4311971, Thermofisher). The plate was then put in a centrifuge and spun at 375 x g for 1 minute before being added to the qPCR machine (7900HT, Applied Biosystems). The ΔCt values were measured and normalised

to housekeeping gene *18S* expression and compared to internal control *GAPDH*. All values were then converted to fold change versus unstimulated controls.

Table 2.9 qPCR preparation mix

Component	Volume (µL)	Catalogue Number
GoTaq qPCR Master Mix	3.0	A600A, Promega
Forward Primer	0.6	VC00026N, Merck
Reverse Primer	0.6	VC00026N, Merck
RNAse Free H_2O	1.1	A600A, Promega
cDNA sample	0.7	
Total Volume	**6µL per well**	

Table 2.10 Human qPCR primer list

Primers

Oligo name	FWD Primer Sequence	Reverse Primer Sequence
Housekeeping Gene Primers		
18S	ACCCGTTGAACCCCATTCGTGA	GCCTCACTAAACCATCCAATCGG
GAPDH	GTCTCCTCTGACTTCAACAGCG	ACCACCCTGTTGCTGTAGCCAA
RPLPO	TGGTCATCCAGCAGGTGTTCGA	ACAGACACTGGCAACATTGCGG
Angiogenesis Primers		
Angiopoietin-1	CAACAGTGTCCTTCAGAAGCAGC	CCAGCTTGATATACATCTGCACAG
Angiopoietin-2	ATTCAGCGACGTGAGGATGGCA	GCACATAGCGTTGCTGATTAGTC
EGF	TGCGATGCCAAGCAGTCTGTGA	GCATAGCCCAATCTGAGAACCAC
EGFR	AACACCCTGGTCTGGAAGTACG	TCGTTGGACAGCCTTCAAGACC
Endoglin	CGGTGGTCAATATCCTGTCGAG	AGGAAGTGTGGGCTGAGGTAGA
Endostatin	GGAGAGATTGGCTTTCCTGGAC	CCTCATGCCAAATCCAAGGCTG
FGFR1	GCACATCCAGTGGCTAAAGCAC	AGCACCTCCATCTCTTTGTCGG
IL-8	GAGAGTGATTGAGAGTGGACCAC	CACAACCCTCTGCACCCAGTTT
Ki67	GAAAGAGTGGCAACCTGCCTTC	GCACCAAGTTTTACTACATCTGCC
MMP-1	ATGAAGCAGCCCAGATGTGGAG	TGGTCCACATCTGCTCTTGGCA
PDGFβ	GAGATGCTGAGTGACCACTCGA	GTCATGTTCAGGTCCAACTCGG
THSP-1	GCTGGAAATGTGGTGCTTGTCC	CTCCATTGTGGTTGAAGCAGGC
TIMP-1	GGAGAGTGTCTGCGGATACTTC	GCAGGTAGTGATGTGCAAGAGTC
TYMP	CACAGGAGGCACCTTGGATAAG	CTGCTCACTCTGACCCACGATA
VEGF	TTGCCTTGCTGCTCTACCTCCA	GATGGCAGTAGCTGCGCTGATA
VWF Primers		
ADAM28M	GATGACACACTCATTCCCTG	CACACAGCATGTCCTTTGCA
ADAM28S	CTGTGCATGTGCGAAGGAAA	TTCTGTCCCATCCCACAGTA
VWF	CCTTGAATCCCAGTGACCCTGA	GGTTCCGAGATGTCCTCCACAT

2.10 Angiogenesis Assay

Angiogenesis assays were performed to assess vasculogenic mimicry in breast cancer cells. A reduced growth factor membrane extract (Cat: 3533-005-02, R&D Systems) was allowed to thaw at 4°C overnight. A sterile 20µL rack of tips was chilled in a -20°C freezer overnight. The following morning both the basement membrane extract and chilled tips were put on ice to keep them cool. Immediately after putting the basement membrane on ice it was quickly spun down in a table top centrifuge to remove any bubbles from the viscous solution. Subsequently, 10µL of the basement membrane was added to an angiogenesis µ-slide (Cat: 81506, Ibidi GmbH, Germany). Upon addition of the basement membrane, the angiogenesis µ-slide was tapped firmly down forcing the basement membrane extract into a uniform layer. The angiogenesis µ-slide was then incubated at 37°C for 30 minutes to allow the basement membrane to polymerise.

MDA-MB-231 and MCF-7 cells cultured as described in section 2.2.1, were washed with pre-warmed PBS before being trypsinised for 5 minutes at 37°C. Trypsinisation was stopped by adding complete media to the flask and the cell suspension was centrifuged at 375 x g for 5 minutes. Cell count was calculated with a haemocytometer and cells suspended at a density of $1x10^5$ cells/mL in opti-MEM™ serum free media to a final volume of 120µL. Cell suspensions were stimulated with either VEGF, recombinant VWF or in combination with various inhibitors bevacizumab (Cat: MAB293, Bio-techne), Cetuximab (Cat: HY-P9905 MedChemExpress), RAP (rH-LRPAP Cat: 296-LR, RnD Systems), low molecular weight heparin (LMWH, Tinzaparin) (Innohep, 4500IU, Leo Pharma), concentrations used outlined in Table 2.11. Following the polymerisation of the basement membrane on the angiogenesis µ-slide the cell suspensions were added in duplicate at 50µL per well and left to incubate at 37°C for 6h in a humidified petri dish.

Following 6h incubation, the angiogenesis slides were imaged using a Zeiss Axio Vert microscope. Images of each well were taken in brightfield at 20x magnification. Images were then collected and established angiogenic phenotypic properties including mesh formation, number of nodes and junctions were quantified using the angiogenesis analyser plug-in on ImageJ.[224] The data was compiled and values were normalised to the negative controls and analysed using GraphPad prism.

Table 2.11 Angiogenesis Assay stimulants

Component	Concentration(s)	Catalogue Number
VWF	100-200nM	Cat: 00944-7553-02
VEGF	2µg/mL	100-20, Peprotech
Bevacizumab (α-VEGF)	200nM	MAB293, Bio-techne
Cetuximab (α-EGF)	150nM	HY-P9905, MedChemExpress
RAP	2µg/mL	4296-LR, RnD Systems
LMWH	100IU/mL	Innohep , 4500IU

2.11 Cellular migration assays

2.11.1 Scratch wound assay

To assess tumour cell migration, firstly a live cell imaging system (Cell Discoverer 7, Zeiss) was used to measure scratch wound assay closure over time. An *in vitro* system of 2-well silicon inserts (Cat: 80209, Ibidi), cells could be added into each chamber of the insert and provide a consistent 500µm gap or 'wound' for cells to migrate into upon the removal of the insert. Cellular movement was then imaged at 1h intervals for 72h.

Breast tumour cells or non-tumourigenic control breast cells were grown in their respective media until confluent as per cell culture section 2.2. Upon reaching confluency cells were detached using 1mL of trypsin for 5 minutes at 37°C before the reaction was neutralised with complete media. Cells were centrifuged at 375 x g for 5 minutes and then counted using a haemocytometer. MDA-MB-231, MCF-7 and MCF-10A cells were seeded at a density of $5x10^5$ cells/mL whereas HMEC cells were seeded at $2x10^5$ cells/mL owing to their larger size. Each silicon 2-well insert was individually added to a well in a 48-well plate. A 70 µL of breast tumour cell suspension was added to the two wells of the insert while 250µL of PBS was added to the wells immediately surrounding the inserts to maintain humidity levels. The 48-well plate was then incubated for 24h at 37°C allowing the cells time to settle and reach 80-90% confluence.

After 24h the inserts were gently removed with a forceps and the cell gap was checked under the microscope. The cells were then gently washed with PBS and 200µL of opti-MEM™ media added, to sustain cells but prevent significant proliferation. Varying doses of pd-VWF

treatment were applied at this stage. The 48-well plate was then added to the live cell imaging microscope where images were taken for 72h. Following imaging the resulting series of images were analysed on ImageJ. The total wound closure over time was measured as a percentage of total picture size (pixels) versus total available space (pixels), this was normalised against the total available space in the initial image of the series being set as 100%. These values were then plotted in GraphPad Prism.

2.11.2 Transwell migration assay

MDA-MB-231 and MCF-7 cells were cultured as per section 2.2.1 and MCF-10A cells were grown as per section 2.2.2. When cells had reached a confluence of 80-90% they were gently washed with PBS and treated with opti-MEM™ overnight to serum starve the cells. Following serum starvation the cells were detached using trypsin for 5 minutes at 37°C. The lifted cells were given their respective complete media and centrifuged at 375 x g for 5 minutes. Cell viability was determined via trypan blue staining, and cell count was measured by haemocytometer only continuing with the experiment with a >90% population of viable cells. The cells were suspended at a density of $4x10^5$ cells/mL in opti-MEM™. Using a 24-well plate, 500µL of opti-MEM™ ± treatment conditions (pd-VWF or 10% FCS as a positive control) was added to each well. The corresponding 24-well plate 8µm Boyden chamber inserts (Cat: MCEP24H48, Merck-Millipore) were added into each well making sure to prevent bubbles forming on the underside of the insert. When the inserts were added to each well 250µL of the breast cancer cell suspension was added to each insert directly. All the surrounding unused wells were filled with 500µL of PBS to keep the humidity levels regulated during the assay. The 24-well plate was then carefully put into the incubator at 37°C for 24h.

After 24h each insert was removed from their respective wells. A solution of CellTracker™ Green CMFDA Dye at a final concentration of 5µM was added to each well to incubate for 30 minutes at 37°C. After 30 minutes the 24-well plate was removed and the media in each well was aspirated off. Each well was washed with PBS avoiding lifting any of the attached cells. For final imaging, 200µL of opti-MEM™ media was added to each well. Using the Nikon eclipse TS100 microscope images were taken of each well with a green fluorescent filter at 470nm at 20x magnification. As the green CMFDA dye is only taken up and metabolised by live cells that had migrated it allowed for the selection of viable cells which have actively undergone

migration. Total cell numbers were quantified using ImageJ software and results graphed using GraphPad Prism.

2.11.3 Invasion Assay

An invasion assay was performed to measure the ability of cancer cells to break down a basement membrane matrix produced by Engelbreth Holm-swarm mouse sarcoma tumour, through proteolytic enzyme activity.

MDA-MB-231 cells were cultured as described in section 2.2.1. Upon reaching a confluence of 80-90% the cells were washed with PBS and serum starved overnight with opti-MEM™. 8µm inserts containing extracellular matrix (ECM) (Cat: ECM 554, Merck Millipore) were placed in a separate 24-well plate. Into each 300µL of pre-warmed opti-MEM™ media was added to hydrate the ECM for at least 30 minutes. Subsequently, the serum starved cells were washed with PBS before being trypsinised for 5 minutes at 37°C. The trypsinisation was neutralised with complete media before the cell suspension was centrifuged at 375 x g for 5 minutes. The cell pellet was resuspended and cell number and cell viability determined with trypan blue using a haemocytometer. The experiment was only allowed to continue with a cellular viability >90%. The cell suspension was made to a concentration of $1x10^6$ cells/mL and a mixture of 500µL opti-MEM™ solution ± pd-VWF or 10% FCS treatment was applied to the desired wells in a 24-well plate. After the insert had been hydrated for 30 minutes the media on top of the inserts was aspirated off where they were then placed in the desired wells with a forceps. The prepared cell suspension was then added into each insert in a final volume of 250µL of serum free opti-MEM™ per insert and added to the pre-treated wells. The invasion assay 24-well plate was then incubated at 37°C for 72h.

After 72h the inserts were removed from the 24-well plate and the media inside each insert was aspirated off. The media in the bottom of each well was aspirated and the well gently washed with PBS. Consequently, 225µL of cell dissociation buffer was applied to each well and the respective inserts were added into their wells with the dissociation buffer. The inserts were incubated at 37°C for 30 minutes, agitating the plate slightly during the incubation. After the cell dissociation was completed the inserts were removed and a cell lysis buffer and CyQuant GR dye® mixture (74:1) was made up. The cell lysis dye mixture was pipetted into

each well at a volume of 75µL and allowed to incubate for 15 minutes at room temperature. Following cell lysis the cell lysis mixture was homogenised and 200µL of each solution was added into a 96-well corning™ black plate (Cat: 10022561, Fisher Scientific). Fluorescence was measured as a direct representation of total cellular ECM invasion through the insert and quantified by ascent software on the Fluoroskan Ascent fluorimeter. Cells that had invaded were lysed with the cell lysis buffer and the CyQuant GR dye® exhibits fluorescent signalling when bound to the exposed cellular nucleic acids which are proportional to the number of invaded cells.[225] Finally values were normalised to unstimulated MDA-MB-231 cells and graphed via GraphPad Prism.

2.12 VWF induced breast cancer cell secretome analysis

2.12.1 Supernatant retrieval for ELISA Analysis

MDA-MB-231 cells were cultured as normal, described in section 2.2.1 Upon reaching 80-90% confluence, the cells were trypsinised for 5 minutes at 37°C, before the uplifting process was stopped by using complete media. Cells were centrifuged for 5 minutes at 375 x g where they were quantified by haemocytometer and seeded into 12-well plates at $1x10^5$ cells/mL in 1mL complete media. The cells were then incubated until they reached 70-80% confluence. The MDA-MB-231 cells were then gently washed with PBS before being treated with 750µL of opti-MEM™ solution ± treatment conditions. Dependent on the experimental conditions, cells were stimulated for a range of 6-48h at 37°C. Following sufficient incubation the 12-well plate was taken out and the supernatant was aspirated from the samples. Supernatants were centrifuged at 375 x g for 5 minutes and then aliquoted in 250µL samples and stored-20°C until later use.

2.12.2 MMP-9 ELISA

Matrix metalloproteinase-9 (MMP-9) concentration was determined by measuring the supernatant releasate levels of stimulated MDA-MB-231 cells through an MMP-9 ELISA kit (Cat: DY9115-05, R&D systems). The ELISA kit was used as per the manufacturer's instructions. The provided capture antibody was diluted in PBS to a concentration of 1µg/mL and coated on a microtitre 96-well plate at room temperature at 50µL per well. Following overnight

incubation the plate was washed three times with 0.1% PBS-T. A solution of reagent diluent was made up composed of 3% BSA in PBS where it was then filtered with 0.22µm filter. After making up the reagent diluent, 200µL of the reagent diluent was added to every well and incubated at room temperature for 1h. The plate was then washed 3 times in 0.1% PBS-T. MDA-MB-231 cell supernatants were then prepared in a serially diluted gradient starting from neat and diluting down eight-fold where they were then added in duplicate at 50µL per well. A provided standard was made to a concentration of 2000pg/mL and serially diluted down to 31.2pg/mL, with a negative control added consisting of the sample diluent (opti-MEM^{TM}). The plate was then left to incubate at room temperature for 2h, where they were subsequently washed three times with 0.1% PBS-T. To detect bound MMP-9, 50µL of MMP-9 detection antibody was made up at 150ng/mL for each well and was allowed to incubate for another 2h at room temperature. The detection antibody was then washed off with 0.1% PBS-T 3 times. Subsequently 50µL of streptavidin-HRP solution (1/40 dilution in reagent diluent) was added to each well and incubated for 30 minutes at room temperature, making sure to keep away from direct light. This was then washed three times with PBS-T. Finally, 50µL of TMB substrate was added to each well where it was allowed to incubate for 20 minutes away from direct light. The reaction was then terminated with 25µL of 1M H_2SO_4. Absorbance levels were measured at 450nm and a standard curve was generated from the provided standard values (pg/mL) versus optical density of the standard. The standard curve was made linear by converting the values into a logarithmic scale, where the equation of the line and r^2 values were determined and used to calculate MMP-9 concentrations via Microsoft excel.

2.12.3 VEGF ELISA

Vascular endothelial growth factor (VEGF) concentration was determined by measuring the supernatant releasate levels of stimulated MDA-MB-231 cells through a VEGF ELISA kit (Cat: DY293B-05, R&D systems). The kit was used according to the kit insert and as detailed in section 2.12.2, with antibodies specific to VEGF outlined in Table 2.12.

Table 2.12 ELISA concentration ranges

ELISAs	Working Concentrations			Catalogue number
	Capture (µg/mL)	Detection (ng/mL)	Standard Range (pg/mL)	
MMP-9	1	150	200-31.2	DY9115-05, R&D Systems
VEGF	1	100	2000 – 31.2	DY293-05, R&D Systems

2.13 Assessing the effect of VWF on breast cell viability

2.13.1 Annexin V Cell Apoptosis Assay

Tumour cell apoptosis was assessed using the annexin V apoptosis assay (Cat: 640914, Biolegend) according to the manufacturer's instructions. MDA-MB-231, MCF-7 and MCF-10A cells were cultured as described in section 2.2.1 and 2.2.2. Cells were washed with PBS and then trypsinised for 5 minutes at 37°C. Following cell detachment, complete media was applied and the suspension centrifuged for 5 minutes at 375 x g. Cell numbers were counted with a haemocytometer. Cells were seeded into a 24 well plate at 8 x 10^5 cells/mL and incubated at 37°C overnight.

The cells were then treated ± pd-VWF or positive control actinomycin (Cat: A9415, Merck), to induce cell death, for 6 and 24h before analysis. Following treatment the cell supernatant was collected before the cell monolayer was gently detached using Trypsin:EDTA (0.025%:0.5mM) (Cat: SM-2004-C, Merck-Millipore) and added to the supernatant. This was done to make sure any floating cells were also measured via flow cytometry as a true indication of total live and dead cells. The collected cells were suspended in complete media before being centrifuged at 375 x g for 5 minutes. Following centrifugation cells were resuspended in the 200µL of the provided binding buffer and stained with 5µL of FITC annexin V and 5µL propidium iodide. Cells were incubated for 15 minutes on ice and in the dark. The proportion of apoptotic cells were then measured using flow cytometry (BD FACSCanto System). Cells were divided into quadrant gates based on propidium iodide and annexin V FITC signalling intensity. Healthy cells were negative for both, necrotic cells were defined by being positive for propidium

iodide and negative for annexin V FITC, early apoptotic cells are only positive for annexin V FITC and late apoptotic cells display positive signals for both annexin V FITC and propidium iodide. Data was analysed using FlowJo and graphed using Graphpad Prism.

2.13.2 Cell Cycle Analysis

MDA-MB-231 cells were grown to confluency following the procedure outlined in the cell culture section 2.2.2. Cells were then uplifted using trypsin and the reaction catalysed using complete media. A 2mL suspension of cells at $2x10^5$cells/mL were then seeded into 6 well plates. When the wells reached 80-90% confluence each well was washed with PBS before being treated with their respective conditions, keeping some cells in complete media and preventing cellular proliferation in the rest using serum starved opti-MEM™ solution ± treatment conditions. After 24h the cells were washed and then harvested using trypsin, each well was counted and cells seeded at equal density into Eppendorf tubes. Cells were centrifuged and supernatant removed before cold 70% ethanol was added to the cells in a dropwise manner, while simultaneously vortexing the pellet, to prevent cell clumping. Cells were fixed in ethanol at 4°C for 30 minutes. Samples were washed with PBS and centrifuged at 8050 x g for 5 minutes to consolidate the cells into a pellet. Making sure not to disturb the pellet, the supernatant was removed. The cells were then treated with 50µg/mL RNAse for 30 minutes, before being stained with propidium iodide for 5 minutes and analysed via flow cytometry. Single cell populations were identified and doublets excluded using forward, side scatter and width. The subsequent population was plotted as a histogram using PI against cell count the resulting two peaks denote the G0/G1, S and G2 cell cycle phases and were quantified.

2.13.3 MTS Viability Assay

MTS assays are conducted as a means of measuring cellular viability, cell proliferation and cell cytotoxicity in response to stimulants or drugs. It is a colourimetric assay that measures the reduction of MTS tetrazolium (3-(4,5-dimethylthiazol-2-yl)-5-(3-carboxymethoxyphenyl)-2-(4-sulfophenyl)-2H-tetrazolium) into formazan by the presence of viable mammalian cells. This conversion is mediated by NAD(P)H-dependent dehydrogenase enzymes available in

metabolically active mammalian cells.[226] The formazan product is directly proportional to the number of viable cells in the well which can then be measured colourimetrically at an absorbance of 490nm.

This assay was performed using the Celltiter 96 AQ_{ueous} one solution™ cell proliferation assay (Cat: G3582, Promega). Confluent cells were seeded in duplicate into a 96-well plate at $1x10^5$ cells/mL at a volume of 50µL (5000 cells per well total). The cells were then treated with a 50µL solution of their respective media ± cellular stimulants (Table 2.13) to measure their effect on cellular viability. The cells were then incubated at 37°C for pre-determined lengths of time ranging from 6 to 72h dependent on experimental conditions. Following sufficient incubation, 20µL of the Celltiter 96 AQ_{ueous} one solution™ was added to each well and incubated for 2h at 37°C. Cell viability was measured at 490nm absorbance and the degree of resultant proliferation/ cytotoxicity was calculated by normalising the values against untreated controls, expressed as a percentage change from normal controls.

Table 2.13 MTS assay stimulants

Component	Time Point(s)	Catalogue Number
VWF	24h, 48h, 72h / 6h	Plasma-derived / recombinant
Cetuximab	6h, 24h	HY-P9905, MedChemExpress

2.14 *In vivo* study

2.14.1 Compliance with ethical standards

All experiments were conducted under the guidelines from 2010/63/EU of the protection of animals for scientific purposes. Protocols were reviewed and approved by RCSI Research and Ethics Committee (REC) prior to licensing. Experiments were licensed and approved by the health products regulatory authority under project authorisation code AE19127 / P067.

2.14.2 Mice

Female NOD.CB17-$Prkdc^{scid}$ mice were acquired from Charles River at 6 weeks of age. NOD.CB17-$Prkdc^{scid}$ mice are bred to express homozygous severe combined immune deficiency spontaneous mutation $Prkdc^{scid}$, defined by the absence of functional T and B cells.

Consequently, NOD.CB17-Prkdc^{scid} mice represent an excellent mouse model to accept allogeneic and xenogeneic grafts in tumour implantation experiments.[220] Upon arrival mice were housed in cages in a scantainer; a specially ventilated cabinet that filters the air flow mice are exposed to and thereby preventing exposure of microorganisms to the immunocompromised mice. The mice were housed for two weeks upon arrival allowing them to acclimatise and settle down before any experiments were carried out. All bedding, cages water and food provided for the NOD.CB17-Prkdc^{scid} mice were autoclaved. Any experiments carried out on the NOD.CB17-Prkdc^{scid} mice were performed in a specialised pathogen free environment to minimise the risk to the immunocompromised animals.

2.14.3 Luciferase-tagged breast cancer cell culture for implantation

Luciferase-tagged MDA-MB-231 cells were cultured as described in 2.2.6. Upon reaching 80-90% confluence the cells were processed for the xenograft implantation of tumour cells into mice. The luciferase-labelled MDA-MB-231 cells were washed with PBS and trypsinised for 5 minutes at 37°C. Following trypsinisation the reaction was neutralised with complete media. The cell suspension was then centrifuged at 375 x g for 5 minutes and cell counted via haemocytometer. A working cell suspension of luciferase-tagged MDA-MB-231 at 5x10^5 cells/mL in PBS were used for implanting into the NOD/SCID mice.

2.14.4 Orthotopic implantation of primary tumour in xenograft mouse model

An orthotopic xenograft mouse model was used to assess primary and metastatic growth of breast cancer in mice. This method was used to replicate the metastatic process of human breast cancer metastasis. Female NOD/SCID mice were reared to an age of 8-12 weeks before the xenografting procedure could begin. Upon reaching sufficient age and passing health scoring checks they were anaesthetized with 4% isoflurane and placed on a heating mat to maintain a 37°C body temperature. The hair was removed from the abdomen of the mice prior to implant. The implant area was swabbed with 70% ethanol before injecting with a BD Microfine$^+$ 0.5mL insulin syringe 30G x 8mm (Cat: 230-45094, BD), with a pre-prepared sample of luciferase-labelled MDA-MB-231 cells in 50µL aliquots of 5x10^5 cells/mL into the fourth right inguinal mammary fat pad. Upon injection of the cells the mice were carefully monitored

as they were allowed to recover on a heating mat. In the days following primary tumour injection the mice were routinely screened and scored every other day for signs of adverse effects whilst primary tumour growth was measured ½(length x width)^2 using an electronic callipers. Any mice that scored above the threshold of 6 on the associated project welfare checks were humanely euthanized.

2.14.5 Primary Tumour Resection

The growth in tumour size was regularly measured in the mice post-implantation. The mice were deemed ready for tumour resection when their tumour volume reached >400mm^3 in size, which typically takes 4-6 weeks post-injection. Tumour volume was measured with a callipers using the formula ½(Length x width)^2. Tumour resection is performed as it allows for further study of the metastatic process longitudinally. Resection can extend the life-span of tumour-bearing mice by reducing complications associated with a large primary tumour including ulcerations, infections and organ invasion. When the mice reached sufficient tumour burden they were first given analgesia of 0.1mg/kg buprenorphine for 30 minutes prior to the resection procedure following that they were anaesthetized with 4% isoflurane and their body temperature maintained using a heat mat at 37°C. When the mice were anaesthetized the instruments were sterilised using a bead steriliser. The hair free tumour site was cleaned with a 70% ethanol swab and betadine solution. In a two person procedure, an incision was made in the skin at the base of the tumour with the tumour carefully excised from surrounding tissue. In cases where the primary tumour had locally invaded into surrounding tissue (peritoneal invasion) the tumour was delicately detached and peritoneal wall switches with dissolvable sutures. Following tumour removal the initial incision was sterilely closed using dissolvable 4-0 Vicryl sutures with a cutting needle. After tissue resection the mice were monitored on heating mats until they recovered, any immediate adverse effects were noted and acted upon. Subsequently, 8h post-surgery analgesia regime using 0.1 mg/kg buprenorphine was administered to the mice. A daily scoring system was performed to check for poor response to tissue resection, with wound re-openings resulting in mice being re-anaesthetized and corrected.

2.14.6 Examining the anti-metastatic effects of VWF

Three days after tumour resection, the xenografted mice were commenced on treatment with an anti-VWF antibody or an anti-IgG control (20µg/mL) (Cat: X0936, DAKO), where they were dosed twice weekly via tail vein injection for a maximum of 10 weeks or until metastatic invasion to the lungs was detected. Rates of metastasis were assessed by weekly non-invasive imaging (IVIS spectrum, Perkin Elmer). The bioluminescent imaging was used to detect luciferase tagged MD-MB-231 cells within the mice. Prior to imaging the mice were injected subcutaneously with 150mg/kg luciferin (Cat: 122799, Perkin Elmer) and anaesthetized with 4% isoflurane in an induction chamber. The anaesthetized mice were gently positioned on their backs and connected to a continuous flow of 2% isoflurane within the IVIS spectrum machine using individual nose cones. Bioluminescence images were then acquired of the mice, displaying where the luciferin tagged MDA-MB-231 cells were within the mice. Following imaging the mice were placed on a heating mat and allowed to recover. The bioluminescence imaging was repeated once a week until the mice started to show strong fluorescent signals in secondary sites including the lungs.

2.14.7 Termination of the experiment and organ harvest

Mice reaching the end point of the experiment either through scoring checks or the natural end point (significant lung metastasis) underwent humane euthanasia. Mice were given an intra-peritoneal injection of anaesthetic ketamine/ medetomidine mix 75mg/kg / 1mg/kg. The mouse was then closely observed until the level of anaesthesia was sufficient resulting in a loss of its righting reflex and no response to the pinch test (5 minutes after anaesthesia). At this time blood was collected by cardiac puncture within a sodium citrate collection tube. Following blood collection the organs were harvested for further analysis and cervical dislocation performed on the animal. Organs were treated with a luciferin solution before being scanned through scanned for bioluminescent signalling following harvest to assess tumour burden within each organ.

2.15 Statistical Analysis

Experimental data was analysed with GraphPad Prism version 9.0 (GraphPad Software, San Diego, USA). For clinical data the results were checked for normality. Upon determining distribution normality the data was expressed as median values ± interquartile range for non-parametric or mean ± SEM/ or SD. Single variant data with normal distributions were analyzed with Student's unpaired two-tailed *t*-test. Non-normally distributed quantitative data were compared using the Mann-Whitney U test. Where appropriate the Spearman correlation coefficient followed by a linear regression was used to determine that correlations between clinical parameters were significantly non-zero. All non-clinical data were assessed for normality using the Shapiro-Wilks test for Gaussian distribution. One way analysis of variance (ANOVA) was performed where multiple data points were measured against a single variable. ANOVAs were conducted using either Dunnetts multiple comparison test where all values were compared to a singular control or Tukeys multiple comparison test where each value was compared against one another. Our time to metastasis data was analysed through survival curve analysis log-rank Mantel-Cox test. In all tests used and values were considered significant with *p*-values <0.05.

Chapter 3: Investigating VWF levels in patients with breast cancer and direct interactions between VWF and breast cancer.

3.0 Introduction

3.0.1 VWF as a biomarker of interest in cancer; thrombosis and survival

The link between cancer and coagulation is well established, it was proposed as early as 1865 by Armand Trousseau who noted migratory thrombophlebitis could be used as a diagnostic tool for cancer.[227,228] In fact, VTE is the second most common cause of death in cancer patients.[98] Correspondingly, active cancer accounts for up to 20% of the overall incidence in VTE.[229] Perhaps this is not surprising as dysregulation in the haemostasis system, both primary and secondary, is now recognised as an important factor for malignant progression.[230]

In breast cancer, platelets have long been associated with cancer progression. Platelets have been shown to coat tumour cells and promote invasion and metastasis, but further to this they enable tumour cell adhesion to the endothelium and promote angiogenesis.[230,231] In addition to platelets, specific coagulation factors have reported roles in breast tumour development. For example, tissue factor in breast cancer is expressed directly by tumour cells and also the tumour stroma which can contribute to breast cancer progression through enhanced proliferation and invasion.[232] Separately, thrombin has been shown to induce tumour growth, migration and invasion in an epidermal growth factor receptor (EGFR) dependent mechanism in inflammatory breast cancer.[233] In two similar independent studies it was observed that patients with early and recurrent breast cancer had enhanced levels of several coagulation activation markers including, prothrombin fragment F1+2, TAT and D-dimer.[234,235] Using multivariate analysis Giaccherini *et al*. identified prothrombin fragment F1 + 2 as an independent risk factor for disease recurrence during follow-up of breast cancer patients who had undergone surgical resection.[235] Incidentally, Mandoj *et* al. observed that D-dimer and FVIII levels in early breast cancer patients had prognostic potential in both univariate and multivariate models for overall survival.[234] More recently, increased thrombin generation potential has been reported in specific breast cancer cohorts which was associated with a high risk of cancer recurrence.[236] These data suggest that specific coagulation factors as well as markers of coagulation activation are markedly elevated in patients with breast cancer and accumulating evidence indicates that this not only contributes to potential risk of thrombosis in this cohort but also tumour progression.

Examination of plasma levels of several procoagulant factors, including fibrinogen, VWF, prothrombin, FVII, FVIII, FIX, FX and FXI, in a large cohort of VTE patients revealed that the

FVIII and VWF levels were the strongest predictors for rates of venous thrombosis.[97] In fact, both FVIII and VWF plasma levels were associated with the highest VTE risk.[96,97] In a longitudinal population study of 19,237 healthy individuals examined for incidence of VTE, elevated plasma VWF:Ag and FVIII were described as common, independent and dose-dependent risk factors for VTE.[237] Importantly, similar observations have been reported in cohorts of patients with CAT. Specifically, VWF:Ag levels were predictive of VTE in a number of cancers, even after adjustment for patient related factors.[203]

Perhaps even more interesting was the observation that elevated VWF plasma levels were also associated with poorer overall survival.[203] In this study of 795 cancer patients with heterogeneous solid tumour malignancies in an Austrian registry, the probability of survival after 2 year of study enrolment in patients with VWF above the 75th percentile was 35.0% compared to 67.7% survival in patients with VWF plasma levels below the 25th percentile. Correspondingly, reduced plasma ADAMTS13 activity, a known regulator of plasma VWF activity, was also associated with significantly poorer survival. Moreover, using multivariable Cox regression analysis to adjust for confounding factors, including age, sex and cancer type, both VWF and ADAMTS13 levels remained statistically significant for VTE as well as survival probability in cancer patients, suggesting these factors may serve as independent prognostic biomarkers for both risk of CAT and clinical outcome.

Elevated VWF:Ag has been described in a number of specific cancer cohort studies, outlined in Table 1.1. Several of these studies have also reported potential prognostic significance of VWF levels with disease progression and overall survival. VWF:Ag and ADAMTS13 activity were reported as biomarkers in the early diagnosis of hepatocellular carcinoma in cirrhotic patients.[107] Additionally, VWF:Ag correlates with poorer overall survival in colorectal cancer, ovarian cancer, glioblastomas, and oesophageal and lung cancer.[102–105] However, VWF is an acute phase protein that is released upon endothelial insult or damage as seen in models of inflammation, sepsis, and cerebral malaria.[135,136,171,212] Nevertheless, accumulating evidence suggests that VWF may have extra-haemostatic roles in angiogenesis, immune cell recruitment, inflammation and direct interaction with tumour cells.[3] The mechanism underpinning increases in VWF:Ag levels in cancer settings are unknown but endothelial cell activation has been proposed.

Several studies have reported that tumour cell supernatants induce VWF release from endothelial cells *in vitro*.[148–155,157] Results from Nossent *et al*, examining VWF propeptide levels, concluded that high VWF:Ag levels linked with thrombosis were primarily mediated by endothelial VWF release.[96] Furthermore, VWF release triggered by Lewis lung carcinoma cells (LLC) resulted in a 6-fold increase in *VWF* gene expression, highlighting the tumour cells may not only induce the release of stored VWF from WPB in endothelial cells but also promote enhanced gene expression.[238] It is interesting to note that VWF:Ag levels also increase with disease progression in cancer cohorts and presence of metastasis (Table 1.1). Taken together, these data indicate that elevated VWF:Ag levels in cancer patients may not be merely an innocent bystander of prognostic relevance but instead may contribute to cancer progression directly.

3.0.2 VWF-tumour cell interactions

VWF has been reported to directly adhere to a variety of cancer cells both statically in the absence of shear stress, and in cases of cellular perfusion where VWF can arrest circulating tumour cells.[186,187,190,239,240] Interestingly, work from Bauer *et al* highlighted the significant accumulation of intraluminal VWF within the tumour vasculature of malignant melanoma from both patients and murine models.[148] Tumour-induced release of these adhesive VWF multimer strings contributed directly to platelet-rich thrombi deposition within the vasculature. Moreover, extensive platelet-thrombi and clot formation was observed in an *in vivo* transgenic murine model of melanoma which appeared to promote the arrest of melanoma tumour cells within the brain microvasculature and subsequently aided metastasis. Most crucially this effect was reduced by inhibiting VWF with a targeted antibody.[241]

Several other tumour cell types have also been reported to induce endothelial cell activation and thus mediate VWF multimer release. For example, Goerge *et al*, showed HT-29 colon carcinoma cells could induce rapid acute activation of both macro- and microvascular endothelial cells resulting in VWF release in static and shear flow conditions.[157] In contrast, the binding of VWF to human breast cancer cell line MCF-7 has been reported to be mediated by tumour expression of a GPIbα-related protein.[187] This interaction has been proposed to constitute a key initial event in breast tumour cell-induced platelet adhesion and aggregation. This may be important in the context of tumour metastasis since, previous studies have

shown that tumour cells form heteroaggregates with platelets in the circulation which contribute to blood-borne dissemination of circulating tumour cells.[242]

Collectively, emerging evidence suggests that VWF-tumour interactions may serve as an important bridging step in facilitating circulating tumour cell sequestration and binding to the endothelial vessel wall, a key step in the metastatic cascade. This is further evident in specific tumour cell populations which directly acquire *de novo* VWF expression.[118,137–144] Specifically, VWF expression in osteosarcoma and glioma tumour cells was also associated with significantly increased platelet adhesion, transmigration and extravasation. In keeping with this, siRNA knock down of tumour expressed VWF in malignant glioma cell line U251 and osteosarcoma lines SAOS2 and KHOS cells significantly reduced tumour adhesion to endothelial cells and platelets both statically and under shear conditions. Moreover, VWF knockdown in these cells attenuated transendothelial migration of SAOS2 and U251.[243] These data suggest that tumour cells may interact with VWF, perhaps via binding within the circulation or direct expression, and that this may contribute to not only tumour-platelet interactions but also tumour-endothelial cell binding. This may not only contribute to enhanced risk of thrombosis for cancer patients but critically, both of these features are key for tumour cell dissemination *in vivo* and thus may directly promote metastasis. Consequently, the aim of this study was to firstly assess VWF expression and plasma levels in patients with breast cancer and examine the potential role of VWF as a novel clinical biomarker. Secondly, we sought to investigate VWF-breast tumour cell interactions and whether this may contribute to breast tumour dissemination including adhesion to the endothelial vessel wall.

3.1 VWF levels in breast cancer

3.1.1 Relapse free survival analysis of breast cancer patients with high VWF mRNA expression

Using the KM plotter *in silico* software tool, the effect of VWF mRNA expression on patient survival risk in subgroups of patient with breast cancer was assessed.[206] This online tool compiles transcriptomic datasets with follow up clinical outcome from the GEO repository. In this way we could determine if VWF expression may represent a prognostic target associated with breast cancer disease progression and clinical outcome. To firstly determine the differential expression of VWF at a transcriptional level in breast cancer patients of all molecular subtypes, the KM plotter online tool grouped patients into tumour grade and assessed for relapse free survival set to a 10 year limit. Relapse free survival was performed using Cox proportional hazards regression. VWF gene expression was dichotomized to levels above the median (high expression) or below the median (low expression) before Kaplan-Meier plots were generated.[206]

Interestingly, in grade 1 and 2 breast cancers there was a non-significant difference in survival between high and low VWF mRNA expression in cancerous breast tissue (Figure 3.1 A-B). In contrast however, patients with grade 3 breast cancer were found to have a decreased survival when VWF was highly expressed within the tumour tissue. Although, this did not reach statistical significance ($p = 0.061$), the data appeared to be trending toward significance and had a reported hazards ratios (HR) of 1.2 (95% confidence intervals (CI) 0.99-1.45) (Figure 3.1 C). Together these data suggest that as the grades of the breast tumour advances, high VWF mRNA expression may correlate with poorer prognosis for breast cancer patients.

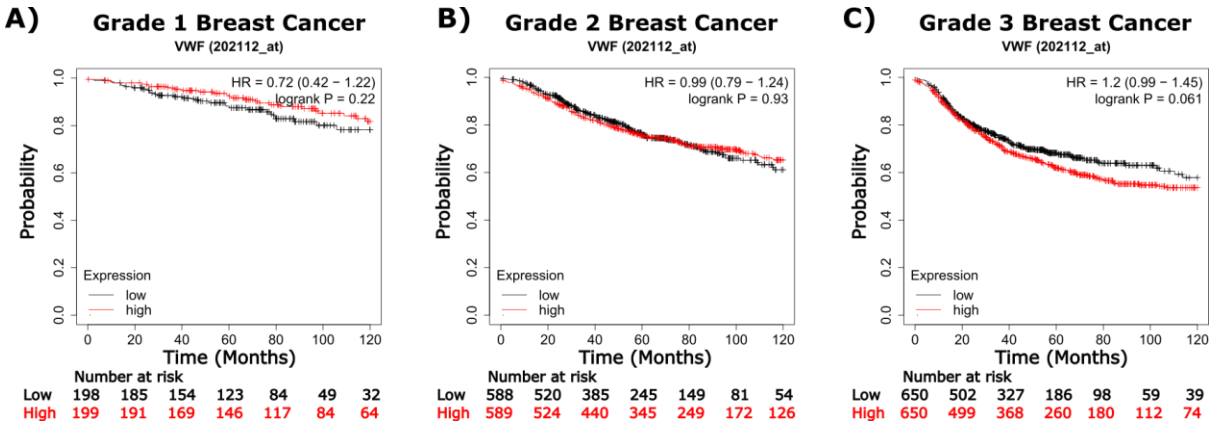

Figure 3.1 Analysis of disease free survival in patients with high VWF mRNA expression in breast cancer: Kaplan-Meier survival curve for relapse free survival in breast cancer patients generated from high VWF expression versus low VWF expression on KM plotter. Analysis was stratified by grouping breast tumours with increasing tumour grade; **A)** grade 1 (p = 0.22 HR = 0.72) **B)** grade 2, (p = 0.93, HR = 0.99) **C)** grade 3 (p = 0.061, HR = 1.2). Relapse free survival was plotted as a probability of survival on the y-axis against time in months on the x-axis. Populations were assessed for significance using cox proportional hazards regression.

3.1.2 Survival analysis of breast cancer patients with high VWF protein expression

Next, VWF protein expression was analysed by the KM plotter *in silico* software.[207] VWF expression data was available from 65 breast tumours of all subtypes. The tissue samples had been evaluated for proteomic expression using a liquid chromatography/ mass spectrometry based proteome analysis.[208] VWF expression levels were divided into high and low expression to measure survival length.[207] KM plots were generated for overall survival and the two values compared by cox proportional hazards regression, measuring HRs, 95% CI and log-rank p-values. The thresholds were compared between upper and lower quartile and a false discovery rate (FDR) computed. Significance was accepted where $p \leq 0.05$ and FDR ≤ 0.2.

High VWF expression, at a protein level, was associated with a significantly with poorer overall survival in patients with breast cancer. This trend was observed in a heterogeneous cohort of subtypes of breast cancer at various stages (Figure 3.2 A). This trend was also observed when patients were sub-selected for advanced, grade 3 tumour stratification (Figure 3.2 B). The high VWF expression group had an upper quartile for survival of 23 months vs 97 months for patient samples associated with low VWF expression. Despite the total number of patients with grade 3 cancer being small, high VWF expression in this group was associated with a HR of 7.52 versus a HR of 3.34 for all breast cancer stages, ($p < 0.05$, FDR ≤ 0.2, Figure 3.2 B). Expectedly, deaths in the grade 3 sub-population were front loaded, with over 50% of deaths occurring within the first 4 years, likely reflecting the aggressive and advanced nature of the disease. Altogether, the data analysis points to a role for VWF as a potential biomarker in breast cancer disease progression, specifically in late stages of tumour advancement.

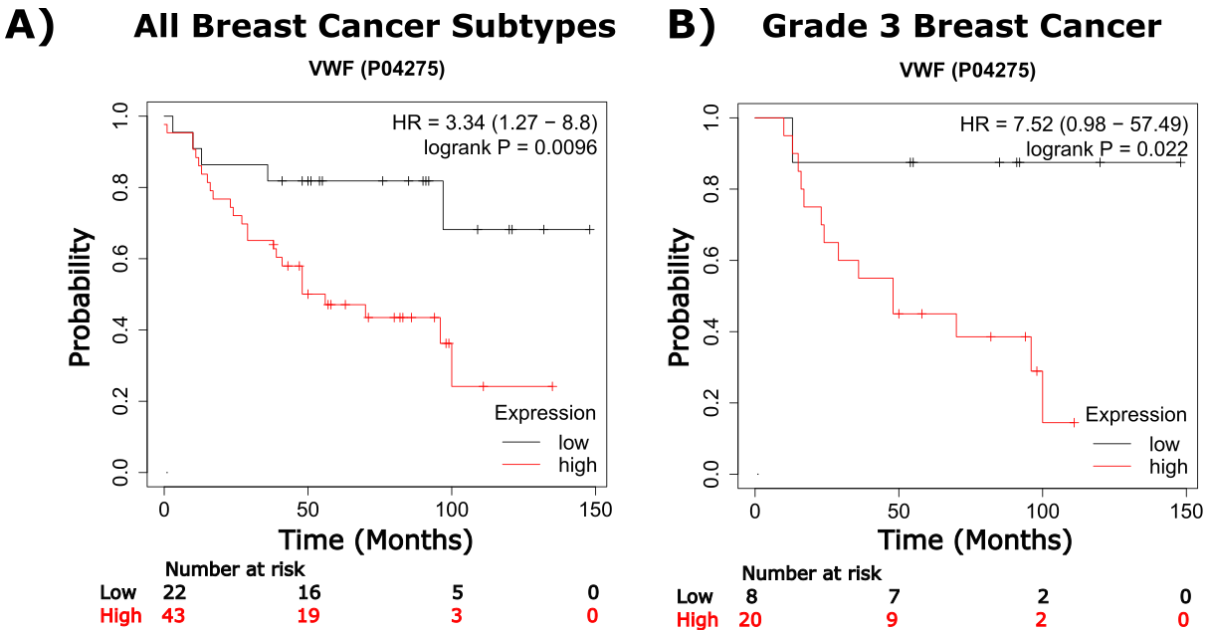

Figure 3.2 Poorer overall survival in breast cancer patients with high VWF protein expression: Kaplan-Meier survival curves for overall survival in patient proteomic profiles expressing high or low VWF protein levels were generated through the KM plotter online tool. The effect of VWF protein expression on overall survival for breast cancer patients was analysed in **A)** all breast cancers of heterogeneous subtype and grade N=65 (p = 0.0096, FDR = 0.2) and **B)** grade 3 breast cancer tissues N=28 (p = 0.022, FDR = 0.2). Samples were assessed for significance using Cox proportional hazards regression, and the FDR was calculated to account for false detection.

3.1.3 Elevated plasma VWF:Ag levels in early and metastatic breast cancer cohorts

After identifying that VWF may be differentially expressed in patients with breast cancer and associate with survival, we sought to quantify systemic plasma VWF:Ag levels in established prospective cohorts of patients with either early (CHAMPion) or advanced breast cancer (TuFClot), clinical parameters of the cohorts outlined in table 3.1.[1,2]

The CHAMPion study represents patients with early breast cancer with all patients only recruited if they were treatment naïve without a previous history of cancer. The median age of the patients recruited in the CHAMPion study was 60 years (range; 32-79) for ductal carcinoma in situ (DCIS) and 59 years (range; 24-84) for invasive cancer. The TuFClot study specifically recruited breast cancer patients with evidence of new metastatic disease or radiological advancement. The median age of the patient cohort was 59 years (range; 36-82 years). All patients within the TuFClot study had evidence of metastasis to liver, bone, lungs or brain. Moreover, 77.5% of the cohort had breast cancer metastasis at multiple sites.

Plasma VWF:Ag levels were measured in both breast cancer cohorts as well a gender- and aged-matched healthy control group using a specific ELISA.[156] Our data shows that patients with early breast cancer had elevated VWF:Ag levels compared to a healthy control population (median 130 IU/dL interquartile range (IQR) 99.6 - 279.8) vs 89.1 IU/dL (IQR 65.2 - 117) $p<0.01$, Figure 3.3). Moreover, VWF:Ag levels were more markedly increased in patients with metastatic breast cancer, compared to healthy controls (217.3 IU/dL (IQR 162.4 - 289.4) vs 89.1 IU/dL $p<0.0001$, Figure 3.3). Of note, the metastatic disease patient group also displayed a significant increase in VWF:Ag compared to early breast cancer patients (Figure 3.3).

Table 3.1 Clinical characteristics of patients recruited to CHAMPion and TuFClot studies

Characteristics	CHAMPion Values (n=130)	TuFClot Values (n=44)
Demographics		
Median Age, years (range)	61 (35-84)	60 (36-82)
Haematological Parameters – Median (IQR)		
VWF (IU/dL)	130 (99.6 - 279.8)	217.3 (162.4 - 289.4)
TAT (ng/mL)	3.49 (2.2925 - 6.255)	5.85 (4.275 - 9.225)
Fibrinogen (g/L)	3.3 (2.8 - 3.9)	3.35 (3 - 4.39)
D-Dimer (ng/mL)	452.5 (291.75 - 621.75)	885 (465.5 – 1368)
Receptor Status		
ER^+, PR^+, $HER2^+$ – *n* (%)	7 (5.38%)	2 (4.55%)
ER^+, PR^+, $HER2^-$ – *n* (%)	77 (59.23%)	16 (36.36%)
ER^+, PR^-, $HER2^+$ – *n* (%)	2 (1.53%)	3 (6.82%)
ER^+, PR^-, $HER2^-$ – *n* (%)	16 (12.3%)	7 (15.91%)
ER^-, PR^+, $HER2^+$ – *n* (%)	0 (0%)	0 (0%)
ER^-, PR^+, $HER2^-$ – *n* (%)	0 (0%)	0 (0%)
ER^-, PR^-, $HER2^+$ – *n* (%)	10 (7.69%)	8 (18.18%)
ER^-, PR^-, $HER2^-$ (Triple Negative) – *n* (%)	18 (13.84%)	8 (18.18%)
Metastatic Status		
No Metastasis – n (%)	14 (10.77%)	3 (6.82%)
≤1 Metastatic site – n (%)	103 (79.23%)	15 (34.09%)
≥2 Metastatic sites – n (%)	13 (10%)	26 (59.09%)
Metastatic sites		
Lung – n (%)		24 (54.55%)
Liver – n (%)		22 (50%)
Bone – n (%)		26 (59.09%)
Brain – n (%)		4 (9.09%)
Post Recruitment Treatment		
Adjuvant Radiation Therapy – n (%)	88 (67.69%)	
Adjuvant Hormone Therapy – n (%)	90 (69.23%)	
Adjuvant Chemotherapy – n (%)	41 (31.54%)	

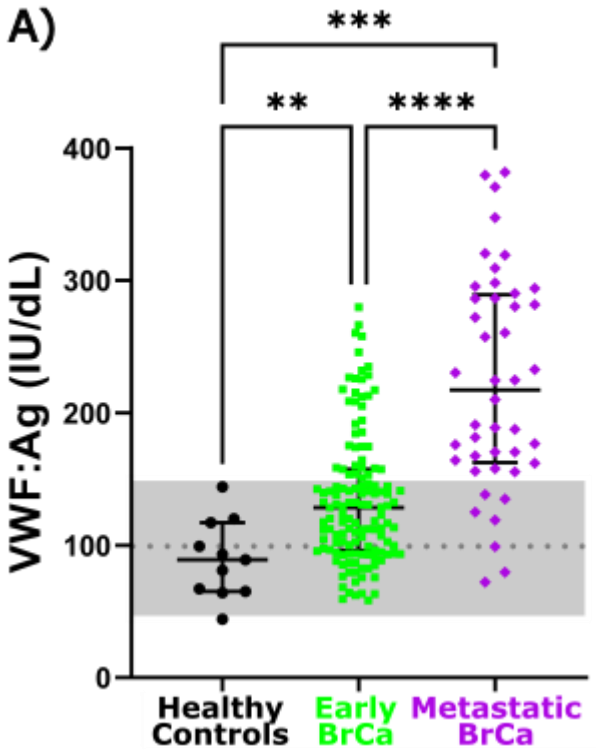

Figure 3.3 Plasma VWF:Ag levels are elevated in patients with early and metastatic breast cancer: VWF levels were quantified in patient samples from the CHAMPion (N=130) and TuFClot (N=44) cohorts using VWF:Ag ELISA, values and compared to age and gender matched healthy control group (N=11). The reference range displayed in the grey region with the dotted line representing the median VWF:Ag levels of a healthy population. Data was graphed as a median with interquartile range, significance was calculated through one way ANOVA using Tukeys multiple comparison test and with significance levels denoted as ** $p \leq 0.001$ and **** $p \leq 0.0001$.

3.2 VWF:Ag correlates with plasma markers of coagulation activation

3.2.1 Thrombin Antithrombin III (TAT) complexes correlation with VWF:Ag levels

Previous studies have reported dysregulation in haemostatic pathways as an early feature in breast cancer patients.[244] Procoagulant markers including TAT complex have been measured in both the CHAMPion and TuFClot cohorts and are significantly elevated.[1,2] TAT complex plasma concentration is a commonly used marker of coagulation activation and a surrogate marker for activated thrombin.[1] Given the elevated VWF:Ag levels observed in our breast cancer cohorts, we sought to assess whether these levels may correlate with other established markers of coagulation activation. Spearman's non-parametric analysis of both the CHAMPion and TuFClot cohorts found that plasma TAT complexes did not correlate with plasma VWF:Ag levels. Both the CHAMPion cohort (r_s=0.042, r^2=0.006, p=0.385) (Figure 3.4 A) and TuFClot cohort (r=0.11, r^2=0.067, p = 0.102) (Figure 3.4 B) displayed very weak associations that did not reach significance.

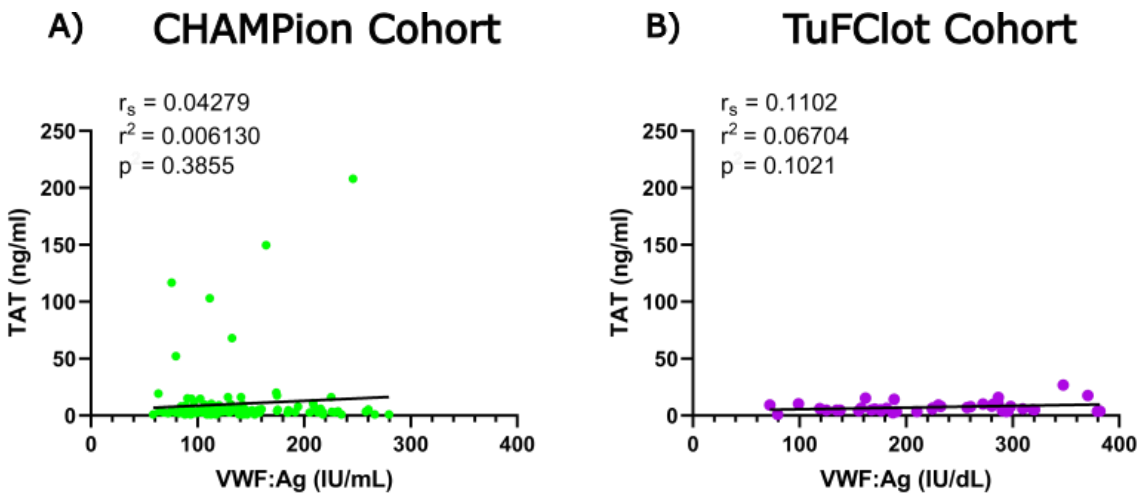

Figure 3.4 Plasma VWF:Ag and thrombin antithrombin III levels do not correlate in breast cancer patients: Measured plasma VWF:Ag levels were correlated against TAT levels from the **A)** CHAMPion (N=125) and **B)** TuFClot cohorts (N=41). Analysis was carried out using Spearman rank correlation for non-parametric data. The Spearman correlation coefficient (r_s) denoted strength of correlation. A linear regression analysis was also conducted, deriving a value for slope of the line (r^2), a significant relationship between parameters was assessed with * $p \leq 0.05$ considered significant.

3.2.2 Plasma fibrinogen correlation with VWF:Ag levels

Plasma fibrinogen levels were also assessed for correlation with VWF:Ag levels. Fibrinogen which is converted to fibrin by thrombin, not only plays and key role in thrombosis formation but more recently has been shown to be elevated in patients with cancer and contributes directly to disease progression and metastasis.[245–247]

Using Spearman's correlation for non-parametric distribution and a linear regression analysis, plasma fibrinogen and VWF:Ag levels showed a positive weak to moderate correlation in both cohorts and a significant non-zero slope of the line; the CHAMPion cohort (r_s=0.375, r^2=0.149 $p \leq 0.0001$, Figure 3.5 A) and TuFClot (r_s =0.359, r^2 = 0.136 $p \leq 0.05$, Figure 3.5B).

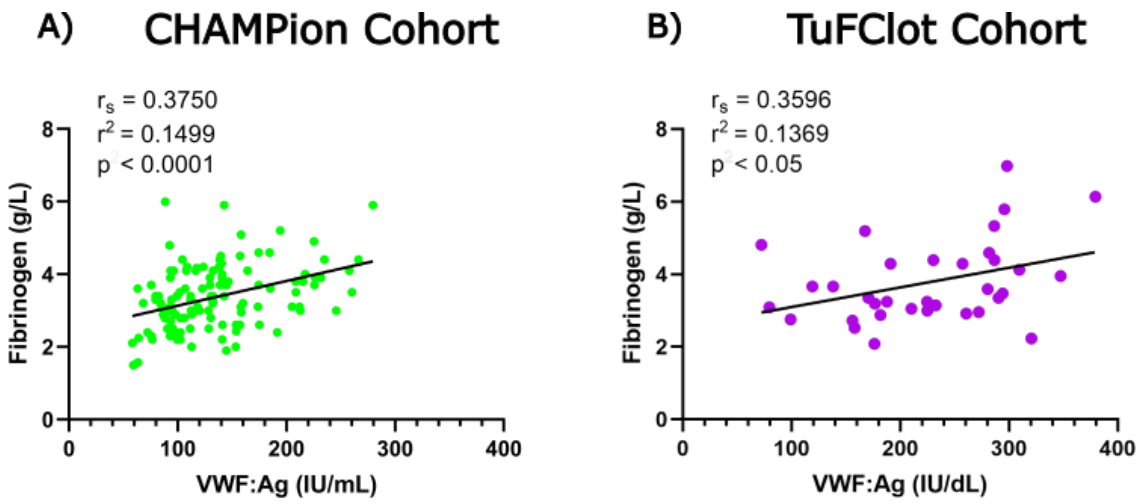

Figure 3.5 VWF:Ag and fibrinogen levels positively correlate in breast cancer patients: Measured plasma VWF:Ag levels were correlated against fibrinogen levels from the **A)** CHAMPion (N=121) and **B)** TuFClot cohorts (N=34). Analysis was carried out using Spearman rank correlation for non-parametric data. The Spearman correlation coefficient (r_s) denoted strength of correlation. A linear regression analysis was also conducted, deriving a value for slope of the line (r^2), the relationship between parameters was assessed to determine significance * $p \leq 0.05$, **** $p \leq 0.0001$.

3.2.3 D-dimer correlation with VWF:Ag levels

VWF:Ag levels were also correlated against plasma D-dimer levels, the end product of fibrinolysis and a well-established marker of coagulation activation.[248] D-dimer levels have previously been shown to be significantly elevated in a vast range of cancer types from haematological to solid tumours, including breast cancer. Furthermore, D-dimer in these cancer cohorts were found to associate with clinical stage and metastasis and were proposed to be a useful prognostic tool in cancer analysis.[249,250]

Interestingly, increasing plasma VWF:Ag in patients with breast cancer showed a moderate correlation with plasma D-dimer levels in patients with both early and late stage breast cancer. However, while analysis of patients in the CHAMPion cohort with Spearman correlation and linear regression analysis revealed that plasma D-dimer and VWF:Ag were significantly associated they did not have a slope of the line that was significantly non zero, meaning VWF levels had no predictive power for D-dimer levels in early breast cancer. (r_s=0.355, r^2=0.020 p=0.103, Figure 3.6 A). In contrast, the TuFClot cohort displayed a significant association between D-dimer and VWF:Ag and a slope of the line that was significantly non-zero (r_s=0.359, r^2=0.148 $p \leq 0.05$, Figure 3.6 B).

Taken together, the elevated plasma VWF:Ag levels observed in both patients with early and advanced stage breast cancer correlated with specific markers of coagulation activation, including fibrinogen and D-dimer. However no association was seen for TAT complexes in these patients.

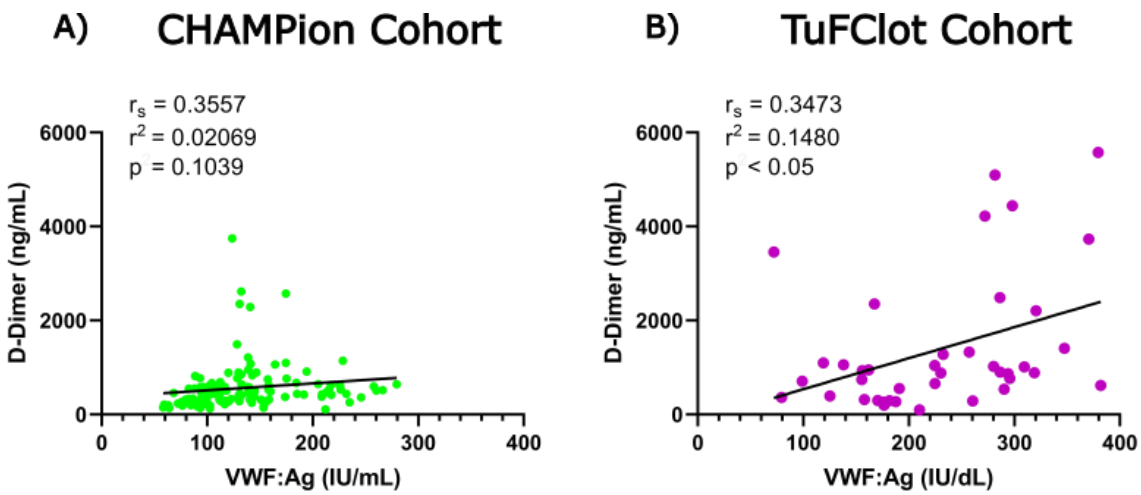

Figure 3.6 VWF:Ag and D-dimer levels positively correlate in breast cancer patients: Measured plasma VWF:Ag levels were correlated against D-dimer levels from the **A)** CHAMPion (N=129) and **B)** TuFClot cohorts (N=40). Analysis was carried out using Spearman rank correlation for non-parametric data. The Spearman correlation coefficient (r_s) denoted strength of correlation. A linear regression analysis was also conducted, deriving a value for slope of the line (r^2), the relationship between parameters was assessed to determine significance * $p \leq 0.05$, **** $p \leq 0.0001$.

3.2.4 VWF:Ag correlates with clinical outcome in patients with breast cancer

As discussed previously, VWF has been reported as a prognostic biomarker in colorectal, ovarian, glioblastomas and lung cancer where increased plasma levels associated with disease progression and poorer clinical outcome.[102–105] While elevated VWF levels have previously been reported in a small cohort of patients with breast cancer, it has not been fully assessed as a prognostic biomarker.[111–113] Thus, we examined whether plasma VWF:Ag may correlate with clinical outcome in our two breast cancer cohorts. Correlations were assessed using Spearman's rank coefficient to assess the association and linear regression analysis for the slope of the line. Since the CHAMPion cohort consists of early stage, newly diagnosed breast cancer patients, the PREDICT online tool was implemented as a surrogate marker to detail expected clinical outcome in this cohort. The PREDICT breast cancer prognostication tool provides expected survival outcomes of patients based on comparative clinical characteristics of each patient.[251] As such correlations with expected survival outcomes against VWF:Ag plasma levels could be derived for the CHAMPion cohort. However, two year survival data (in days) was available in the TuFClot, where patients had advanced metastatic disease. Therefore VWF:Ag levels were correlated against survival data (in days) for the TuFClot cohort.

In keeping with the early disease status of the patients, survival, based on the PREDICT score, was high with 86% of the patient population calculated as having a score greater than 50%. Perhaps unsurprisingly, no significant association or slope of the line was observed for VWF:Ag levels and the PREDICT score in this cohort (r_s=-0.081, r^2=0.001, p=0.711, Figure 3.7 A). Conversely however, in the metastatic breast cancer cohort, higher VWF:Ag levels were found to be inversely proportional to patient survival, the correlation was moderate to strong with a significant slope of the line (r_s=-0.475, r^2=0.001, $p \leq 0.05$, Figure 3.7 B). Furthermore, comparing VWF:Ag levels in those who died within 1 year of study enrolment versus those who remained alive beyond 1 year, statistically higher VWF:Ag levels were observed (median 189.3 (IQR 155.8 – 281.8) versus 281.7 (IQR 179.6 – 333.3) $p \leq 0.05$, Figure 3.7 C). This novel observation reveals that increased plasma VWF:Ag levels were associated with higher early mortality in breast cancer patients with metastatic disease.

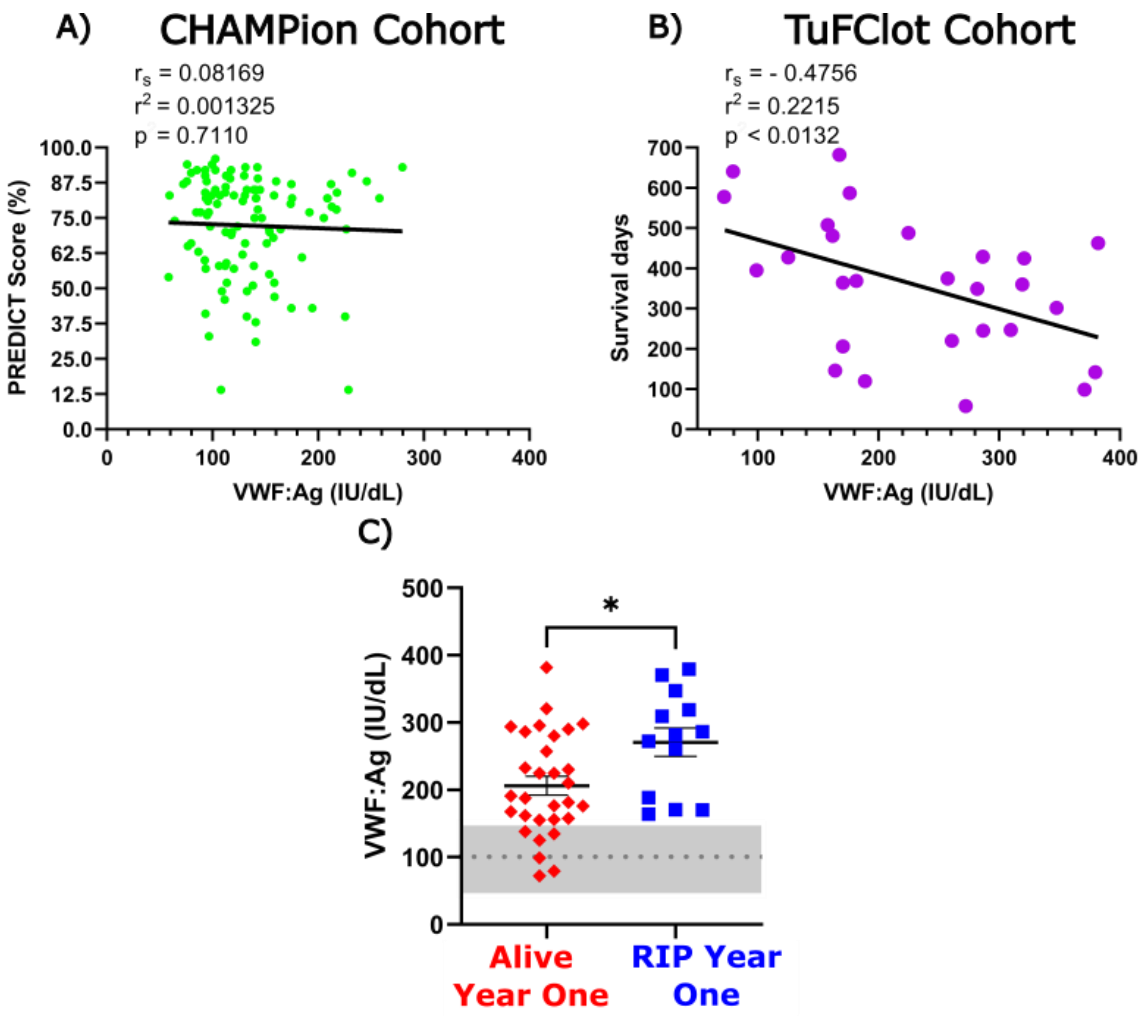

Figure 3.7 VWF:Ag survival correlation of patients with breast cancer: Measured plasma VWF:Ag levels were correlated against patient survival. **A)** Patient survival was calculated over 5 years with values adjusted with the PREDICT web-based prognostication tool for expected survival in the early breast cancer CHAMPion cohort (N=106). **B)** 2 year patient survival (N=27) was measured against plasma VWF:Ag in the metastatic TuFClot cohort. Values were correlated using Spearman rank correlation for non-parametric data. The Spearman correlation coefficient (r_s) denoted strength of correlation. A linear regression analysis was also conducted, deriving a value for slope of the line (r^2), the relationship between parameters was assessed to determine significance **C)** Patient plasma VWF:Ag levels from the TuFClot cohort (N=43 (30 vs 13)) were separated into two groups based on survival beyond one year. The results were collated and plotted as median VWF:Ag levels between patients who died within one year of enrolment and those that survived The median value for VWF:Ag (IU/dL) in a healthy population was depicted with a dotted line and the reference range displayed as a grey bar. Statistical significance was calculated with a student t-test, * $p \leq 0.05$.

3.3 In vitro VWF-breast cell adhesion analysis

3.3.1 Interaction of invasive MDA-MB-231 breast cancer cells with VWF

A number of *in vitro* studies have described that tumour cells can directly interact and bind purified VWF.[187,190,240] Moreover, recently it has been shown that this interaction may occur within the circulation. For example, plasma VWF bound in a preferential manner to melanoma tumour rather than leukocytes within whole blood.[240] Given the markedly elevated plasma VWF:Ag levels we described in patients with breast cancer we next sought to characterise the interaction between breast cancer cells directly. MDA-MB-231 breast cancer cells represent a human immortalised triple negative breast cancer cell line that is highly metastatic.[214] These cells rapidly undergo blood-borne metastasis *in vivo* and have been reported to interact with platelets and other coagulation derived factors as they undergo metastasis.[252,253] We thus selected MDA-MB-231 cells as a model for breast cancer cells which undergo haematogenous metastatic spread with potential for interactions with blood-borne proteins including VWF.[213,220]

MDA-MB-231 cell adhesion to human recombinant VWF was assessed at increasing concentrations in a static adhesion assay using flow cytometry. The assay was conducted in the presence and absence of ristocetin, which has been shown to induce structural unfolding of the VWF A-domains, similar to the multimer unwinding seen under conditions of shear stress within blood flow.[254] The interaction was quantified by measuring VWF-bound breast tumour cells with a specific anti-VWF antibody and corresponding Alexa-488 Fluor secondary antibody.

The results show that treating MDA-MB-231 cells with VWF at doses of 50nM (~100IU/dL) which are considered physiological levels there was no adhesion observed. However, by increasing concentrations to 200nM VWF which represent those found in our breast cancer patients we found a significant direct interaction between VWF and the MDA-MB-231 cells with around a 2 fold increase in adhesion (Figure 3.8). Interestingly, the addition of ristocetin markedly enhanced VWF adhesion to breast tumour cells at higher concentrations leading to 4 and 5 fold increases in binding for 100nM and 200nM VWF treatments respectively (Figure 3.8 D).

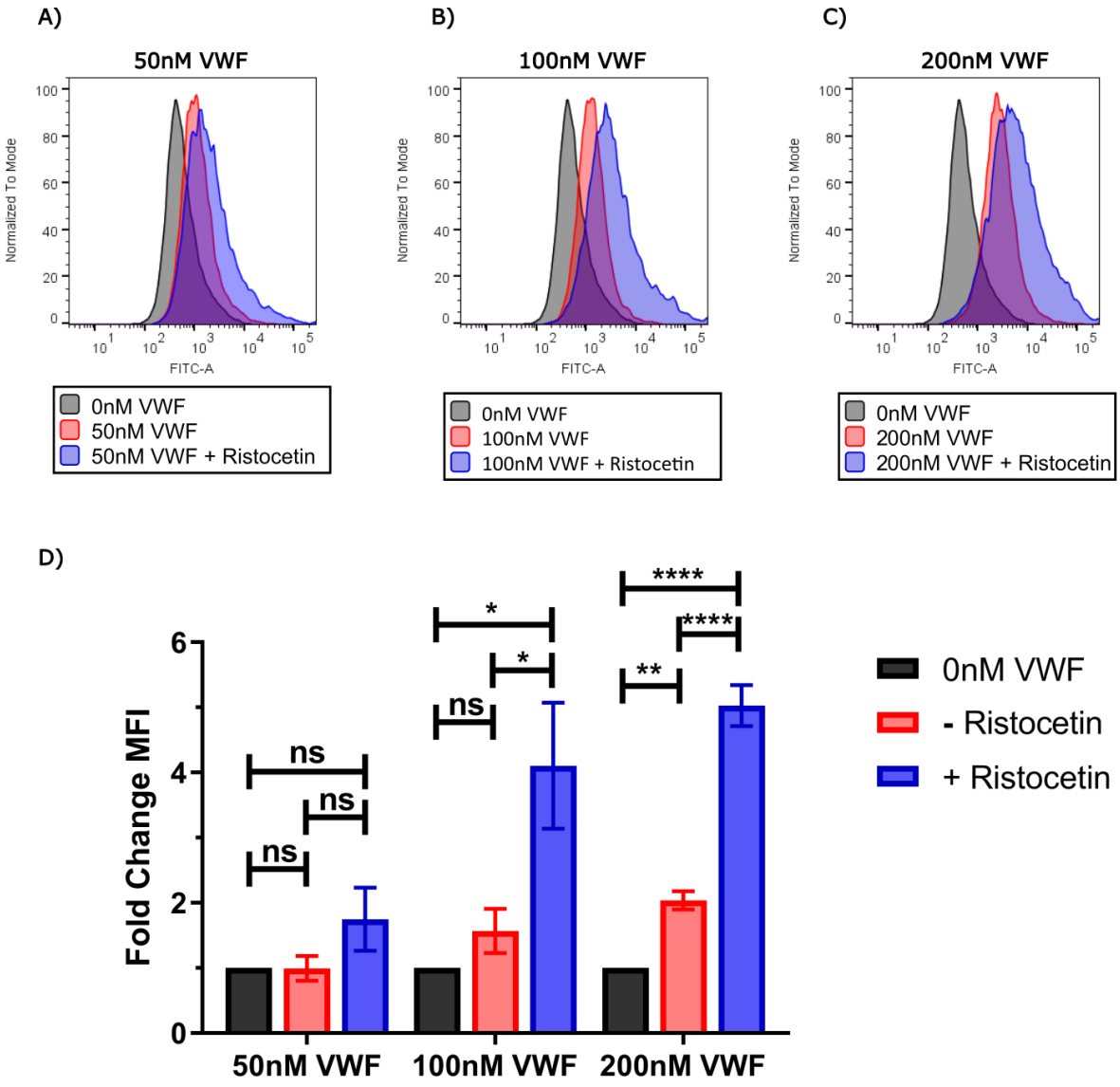

Figure 3.8 MDA-MB-231 cells adhere to VWF in a dose dependent manner dependent on ristocetin: MDA-MB-231 cell adhesion to recombinant VWF was measured under static conditions (N=3), cells were treated with increasing doses of recombinant VWF shown in representative histograms **A)** 50nM VWF ± ristocetin **B)** 100nM VWF ± ristocetin **C)** 200nM VWF ± ristocetin. **D)** Fold change in MFI values from VWF adhesion to MDA-MB-231 cells were normalised against untreated stained controls and graphed ± SEM. Significance was determined by ordinary one-way ANOVA with Tukeys multiple comparison test, * $p \leq 0.05$, ** $p \leq 0.01$, **** $p \leq 0.0001$.

3.3.2 Pre-metastatic MCF-7 adhesion to VWF

MCF-7 breast cancer cells represent a hormone receptor positive, pre-metastatic breast cell line.[216] We measured VWF binding capacity on MCF-7 cells via flow cytometry as outlined in 2.4. Our analysis showed that MCF-7 cells bound VWF with greater avidity than the MDA-MB-231 cells without the addition of ristocetin, reaching around a 2 fold increase in MFI from the untreated control cells at 50, 100 and 200nM VWF (Figure 3.9). In the absence of ristocetin, maximal VWF adhesion, was observed at 50nM, with no further significant increase observed at higher VWF concentrations. In contrast, the addition of ristocetin resulted in further increase in VWF binding to MCF-7 cells for (2 fold at 50nM vs 4 fold at 200nM) (Figure 3.9 D).

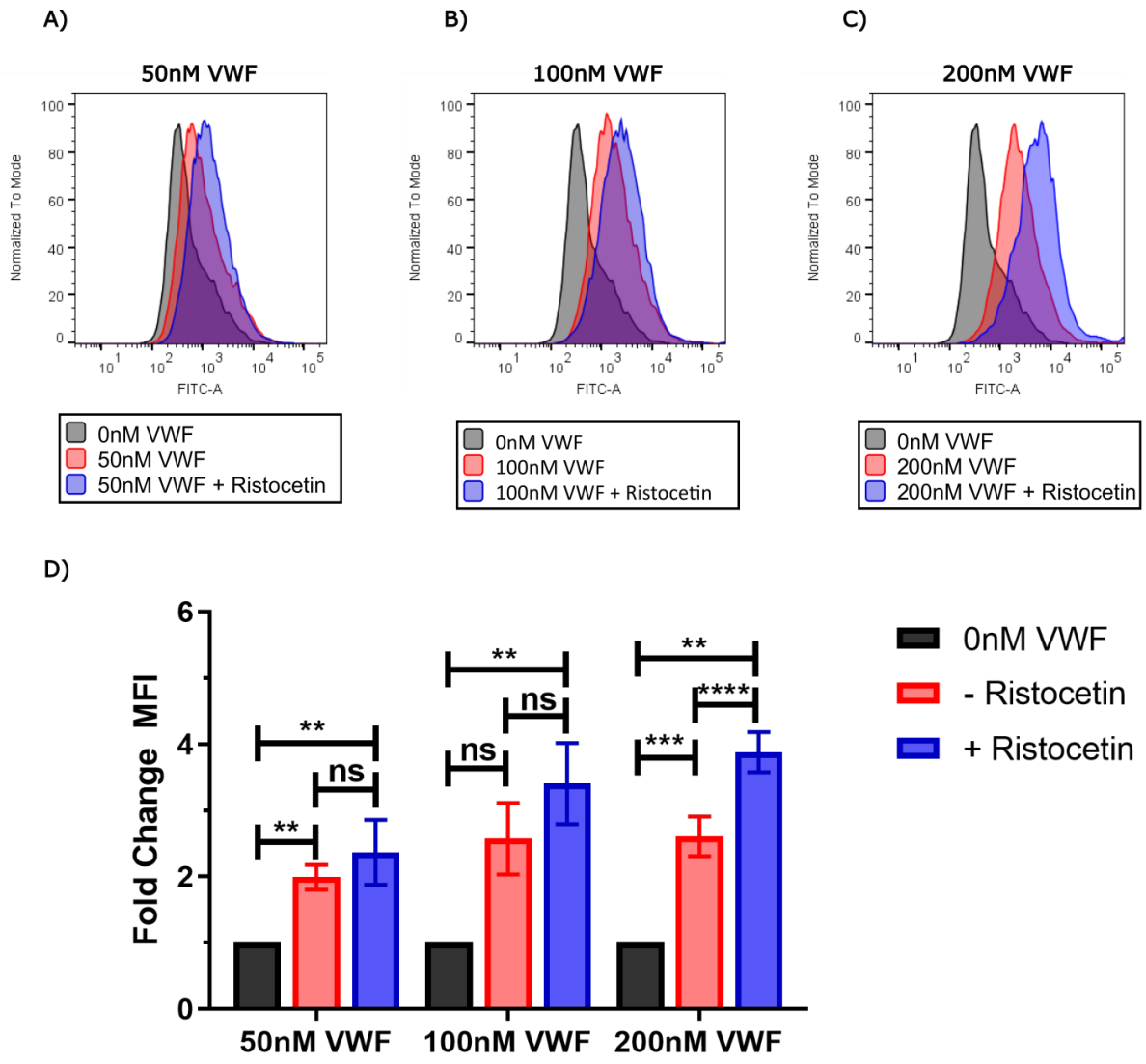

Figure 3.9 MCF-7 cells adhere to VWF in a dose dependent manner independent of ristocetin: MCF-7 cell adhesion to recombinant VWF was measured under static conditions (N=3), cells were treated with increasing concentrations of recombinant VWF in representative histograms **A)** 50nM VWF ± ristocetin **B)** 100nM VWF ± ristocetin **C)** 200nM VWF ± ristocetin. **D)** Fold change in MFI values from VWF adhesion to MCF-7 cells were normalised against untreated stained controls and graphed ± SEM. Significance was determined by ordinary one-way ANOVA with Tukeys multiple comparison test ** $p \leq 0.01$, **** $p \leq 0.0001$.

3.3.3 Non-tumourigenic MCF-10A adhesion to VWF

The cell line MCF-10A is a non-tumourigenic, yet immortalised cell line and as such are used as a model for normal breast tissue.[217,218] Using the same static binding assay as previously described with MCF-7 and MDA-MB-231 cells, VWF-MCF-10A adhesion was quantified via flow cytometry. The data shows that MCF-10A cells bind in a dose dependent manner to VWF from 50nM to 200nM (Figure 3.10). However, adhesion of VWF was found to be much lower than with tumourigenic cell line counterparts MCF-7 and MDA-MB-231. While MCF-10A cells adhered to VWF without ristocetin at the around the same fold rate as MDA-MB-231 (2-fold), addition of ristocetin had minimal effect on further influencing the adhesion any further (Figure 3.10 D).

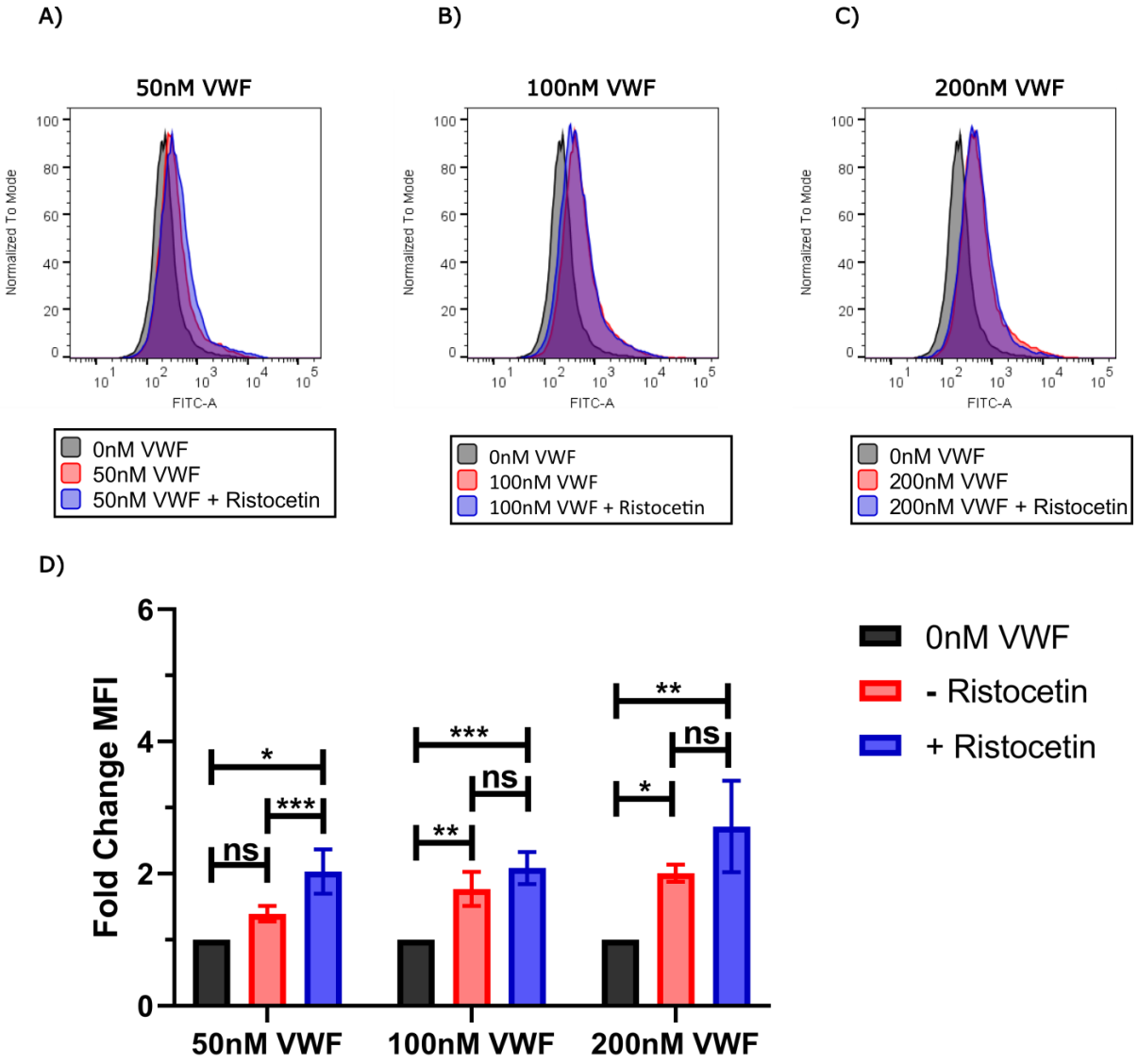

Figure 3.10 VWF adhere to MCF-10A cells but a lower affinity: MCF-10A cell adhesion to recombinant VWF was measured under static conditions (N=3), cells were treated with increasing concentrations of VWF shown in representative histograms **A)** 50nM VWF ± ristocetin **B)** 100nM VWF ± ristocetin **C)** 200nM VWF ± ristocetin. **D)** Fold change in MFI values from VWF adhesion to MCF-10A cells were normalised against untreated stained controls and graphed ± SEM. Significance was determined by ordinary one-way ANOVA with Tukeys multiple comparison test *p ≤ 0.05, ** p ≤ 0.01, *** p ≤ 0.001.

3.3.4 Primary HMEC adhesion to VWF

The HMEC are primary cells derived from female mammary epithelial tissue, these cells are non-immortalised and are the truest representation of non-cancerous mammary epithelial tissue.[219] Therefore we used HMEC as another control to assess the adhesion of VWF to breast cells.

VWF adhesion to HMEC was negligible (Figure 3.11). Interestingly, VWF adherence to HMEC only reached significance at 100nM without ristocetin treatment however these levels were only marginally above the baseline stained controls at ~1.5 fold increase (Figure 3.11 D) and likely reflect natural variability within the assay. The addition of ristocetin to VWF adhesion with HMEC showed no change over all concentrations assessed.

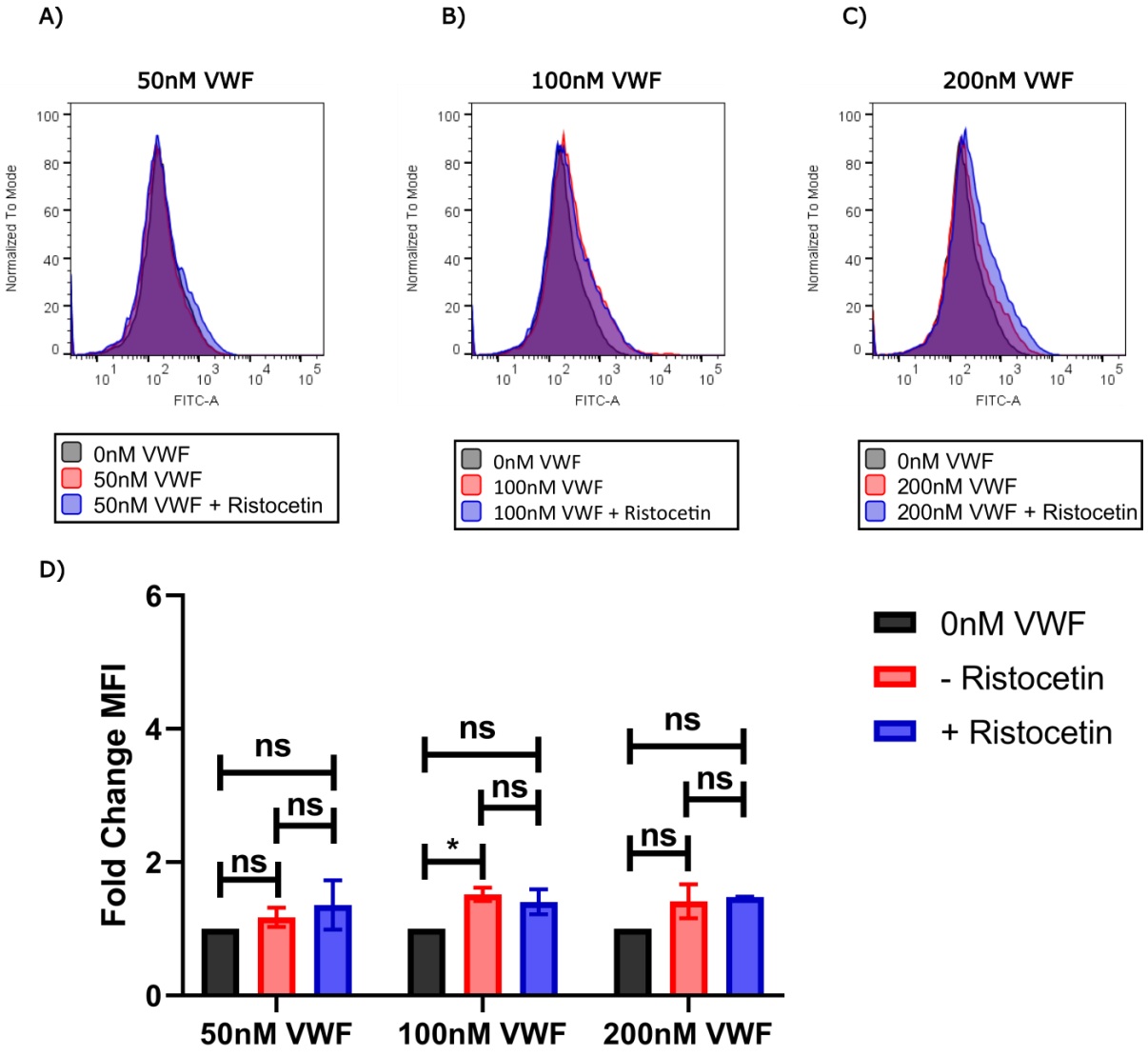

Figure 3.11 Primary HMEC do not adhere to VWF: HMEC adhesion to recombinant VWF was measured under static conditions (N=3), cells were treated with increasing concentrations of VWF shown in representative histograms **A)** 50nM VWF ± ristocetin **B)** 100nM VWF ± ristocetin **C)** 200nM VWF ± ristocetin. **D)** Fold change in MFI values from VWF adhesion to HMEC were normalised against untreated stained controls and graphed ± SEM. Significance was determined by ordinary one-way ANOVA with Tukeys multiple comparison test * $p \leq 0.05$.

3.3.5 The role of calcium on breast cell adhesion to VWF

A previous study reported that VWF adhesion to melanoma tumour cells required the addition of divalent manganese cations.[255] Despite manganese not being present in our experimental set up for the flow cytometry static binding assay we noted that the binding buffer solution used contained 1mM calcium, also a divalent cation. As a result we sought to further characterise the role of Ca^{2+} in our assay.

The VWF-breast tumour adhesion assay was repeated in buffer with and without calcium supplementation. For all three breast cell lines used, no significant VWF adhesion was observed in the absence of calcium ions (Figure 3.12). However, supplementation of 1mM calcium saw a restoration in VWF binding to previous levels, highlighting that VWF-breast tumour interactions are significantly dependent on the presence of calcium ions.

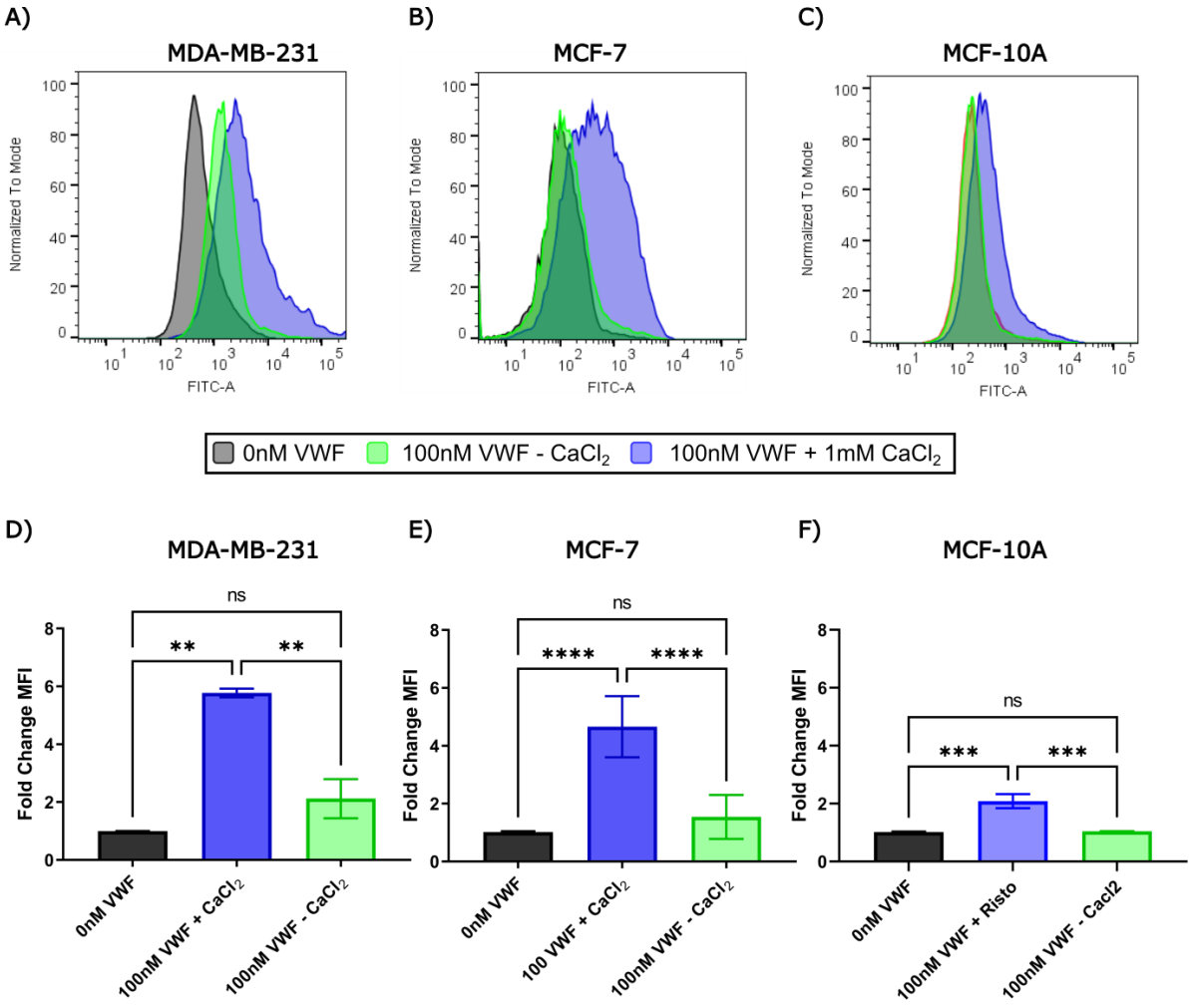

Figure 3.12 VWF adhesion to breast cancer cells is dependent on calcium: Breast cell lines MDA-MB-231 (N=3), MCF-7 (N=5) and MCF-10A (N=3) were assessed for static adhesion of recombinant VWF in the presence and absence of supplemented calcium. 100nM VWF + ristocetin was applied to each cell line in binding buffer supplemented with/without 1mM calcium chloride, representative histograms **A)** MDA-MB-231, **B)** MCF-7 and **C)** MCF-10A. Fold change in MFI was calculated by normalising against an untreated controls of each respective cell line. Data was graphed as fold change in MFI ± SEM for each cell type **D)** MDA-MB-231 **E)** MCF-7 **E)** MCF-10A. Significance was calculated by using one way ANOVA with Tukeys multiple comparisons test, ** $p \leq 0.01$, *** $p \leq 0.001$, **** $p \leq 0.0001$.

3.3.6 LWMH Inhibits VWF-breast cancer cell adhesion

The addition of ristocetin significantly enhanced VWF adhesion to both MDA-MB-231 and MCF-7 to varying degrees. The effect of ristocetin in promoting the unfolding of the VWF A-domains has been well characterised and essential in facilitating VWF-platelet GPIbα interactions in vitro.[256] Interestingly, VWF has a heparin binding region within the A1 domain.[257] Furthermore, heparin has been described to play an inhibitory role in platelet adhesion by blocking GPIb adhesion to platelets through the VWF A1 domain.[205] This may be partly due to their binding sites being in close proximity within the A1 domain, where both GPIb and heparin compete for the same electrostatically charged region in the A1 domain.[258] To further assess a potential role for the A1 domain, based on our ristocetin data, we examined whether LMWH could reduce VWF adhesion to breast cancer cells.

To examine the potential inhibitory role of LMWH, MDA-MB-231 and MCF-7 cells were treated with 100IU/mL of LMWH and 100nM VWF plus ristocetin for 30 minutes. VWF adhesion at 100nM, in the presence of ristocetin, was quantified in cells that were treated with LMWH and compared against untreated. Treatment of LMWH significantly attenuated VWF-breast tumour cell adhesion (Figure 3.13). These data suggest that LMWH inhibits VWF-breast tumour interactions. Whether this inhibitory effect is due to LMWH competing with VWF for binding a specific tumour receptor or that LMWH directly binds the VWF A1 domain and shields breast tumour adhesion sites remains to be fully elucidated.

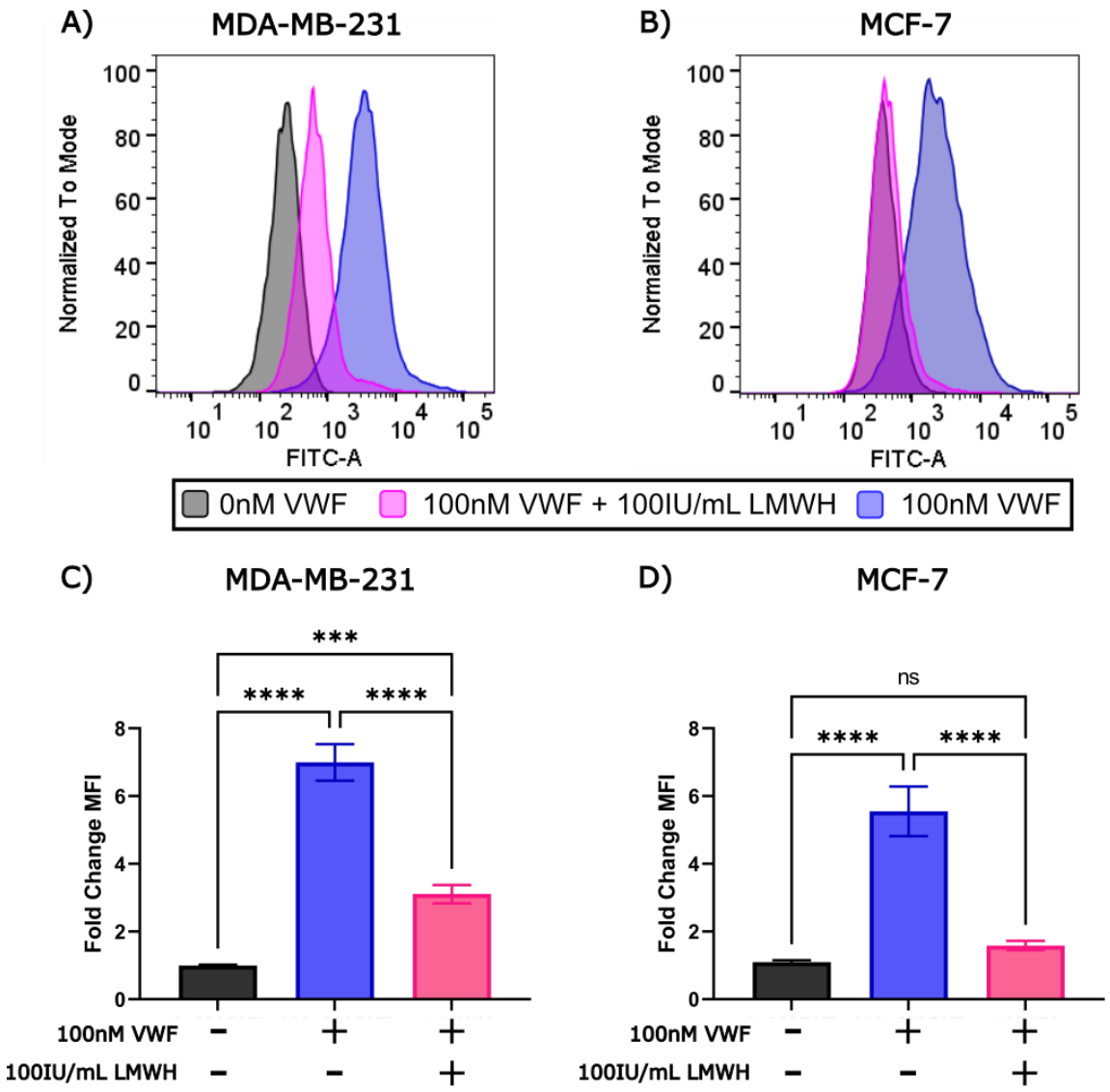

Figure 3.13 LMWH inhibits VWF adhesion to breast cancer cells: MDA-MB-231 (N=6) and MCF-7 (N=5) cells were treated with a combination of 100IU/mL LMWH and 100nM recombinant VWF + ristocetin. VWF adhesion was measured by flow cytometry, representative histograms of LMWH inhibition of VWF adhesion to **A)** MDA-MB-231 and **B)** MCF-7. Fold change in MFI was calculated by normalising VWF bound MFI levels against untreated stained control cells for each cell type. LMWH inhibition of VWF adhesion was graphed in **C)** MDA-MB-231 and **D)** MCF-7 cells as fold MFI change ± SEM. Significance was determined using one way ANOVA with Tukeys multiple comparison test, *** $p \leq 0.001$, **** $p \leq 0.0001$.

3.3.7 VWF binding to breast cancer cells, enhances their adhesion to an endothelial layer

Endothelial cells can serve as a key barrier in preventing haematogenous metastasis of cancer cells from spreading to a secondary site. To overcome this, circulating tumour cells need to undergo firm adhesion to the endothelium as a key prerequisite step in allowing haematogenous extravasation across the vessel wall.[259] VWF expressing SAOS2 osteosarcoma and U251 glioma cells display significantly enhanced adhesion to the endothelial layer compared to VWF siRNA KO cell counterparts, suggesting the surface bound VWF on tumour cells may promote their anchorage with endothelial cells[143] With this in mind we investigated the role of VWF once bound to our invasive MDA-MB-231 breast tumour cells, in mediating their adhesion to primary HUVEC.

As a highly invasive cell line that has been described to undergo haematogenous dissemination, by circulating through the blood in mouse models we used MDA-MB-231 cells to assess the ability of VWF to affix the invasive breast cancer cell line to an endothelial layer.[213,220] MDA-MB-231 cells with and without pre-bound VWF were added to the HUVEC layer for 2, 5, 10 or 20 minutes. MDA-MB-231 cells with pre-bound VWF affixed to the HUVEC layer at a higher rate than the native MDA-MB-231 with no VWF bound (Figure 3.14 A-E). The area under the curve (AUC) analysis showed that native MDA-MB-231 baseline adhesion (225.9 ± 44.86) was significantly lower than VWF treated MDA-MB-231 cells (372 ± 20.4, $p \leq 0.05$) over the 20 minute interval (Figure 3.14 F).

Taken together, the data suggests that circulating breast tumour cells may directly bind the elevated VWF antigen within the blood of patients as they undergo haematogenous dissemination. Once surface bound, VWF on the breast tumour cells may serve to facilitate breast tumour-endothelial tethering, a key step in the metastatic pathway, either through more rapid adhesion rates and or firmer adhesion events.

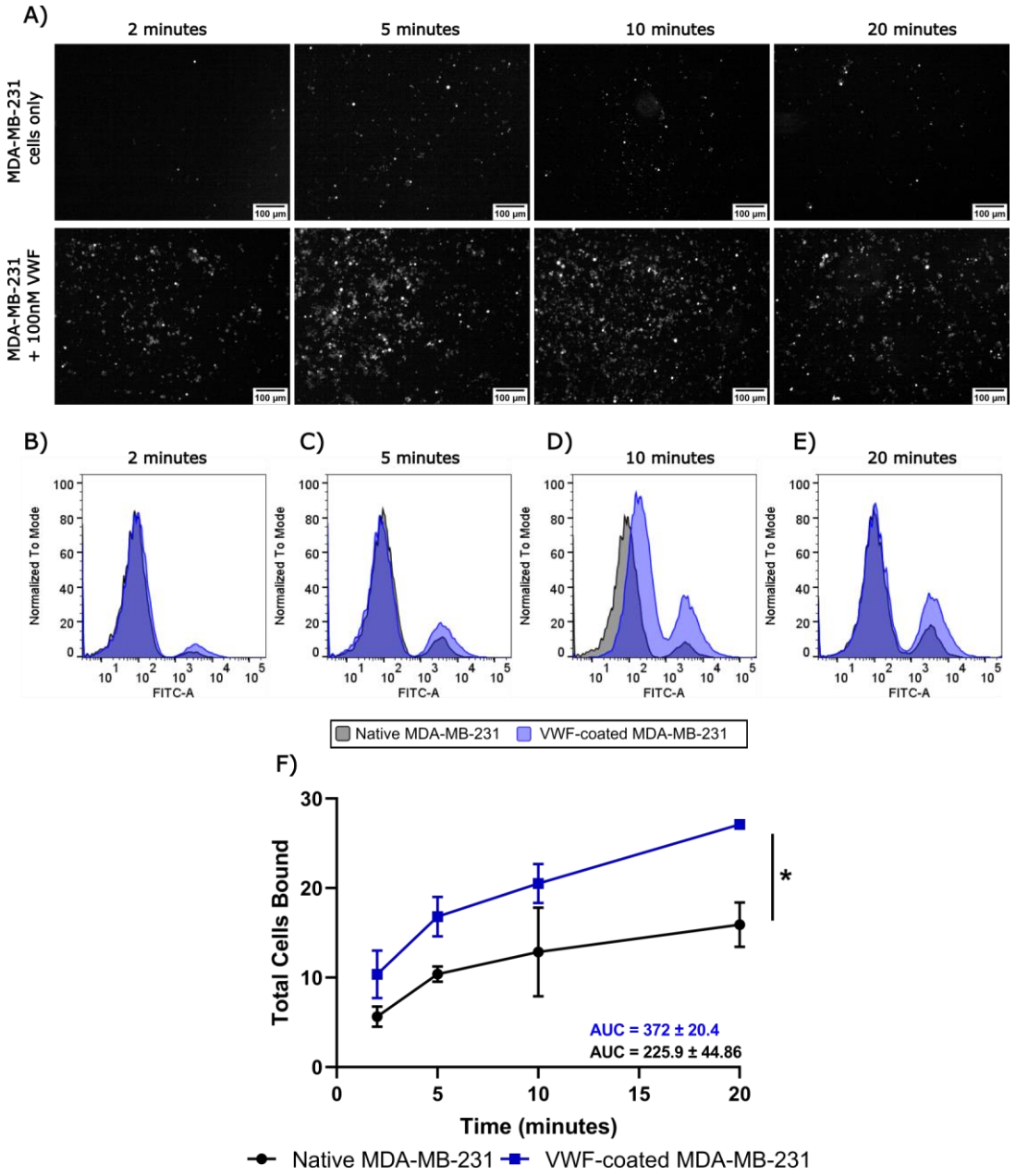

Figure 3.14 VWF promotes adhesion of cancer cells to the endothelium over time: MDA-MB-231 cancer cells were fluorescently stained before being treated ± 100nM recombinant VWF + ristocetin (N=3). Both the VWF-bound and native untreated cells were added to a HUVEC monolayer for 2, 5,10 and 20 minutes in separate wells before unbound tumour cells were washed off. **A)** Images at 10x magnification were taken for each condition at the corresponding time points. Cells were then uplifted and stained with endothelial CD31 marker. The static adhesion co-culture was measured by flow cytometry to identify FITC labelled MDA-MB-231 cells and represented as histograms **B)** 2 minutes **C)** 5 minutes **D)** 10 minutes **E)** 20 minutes. **F)** The percentage of MDA-MB-231 cells in the total cell population were plotted over time for both untreated and VWF bound MDA-MB-231 cells. Data was analysed as area under the curve with values presented with a mean ± SEM significance was determined using a student t-test, * $p \leq 0.05$.

3.4 Breast cancer cell adhesion to endothelial cells

3.4.1 VWF adhesion to MDA-MB-231 cells under shear flow

VWF is a dynamic multimeric protein and through forces induced by blood shear stress within the vasculature, VWF multimers are unwound resulting in the exposure of binding sites for circulating platelets and leukocyte adhesion.[15,260] In response to endothelial cell stimulation or damage, UL-VWF multimers are released and anchored to the endothelial cell surface where the tensile stresses of blood shear expose cryptic A-domains of the VWF structure. These forms of VWF display greater adhesive properties and are the most prothrombotic.[76,78] Thus, given the direct interaction between VWF and breast tumour cells under static conditions, we next sought to examine whether VWF multimers may serve as an adhesive platform for circulating breast tumour cells under shear stress. Firstly, we optimised the assay using a purified system *in vitro* system, a laminal flow slide was coated with 100nM VWF where labelled invasive MDA-MB-231 cells were perfused across it. The system was designed to model the shear rates experienced in venous blood flow.

MDA-MB-231-VWF adhesion events were recorded, with stable binding events measured through surface coverage and real-time tumour tracking and adhesion rates analysed by $K_{[on]}$ and $K_{[off]}$ values using u-track particle tracking analysis as previous.[156] VWF coating resulted in a large increase in surface coverage of perfused breast tumour cell compared to the uncoated control surface (100.2 ± 12.65 cells/mm^2 vs 26.9 ± 27.45 ± 9.26 cells/mm^2 $p<0.001$, Figure 3.15 A-B). In keeping with our previous findings, addition of 100IU/mL LMWH to the perfusion media resulted in a complete ablation of breast tumour binding and surface coverage (26.9 ± 8.04 cells/mm^2, Figure 3.15 A-B). Furthermore, the addition of LMWH also decreased the $K_{[on]}$ value, indicative of tumour cells no longer able to adhere to exposed VWF strings (Figure 3.15 C, 2.66 ± 0.51 cells/mm^2/s vs 0.913 ± 0.26 cells/mm^2/s) but also increased the $K_{[off]}$ value (Figure 3.15 D, 0.017 ± 0.005 1/s vs 0.070 ± 0.02 1/s), suggesting that any tumour adhesion events which did occur were transient in nature and not firmly attached to the immobilised VWF on the surface.

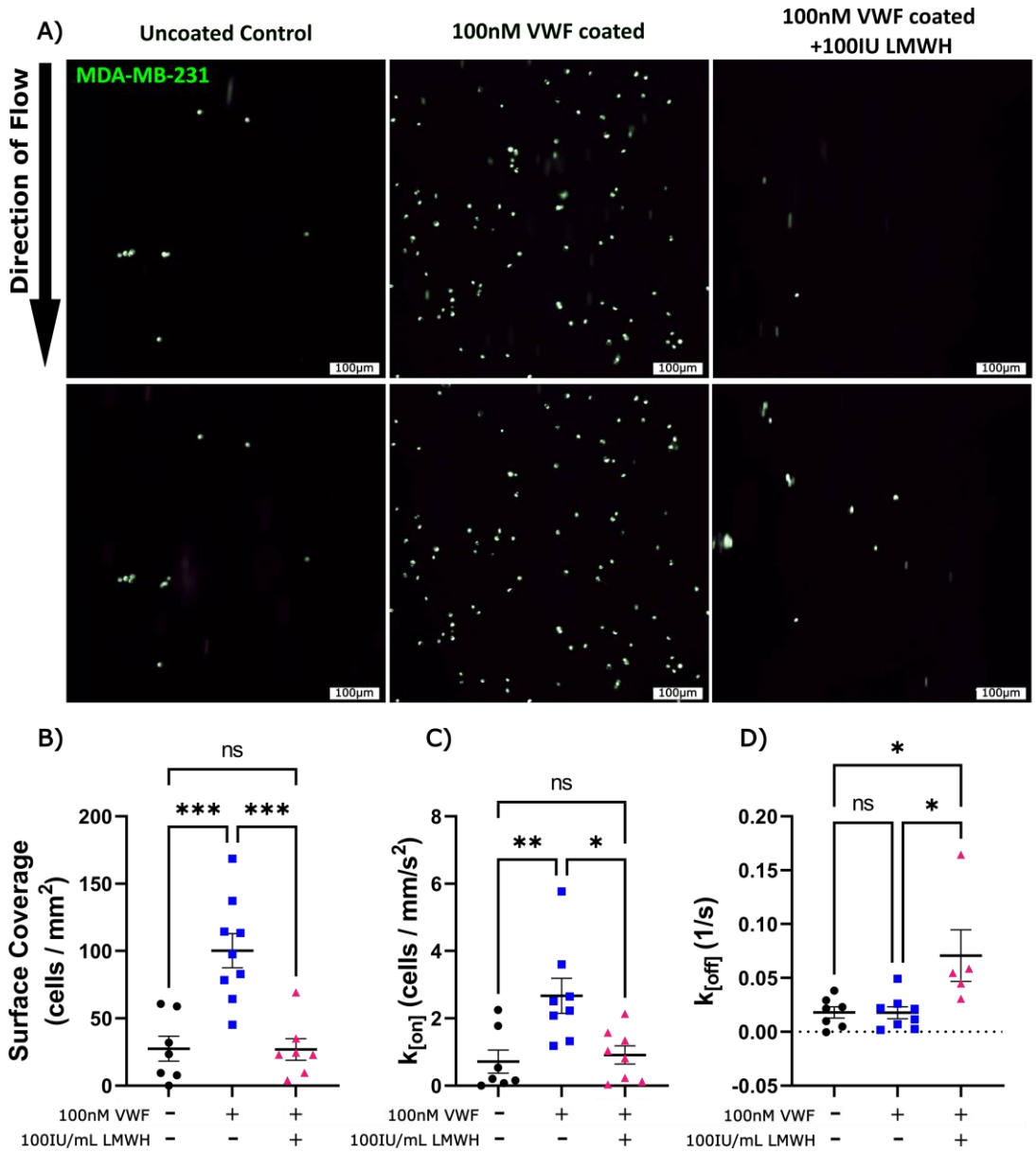

Figure 3.15 Immobilised VWF arrests MDA-MB-231 cells under perfusion: MDA-MB-231 cells were perfused at a flow rate of 0.2 ml/min resulting in venous shear stress of 0.25 dyn/cm^2. The channels of an ibidi flow slide were either coated with 100nM pd-VWF or untreated. Fluorescently labelled MDA-MB-231 cells ± 100IU LMWH treatment were perfused across the channels and recorded at 10x magnification for up to 700 frames. **A)** Representative images of cellular perfusion were taken at different time points to highlight differences in surface coverage of breast tumour cells under different experimental conditions. Tumour cell arrest was measured by **B)** stable adhesion through surface coverage (cells/mm^2), **C)** attachment rates $K_{[on]}$ (cells/mm^2/s), **D)** detachment rates $K_{[off]}$ (1/s). Data is presented as the mean ± SEM of at least 3 independent experiments. Significance was determined through one way ANOVA using Tukeys multiple comparisons test, * $p \leq 0.05$, ** $p \leq 0.01$, *** $p \leq 0.001$.

3.4.2 VWF multimers secreted from endothelial cells contribute to enhanced adhesion of breast cancer cells under shear flow

Circulating monocytes, leukocytes and platelets have all been described to be firstly recruited by and then attached to VWF multimer strings in *in vitro* and *in vivo* models.[167,261,262] Importantly, these UL-VWF multimeric structures have been previously reported in cancer patients. In particular, biopsies from patients with malignant melanoma reveal significant accumulation of VWF multimers and platelet-rich thrombi as a result.[148,181] Recently published data by our group highlights that endothelial cell activation and VWF multimer release is also induced by breast cancer cells.[156] Under shear conditions, platelets immobilized on VWF multimers have been shown to mediate tethering, rolling and firm adhesion of colonic cancer lines.[263] Under these conditions, VWF played a critical role in enabling firm adhesion of the tumor cells to the immobilized platelets. Our data suggests that VWF can mediate the firm adhesion of perfused MDA-MB-231 breast tumour cells independent of platelets. We further evaluated this using activated endothelial cells which release adhesive VWF multimers in response to PMA stimulation under shear stress and quantified adhesion of MDA-MB-231 under flow perfusion.

Analysis of MDA-MB-231 adhesion revealed that they bound with significant affinity to the activated endothelial cell surface under venous shear stress (Figure 3.16 A). To confirm a role for VWF multimers in contributing to this adhesion, a polyclonal anti-VWF antibody was added to the perfusion media. This resulted in an ablation of surface coverage vs isotype control treatment (2.54 ± 0.31 cells/mm^2 vs 43.05 ± 5.71 cell/mm^2, $p<0.001$ Figure 3.16 A-B). Correspondingly, inhibition of VWF caused attachment rates to the endothelial layer to decrease (1.83 ± 0.90 cells/mm^2/s^{-1} vs 6.70 ± 0.67 cells/mm^2/s^{-1}, $p<0.01$ Figure 3.16 C). In further support of this, a significant increase in the detachment rate was observed following anti-VWF treatment compared to the isotype control (Figure 3.16 D). Taken together, these novel data suggest the VWF multimers released from activated endothelial cells can serve as an adhesive platform for circulating triple negative breast tumour cells independent of immobilized platelets.

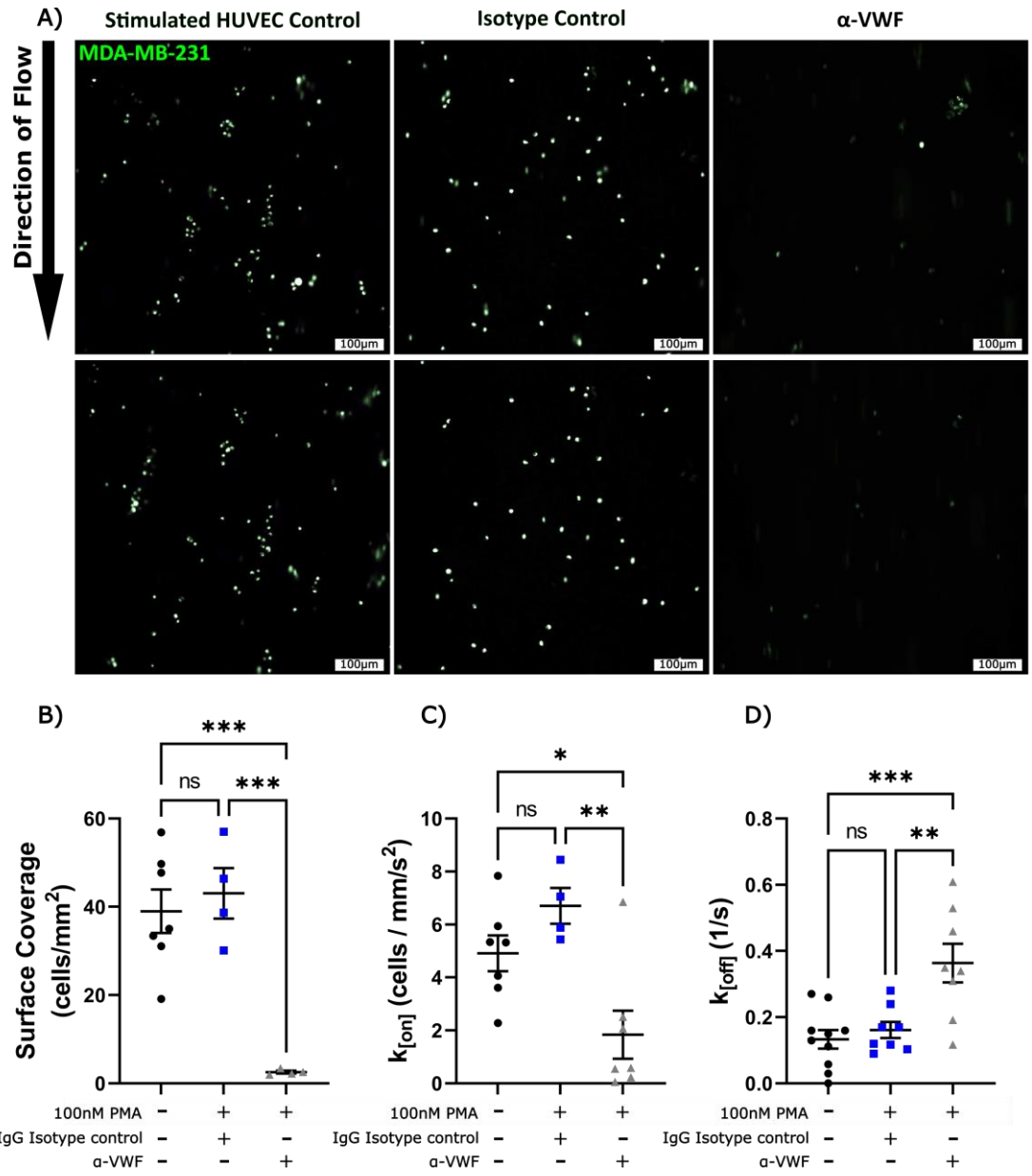

Figure 3.16 VWF multimer strings recruit MDA-MB-231 cells to the endothelial cell surface: HUVEC monolayers were cultured on ibidi channel slides and stimulated with 100nM PMA to ensure maximal release of VWF. MDA-MB-231 cells were fluorescently labelled before being perfused over the HUVEC monolayer at a venous shear stress of 0.25dyn/cm^2 in the presence of either an anti-VWF antibody or species matched isotype control (20µg/mL). Adhesion events were imaged at 10x magnification for up to 700 frames. **A)** Representative images of cellular perfusion were taken at different time points to highlight differences in surface coverage of breast tumour cells under different experimental conditions. Tumour cell adhesion was quantified by **B)** stable adhesion through surface coverage (cells/mm^2), **C)** attachment rates $K_{[on]}$ (cells/mm^2/s), **D)** detachment rates $K_{[off]}$ (1/s). Data is presented as the mean ± SEM of at least 3 independent experiments. Significance was determined through one way ANOVA using Tukeys multiple comparison test, * $p \leq 0.05$, ** $p \leq 0.01$, *** $p \leq 0.001$.

3.4.3 LMWH inhibits adhesion of breast cancer cells to the endothelium under shear stress conditions

Taking the results further, we explored the ability of LMWH to prevent MDA-MB-231 adhesion to the HUVEC layer under flow. Corresponding to our previous data, perfusion of MDA-MB-231 cells in media containing 100IU/mL LMWH dramatically decreased stable MDA-MB-231 attachment to the endothelial cell surface, resulting in decreased surface coverage compared to the PMA stimulated control (38.99 ± 4.91 cells/mm^2 vs 6.34 ± 1.69 cell/mm^2 Figure 3.17 A-B). Furthermore while there was no change in the number of attachment events $K_{[on]}$ the detachment rates in LMWH conditions were significantly increased (0.1329 ± 0.0281 s^{-1} vs 0.2833 ± 0.01282 s^{-1}, Figure 3.17 D). These data suggest that LMWH can block adhesion of MDA-MB-231 cells to the activated endothelial layer and perhaps prevent haematogenous metastatic invasion.

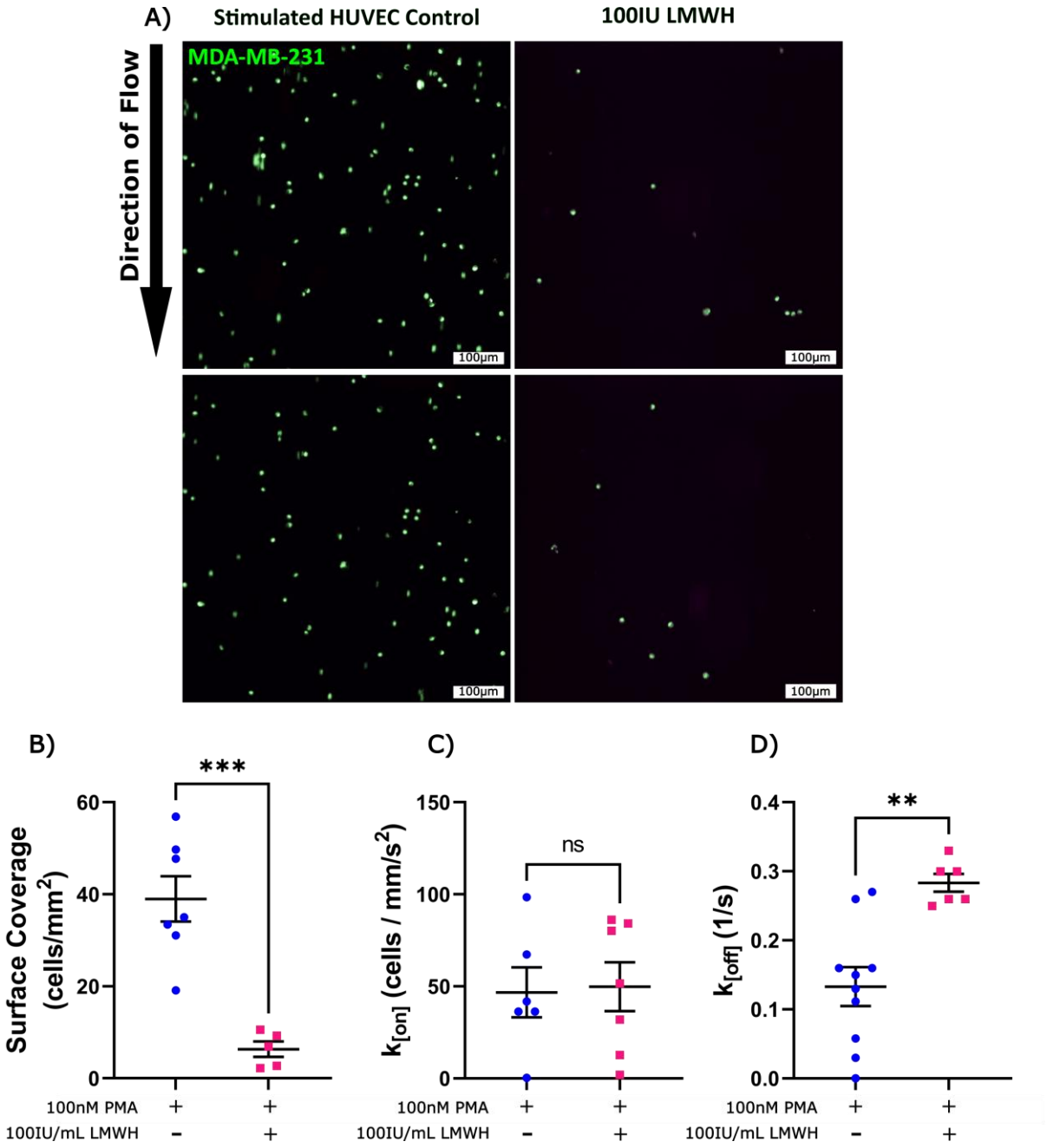

Figure 3.17 LMWH inhibits VWF multimer strings recruitment of MDA-MB-231 cells to the endothelial cell surface: HUVEC monolayers were cultured on ibidi channel slides and stimulated with 100nM PMA to ensure maximal release of VWF. MDA-MB-231 cells ± 100IU/mL LMWH solution were fluorescently labelled before being circulated over the HUVEC monolayer at a venous shear stress of 0.25 dyn/cm^2. Adhesion events were imaged at 10x magnification for up to 700 frames. **A)** Representative images of different experimental conditions were captured Tumour cell adhesion was quantified by **B)** stable adhesion through surface coverage (cells/mm^2), **C)** attachment rates $K_{[on]}$ (cells/mm^2/s), **D)** detachment rates $K_{[off]}$ (1/s). Data is presented as the mean ± SEM of at least 3 independent experiments. Significance was determined through student t-test, ** $p \leq 0.01$, *** $p \leq 0.001$.

3.5 Discussion

Malignancy drives a prothrombotic environment resulting in an increased risk of venous thrombosis for patients with cancer. Specifically, breast cancer is associated with a 3-4 fold increased risk of VTE. This risk increases further in patients with metastatic breast cancer and in those receiving chemotherapy, with VTE rates of up to 17.5% reported.[264,265] The mechanisms underpinning cancer associated thrombosis are multifactorial and may be cancer type specific. Nevertheless, understanding the pathophysiology is of direct clinical relevance, since multivariate analysis has demonstrated that VTE in breast cancer patients is associated with reduced 2 year survival (hazard ratio 2.3; 95% CI, 2.1-2.6).[266] Moreover, tumour mediated coagulation activation not only contributes to risk of thrombosis in patients with cancer but accumulating evidence suggests that it actively promotes cancer progression by contributing to tumour cell proliferation, angiogenesis and blood-borne metastasis.[230]

Interestingly, novel functions for VWF have been associated with the hallmarks of cancer.[267] For example, VWF has been described as an angiogenic regulator, influencing endothelial cell angiogenesis.[3,73] Recently, VWF has been shown to directly promote proliferation of smooth muscle cells and contribute to wound healing.[268] Additionally, VWF is thought to be an inflammatory mediator, with evidence it contributes to vascular permeability,[3,175,269] as well as facilitating immune cell extravasation by tethering and adhering cells to the endothelium.[3,172] Finally, VWF contributes as a coagulopathic agent, where it has been found to be a risk factor for VTE in several solid tumour malignancies.[3,97,270] Given previous studies reporting significantly elevated VWF plasma levels in cancer patients, which associate with advanced disease stage, we sought to investigate the role of VWF specifically in a breast cancer cohort and to examine whether VWF may interact directly with breast cancer cells and promote aspects of disease progression.

3.5.2 Clinical findings on VWF in breast cancer

Therefore we assessed the relative survival probability of breast cancer patients with high VWF expression at both gene and protein level from a publically available database (KM Plotter).[206,207] Kaplan-Meier curves generated from available records in the GEO repository revealed that while higher VWF mRNA levels were not associated with poorer survival, stratifying patients into groups based on increasing grade of breast cancer revealed a stronger trend towards reduced survival probability in the high *VWF* expression cohort, although this

did not reach statistical significance (p=0.061). A single previous report in patients with breast cancer revealed that VWF mRNA expression was significantly related to breast tumour histology.[271] Specifically, breast cancer patients with invasive lobular carcinoma (ILC) had higher VWF expression than patients with invasive ductal carcinoma (IDC) and other histology presentations. However, *VWF* expression in either ILC or IDC was not related to patient survival. Nevertheless, Kaplan-Meier analysis revealed that high VWF protein expression was associated with significantly higher mortality rates. Incidentally, when patients with grade 3 breast tumour were sub-selected for analysis, high VWF protein expression doubled the HR score compared to the heterogeneous breast cancer grade population.

It is interesting to note that mRNA and protein samples in these databases were derived from breast tumour samples. Under normal healthy conditions, *VWF* gene and thus protein expression is restricted to endothelial cells and megakaryocytes.[9] There are a few reports of acquired *de novo* VWF expression in specific tumour cells, including glioma and osteosarcoma, however the relative total VWF protein expressed in these tumour cells is an order of magnitude less than that reported with human endothelial cells in these studies.[118,137–139,141–144,272] Moreover, we have not observed any VWF gene expression in our breast cancer cell lines included in this study [Appendix I, Figure 7.1]. It is likely that within the tumour samples, a significant amount of tumour vasculature is also represented including, microvessels of arterioles, capillaries and venules all capable of expressing and secreting VWF. In fact, human skin biopsies of melanoma tumour and healthy tissues showed differential VWF levels on staining, with healthy tissues having increased endothelial wall localised VWF staining and tumour samples with greater luminal deposition of VWF.[148] Additionally, a similar pattern of VWF staining was observed in quiescent and tumour activated endothelium in immunohistochemistry analysis of tumour biopsies from patients with urothelial bladder cancer.[153] Taken together, our data suggest that local VWF expression within tumour tissues may be associated with poorer probability of survival in patients with breast cancer. Of note, the increased mortality associated with higher VWF expression was most marked in patients with higher grade breast tumours, which indicates that VWF could play a key role in late stage breast cancer.

In silico analytical tools provide a preliminary view of both gene and protein levels in a cancer setting. However, these tools are not without limitations. The data from *in silico* datasets are

sourced from varied studies with different recruitment dates and no standardised model of treatment or disease sample processing between cases. Furthermore, when assessing VWF levels, surgery and varied chemotherapies can contribute to increased VWF secretion from the endothelium. Therefore, the use of *in silico* models in this thesis was as a preliminary tool to assess whether VWF was a viable candidate before more robust patient sampling and *in vitro* analysis was conducted.

In keeping with previous reports, we observed elevated systemic levels of VWF in patients with breast cancer compared to healthy controls.[111–113,156] In fact an incremental increase in plasma VWF:Ag was observed between patients with newly diagnosed early stage breast cancer versus patients with advanced stage metastatic disease. Of relevance all blood samples taken within these cohorts were done before chemotherapeutic treatment. This data lends credence to the hypothesis that VWF may be playing distinct roles at later stage metastatic disease. The biological mechanisms underpinning elevated VWF levels in cancer patients have not been fully defined however our recent work highlights a key role for VEGF-A secreted by breast tumour cells MDA-MB-231 and MCF-7 in triggering endothelial cell activation and VWF multimer release in vitro.[156] In keeping with our clinical data, VWF release was greatest in metastatic MDA-MB-231 cells which secrete high levels of VEGF-A.

We tracked patient survival against plasma VWF:Ag levels in both the CHAMPion and TuFClot cohorts. According to cancer research UK, 95% of women diagnosed with breast cancer survive for 1 year or more and 85% of women survive 5 years or more.[273] Perhaps it is unsurprising that no correlation between VWF:Ag levels and estimated predicted survival were found in the CHAMPion cohort due to the low frequency of mortality in this early stage group. Importantly, women diagnosed with late stage cancer have a markedly poorer prognosis with only 66% likely to survive beyond a year.[273] Our data showed that within the metastatic TuFClot cohort, VWF:Ag levels inversely correlated with 2 year survival. While patient plasma samples used for VWF:Ag measurement were taken before treatment, varying treatment options available to patients depending on performance status, cancer aggressiveness or other treatment related toxicities may have some effect on overall survival.

It is interesting to note that while elevated VWF:Ag levels have been reported in a number of cancer types (Table 1.1), data on the potential association with patient survival is limited to ovarian, glioblastoma and gastric cancers cohorts.[102–105] To date VWF:Ag levels have been

linked as a prognostic indicator of invasive breast cancer stage in recurrent cancer. [274] However, no report has measured VWF levels following chemotherapeutic treatment to assess whether VWF levels track with response to cancer treatment. Despite this VWF may play a prognostic role predicting beyond recurrence through quantifiable increases in the early onset of breast cancer.[274] Indeed, our novel findings suggest that plasma VWF levels can be a prognostic biomarker of interest in the setting of breast cancer and that it may be playing a role in breast cancer disease progression, beyond being an epiphenomenon of acute phase endothelial activation.

Of note, both chemotherapeutics and surgery are associated with inflammation and endothelial release of VWF, which should under our current hypothesis lead to greater cancer progression.[116,275] However, these increases in VWF levels are typically an acute phase response and will decrease rapidly following treatment. Furthermore, both surgery and chemotherapy act to reduce the total number of cancer cells. Therefore, with fewer cancer cells the ability of VWF to influence tumour cell metastasis would in turn be reduced. Secondly, there would be fewer cancer cells systemically increasing VWF, as such, it would be expected that plasma VWF:Ag levels would be reduced. It would be interesting to perform a longitudinal study of the VWF levels of patients throughout treatment to assess the relative shifts in VWF:Ag levels.

Using data available from the CHAMPion and TuFClot cohorts, correlations of existing procoagulant parameters were made against VWF:Ag levels. Despite previous studies reporting that TAT complex levels showed a strong association with poorer year 1 survival in both the CHAMPion and TuFClot cohorts, we observed no correlation between VWF:Ag and TAT complexes.[1,2] TAT complexes form covalently following thrombin generation and are thus a marker for sustained thrombin formation, a key step in secondary haemostasis, as well as a marker for the consumption of antithrombin. It is notable that thrombin has been shown to increase immune evasion, tumour growth and metastasis in specific cancer subtypes.[276,277] However, since plasma VWF levels are regarded as a marker of endothelial activation or dysfunction and contributes to primary haemostasis, it is perhaps unsurprising that VWF and TAT do not directly correlate with each other.[278] Nevertheless, these data indicate that coagulation activation and endothelial dysfunction are features in patients with metastatic breast cancer and may contribute to poorer clinical outcomes.[276,277]

Contrastingly, in both the CHAMPion and TuFClot cohort fibrinogen levels were found to directly correlate with plasma VWF:Ag. Fibrinogen is converted into an insoluble fibrin network, the final product of the haemostatic system, through the proteolytic effect of thrombin.[279] Although fibrinogen is an acute phase protein, hyperfibrinogenemia is increasingly recognized as an important risk factor influencing cancer development and outcome.[280–282] Fibrinogen is a large dimeric molecule with a number of integrin and non-integrin binding motifs which allow it to interact with various immune cells and also tumour cells directly.[283] Studies have revealed that fibrin(ogen) contributes to impeding immunosurveillance of NK-cells and thus promotes metastasis.[284] The observed novel correlation between plasma VWF:Ag and fibrinogen levels in both our early and metastatic breast cancer cohorts may suggest some shared mechanism through which both act in cancer settings. A recent study has observed that endothelial-derived VWF can accelerate fibrin clotting within engineered microvessels, although this appeared to occur in the absence of any direct interaction between VWF and fibrin(ogen).[285] Perhaps, VWF:Ag and fibrinogen levels correlate in our analysis due to shared roles in excessive clot formation or coagulopathy, reportedly induced by many tumour types.[286–288] Correspondingly, D-dimers, a degradation product of cross-linked fibrin that occurs during clot formation,[289] also significantly correlated with plasma VWF:Ag in the metastatic TuFClot cohort.

3.5.2 In vitro findings on the role of VWF in breast cancer

Several studies have reported that VWF may interact with tumour cells under both static and shear stress conditions.[168,187,190,239,240] However, to date this has not been robustly assessed in breast cancer, using cell lines of distinct molecular subtype. Notably, VWF adhered to breast cancer cells MDA-MB-231 and MCF-7 avidly, as well as to immortalised MCF-10A cells to a lesser extent. Importantly, VWF displayed negligible binding with control non-neoplastic primary mammary epithelial cells (HMEC).

Critically, the addition of ristocetin significantly enhanced VWF binding to both MDA-MB-231 and MCF-7 breast cancer cells. Ristocetin modulates the VWF A-domain structure by binding two sites flanking the VWF A1 domain Cys1237–Pro1251 and Glu1463–Asp1472 resulting in allosteric conformational unfolding of the cryptic GPIb binding region within A1 domain of VWF.[256] This mimics the effect of shear stress *in vivo* and allows platelet-VWF interactions.[290] More recently, ristocetin has also been reported to enhance ADAMST13 proteolysis of VWF

in vitro, highlighting that the conformational unfolding may not be limited to just the A1 domain but also the A2 domain. [256] As such, our data suggests that while limited binding between VWF and breast tumour cells can occur in the absence of ristocetin perhaps via a non-cryptic VWF binding site, the significant increase in binding following addition of ristocetin may point to a key binding site within the VWF A1-A2 region which become exposed after unwinding of the globular VWF structure. This interaction may be of particular importance *in vivo* whereby the presence of shear stress would be permissive for breast tumour cell-VWF interactions within the vasculature, and in particular newly secreted endothelial tethered VWF which experiences high tensile forces.

As described, adhesion to VWF has been shown both statically and under fluidic stress in a variety of tumour types including melanoma, breast, gastric and colonic cells.[168,183,190,204,239,240,291,292] In mouse melanoma B16-BL6 cells, adhesion to recombinant VWF was shown to occur independent of ristocetin and shear stress.[190] However, VWF-tumour cell adhesion in other studies have been shown to occur both in conjunction with platelets and directly when under flow.[118,168,187,239] For example, in BGC823 gastric cancer cells perfused over surface bound platelets the addition of recombinant VWF more than doubled the total adherent cells over a 60 minute interval.[118] Moreover, anti-VWF antibody treatment halved the baseline adhesion of the gastric cancer cell adhesion. It is unclear whether shear stress is a requirement in the adhesion of tumour cells to VWF as different tumour receptors may likely target unique regions or epitopes of VWF, some of which may be readily accessible within its structure in the absence of shear stress.

Our data highlights that adhesion of VWF to breast cells was found to be dependent on calcium ion supplementation. This is in agreement with findings by Terraube *et al* who reported that VWF binding to murine B16-Bl6 melanoma cells was dependent on divalent Mn^{2+} ions.[190] However, this contrasts the effects seen in human M21 melanoma cells where the use of physiological concentrations of Ca^{2+} reduced $\alpha_v\beta_3$ receptor mediated tumour cell arrest to VWF.[239] Importantly, calcium concentrations used in our assay are within the physiological range of blood calcium levels, suggesting the circulating breast tumour cells may be capable of interacting with VWF *in vivo*.[293] A variety of integrins are known to be regulated by divalent cations, resulting in conformational changes of integrins into their active state.[294] These findings may point to an important role for integrins in contributing to VWF-breast

tumour interactions. Further specific studies on key breast tumour receptors of interest in mediating VWF adhesion are assessed and characterised in the next chapter.

Notwithstanding this, we observed a significant role for LMWH in inhibiting VWF-breast tumour interactions. Structural studies of VWF have described two heparin binding domains within the A-domains of VWF.[295] Furthermore, LMWH has been described to interact with the GPIb binding region within the A-domain of VWF and thereby inhibit subsequent platelet interactions.[205] This inhibitory effect of LMWH would be in keeping with our hypothesis for a key VWF tumour binding motif within the A1 domain or indeed flanking regions within VWF. However, currently our results are unable to delineate whether LMWH inhibits breast tumour cell adhesion to VWF through interaction with the VWF and the A-domains directly, or interaction with the breast tumour cells via as of yet unidentified heparin-sensitive receptor or perhaps through both mechanisms.

Importantly, LMWH is a widely used thromboprophylaxis agent for the treatment and management of cancer associated thrombosis.[296] Early clinical studies assessing its use in patients pointed to a potential long-term survival benefit in a small group of cancer patients with good prognosis on enrolment.[193,194] In support of this, several pre-clinical studies have now indeed demonstrated anti-metastatic properties of LMWH in tumour models, including breast cancer.[297–299] It is important to note that while anti-metastatic roles have been attributed to LMWH in these pre-clinical studies, the concentrations used in these studies are in excess of therapeutic dosing and may not be fully representative of clinical results. However, despite the biological mechanisms remaining poorly defined, it is possible that the VWF-tumour interactions may represent a novel anti-metastatic target of LMWH.

Previous studies have revealed that VWF mediated adhesion to the endothelium, as reported in malignant glioma, osteosarcoma, LLC and melanoma cells could enhance cellular transendothelial migration.[243,300] Similarly, our results showed that VWF assisted MDA-MB-231 adhesion to the endothelium. These results imply a potential advantage for circulating breast tumour cells to accumulate VWF from the circulation in order to adhere to the endothelial layer of the vascular wall. While the receptor basis for enhanced endothelial adhesion remains to be determined in this context, previous studies have reported that VWF can self-associate along the endothelium but also directly bind specific endothelial receptors including αvβ3.[262,301] Conversely, the accumulation of plasma VWF on surface of melanoma

tumour cells *in vitro* has been described to attenuate tumour binding to the endothelium.[240] Using single molecular force spectroscopy, the authors propose that VWF binding to heparan sulphate chains on melanoma cells promoted the repulsion of circulating tumour cells from the blood vessel wall to counteract metastasis. The receptors involved in VWF-tumour adhesion are clearly a decisive element in the subsequent effects on tumour cell biology, including perhaps endothelial adhesion. This will be further examined in data presented in the next chapter.

Notwithstanding these apparent paradoxical roles for tumour bound VWF, there is significant clearer evidence for the role of endothelial VWF multimers tethering circulating cells and contributing to their extravasation. A previous report has shown that immobilised VWF could cause cellular arrest of M21 melanoma cells that were under dynamic flow conditions.[239] Similarly, our recent findings, define a novel role for breast tumour cell secreted VEGF-A in inducing the release of VWF multimers from endothelial cells *in vitro*.[156] These adhesive multimers have been described to tether circulating platelets, erythrocytes and immune cells.[167,302,303] Our findings now demonstrate for the first time that VWF multimers released from activated endothelial cells can also bind circulating breast tumour cells in a platelet-independent manner under shear stress. Activation of an endothelial monolayer promotes the release of VWF multimers resulted in enhanced adhesion of MDA-MB-231 breast cancer cells to the endothelium. The dependence of VWF was confirmed using an anti-VWF treatment which ablated MDA-MB-231-endothelial attachment. These data provide evidence of VWF as a novel adhesive mediator for triple negative breast tumour-endothelial interactions. Interestingly, galectin-3 expressed on activated endothelium has also been reported to facilitate adhesion of breast cancer cells via interaction with tumour-associated Thomsen-Friedenreich antigen.[304,305] Galectin-3 is known to be complexed with VWF within WPB of the endothelium, and co-localises along VWF multimer strings released from stimulated EC.[306] Further studies may be warranted to examine the contribution of galectin-3-VWF complex in tethering circulating breast tumour cells.

Of note, a limitation of using PMA in our assays to induce endothelial activation and subsequent release of VWF may is that it may result in the further upregulation of cell adhesion factors on the endothelial layer. Upregulation of other adhesion molecules that are distinct from VWF could make the endothelial cells more adherent to the circulating breast

cancer cells. However, work from our group has determined that VEGF-A another endothelial activator also shown to induce VWF release caused similar levels of breast tumour binding in our perfusion assay.[156] Furthermore, unpublished work determined that stained VWF multimers induced by PMA stimulation directly interacted with circulating breast cancer cells under fluidic stress.

Congruent to our previous data LMWH treatment prevented MDA-MB-231 adhesion to endothelial associated-VWF. Of further interest, in the presence of LMWH small numbers of MDA-MB-231 cells were still able to adhere to the endothelial layer at the same rate $K_{[on]}$ however they detached at a greater rate ($K_{[off]}$) than the untreated cells. This could indicate a two-step process in VWF-mediated breast tumour cell adhesion, where multiple receptors are used to facilitate initial transient tethering followed by firm VWF adhesion.[261] In concordance with this, work by Feinauer *et al*. demonstrated that LMWH treatment in a brain metastasis model reduced tumour induced clot formation in Jimt1 breast cancer cells and A2058 and H1 melanoma cells. Subsequently, the LMWH treatment was able to significantly reduce the number of arrested Jimt1 breast cancer cells in the brain.

Similar observations has been reported for VWF-leukocyte interactions under shear stress that facilitate leukocyte diapedesis. Endothelial released VWF has been shown to modulate leukocyte recruitment, adhesion and extravasation under conditions of shear stress, providing a novel link between inflammatory pathways and thrombosis.[147,167] The ability of VWF to directly adhere breast cancer cells in to the endothelial layer in a manner representative of leukocyte adhesion could suggest that MDA-MB-231 breast cancer cells can utilise similar pathways as leukocytes to transmigrate through the endothelium. Of particular note, work by Aymé *et al* identified that by targeting the A1 domain of VWF, leukocyte recruitment and VWF-mediated vascular permeability were attenuated.[173] Together, we hypothesize that VWF multimer strings released from the endothelium due to breast tumour cell activation may promote tumour cell attachment perhaps with a particularly important role for the VWF-A1 domain in mediating this binding.

In summary, our results demonstrate that patients with breast cancer have elevated plasma levels of VWF and in particular patients with metastatic disease have the highest levels which correlate inversely with survival. We report for the first time on the characterisation of breast tumour-VWF interactions under both static and shear stress conditions and importantly, our

data that shows VWF released from activated endothelial cells can directly bind circulating MDA-MB-231 breast cancer cells, promoting their endothelial adhesion. This may be of particular importance in the context of development of the early metastatic niche whereby disseminating breast tumour cells undergo blood borne metastatic and extravasate from the vasculature to colonise distal tissues.

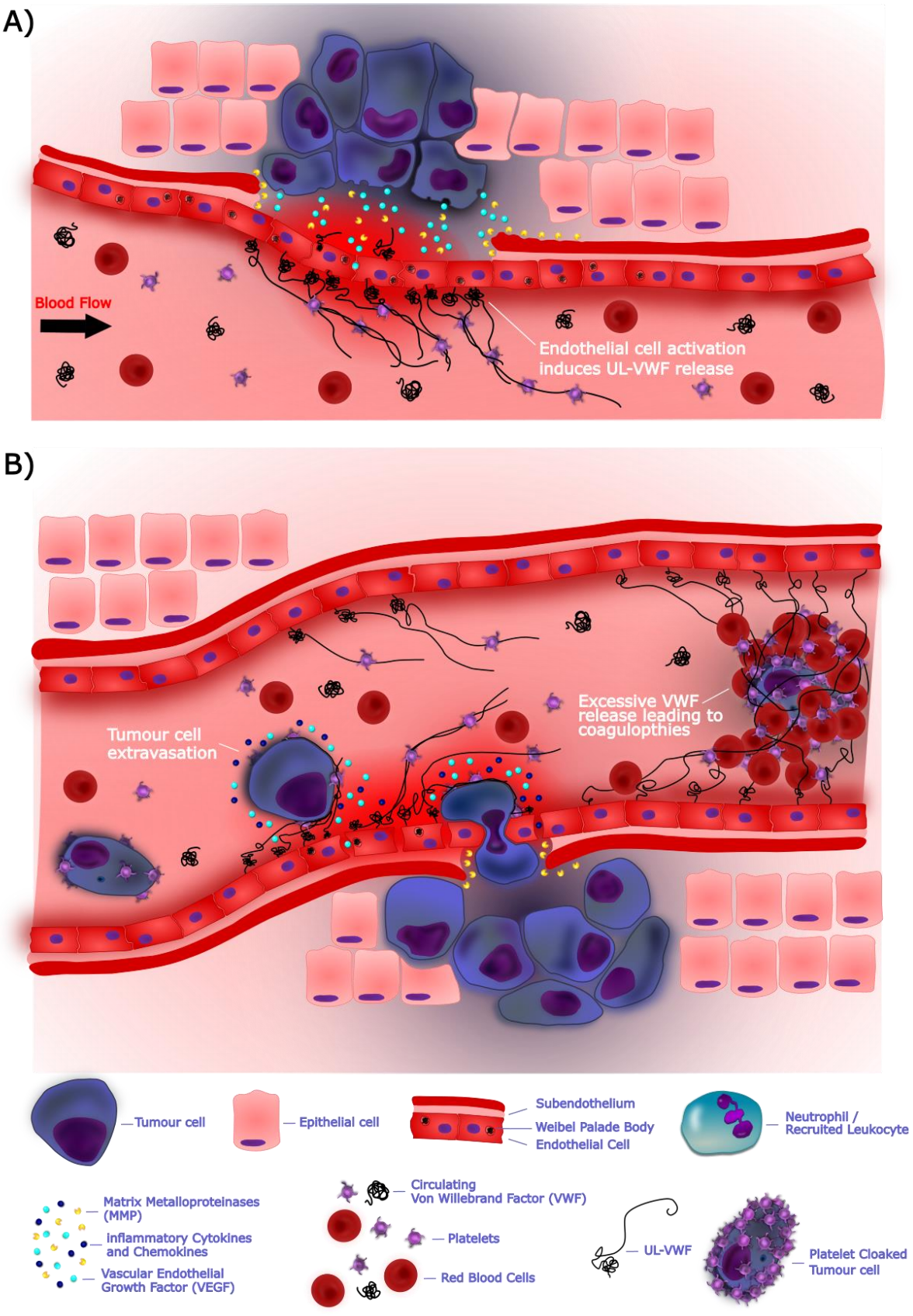
A)
Blood Flow
Endothelial cell activation
induces UL-VWF release
B)
Tumour cell
extravasation
Excessive VWF
release leading to
coagulopthies
Tumour cell
Epithelial cell
Subendothelium
Weibel Palade Body
Endothelial Cell
Neutrophil /
Recruited Leukocyte
Matrix Metalloproteinases
(MMP)
Inflammatory Cytokines
and Chemokines
Vascular Endothelial
Growth Factor (VEGF)
Circulating
Von Willebrand Factor (VWF)
Platelets
Red Blood Cells
UL-VWF
Platelet Cloaked
Tumour cell

Figure 3.18 Elevated VWF in breast cancer: **A)** Upon the onset of cancer development plasmatic VWF:Ag levels begin to elevate beyond those of healthy patients, in a mechanism believed to be induced by tumour cell activation of the endothelium. The levels of systemic VWF:Ag are gradually elevated and correspond with breast tumour progression, with higher VWF:Ag levels strongly associated with mortality. **B)** The highly elevated plasma VWF:Ag representative of metastatic tumours correlate with the upregulation of other haemostatic factors like fibrin and D-dimer, collectively contributing to the enhanced thrombotic events, like venous thromboembolism described in patients with cancer. Additionally, activated endothelial cells with anchored VWF strings can adhere to the circulating breast cancer cells as they disseminate through the blood, where it is thought that VWF may be able to promote metastasis and migration in tumour cells attached to the endothelium.

Chapter 4: Investigating the role of breast tumour receptors in mediating VWF adhesion.

4.0 Introduction

4.0.1 Understanding the adhesive capabilities of VWF

VWF is a multidomain protein capable of interacting with several ligands including collagens, FVIII as well as a diverse array of endothelial and platelet adhesion receptors and integrins such as P-selectin, $\alpha_{iib}\beta_3$, $\alpha_v\beta_3$ and GPIbα, all of which are key in mediating its role in haemostasis.[16,30,31,307–309] Within the circulation, VWF exists in a globular configuration, with both the platelet binding site, GPIbα in the A1 domain, and the ADAMTS13 cleavage site in the A2 domain remaining cryptic or non-exposed.[18,19,260,310] However, upon vessel damage, VWF is tethered to exposed collagens on the sub-endothelial vessel wall and subject to increased shear stress triggering the VWF multimers to adopt an elongated structure, exposing the GPIbα binding site within the A1 domain.[311,312] This conformationally active VWF is perfectly suited to anchor flowing platelets and thereby enable primary haemostasis. Moreover, the tensile stress of attached platelets subsequently assists ADAMTS13 proteolysis of VWF multimers, likely associated with exposure of the cryptic ADAMTS13 cleavage site within the A2 domain.[313] This serves to limit the haemostatic activity of VWF and prevent excessive thrombi formation.

However, more recently, this conformational activation of VWF A-domains has also been highlighted as a key regulatory feature of its interaction with other receptors and ligands including low density lipoprotein related protein-1 (LRP1), P-selectin glycoprotein ligand-1 (PSGL-1) and β2 integrins on leukocytes.[222,261,314] While a variety of receptors can interact with the specific regions of VWF due to shear stress exposure of the A-domains, many other interactions have been described in the N-terminal D'-D3 regions as well as the C-terminal A3-CK domains within the multimerised dimeric bouquet crystal structure that has been described for VWF.[9] For example, FVIII adheres to the D'D3 domain of VWF that is accessible independent of shear induced unfolding.[16] Furthermore, VWF-monocyte binding occurs via two Leucine-Leucine-Glycine (LLG) motifs within the D3 and A2 domains proposed to be consensus integrin binding sequences.[315] Additionally, VWF-murine melanoma tumour cell interactions are hypothesized to be mediated via an RGD sequence located in the C4-domains of VWF.[15,190,316]

A key feature of newly secreted VWF is its ability to tether cells to the endothelial layer utilizing the multiple binding sites along its large structure. This role is essential in mediating

primary haemostasis where endothelial insult or damage results in the release of VWF from WPB as UL-VWF multimers.[76] Released VWF multimers have been proposed to be anchored to the endothelium through either $\alpha_v\beta_3$ or P-selectin clusters on the endothelial surface.[307,317] Exposure to the fluidic shear stress of the blood promotes these VWF multimer strings to unwind.[260] Interestingly however, only a subset of about one third of endothelial associated VWF strings are found to become platelet decorated under varying shear stresses, highlighting, as of yet, unknown further regulatory mechanisms for VWF-platelet tethering.[262]

In a systematic review of the interactions between endothelial associated VWF and circulating cells, including leukocytes and erythrocytes, it was found that the majority of these interactions require exposure of the VWF A1-domain to high shear conditions.[303] Furthermore, while these interactions with endothelial VWF can occur directly or indirectly, almost all were dependent on the presence of platelets, highlighting platelet-decorated VWF multimers as a key adhesive platform for circulating cells along the endothelium. More specifically, endothelial released VWF has been described to bind red blood cells (RBCs), sickle cell disease RBCs, malaria-infected RBCs, neutrophils, monocytes and T and B cells through platelet-dependent mechanisms. [147,167,261,302,303,318,319] Although, the biological role of these adhesive events is not fully elucidated, under pathophysiological conditions such as sickle cell disease and malaria, VWF tethering of RBCs was found to contribute to sequestration and potential vessel occlusion.[261,302] Moreover, adhesion of immune cells to endothelial released VWF increases immune cell diapedesis across the endothelial layer.[147,167,172] Altogether, these extensive binding sites along its structure make VWF a prominent intermediate molecule in modulating cellular adhesion within the circulation (Figure 4.1). Growing evidence now also indicates that in the setting of cancer, VWF may bridge tumour cells to the endothelium both with the help of platelets via heteroaggregate formation and through direct tumour adhesion.[143,156]

4.0.2 VWF-platelet heteroaggregate adhesion of cancer cells

A plethora of functions have been ascribed to platelets in promoting tumour metastasis, where platelet aggregates can cloak circulating tumours to prevent immune detection as well as aiding cellular tethering to the endothelium.[242] Strikingly, platelet-tumour cell clusters may be mediated by the intermediary activity of VWF that can link multiple platelets to a tumour cell in heteroaggregate formations.[143,320]

The functional mechanisms behind platelet-VWF-tumour cell generation of heteroaggregates in cancer is not fully understood. However, as the primary receptor for initial VWF-platelet interactions, GPIbα is a compelling target in heteroaggregate formation and metastasis, especially since GPIbα has been reported to express on some cancer cells.[187,241,321,322] In a model of murine LLC, experimental metastasis targeting the GPIbα-VWF axis with antibody treatment reduced platelet aggregation by around 60%, and decreased surface pulmonary nodules in a metastatic *in vivo* model.[184] Similarly, an anti-GPIbα antibody with an epitope specifically targeting the VWF binding site of GPIbα also significantly reduced pulmonary metastasis in a murine model of human breast cancer. Of note, this resulted in a reduction of not only platelet aggregation to tumour cells but also tumour cell interaction with endothelial cells. Concordantly, in an *in vitro* assessment of colon tumour cells, polyclonal anti-VWF antibody treatment reduced platelet adhesion of CT26 and HCT8 colon cancer cells 75% and 81% respectively, indicating that platelet adhesion to tumour cells is strongly regulated by VWF.[189] These data highlight a role for platelet-VWF-tumour cell interactions and heteroaggregate formation, and in particular with the GPIbα-VWF axis, in contributing to metastasis.

Strikingly, the GPIbα receptor is not only expressed on platelets but has also been reported to express directly by specific tumour cells including on the surface of breast cancer cell, MCF-7.[187,188] Furthermore, these pseudo-GPIbα variants acted in a functionally distinct manner from platelet GPIbα, not requiring shear stresses to induce VWF adhesion and platelet aggregation.[187] Through adhesion of GPIbα on the platelet surface or direct expression by tumour cells, VWF may mediate tumour cell heteroaggregate formation. These heteroaggregates confer a metastatic advantage with platelets thought to cloak circulating cells but also potentially enabling endothelial attachment under fluidic shear stresses.[186] Collectively, as one of the primary ligands for GPIbα, multimeric VWF may be able to adhere to circulating tumour cells and facilitate the pro-metastatic heteroaggregate formation by bridging platelets and tumour cells at multiple binding sites along its multimeric structure.

However, the VWF-GPIbα interaction is not the sole mediator of platelet-VWF-cancer cell heteroaggregation. Work by Oleksowicz *et al*. found that MCF-7 breast cancer cell induced platelet heteroaggregation was reduced using a number of blocking agents.[204] Critically, it was found that while inhibiting GPIbα reduced heteroaggregation, the greatest effect was found

by blocking GPIbα in conjunction with VWF, indicating that VWF is mediating this effect both dependently and independently of GPIbα. Accordingly, VWF overlaid on a surface immobilised platelet layer firmly adhered LS174T colon cancer cells under dynamic flow conditions, while conversely, an overlaid fibrinogen layer had no effect.[183] Interestingly, using the same anchored platelet layer flow system with COLO205 colon cancer cells, overlaid VWF was once again responsible for firm adhesion of the tumour cells. Notably, COLO205 tethering to the VWF-platelet complex was initiated with platelet P-selectin.[183] Interestingly, VWF-mediated $\alpha_{iib}\beta_3$ upregulation on the platelet surface also promoted heteroaggregation of fibrosarcoma HT-1080 cancer cells.[323]

Our recently published work describes novel mechanisms through which platelets and tumour cells cumulatively stimulate the endothelium to induce VWF release.[156] Enhanced platelet-tumour cell mediated VWF release resulted in an increase in the adherence of tumour cells directly to the endothelial layer.[156] Altogether these data highlight that VWF may facilitate indirect adhesion of tumour cells through the use of platelet GPIbα and by upregulating the expression of other platelets receptors. However, VWF may also be able to directly adhere to cancer cells where it can act as a nucleation point to enhance platelet adhesion and subsequently promote metastasis through heteroaggregation and other mechanisms.

4.0.3 Direct interaction of VWF and tumour cells.

Interestingly, independent from platelets, VWF has been described to directly adhere to tumour cells. Neirodzik *et al*. determined that HM29 melanoma cells as well as HCT8 and CT26 colon cancer cells could adhere directly to VWF-coated microtitre plates.[292] Tumour adhesion in this assay was inhibited by treating with an anti-VWF antibody confirming specificity of the interaction.

A variety of integrins are highly expressed on tumour cells and are known to interact directly with VWF in particular via the RGD binding motif within the C domains of VWF.[308] In fact, integrin expression is an important factor in the metastatic potential of a cancer cell, for example, a subset of MDA-MB-451 breast cells exhibited a more aggressive metastatic phenotype when stably expressing $\alpha_v\beta_3$ on their surface, proposed to result from activated $\alpha_v\beta_3$ on tumour cells supporting their arrest to the endothelium.[324] Carlson *et al*. proposed that $\alpha_v\beta_3$ integrin in conjunction with VWF promotes survival and dissemination of breast

tumour cells. Specifically, $\alpha_v\beta_3$ expression allowed direct interaction with VWF at the perivascular niche and conferred a chemoresistant phenotype in disseminated breast tumour cells by affixing the tumour cells to the perivascular cells *in vivo*.[291] Moreover, in a static adhesion model, VWF binding to BL16/BL6 melanoma cancer cells could be inhibited 65% with an antibody against the β_3 integrin subunit.[190] Correspondingly, Pilch and colleagues were able to inhibit VWF mediated M21 cellular adhesion by blocking $\alpha_v\beta_3$ integrins under perfusion, with the authors postulating that the $\alpha_v\beta_3$-VWF interaction may promote metastasis through tumour cell arrest and colonisation.[239]

In contrast to these pro-metastatic and pro-survival functions of tumour $\alpha_v\beta_3$-VWF interactions, other studies have described a pro-apoptotic role for VWF.[101,255] Interestingly, it was found in a host of tumour cells (MCF-7, 769P and HepG2) that VWF signalling through $\alpha_v\beta_3$ resulted in increased apoptosis.[101] Notably, VWF has also been shown to induce apoptosis and subsequently cell death in B16/BL6 melanoma cells that had previously been identified to adhere to VWF through the $\alpha_v\beta_3$ receptor.[255]

In addition to integrins, other adhesive receptors have also been identified in mediating direct VWF-tumour cell interactions. In an experiment using colon cancer cells, VWF-mediated adhesion of tumour cells to HUVEC was not inhibited by targeting a variety of integrin subunits including α_{iib}-, β_1- and β_3.[168] This indicates that other tumour receptor(s) may be key in facilitating adhesion of the HRT-18 colon cancer cell line to endothelial VWF. Recently, it has been reported that expression of heparan sulphate a highly negatively charged glycosaminoglycan on the surface of melanoma cell lines MV3, IGR37 and B16F10 was directly proportional to the ability of these tumour cells to bind VWF *in vitro*.[240] Additionally, siRNA knockdown of heparanase in B16F10 cells, known to cleave heparin sulphate showed a slight increase in the ability of VWF to adhere. Notably, by using a recombinant VWF fragment with the A1-domain deleted the authors proposed heparan sulphate mediated adhesion of melanoma tumour cells to VWF occurred through the A1 domain. Contradictory to other reports, atomic force microscopy discerned that this tumour heparan sulphate-VWF complex showed strong repulsive forces for subsequent melanoma tumour-endothelial adhesion and resulted in reduced metastasis in an experimental murine model of melanoma.[240]

Cumulatively the literature suggests that VWF can interact both indirectly with tumour cells via platelets but also directly through a diverse array of receptors. Moreover, the functional

consequences of these interactions are varied and are likely receptor dependent and cancer type specific. Therefore, after determining that VWF can preferentially bind to breast cancer cells we aim to identify the key VWF domains that interact with breast cancer cells. Furthermore, a targeted approach of assessing the expression of receptors previously described to adhere to VWF on breast cancer cells will inform us of potential receptor candidates in VWF-breast cancer interaction. Thus understanding the key receptors involved in mediating VWF-breast tumour cell binding will be key in delineating the downstream functional effects of this novel binding interaction.

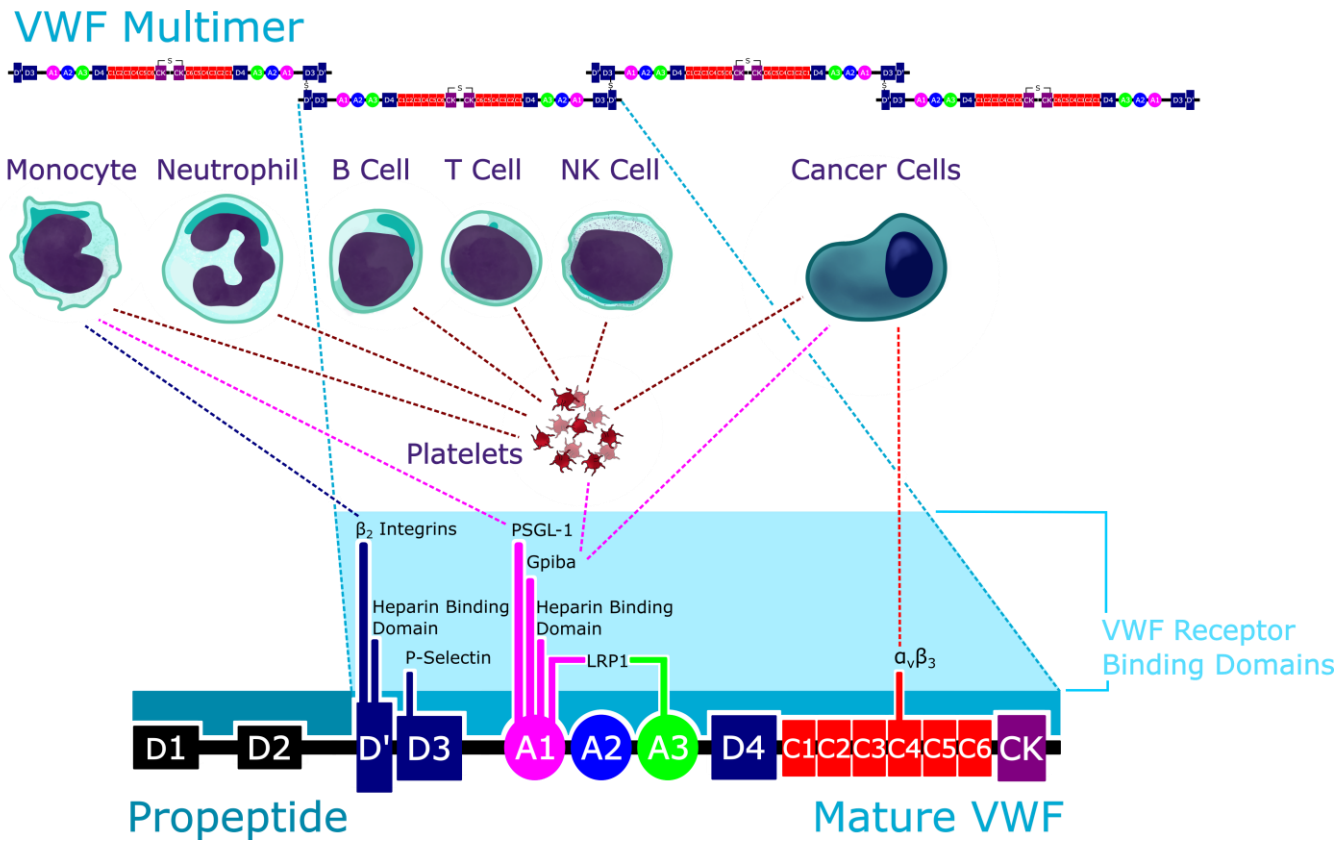

Figure 4.1 The multiple binding partners of the multimeric VWF structure: VWF is a multidomain protein capable of interacting with many receptors due to the diverse binding regions along its surface. The concatenated nature of VWF facilitates its function as an intermediary link between multiple cell types where it is thereby capable of indirectly enabling platelet mediated adhesion to circulating immune cells (monocytes, neutrophils, B Cells, T Cells and NK cells) as well as directly bridging endothelial cells to circulating cells.[147,167,172,261,302,303,318,319] Of note, due to its repeating multimeric structure VWF is capable of bridging two receptors that adhere to the same VWF domain together through the other exposed domains further along its structure, including two of the same receptor type if necessary as seen in platelet decorated VWF string structures.[89,262] VWF has been reported to mediate direct endothelial-tumour cell interactions as well as indirect platelet-VWF-tumour heteroaggregate formations.[143,156,187,239]

4.1 Characterising specific VWF domains is important in regulating binding to breast tumour cells

4.1.1 MDA-MB-231 breast cancer cell adhesion to truncated VWF domain fragments

As discussed above, VWF is composed of a multitude of distinct domains that contribute to its haemostatic properties with the vessel wall but also its cellular adhesive properties with erythrocytes, immune cells and tumour cells within the circulation (Figure 4.1). Specifically, VWF domains are arranged in this order: D1-D2-D'-D3-A1-A2-A3-D4-B1-B2-B3-C1-C2-C3-C4-C5-C6-CK, where the D1-D2 domains, which comprise the VWF propeptide are cleaved during post-translational processing but are co-released with the mature protein (D'-CK) into the circulation.[14] To characterise the regions of VWF involved in mediating adhesion to breast cancer cells, a variety of truncated VWF fragments (D'A3, A1A2A3 and A3-CK, Figure 4.2 A) were generated. Direct binding of these VWF fragments to both MDA-MB-231 cells and MCF-7 cells was assessed by flow cytometry.

The binding profiles of each VWF domain to breast tumour cells was detected using a specific anti-Histidine fluorescently labelled antibody, thus allowing a direct comparison between each of the HIS-tagged VWF fragments (Figure 4.2). We observed that the D'A3 region had the most marked increase in adhesion with MDA-MB-231 cells with a 2 fold change in MFI from normalised values (Figure 4.2 B+C). Although both the A1A2A3 and A3-CK domain fragments could also mediate binding to MDA-MB-231 cells, the relative contribution of these domains was significantly less than the N-terminal VWF fragment consisting of D'A3. The data suggests that VWF is able to adhere to MDA-MB-231 cells perhaps via multiple binding regions but with a key binding site localised within the D'A3 domains.

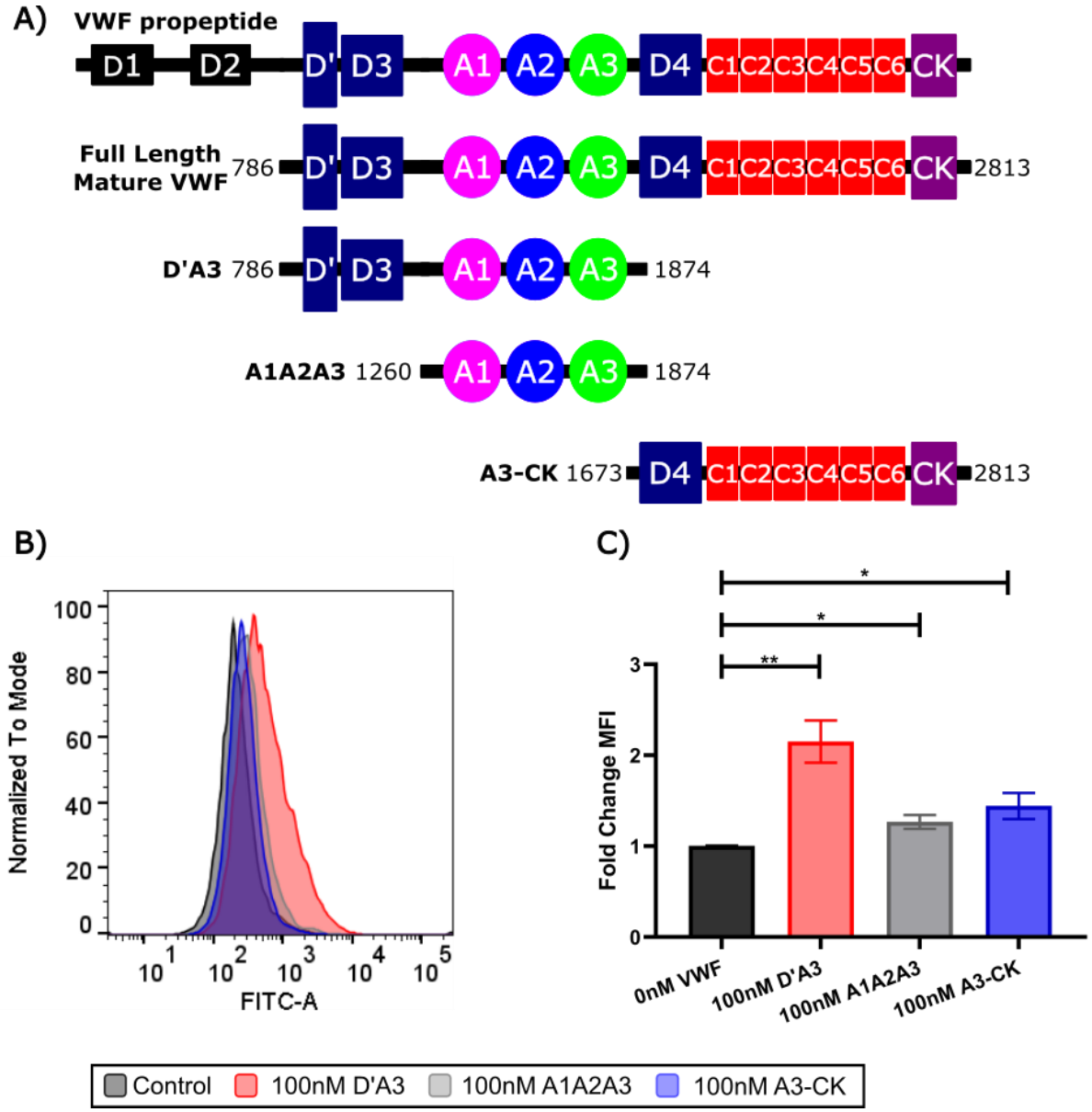

Figure 4.2 Assessing MDA-MB-231 adhesion to truncated VWF domains: MDA-MB-231 cell adhesion to recombinant truncated VWF domains (N=4) were assessed under static conditions by flow cytometry. A) Representative flow cytometry histogram of cells treated with 100nM concentration of each truncated VWF fragment + ristocetin for all fragments. **B)** Fold change in MFI values from VWF fragment adhesion to MDA-MB-231 cells were normalised against untreated stained controls and graphed ± SEM. Significance was determined through student t-test against the normalised control test * $p \leq 0.05$, ** $p \leq 0.01$.

4.1.2 MCF-7 breast cancer cell adhesion to truncated VWF domain fragments

Adhesion of VWF truncated domains was also performed with breast cancer cell line MCF-7. Similarly to our findings with MDA-MB-231 cells, we observed that D'A3 was the primary binding domain of VWF to MCF-7 cells (Figure 4.3). In contrast however, the A1A2A3 domain had no significant binding with the MCF-7 cells while the A3-CK domain displayed a very small ability to adhere to MCF-7 cells. Altogether, the D'A3 region of VWF was found to adhere to both breast cancer cells with a greater avidity than other VWF fragments spanning the mature protein.

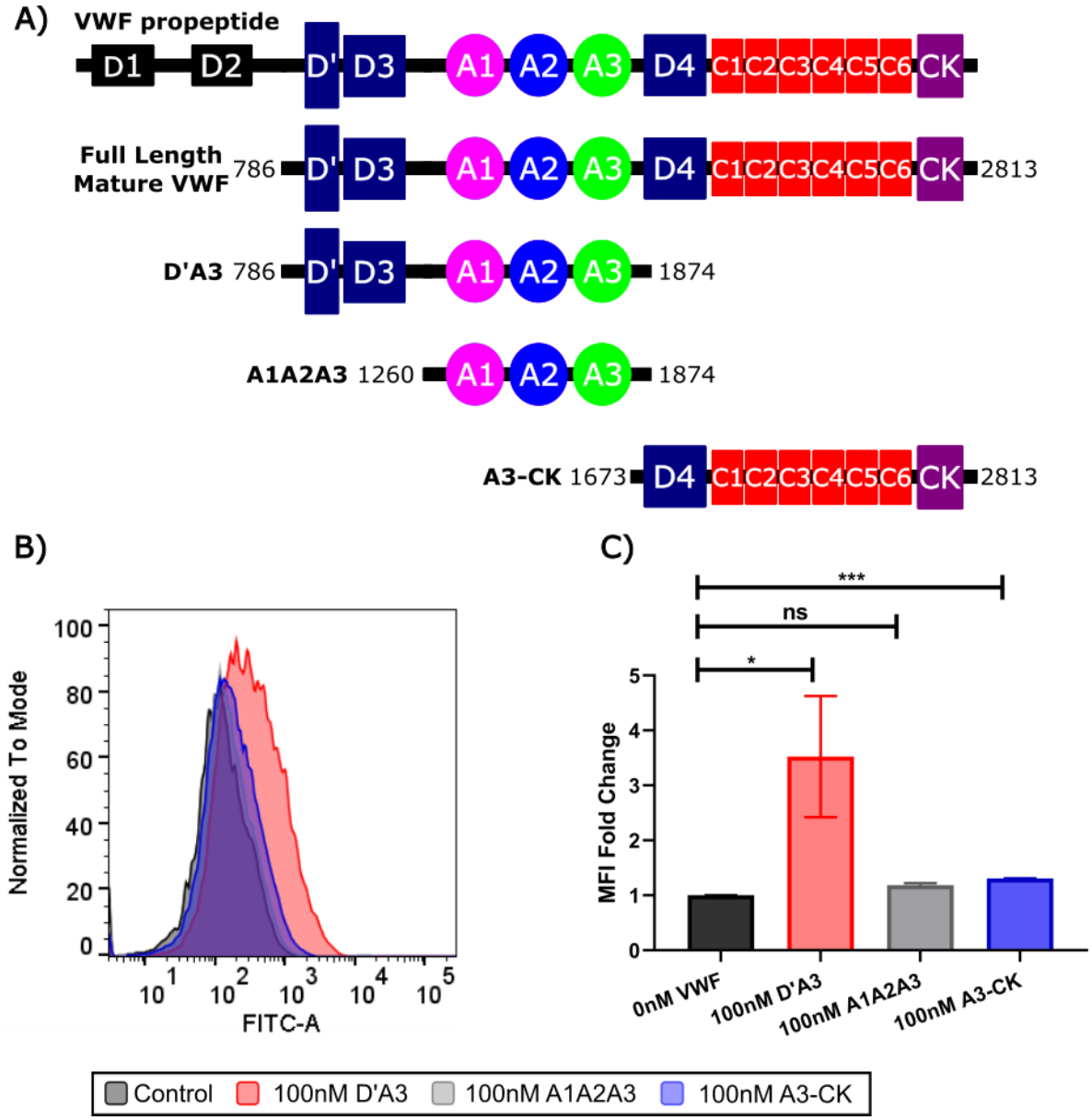

Figure 4.3 Assessing MCF-7 adhesion to truncated VWF domains: MCF-7 cell adhesion to recombinant truncated VWF domains (N=3) were assessed under static conditions by flow cytometry. A) Representative flow cytometry histogram of cells treated with 100nM concentration of each truncated VWF fragment. **B)** Fold change in MFI values from VWF fragment adhesion to MCF-7 cells were normalised against untreated stained controls and graphed ± SEM. Significance was determined through student t-test against the normalised control test* $p \leq 0.05$, *** $p \leq 0.001$.

4.2 Differential receptor expression on MCF-7 and MDA-MB-231 cells

4.2.1 P-selectin glycoprotein ligand 1 expression on MCF-7 and MDA-MB-231 cells

As discussed above, VWF has a diverse array of receptor partners it can interact with in a number of settings from normal haemostasis to pathological disease including inflammation, malaria, sickle cell disease and cancer.[303,325] After isolating the D'A3 region of VWF as the predominant interactive site for VWF with both MDA-MB-231 and MCF-7 cells we sought to characterise breast tumour expression of a number of key receptors known to adhere to VWF via this region. We thus generated a list of potential candidates to challenge VWF-breast cancer adhesion. PSGL-1, has been identified as an adhesion partner for the A1-domain of VWF for the adhesion to leukocytes facilitating both rolling and stable adhesion of leukocytes under flow.[261] On assessing its expression on breast tumour cells, we observed PSGL-1 was exclusively expressed on the surface of MDA-MB-231 cells with a 2-fold increase in MFI detected using an anti-PSGL-1 antibody compared to an isotype control (Figure 4.4). No expression of this candidate receptor was observed on MCF-7 cells.

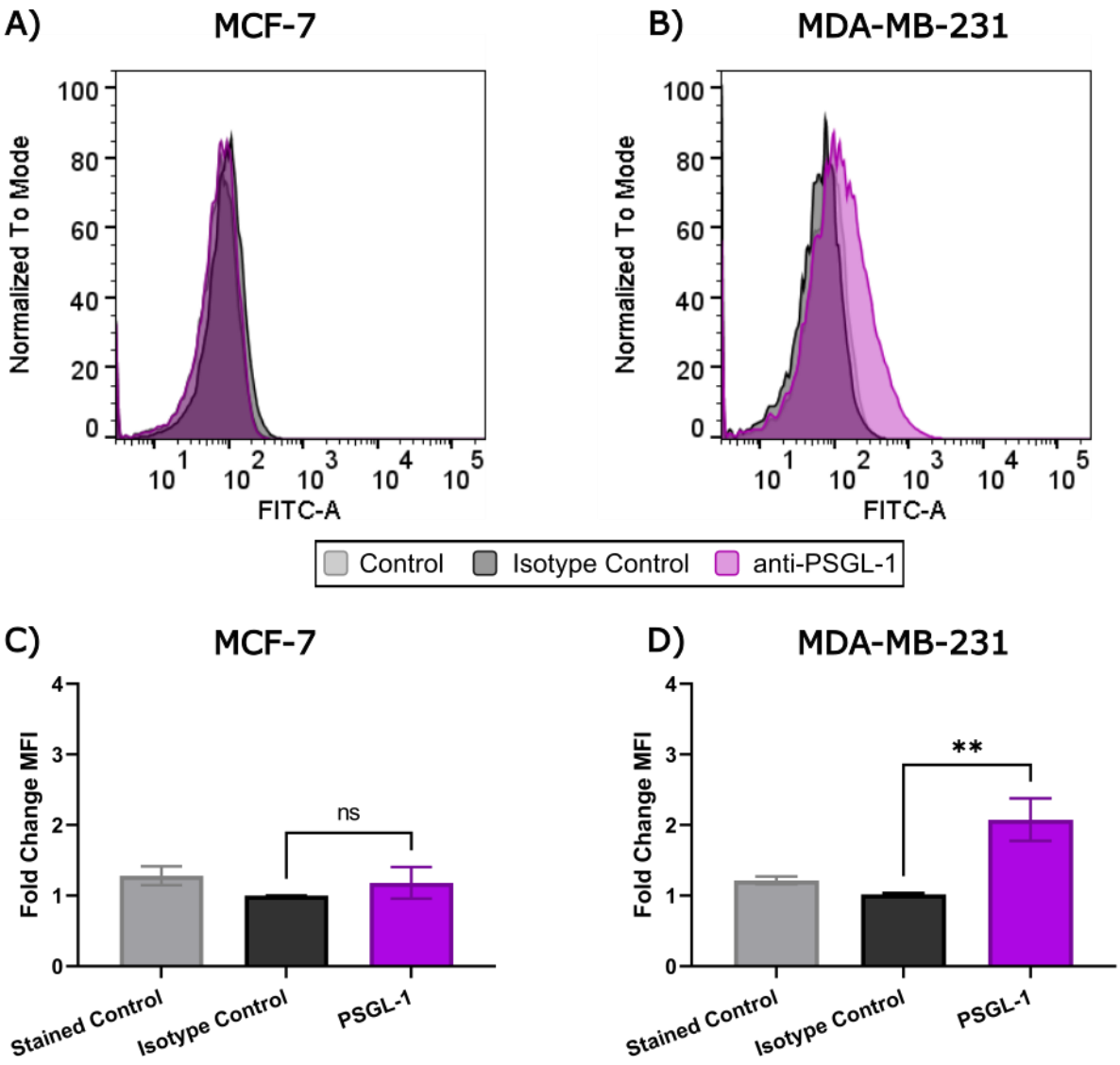

Figure 4.4 PSGL-1 surface expression on MCF-7 and MDA-MB-231 breast cancer cells: Breast tumour cell surface expression of PSGL-1 was measured (N=5) with an anti-PSGL-1 detection antibody along with an isotype control antibody. Expression of the PSGL-1 receptor was displayed in representative histograms for **A)** MCF-7 and **B)** MDA-MB-231 cells. Fold changes in MFI values for PSGL-1 expression were normalised against isotype controls and compiled into graphs ± SEM **C)** MCF-7 and **D)** MDA-MB-231 cells. Significance between treatment conditions were calculated by student t-test ** $p \leq 0.01$.

4.2.2 P-selectin expression on MCF-7 and MDA-MB-231 cells

P-selectin and VWF have been described to interact, both proteins are co-packaged within WPB in endothelial cells as well as α-granules in platelets. Upon WPB exocytosis P-selectin clusters on endothelial cells have been described to anchor VWF along the endothelial cell surface under flow in a calcium dependent manner, allowing for VWF string formation.[307,317] P-selectin adhesion to VWF within WPB appears to occur through the D'D3-domain of VWF and luminal domain of P-selectin.[326] Under our assays conditions, neither MDA-MB-231 cells nor MCF-7 cells expressed P-selectin. The fold change in MFI was not significantly different from matched isotype control in both MDA-MB-231 (MFI 0.98 ± 0.006) and MCF-7 cell lines (MFI 1.0 ± 0.05), respectively, (Figure 4.5).

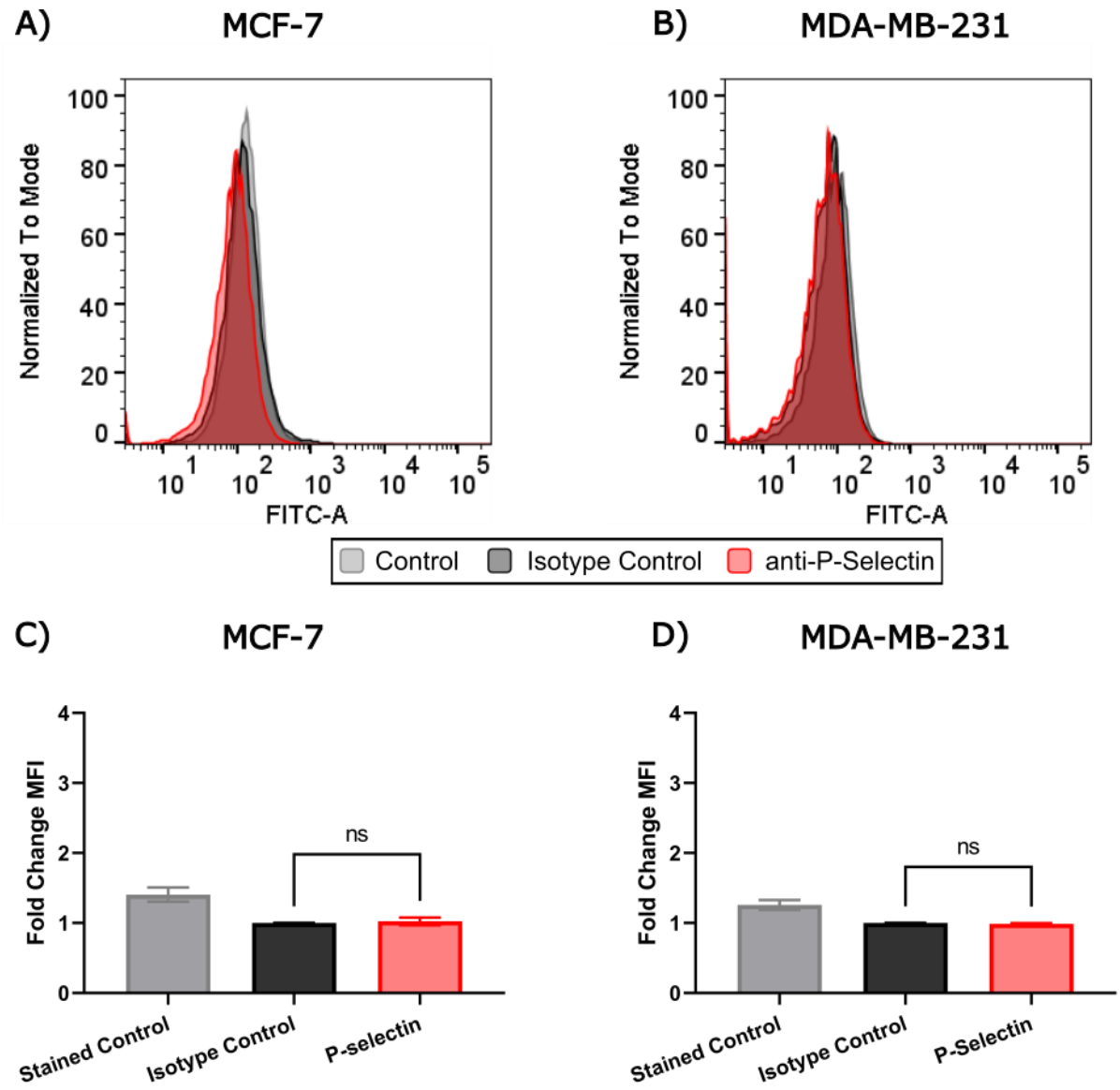

Figure 4.5 P-Selectin surface expression on MCF-7 and MDA-MB-231 breast cancer cells: Breast tumour cell surface expression of P-Selectin was measured (N=3) with an anti-P-selectin detection antibody along with an isotype control antibody. Expression of P-Selectin was displayed in representative histograms for **A)** MCF-7 and **B)** MDA-MB-231 cells. Fold changes in MFI values for P-Selectin expression were normalised against isotype controls and compiled into graphs ± SEM **C)** MCF-7 and **D)** MDA-MB-231 cells. Significance between treatment conditions were calculated by student t-test * $p \leq 0.05$.

4.2.3 $\alpha_v\beta_3$ expression on MCF-7 and MDA-MB-231 cells

Another key receptor for VWF is $\alpha_v\beta_3$ with an interactive binding site within the C-domain of VWF.[327] Considering the small yet still significant adhesion we observed for the A3-CK domain of VWF to MDA-MB-231 cells we examined the expression of this integrin on breast tumour cells. Huang *et al.* have proposed that VWF multimer adhesion and subsequent platelet tethering along the endothelium under shear stress occurs via $\alpha_v\beta_3$ receptors which can anchor VWF multimers to unwind and facilitate platelet adhesion.[262] Furthermore, siRNA Knockdown of VWF in HUVEC was linked with dysregulated $\alpha_v\beta_3$-mediated endothelial angiogenesis, implying an ability of VWF to signal through $\alpha_v\beta_3$.[73] It has been proposed that VWF may induce apoptosis in a number of cancer cells, MCF-7, 769P and HepG2 by signalling through the $\alpha_v\beta_3$ receptor expressed on these tumour cells. Interestingly, specific tumour cells can prevent this VWF-apoptotic effect via expression of a novel VWF cleaving protease 'a disintegrin metalloproteinase domain 28' (ADAM28).[101] Altogether, $\alpha_v\beta_3$ is an interesting candidate for VWF adhesion to breast cancer cells. Following flow cytometry analysis, we indeed observed that $\alpha_v\beta_3$ was expressed on MCF-7 cells, (MFI 1.6 ± 0.25 Figure 4.6 A+C) but also highly expressed on MDA-MB-231 cells (MFI 3.3 ± 0.30, Figure 4.6 B+D).

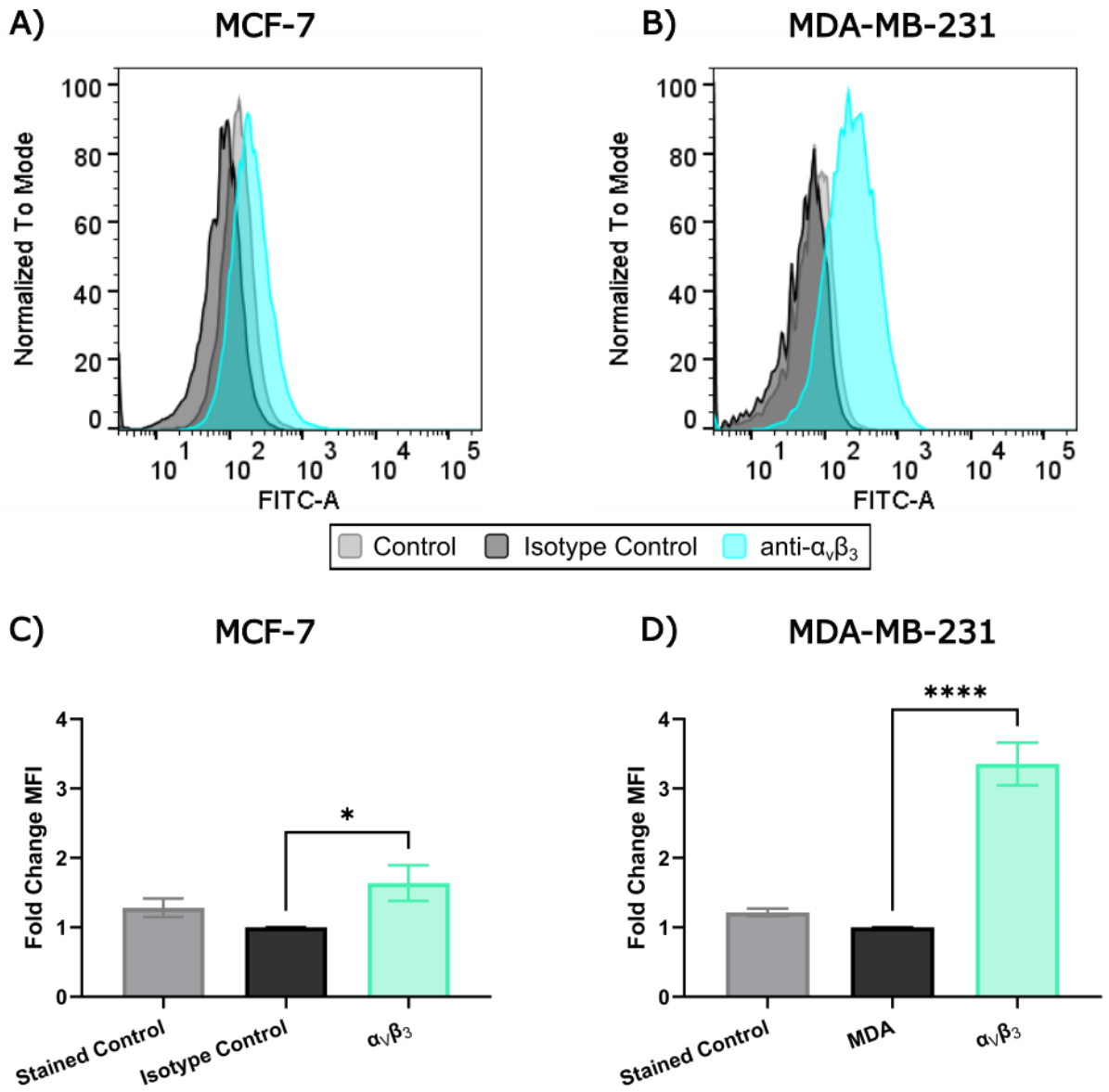

Figure 4.6 $\alpha_v\beta_3$ surface expression on MCF-7 and MDA-MB-231 breast cancer cells: Breast tumour cell surface expression of $\alpha_v\beta_3$ was measured (N=5) with an anti-$\alpha_v\beta_3$ detection antibody along with an isotype control antibody. Expression of the $\alpha_v\beta_3$ receptor was displayed in representative histograms for **A)** MCF-7 and **B)** MDA-MB-231 cells. Fold changes in MFI values for $\alpha_v\beta_3$ expression were normalised against isotype controls and compiled into graphs ± SEM **C)** MCF-7 and **D)** MDA-MB-231 cells. Significance between treatment conditions were calculated by student t-test * $p \leq 0.05$, **** $p \leq 0.0001$.

4.2.4 GPIbα expression on MCF-7 and MDA-MB-231 cells

GPIbα is a well characterised platelet receptor that adheres to VWF. VWF binding to the GPIbα receptor on non-activated platelets is key for the initial tethering events of platelets to the sub-endothelium.[312,328] Subsequently, platelets become activated with the $\alpha_{iib}\beta_3$ platelet receptors adopting an active conformation and forming a high affinity complex with VWF, cross-linked fibrinogen and promoting stable platelet adhesion and aggregation. Binding of VWF to platelet GPIbα receptors is highly dependent on the rate of shear within the vasculature. The VWF residues important for mediating GPIbα binding are located within the VWF A1 domain on either side of the disulphide loop.[329,330]

Interestingly, two groups have independently described the expression of GPIbα or a pseudo-GPIbα receptor on the surface of breast cancer cells including MDA-MB-231 and MCF-7.[187,188] Critically, MCF-7-induced platelet aggregation could be inhibited by targeting this GPIbα expression.[187] However, recent data has shown that Jimt1 breast cancer cells do not express GPIbα on their surface, suggesting differential expression of GPIbα depending on breast cancer cell type.[241] In support of this, immunohistochemistry analysis of GPIbα expression in primary breast tumour samples revealed only 62% of samples staining positively.[321] With this in mind, we assessed tumour expression of GPIbα on MDA-MB-231 and MCF-7 cells. In keeping with previous reports by Suter *et al*, MDA-MB-231 cells demonstrated higher expression of GPIbα than the MCF-7 cells (MFI 2.3 ± 0.11 vs MFI 1.3 ± 0.15, Figure 4.7).[188]

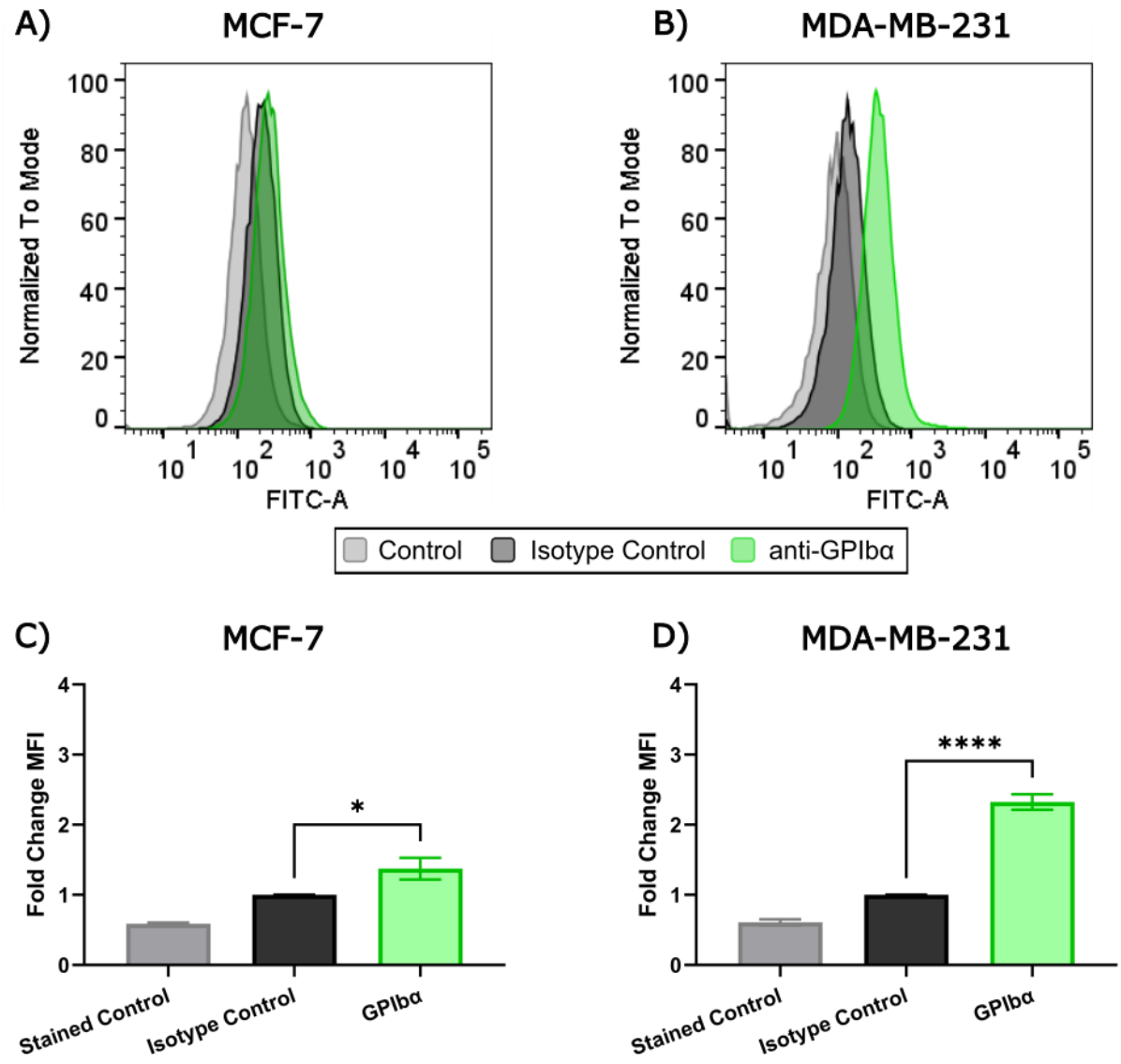

Figure 4.7 GPIbα surface expression on MCF-7 and MDA-MB-231 breast cancer cells: Breast tumour cell surface expression of GPIbα was measured (N=5) with an anti-GPIbα detection antibody along with an isotype control antibody. Expression of the GPIbα receptor was displayed in representative histograms for **A)** MCF-7 and **B)** MDA-MB-231 cells. Fold changes in MFI values for GPIbα expression were normalised against isotype controls and compiled into graphs ± SEM **C)** MCF-7 and **D)** MDA-MB-231 cells. Significance between treatment conditions were calculated by student t-test * $p \leq 0.05$, **** $p \leq 0.0001$.

4.2.5 Low density lipoprotein related protein expression on MCF-7 and MDA-MB-231 cells

Finally, we assessed expression of LRP1, a receptor that is ubiquitously expressed across a myriad of cell types, including many tumour types.[331–333] LRP1 is a promiscuous receptor with many ligands described and has been implicated in both endocytosis and signalling pathways.[334,335] Genome-wide association studies reveal that the *LRP1* gene represents a susceptibility locus for myocardial infarction.[336] the role of LRP1 in myocardial infarction may be in part mediated by its ability to bind and clear FVIII and VWF from the circulation and thus regulate plasma levels of FVIII and VWF.[222,314,336,337] VWF clearance by LRP1 is thought to be mediated by the cluster II and IV domains of the LRP1 receptor which then interact directly with the A1-domain of VWF.[338] Interestingly, this adhesion is facilitated by PEGylation of both A1 and A3 VWF domains.[338] Of note, in a VWF clearance model, adhesion of VWF coated beads to LRP1 seemed to be most effective when exposed to shear forces greater than 2.5dyn/cm^2, however, baseline adhesion was not assessed in the absence of shear stresses.[314] On the basis of this, we measured LRP1 expression in our breast cancer cell lines MDA-MB-231 and MCF-7. Only modest LRP1 expression was detected on MCF-7 cells (Figure 4.8 A+C), however significant LRP1 expression was observed on MDA-MB-231 cells, with the MFI increased 2.5-fold compared to isotype control stained cells (MFI 2.5 ± 0.07 vs. 1.19 ± 0.06, $p<0.001$, Figure 4.8 B+D).

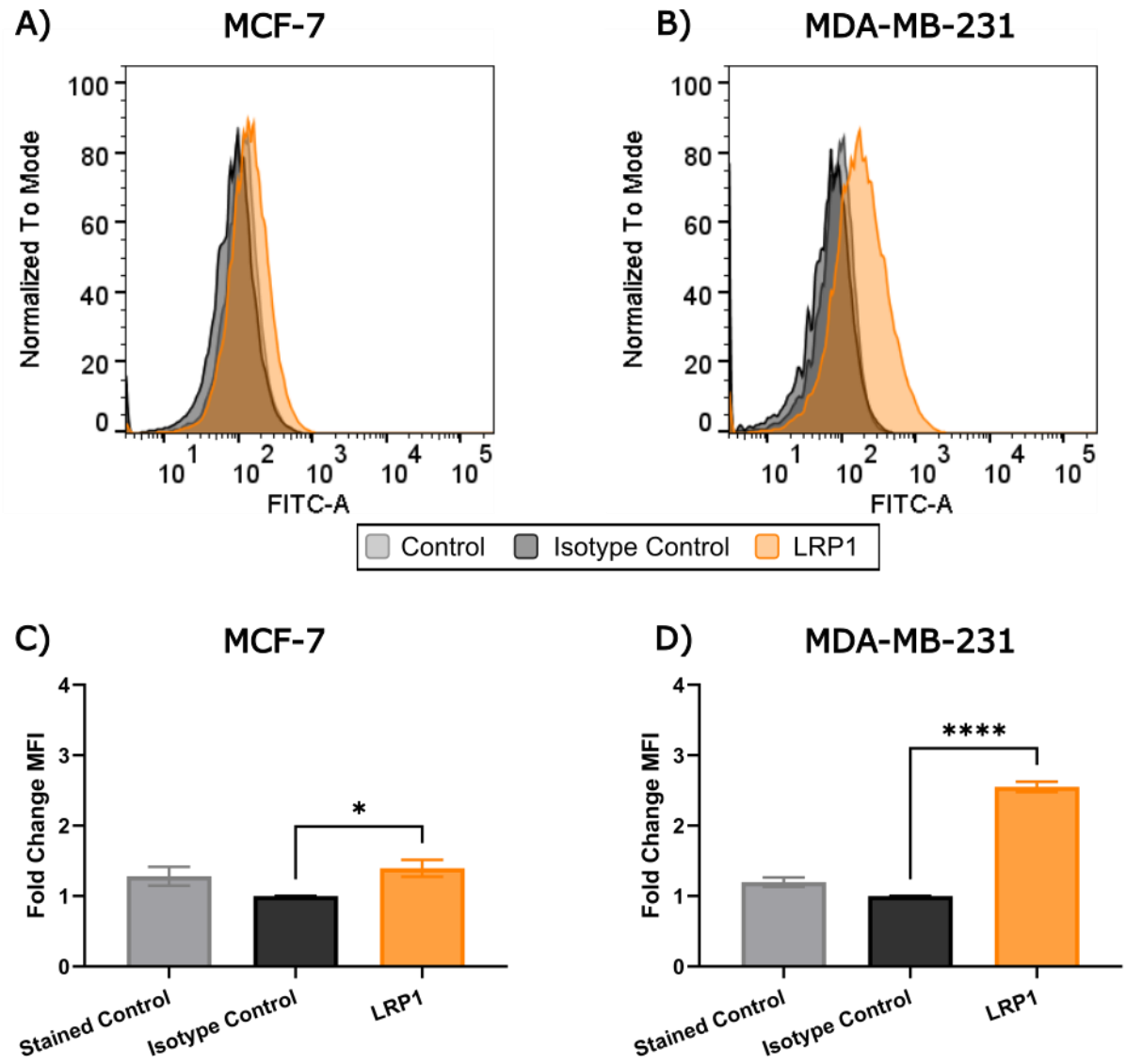

Figure 4.8 LRP1 surface expression on MCF-7 and MDA-MB-231 breast cancer cells: Breast tumour cell surface expression of LRP1 was measured (N=4) with an anti-LRP1 detection antibody along with an isotype control antibody. Expression of the LRP1 receptor was displayed in representative histograms for **A)** MCF-7 and **B)** MDA-MB-231 cells. Fold changes in MFI values for LRP1 expression were normalised against isotype controls and compiled into graphs ± SEM **C)** MCF-7 and **D)** MDA-MB-231 cells. Significance between treatment conditions were calculated by student t-test * $p \leq 0.05$, **** $p \leq 0.0001$.

4.3 Characterisation of MDA-MB-231 tumour receptors mediating VWF-breast cancer cell binding

Taken together, the data points to the diverse array of candidate VWF receptors expressed on MDA-MB-231 cells which may be involved in mediating VWF adhesion (Table 4.1). Having characterised the expression profile of these receptors we next sought to assess their potential role in VWF binding to MDA-MB-231 breast tumour cells using a targeting approach. Our results found no strong candidates for VWF-MCF-7 cell adhesion and thus further work is warranted to characterise the receptors that mediate VWF adhesion to MCF-7 cells. Nevertheless we can conclude an important role for the D'A3 region of VWF and given the key role of ristocetin in our VWF-MCF-7 binding assays, the conformational unfolding of VWF A1 domain is likely to be an important regulatory feature in this direct interaction.

Table 4.1 Expression profile of VWF binding receptors on MCF-7 and MDA-MB-231 cells

	Cell type	
	MCF-7	MDA-MB-231
PSGL-1	**No expression**	**Intermediate expression**
P-selectin	**No expression**	**No expression**
$\alpha_v\beta_3$	**Intermediate expression**	**High expression**
GPIbα	**Low expression**	**High expression**
LRP1	**Low expression**	**High expression**

Expression profile of VWF binding receptors on MCF-7 and MDA-MB-231 cells. Expression levels are notated by the relative MFI fold changes derived through flow cytometry compared to the respective isotype controls: No expression constitutes non-significant fold MFI change, low expression <1.5 Fold change, intermediate expression 1.5-2 fold change and high expression >2 fold change.

4.3.1 The effect of PSGL-1 inhibition on VWF-MDA-MB-231 cell adhesion

Given the robust expression of PSGL-1 receptor on MDA-MB-231 cells, we sought to assess whether targeting this receptor may reduce binding of human recombinant VWF to these breast tumour cell line. Using known anti-PSGL-1 clone KPL-1, reported to prevent L-selectin, P-selectin and VWF adhesion to the PSGL-1 receptor we expected PSGL-1 inhibition would reduce VWF binding to MDA-MB-231 cells.[261,339] Contrastingly, despite pre-treating MDA-MB-231 cells with an anti-PSGL-1 antibody for 30 minutes before addition of 100nM VWF, no significant change in VWF adhesion to the breast tumour cells was observed in comparison to isotype treated cells. Both isotype control and anti-PSGL-1 treated MDA-MB-231 cells displayed comparable binding affinities for VWF (Figure 4.9), suggesting that PSGL-1 may not act as a key VWF receptor for these tumour cells.

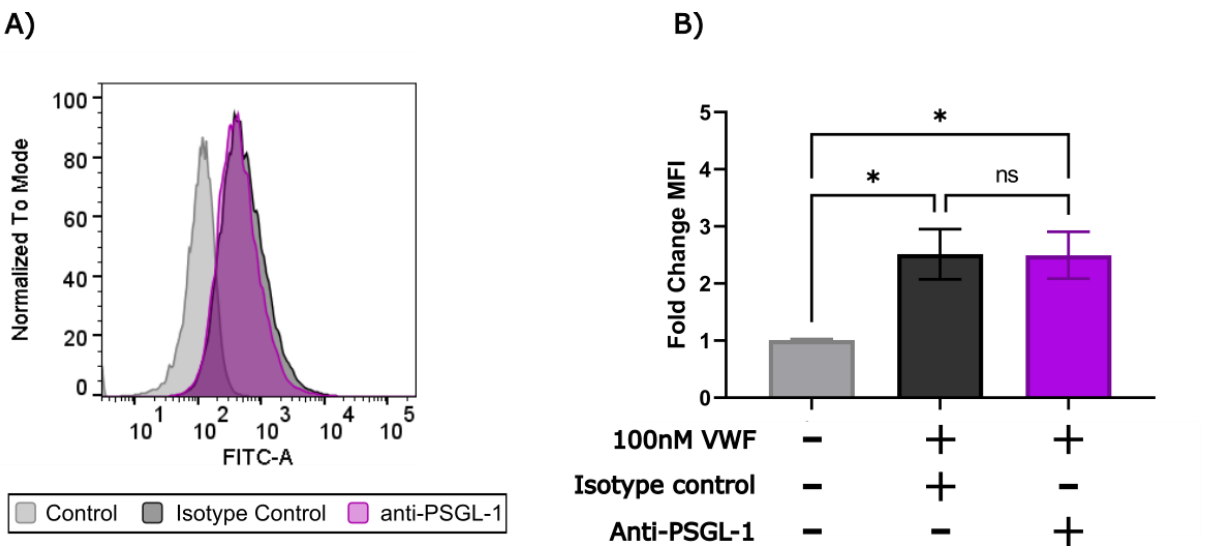

Figure 4.9 PSGL-1 does not mediate VWF-MDA-MB-231 cell adhesion: MDA-MB-231 cells were pre-treated with an anti-PSGL antibody (N=5) or isotype control for 30 minutes at 4°C before 100nM recombinant VWF was added in buffer supplemented with ristocetin and calcium ions, in keeping with our established assay conditions. VWF adhesion was quantified using flow cytometric analysis, with representative histograms depicted in **A)** and **B)** compiled graph of fold change in MFI. Fold changes in MFI were calculated by normalising values against an untreated stained control group and graphed ± SEM. Significance between treatment conditions were determined through one way ANOVA using Tukeys multiple comparisons test, * $p \leq 0.05$.

4.3.2 The effect of RGDS treatment on VWF-MDA-MB-231 cell adhesion

VWF has an RGD binding motif along the C4 domain that can mediate adhesion to a variety of integrins including $\alpha_{iib}\beta_3$ and $\alpha_v\beta_3$.[33,308] Despite the VWF D'A3 region being the predominant binding region to MDA-MB-231 cells in our assays, the VWF A3-CK domain also exhibited significant adhesion to MDA-MB-231 and constitutes a binding region for many integrins. Interestingly, a number of different cancer cells have shown reduced binding affinity to VWF when treated with an RGD-binding peptide.[187,239] In M21 melanoma cells perfused over immobilised VWF, cellular arrest was completely abolished in the presence of an RGD-binding peptide.[239] Correspondingly, recombinant VWF protein with a mutated RGD binding domain (VWF-RGG) failed to adhere to B16-BL6 melanoma cells whereas wild-type VWF showed strong adhesion.[190]

Therefore we targeted integrin binding by pre-treating MDA-MB-231 cells with an RGDS peptide overnight and compared binding to baseline VWF adhesion. Strikingly, RGDS treatment resulted in a significant attenuation of VWF adhesion (MFI 8.01 ± 1.18 vs 4.08 ± 0.82, $p<0.05$, Figure 4.10). This indicates that treatment of MDA-MB-231 cells with an RGDS peptide may block key integrin sites and thus compete for binding with the RGD motif along the VWF C-domain region.

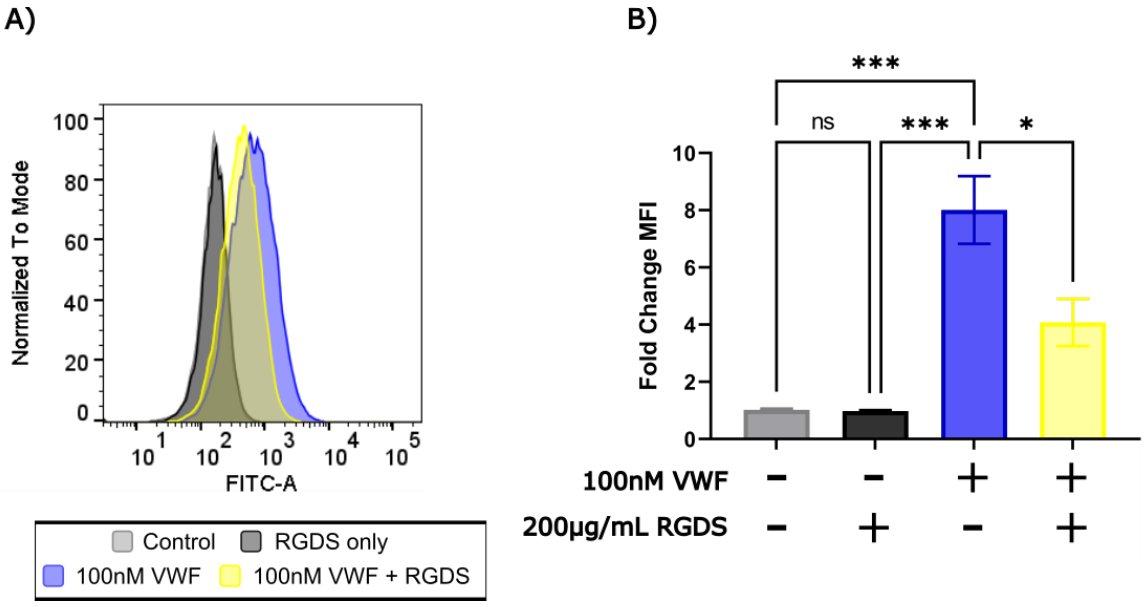

Figure 4.10 RGDS treatment reduces VWF adhesion to MDA-MB-231 cells: An RGDS peptide was pre-treated on MDA-MB-231 cells (N=4) overnight and washed off before 100nM recombinant VWF was added to the MDA-MB-231 breast cancer cells under static conditions. Inhibition of VWF adhesion was quantified using flow cytometric analysis, RGDS treatment was depicted as **A)** a representative histogram and **B)** compiled graph of fold MFI changes. Fold changes in MFI were calculated by normalising values against an untreated stained control group and graphed ± SEM. Significance between treatment conditions were determined through one way ANOVA using Tukeys multiple comparisons test , * $p \leq 0.05$, *** $p \leq 0.001$.

4.3.3 The effect of $\alpha_v\beta_3$ inhibition on VWF-MDA-MB-231 cell adhesion

Our analysis showed that integrin $\alpha_v\beta_3$ was strongly expressed in MDA-MB-231 cells and subsequent inhibition of the VWF-MDA-MB-231 interaction with RGDS peptide hinted at a partial role for integrins in VWF-MDA-MB-231 adhesion. In fact, as characterised by Terraube *et al*. B16-BL6 murine melanoma cells expressed both the α_v and β_3 subunits and the subsequent adhesion of murine melanoma cells to VWF could be inhibited by 65% by targeting the β_3-subunit.[190] Furthermore an anti-β_3 antibody was able to reduce surface bound VWF and platelets from gastric cancer cell line BGC823.[118] Despite evidence for a role for $\alpha_v\beta_3$ in mediating VWF adhesion to other tumour types, our VWF-breast tumour binding assay revealed that blocking $\alpha_v\beta_3$ had no effect on VWF adhesion. Inhibition of $\alpha_v\beta_3$ resulted in comparable VWF adhesion as blocking with a matched isotype control (MFI 3.7 ± 0.41 vs MFI 3.9 ± 0.90, p = 0.9885, Figure 4.11).

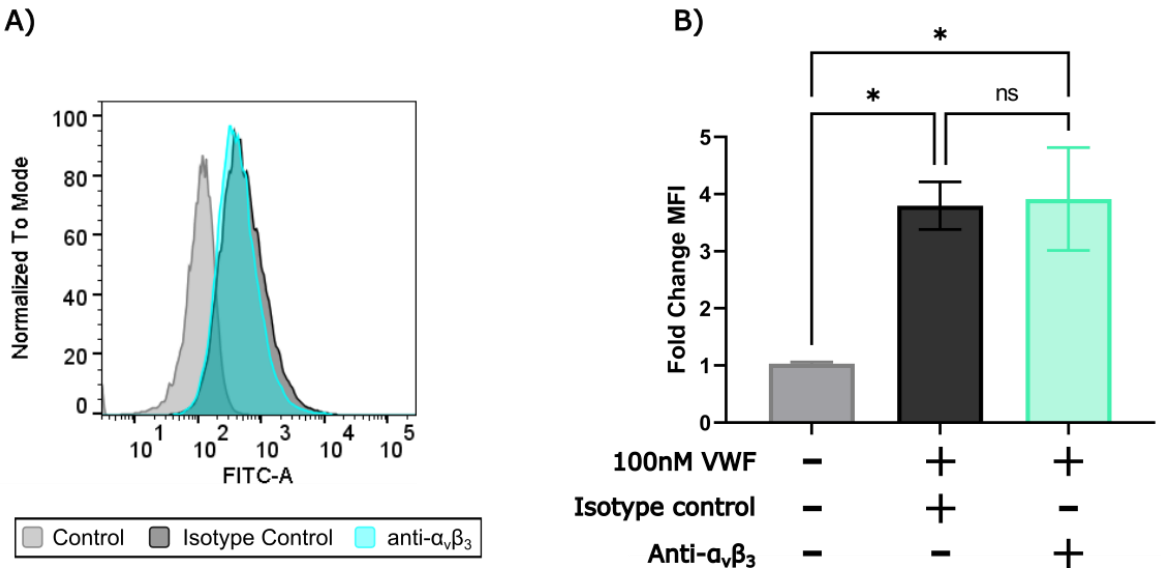

Figure 4.11 $\alpha_v\beta_3$ does not mediate VWF-MDA-MB-231 cell adhesion: MDA-MB-231 cells were pre-treated with an anti-$\alpha_v\beta_3$ antibody (N=3) or isotype control for 30 minutes at 4°C before 100nM recombinant VWF was added in buffer supplemented with ristocetin and calcium ions, in keeping with our established assay conditions. VWF adhesion was quantified using flow cytometric analysis, with representative histograms depicted in **A)** and **B)** compiled graph of fold change in MFI. Fold changes in MFI were calculated by normalising values against an untreated stained control group and graphed ± SEM. Significance between treatment conditions were determined through one way ANOVA using Tukeys multiple comparisons test, * $p \leq 0.05$.

4.3.4 The effect of GPIbα inhibition on VWF-MDA-MB-231 cell adhesion

Congruent with the previous literature, we observed marked expression of GPIbα on the surface of MDA-MB-231 cells.[188] GPIbα-VWF adhesion forms a fundamental process in primary haemostasis as VWF tethers platelets to the sites of vascular injury.[340] GPIbα has few described ligands including thrombin and the A1-domain of VWF.[341] Therefore we inhibited GPIbα on the surface of MDA-MB-231 where adhesion of VWF was subsequently assessed by flow cytometry. Notably, VWF binding was significantly inhibited by approximately 50% following anti-GPIbα treatment of the MDA-MB-231 cells compared to the matched isotype (MFI 2.216 ± 0.41 vs MFI 4.3 ± 0.26, respectively, $p<0.05$, Figure 4.12). This data highlights GPIbα as a relevant receptor in mediating VWF adhesion to MDA-MB-231cell under static conditions.

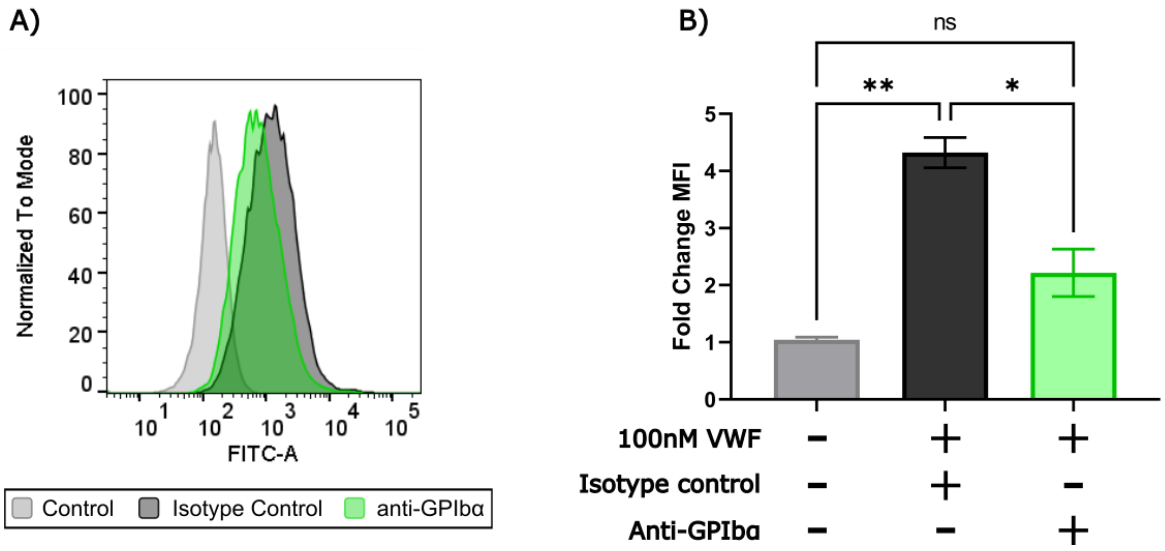

Figure 4.12 GPIbα mediates VWF-MDA-MB-231 cell adhesion: MDA-MB-231 cells were pre-treated with an anti-GPIbα antibody (N=4) or isotype control for 30 minutes at 4°C before 100nM recombinant VWF was added in buffer supplemented with ristocetin and calcium ions, in keeping with our established assay conditions. VWF adhesion was quantified using flow cytometric analysis, with representative histograms depicted in **A)** and **B)** compiled graph of fold change in MFI. Fold changes in MFI were calculated by normalising values against an untreated stained control group and graphed ± SEM. Significance between treatment conditions were determined through one way ANOVA using Tukeys multiple comparisons test, * $p \leq 0.05$, ** $p \leq 0.01$.

4.3.5 The effect of LRP1 inhibition on VWF-MDA-MB-231 cell adhesion

Despite the well characterised interaction between macrophage LRP1 and VWF, there has been no evidence to date of VWF-LRP1 interactions in a tumour setting.[222,342] This may be of particular interest since some reports indicate that tumour LRP1 expression may be associated with enhanced proliferation and pro-invasive features in cancer settings, yet the biological mechanisms and key ligands remain poorly defined.[343–345] Interestingly, LRP1-VWF interactions were inhibited through the use of an anti-LRP1 antibody previously used to assess VWF-LRP1 interactions in macrophages (as of yet unpublished). Therefore, we discerned that treatment of MDA-MB-231 breast cancer cells with the same anti-LRP1 antibody resulted in a partial decrease in VWF adhesion by approximately 50% compared to isotype control treated cells (MFI 2.67 ± 0.36 vs 4.16 ± 0.11, $p<0.05$ Figure 4.13). Altogether, these data suggest that VWF may serve as a novel ligand for LRP1 expressed on MDA-MB-231 breast tumour cells.

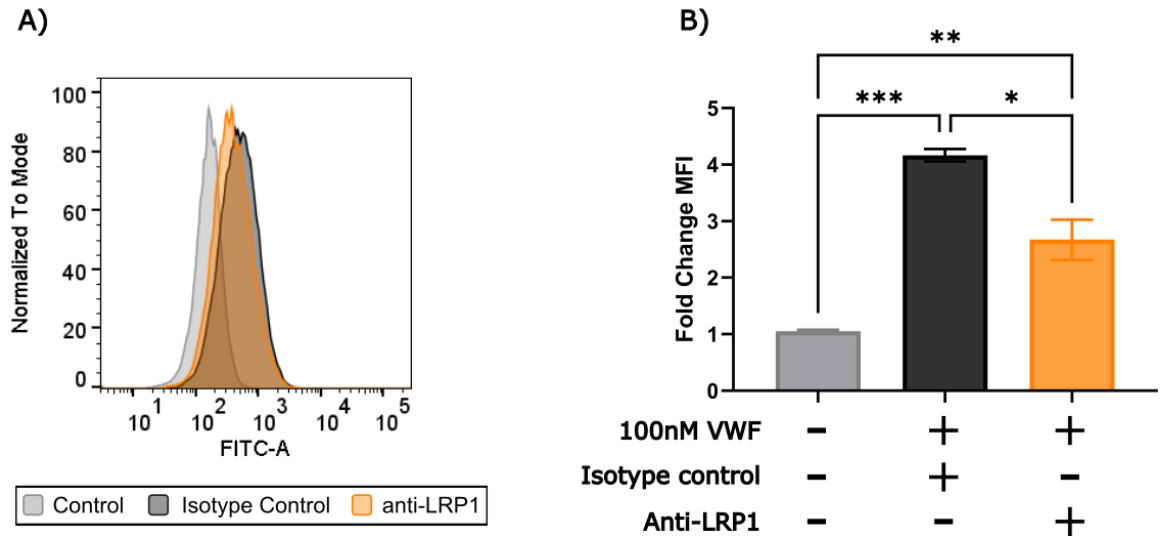

Figure 4.13 LRP1 mediates VWF-MDA-MB-231 cell adhesion: MDA-MB-231 cells were pre-treated with an anti-LRP1 antibody (N=4) or isotype control for 30 minutes at 4°C before 100nM recombinant VWF was added in buffer supplemented with ristocetin and calcium ions, in keeping with our established assay conditions. VWF adhesion was quantified using flow cytometric analysis, with representative histograms depicted in **A)** and **B)** compiled graph of fold change in MFI. Fold changes in MFI were calculated by normalising values against an untreated stained control group and graphed ± SEM. Significance between treatment conditions were determined through one way ANOVA using Tukeys multiple comparisons test, * $p \leq 0.05$, ** $p \leq 0.01$, *** $p \leq 0.001$.

4.4 LRP1 and VWF directly interact on the surface of MDA-MB-231 cells

4.4.1 Imaging VWF and LRP1 interaction

Given the key role of LRP1 in tumour invasion and metastasis and our finding of VWF as a key novel ligand for this tumour receptor, we sought to further confirm a direct interaction between VWF and LRP1 on the surface of MDA-MB-231 cells, by employing a Duolink® proximity ligation assay (PLA). Cells were treated with primary antibodies against VWF (anti-rabbit) and LRP1 (anti-mouse) before the Duolink® PLA was carried out by adding PLUS (anti-rabbit) and MINUS (anti-mouse) PLA® probes to the respective primary antibodies. The probes were subsequently ligated together and thereby produced a unique red fluorescent colour when the two probes were in close proximity to each other indicating that both LRP1 and VWF are co-localised on the cell surface. For initial antibody optimisation, we firstly confirmed LRP1 expression on MDA-MB-231 cells by immunofluorescence with LRP1 expression indeed confirmed by presence of green fluorescence on the tumour cells. (Figure 4.14 A).

Then MDA-MB-231 cells were treated with 100nM VWF, in our optimised binding buffer supplemented with ristocetin and calcium. After washing and incubation with primary antibodies, specific matched secondary PLA probes were added to MDA-MB-231 cells coated on a slide. The presence of red immunofluorescent signal is indicative of co-localisation of both LRP1 and VWF within a 40nm radius on the tumour cell surface. We confirmed the co-localisation of VWF and LRP1 on MDA-MB-231 cells treated with VWF. Moreover, this signal was abolished upon treatment with LRP1 antagonist RAP, once again confirming the specificity of this novel interaction on breast tumour cells (0.12 ± 0.009 vs 0.008 ± 0.005 % area coverage) (Figure 4.14 B-E).

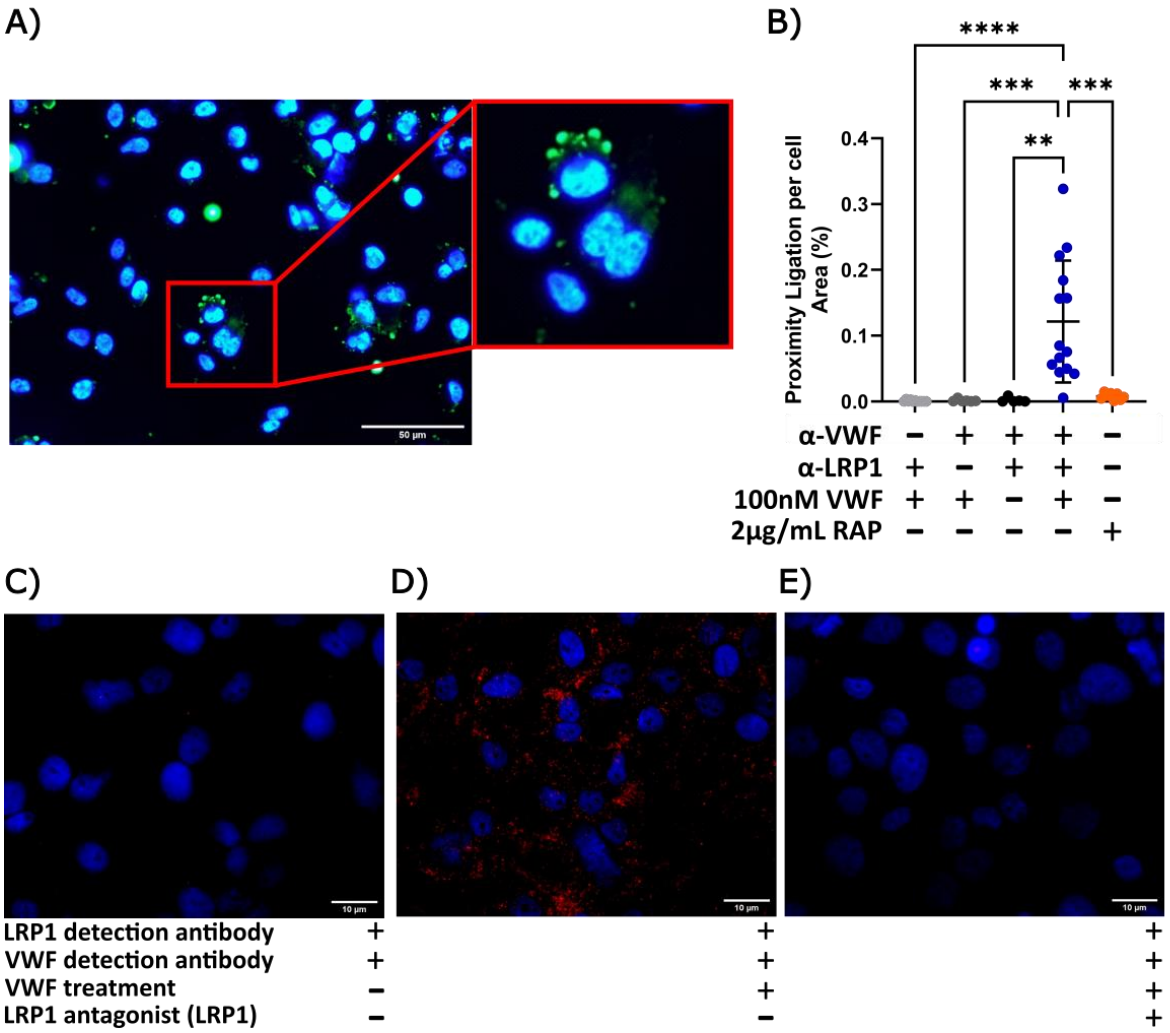

Figure 4.14 Proximity ligation assay for VWF and LRP1 colocalization MDA-MB-231 cells: MDA-MB-231 cells were coated on a 12 chamber microscope slides and treated with an anti-LRP1 or matched isotype control. A fluorescent secondary antibody was added and **A)** stained cells were imaged at 20x magnification. A proximity ligation assay was conducted on MDA-MB-231 cells coated on a 12 chamber microscope slide. Primary antibodies against LRP1 and VWF were added, followed by species specific PLA® probes that were then ligated and fluorescent signal amplified. Signal was only detected if both probes were in close proximity. **B)** data was graphed with signal normalised against number of cells per image ± SD, representative images **C)** No VWF treatment control **D)** 100nM recombinant VWF treatment **E)** 2µg/mL RAP 30 minute pre-treatment and 100nM VWF treatment. Images were processed on ImageJ software. Significance between treatment conditions were determined through one way ANOVA using Tukeys multiple comparisons test, ** $p \leq 0.01$, *** $p \leq 0.001$, **** $p \leq 0.0001$.

4.5 VWF-tumour receptor inhibition of MDA-MB-231 cells adhesion under shear flow

Having defined a key role for breast tumour expressed GPIbα and LRP1 in mediating significant VWF adhesion to MDA-MB-231 cells under static conditions yet in the presence of ristocetin, we then sought to further characterise the role of these two key tumour receptors under conditions of shear flow perfusion to better recapitulate circulatory stresses. Moreover, based on our previous findings defining a role of VWF multimers secreted from endothelial cells in tethering and arresting circulating breast tumour cells along the endothelium, we also assessed the role of breast tumour expressed GPIbα and LRP1 in contributing to this effect.

4.5.1 LRP1 inhibition ablates adhesion of MDA-MB-231 cells to VWF under shear flow

To better understand the potential role of VWF adhesion to LRP1 expressed on the surface of MDA-MB-231 cells during haematogenous metastasis, we assessed the binding interaction under conditions of venous blood shear stress. Importantly, VWF adhesion to macrophage LRP1 has been well characterised with key lysine residues located in the A1 VWF domain and crucially this interaction is dependent on shear stress or ristocetin induced unfolding of VWF.[314,342,346] On the basis of this we determined whether VWF-MDA-MB-231 cell adhesion could be inhibited by targeting tumour LRP1 under flow conditions. MDA-MB-231 cells were treated with a well-established LRP1 antagonist RAP for 30 minutes before being perfused over a layer of immobilised VWF under conditions mimicking venous shear stress rates.[347]

In support of our previous findings, addition of the LRP1 antagonist RAP ablated the adhesion of circulating MDA-MB-231 cells to VWF (Figure 4.15). Stable arrest of RAP treated MDA-MB-231 cells to VWF, as measured by surface coverage was markedly reduced compared to untreated MDA-MB-231 cells (33.94 ± 12.07 cells/mm^2 vs. 93.96 ± 12.95 cells/mm^2 $p<0.01$, Figure 4.15 B). Notably, this residual MDA-MB-231 adhesion in the presence of RAP was comparable to the control uncoated channels (27.45 ± 9.263 cells/mm^2), indicating that only non-specific adhesion of MDA-MB-231 cells remained. Of note, treating MDA-MB-231 cells with LRP1 antagonist RAP resulted in a non-significant downward trend in $K_{[on]}$ values compared to those seen in the VWF coated samples (2.668 ± 0.5187 cells/mm/s^2 vs 1.793 ± 0.7183 cells/mm/s^2, Figure 4.15 C). Furthermore, detachment rates $K_{[off]}$ were significantly increased upon RAP treatment of MDA-MB-231 cells (0.028 ± 0.008 1/s vs 0.14 ± 0.07 1/s, $p \leq 0.05$, Figure 4.15 D). The ability of RAP to diminish surface coverage of MDA-MB-231 cells

and transient binding events under conditions of shear stress is further confirmation of a key role for LRP1 in MDA-MB-231 mediated VWF-adhesion.

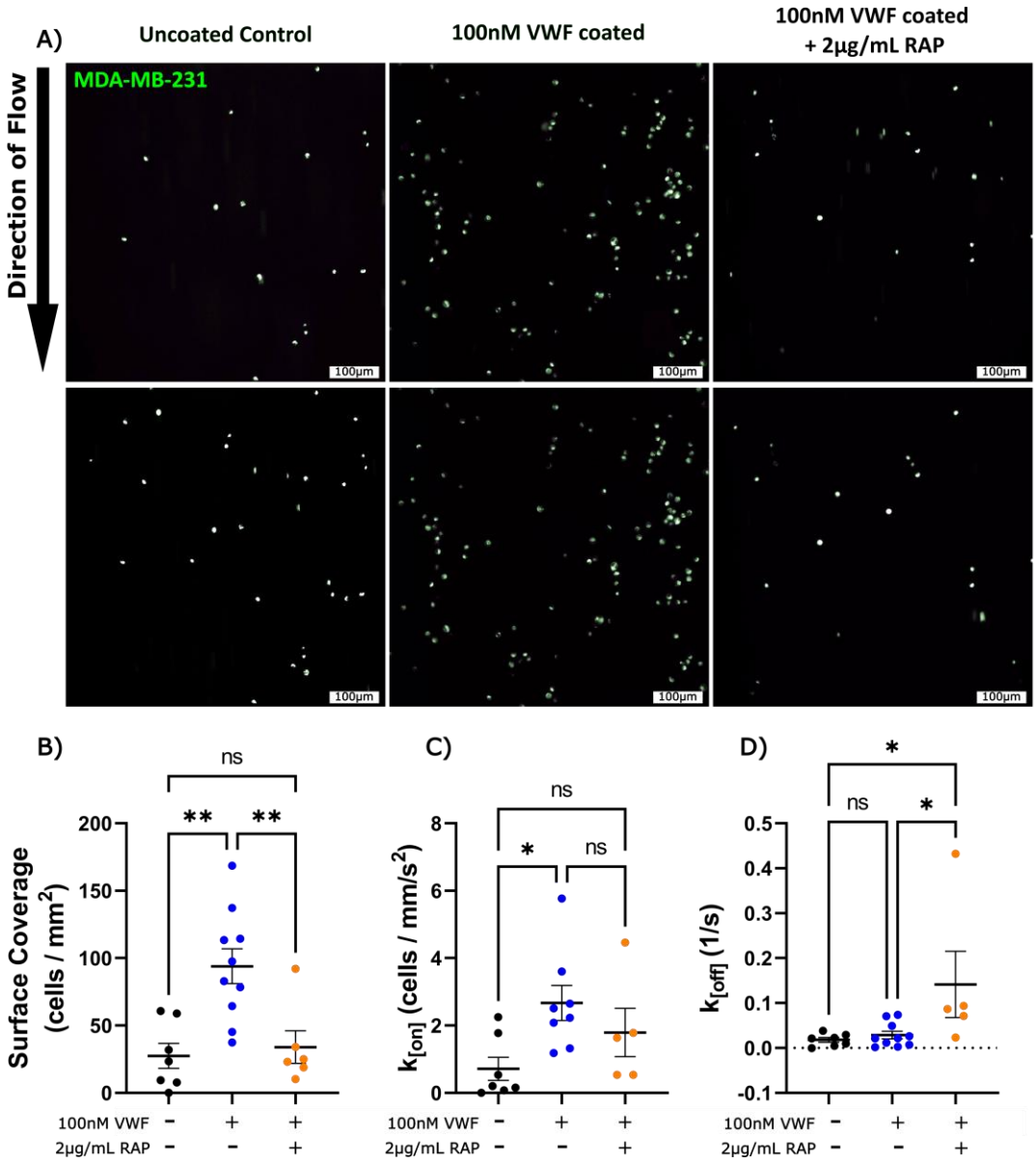

Figure 4.15 LRP1 inhibition ablates adhesion of MDA-MB-231 cells to VWF under shear flow: MDA-MB-231 cells were perfused at a flow rate of 0.2 ml/min resulting in venous shear stress of 0.25 dyn/cm^2. The channels of an Ibidi flow slide were either coated with 100nM pd-VWF or left untreated. Fluorescently labelled MDA-MB-231 cells ± 2µg/mL RAP treatment were perfused across the wells and recorded at 10x magnification for up to 700 frames. **A)** Representative images of cellular perfusion were taken at different time points to highlight differences in surface coverage of breast tumour cells under different experimental conditions. MDA-MB-231 tumour cell arrest was measured by **B)** stable adhesion through surface coverage (cells/mm^2), **C)** attachment rates $K_{[on]}$ (cells/mm^2/s), **D)** detachment rates $K_{[off]}$ (1/s). Data is presented as the mean ± SEM. Significance was determined through one way ANOVA using Tukeys multiple comparisons test, * $p \leq 0.05$, ** $p \leq 0.01$.

4.5.2 LRP1 inhibition abolishes adhesion of MDA-MB-231 to endothelial VWF under shear stress

As previously shown, VWF multimers released from activated endothelial cells promote MDA-MB-231 cell adhesion to the endothelial surface under shear stress. We evaluated the role of breast tumour LRP1 in this assay. In U87 glioblastoma cells LRP1 silencing resulted in decreased migration and invasion in a MMP-2 and MMP-9 dependent manner.[348] Other evidence has shown that when seeded in a 3D collagen matrix, inhibition of LRP1 with RAP or antibody treatment reduced LS174T and HT-29 colon carcinoma proliferation.[344] Most interestingly, there is growing evidence for increased invasiveness in breast cancer cells expressing LRP1.[349–351] Of particular note, LRP1 silencing in MDA-MB-231 cells resulted in morphological changes in MDA-MB-231 cells making them less migratory by reducing cellular protrusions as well as modulating actin polarisation, specifically when seeded on a collagen layer.[352] However the biological mechanisms underpinning these observations are not fully understood. We hypothesise that LRP1 expression on MDA-MB-231 cells may promote their adhesion to the endothelial vessel wall in a VWF-dependent manner and thus contribute to blood-borne metastasis.

In line with the results using immobilised purified VWF, inhibition of LRP1 with RAP in MDA-MB-231 cells severely diminished MDA-MB-231 adhesion to activated endothelial cells. Surface coverage of the endothelial layer was significantly ablated upon RAP treatment versus untreated control conditions (6.06 ± 1.9 cells/mm^2 vs 35.24 ± 4.8 cells/mm^2, $p<0.001$, Figure 4.16 A+B). These data suggest that LRP1 is involved in stable adhesion of MDA-MB-231 breast cancer cells to activated endothelial cells, which, based on our previous data is at least in part dependent on the presence of VWF multimers. Furthermore, endothelial attachment rates of perfused MDA-MB-231 cells, as measured by $K_{[on]}$, were significantly reduced in the presence of RAP (0.34 ± 0.19 cells/mm^2/s vs 3.29 ± 0.92, $p<0.05$, Figure 4.16 C). However, detachment rates, $K_{[off]}$, were found to be unchanged in the RAP treated MDA-MB-231 cells (0.17 ± 0.05 1/s vs. 0.19 ± 0.13, Figure 4.16 D) potentially indicating that blocking LRP1 can prevent initial adhesion to the endothelial VWF, however, there may be other factors involved in tethering cells.

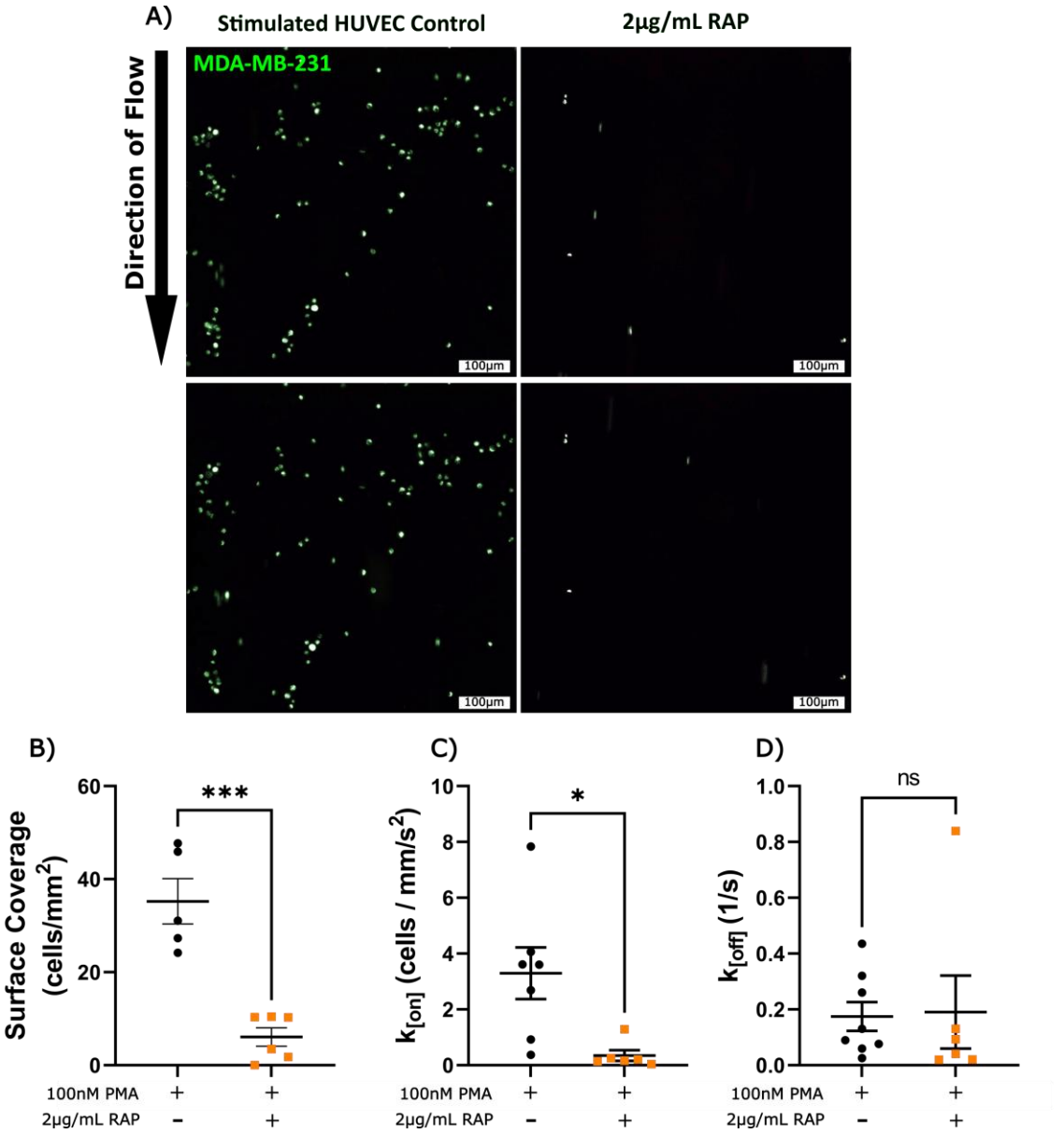

Figure 4.16 LRP1 antagonist RAP inhibits endothelial adhesion of MDA-MB-231 cells: HUVEC monolayers cultured on Ibidi channel slides were stimulated with 100nM PMA to ensure maximal release of VWF. MDA-MB-231 cells were treated with 2µg/mL RAP, LRP1 antagonist, and fluorescently labelled before being perfused over the HUVEC monolayer at a venous shear stress of 0.25dyn/cm^2. Adhesion events were imaged at 10x magnification for up to 700 frames. **A)** Representative images of cellular perfusion were taken at different time points to highlight differences in surface coverage of breast tumour cells under different experimental conditions. MDA-MB-231 breast tumour cell adhesion was quantified by **B)** stable adhesion through surface coverage (cells/mm^2), **C)** attachment rates $K_{[on]}$ (cells/mm^2/s), **D)** detachment rates $K_{[off]}$ (1/s). Data is presented as the mean ± SEM. Significance was determined through one way ANOVA using Tukeys multiple comparison test, * $p \leq 0.05$, *** $p \leq 0.001$.

4.5.3 Inhibition of GPIbα ablates adhesion of MDA-MB-231 to endothelial VWF under shear stress

To further support our data showing inhibition in static adhesion of anti-GPIbα treated MDA-MB-231 cells to VWF, we next examined whether targeting GPIbα on the surface of MDA-MB-231 cells may also inhibit adhesion of these tumour cells to endothelial VWF. Importantly, anti-GPIbα antibodies 1D12 and 2B4 were previously shown to reduce platelet aggregation and metastasis in B16F10 melanoma cells and LLC *in vivo* mouse model.[184] Notably, this study was unable to distinguish whether the inhibitory effect was mediated by targeting GPIbα expressed on platelets, which would comprise the majority of available GPIbα sites or GPIbα expressed on tumour cells directly or perhaps a combination of both.[184] However, treating with anti-GPIbα antibodies was shown to inhibit GPIbα-VWF adhesion which not only prevented LLC adhesion to platelets and platelets to HUVEC but also inhibited LLC adhesion to HUVEC. These data suggest that in lung and melanoma murine models, VWF-platelet-tumour interactions and subsequent tumour-endothelial binding are supported by GPIbα expression. Furthermore, this data was recapitulated in HCT116 colon cancer cells, MDA-MB-231 breast cancer cells and A549 lung cancer cells using an anti-human YQ3 antibody with epitopes overlapping those of the 1D12 and 2B4 antibodies. Considering this treatment removes platelet-tumour cell interaction it is tempting to speculate that in this model VWF is able to bridge both tumour cells and endothelial cells through GPIbα and at least partially prevent the metastatic invasion seen through this. To further define a role for breast tumour expressed GPIbα in promoting a direct interaction with VWF, we pre-treated MDA-MB-231 cells with an anti-GPIbα antibody before perfusing them over an activated endothelial layer in the absence of platelets.

Concordant with inhibition of VWF and MDA-MB-231 cells under static conditions, targeting GPIbα expressed on MDA-MB-231 cells ablated endothelial adhesion of MDA-MB-231 cells. Importantly, as no platelets are present in our assay, in contrast to previous studies, we can confirm inhibition is likely specific to GPIbα expressed on MDA-MB-231 cells. Our data analysis showed that PMA activated endothelial cells and isotype treated endothelial cells had no significant difference in breast tumour surface coverage, although the isotype conditions did display a larger inter-assay variation, while anti-GPIbα treated MDA-MB-231 endothelial adhesion was significantly attenuated (30.21 ± 4.084 cells/mm^2 versus 43.59 ±

13.45 cells/mm^2 versus 8.315 ± 3.358 cells/mm^2, respectively, $p<0.01$ and $p<0.05$, Figure 4.17 A+B). Correspondingly, $K_{[on]}$ attachment rates were dramatically decreased in the anti-GPIbα conditions compared to the isotype control (0.45 ± 0.11 cells/mm^2/s vs. 7.16 ± 1.2 cells/mm^2/s, $p<0.01$, Figure 4.17 C). Finally, detachment rates $K_{[off]}$ resulted in no significant change upon anti-GPIbα treatment compared to control conditions, notwithstanding the significant spread in the data (Figure 4.17 D). These findings reveal for the first time that breast tumour expressed GPIbα can promote direct adhesion of circulating breast tumour cells to endothelial VWF. Altogether, the data points to the potential of multiple receptors expressed on triple negative breast tumour cells including LRP1 and GPIbα, which may be involved in the initial adhesion of circulating breast cancer cells to VWF released from activated endothelium. The role of these receptors in breast cancer and the relative contribution of each *in vivo* remains to be fully examined.

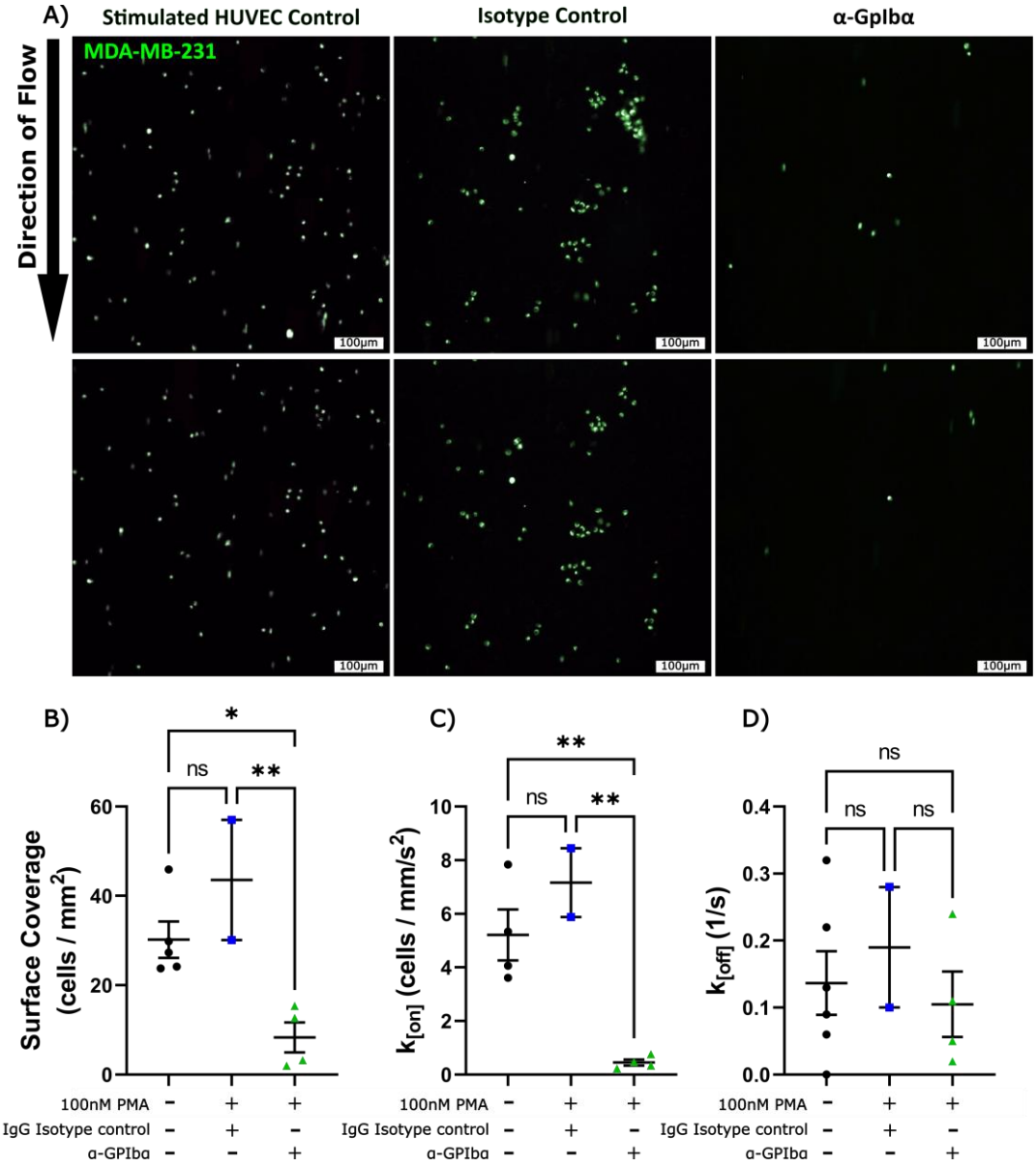

Figure 4.17 anti-GPIbα treatment inhibits endothelial adhesion to MDA-MB-231 cells under shear stress: HUVEC monolayers cultured on ibidi channel slides were stimulated with 100nM PMA to ensure maximal release of VWF in the presence and absence of anti-GPIbα antibody or a species matched isotype control. MDA-MB-231 cells were treated and fluorescently labelled before being perfused over the HUVEC monolayer at a venous shear stress of 0.25dyn/cm^2 in the presence of either anti-GPIbα antibody or a species matched isotype control. Adhesion events were imaged at 10x magnification for up to 700 frames. **A)** Representative images of cellular perfusion were taken at different time points to highlight differences in surface coverage of breast tumour cells under different experimental conditions. Tumour cell adhesion was quantified by **B)** stable adhesion through surface coverage (cells/mm^2), **C)** attachment rates $K_{[on]}$ (cells/mm^2/s), **D)** detachment rates $K_{[off]}$ (1/s). Data is presented as the mean ± SEM. Significance was determined through one way ANOVA using Tukeys multiple comparison test, * $p \leq 0.05$, ** $p \leq 0.01$.

4.6 Discussion

Metastasis, or the spread of tumour cells from their original site to a distal secondary site, is a multifaceted yet not fully understood process. The route of metastatic dissemination can be either lymphatic or haematogenous. The lymphatics are usually the first site of metastasis as it has fewer physical restrictions than the endothelial layer, pericytes and tight junctions of the haematogenous metastasis route.[353] Interestingly however, this route of metastatic spread can ultimately lead to haematogenous metastasis as tumour cells eventually drain out of the left or right thoracic duct into the subclavian vein. Correspondingly, in a prostate cancer study, of the 415 patients that had pelvic or paraaortic lymphatic metastasis, 84% had simultaneous haematogenous spread, displaying the link between the two forms of metastasis.[354] Breast tumours have also been reported to form tumour cell nests that can occur within lymph nodes and develop blood vessels around them. These nests can then integrate into the blood stream for further dissemination but are restricted to blood and not lymphatic vasculature in order to disseminate.[355] Furthermore, it has been shown that some breast cancer tumour nests do not require penetration of the vascular wall in order to enter the circulation.[356] Despite the high mortality rate associated with metastasis, it is estimated that less than 0.01% of circulating tumour cells go on to form distant metastases highlighting the significant complexities involved in blood-borne metastasis.[357–359]

A prerequisite for haematogenous metastasis is tumour adhesion to the endothelial cell wall where cancer cells can subsequently invade through the endothelial barrier via a variety of mechanisms including tight junction remodelling and extracellular matrix break down.[360–362] As previously stated, VWF has been linked with increased tumour cell adhesion and colonisation of the endothelial wall. In an *in vivo* metastasis model, tumour cell arrest of melanoma A2058 cells was linked with extensive clot activation. However, while the VWF signal was not as abundant as platelets through multiphoton laser-scanning microscopy, VWF was found to be located in more specific microvascular regions adjacent to the tumour cells.[241] Concordant with these observations in mice, immunohistochemical analysis of brain metastasis sections from patients with breast cancer depicted VWF adhesion next to breast cancer brain metastases. Furthermore, several reports have shown VWF adhesion to a number of receptors on the surface of several tumour cells both under static binding and shear stress conditions.[187,190,239,240] Despite this, the receptors contributing to VWF-breast

cancer adhesion remain uncharacterised. A number of endothelial receptors including selectins, β1-integrin subunit and β3-subunit have been postulated to contribute to the arrest of circulating tumour cells along the endothelium *in vitro* with an important role also highlighted for tumour cell receptors including tissue factor, $\alpha_5\beta_1$ and $\alpha_v\beta_3$ in modulating tumour-endothelial adhesion.[324,363,364] In fact a recent study has outlined a two-step adhesion process where endothelial cells deposit fibronectin to favour $\alpha_5\beta_1$-mediated cancer cell adhesion.[364] However, potential contribution of endothelial VWF and indeed the receptors involved in promoting VWF-tumour adhesion along the endothelium under fluidic forces has not been fully examined. Given the direct interaction observed between VWF and breast tumour cells *in vitro* and the role of this interaction in facilitating MDA-MB-231 breast tumour cell adhesion to the endothelium under shear flow, we sought to identify the specific regions of VWF as well as breast tumour receptors involved in mediating this effect.

4.6.1 Characterising specific VWF domains that are important in regulating binding to breast tumour cells

Our results showed that VWF adhesion to MCF-7 and MDA-MB-231 cells was mediated by multiple binding domains along the VWF structure. However, VWF adhesion was most prominent within the D'A3 domains of VWF for both cell lines tested, with a small contribution of the A3-CK C-terminal end of VWF in also mediating binding to MDA-MB-231 cells. Interestingly, the degree of adhesion of truncated VWF to the breast cancer cells was not as high as full-length VWF, this is likely due to multiple binding sites along the VWF structure.

While no studies have previously characterised breast cancer adhesion to VWF, interestingly, characterisation of B16-BL6 murine melanoma cell adhesion to recombinant variants of VWF revealed that deletions in the A1 and A2-VWF domains had no effect on adhesion when compared to baseline binding in wild-type VWF.[190] However, deletions in the C-domains, and more specifically, the RGD motif purported to be within the VWF C4-domain both resulted in near complete abolishment of VWF adhesion to the melanoma cells. Accordingly, for human MV3 melanoma cells, deletions in the RGD domain of VWF also severely reduced tumour-VWF adhesion.[240] However, in contrast to the previous study, they also found that a deletion in the A1 domain also displayed significant reduction in tumour adhesion to VWF compared to the wild type VWF. Our novel data delineates a unique role for the D'A3 region of VWF in mediating direct adhesion to MCF-7 breast cancer cells. However, not unlike VWF-melanoma

interactions, multiple sites within VWF may facilitate binding to MDA-MB-231 cells. Moreover, the role of multiple domains in VWF-breast tumour adhesion may indicate a role for multiple candidate receptors that VWF can adhere to on the surface of breast cancer cells.

Of note, while we found that the D'A3 region bound with the greatest affinity in our assays it is interesting that the A1A2A3 domains were unable to replicate the full extent of this adhesion. This is especially interesting as many of the most prominent VWF binding domains exist within the VWF-A1 domain. This result may be due to the amino acid boundaries of the VWF constructs in our assays. It is possible that the additional D'D3 domain within the D'A3 construct confers additional stability to the A1A2A3 domain, conformationally changing the A1 domains to become more permissive to receptor interactions. Interestingly, it has been reported that a linker domain between the D3 and A1 domains exists that modifies VWF A-domain affinity with GPIbα.[365] Furthermore, the flanking regions either side of the A1-domain referred to as N- and C- terminal autoinhibitory modules (NAIM and CAIM) can prevent the A1 adhesive capabilities.[20] It is possible that the truncated A1A2A3 fragments used in our assay have decreased affinity to the tumour cells due to the flanking regions and construct domain boundaries conferring residual inhibition.

We used variant forms of recombinant VWF to assess adhesion to breast cancer cells, this was done both through truncated derivations of VWF for domain analysis and as a full-length recombinant structures for receptor adhesion. Interestingly, it has been reported that plasma-derived and recombinant varieties of VWF have differing functional properties, with a clinical grade recombinant VWF (Vonicog alfa) described to increase the mediation of platelet adhesion to collagen under shear stress, platelet-binding activity and FVIII binding compared to other clinical plasma-derived preparations like haemate-P.[366] It is possible that plasma VWF within patients interact with breast cancer cells differently than our recombinant VWF. However, we have performed breast cancer adhesion experiments using pd-VWF, not shown in the thesis, that demonstrate similar binding profiles to our recombinant protein. Notably, as plasma-derived variants of VWF for clinical use, like Haemate-P, are prepared with greater levels of FVIII along the D'D3 region of VWF it is interesting that the binding to breast cancer cells does not seem to interfere with adhesion. Perhaps indicating that the FVIII binding site within the D'D3 assembly of VWF is not a major factor in breast cancer cell adhesion.

4.6.2 Differential receptor expression on MCF-7 and MDA-MB-231 cells and their role in mediating adhesion to VWF and to the endothelium

It has been proposed that tumour cells can use invasion techniques that are similar to leukocyte extravasation.[358,367,368] Specifically, this process of tumour extravasation is characterized by initial cell capture, tethering, rolling, firm adhesion, and subsequent transmigration through endothelial cells. Evidence has shown that PSGL-1 can mediate immune cell arrest and contribute to the initial stages of endothelial transmigration.[261] Moreover, PSGL-1 has been described to bind directly to VWF through the A1-domain.[261] Therefore, we assessed the potential role of PSGL-1 on breast tumour cells. Despite displaying significant expression of PSGL-1, MDA-MB-231-VWF adhesion was not mediated via this receptor. Notably, the PSGL-1 antibody utilised has been previously characterised as functionally blocking and interferes with the recognition of P- and L-selectin as well as VWF to the PSGL-1 receptor.[261,339] Despite this, our data suggests no role for PSGL-1 in promoting direct interaction between breast tumour cells and VWF *in vitro*.

Integrins are key mediators of direct binding to tumour cells and the subsequent adhesion to the endothelial barrier.[360] Reports of a panoply of integrins that adhere to a range of tumour cells *in vitro* have been highlighted including the β1-subunit, β4-subunit as well as $\alpha_5\beta_1$ and $\alpha_v\beta_3$ heterodimers.[364,369,370] Moreover, expression of $\alpha_v\beta_3$ on 45 different human tumour cell lines seemed to correlate with tumour transmigration.[360,371] Despite evidence of marked $\alpha_v\beta_3$ expression in our MDA-MB-231 cells compared to MCF-7 cells, blocking $\alpha_v\beta_3$ had no effect on VWF adhesion to the triple negative invasive MDA-MB-231 cell line. This is surprising as $\alpha_v\beta_3$ has been isolated as a key VWF binding partner in a diverse range of independent studies within its role in haemostasis but also in a cancer setting directly adhering to tumour cells.[118,190,239,262] Direct VWF adhesion to $\alpha_v\beta_3$ expressed on tumour cells has been reported in gastric cancer cells and in melanoma models.[118,190,239,240] Interestingly, Terraube *et al*. found that inhibiting the integrin β_3-subunit and not the α_v-subunit had the greatest diminution of VWF adhesion to melanoma cells.[190] Furthermore, in gastric BGC823 cancer cells, platelet and VWF adhesion to the cancer cells was prevented by specifically targeting the β_3-subunit.[118] Contrastingly, in an *in vitro* model of colon cancer cell adhesion to the endothelium, inhibition of α_{IIb}-, β_1- or β_3- integrin subunits all demonstrated no significant reduction in VWF mediated

adhesion to the endothelium, suggesting that other integrin-independent mechanisms may also exist for direct tumour-VWF adhesion.[168]

Notably, within our assay we specifically targeted the whole $\alpha_v\beta_3$ heterodimeric receptor complex, perhaps breast tumour adhesion is not localised to the $\alpha_v\beta_3$ receptor but instead another integrin family member with the β_3-subunit. In support of this hypothesis, VWF adhesion to MDA-MB-231 cells was significantly inhibited by targeting the integrin RGD binding motif on VWF with an RGDS peptide. Together, this suggests a role for the RGD-binding motif within VWF in mediating MDA-MB-231 adhesion but also infers a role for tumour integrins in this interaction. Further investigation is warranted to elucidate the specific integrin(s) that may mediate VWF C-domain attachment to MDA-MB-231 breast tumour cells.

The mechano-receptor GPIbα is classically expressed on platelets, which circulate in the bloodstream. GPIbα has only a few described binding ligands including VWF and thrombin.[341] With reports of GPIbα expression on some breast cancer cells including MCF-7 and MDA-MB-231, it is interesting to note that there may be a selective advantage to tumour cells expressing this receptor that are undergoing haematogenous metastasis with enhanced ability to interact circulating and endothelial-bound VWF.[187,188] Furthermore, in a lung adenocarcinoma platelet-mediated metastatic mouse model specifically targeting the VWF-GPIbα axis resulted in a reduction of pulmonary metastasis in a VWF expressing cancer cell line compared to the untreated conditions.[142] Correspondingly, our findings show that targeting GPIbα in our static VWF binding assays indeed inhibited VWF-MDA-MB-231 interactions.

GPIbα expression on tumour cells has been linked with increased platelet aggregation and subsequent platelet-VWF-tumour heteroaggregation.[143,187] Interestingly, in MDA-MB-231 cells with GPIbα expression, adhesion to immobilised VWF resulted in elongation of the cell filopodia which is a hallmark of migration.[188] Furthermore, VWF treatment in these MDA-MB-231 cells displayed enhanced aggregate formation which was inhibited through a monoclonal antibody against the VWF-A1 domain, the GPIbα binding site. Strikingly, while most circulating tumour cells circulate as single cells, those that travel in clusters or heteroaggregates with platelets are much more likely to avoid immune detection and form distant metastasis.[358,372,373] Our novel findings now also suggest that inhibition of GPIbα on

MDA-MB-231 cells ablates adhesion to an activated endothelial layer under shear flow. This is in agreement with the report that found that inhibiting the VWF-GPIbα interaction attenuated not only platelet-endothelial cell and platelet-tumour cell interactions but also tumour-endothelial cell adhesion.[184] Taken together, these data suggest that GPIbα expressed on MDA-MB-231 breast tumour cells may help in bridging tumour cell adhesion to the endothelium through VWF and that GPIbα is at least partially responsible for arresting circulating breast tumour cells to the endothelial cell wall *in vitro*.

The role of LRP1 in cancers is a controversial one, with many reports of LRP1 playing contradictory roles in cancer progression. Indeed, low levels of LRP1 were found to be associated with increased invasiveness and tumour progression in colonic and HCC cell lines as well as colonic, HCC, prostate and melanoma IHC samples.[374–378] However, this is in contrast to accumulating reports of a pro-cancerous role of LRP1, specifically in breast cancer.[344,348,349,351,352,379,380] Intriguingly, it was found in a cohort of Iranian patients with breast cancer that *LRP1* gene levels were lower in those that responded to chemotherapy.[381] In support of this, *LRP1B,* a close homologue of *LRP1* and one of the top 10 mutated genes in human cancer, is largely considered a tumour suppressor for most cancers but not in fact for breast cancer.[350,382,383] Immunohistochemical staining of LRP1B in invasive ductile carcinomas revealed that nuclear LRP1B was associated with poorer survival and, in addition, nuclear expression of LRP1B increased matrigel invasion activity in MCF-7 and T47D breast cancer cells.[384]

In a recent paper it was discerned that MDA-MB-231 breast cancer cells lost self-supported motility upon LRP1 downregulation in both colloidal gold migration assays and scratch assays. This effect was linked to a destabilisation of EGFR levels that was inducible in both tumours and non-neoplastic cells.[380] Furthermore, in a study examining LRP1 expression in several breast cancer cell lines *in vitro*, it was found that cell lines that exhibited greater than 1000 LRP1 sites per cell (MDA-MB-231, BT-20, HS-578T) displayed a direct association with invasiveness as opposed to those that had fewer than 1000 LRP1 sites per cell (MCF-7, HMEC).[349] Moreover, in MDA-MB-231 cells, treatment with 40μg/mL RAP was able to reduce both invasion and migration by nearly half compared to controls. Altogether, it suggests there is a precedent for LRP1 to contribute not only to adhesion but also to cell motility in migration and invasion.

LRP1 and VWF have a well described interaction in the regulation of VWF plasma levels where cluster II and IV of LRP1 on macrophages is described to adhere through the A1 and A3 domains of VWF.[314,338,342] As a result, tumour expressed LRP1 was of particular interest as a candidate VWF receptor. Our results highlight that not only does LRP1 expression significantly increase in the more invasive MDA-MB-231 cell line than the poorly metastatic MCF-7 cells but also that inhibition of LRP1 significantly decreases VWF adhesion to MDA-MB-231 cells. LRP1 adhesion to VWF has been described to be dramatically enhanced by the shear forces experienced in the blood, likely due to a cryptic LRP1 site on folded VWF.[314,342] Congruent to this, our novel data demonstrates that tumour LRP1 inhibition abolished direct adhesion of MDA-MB-231 tumour cells to both immobilised VWF as well as endothelial associated VWF strings under fluidic stress. This inhibitory effect was confirmed by two distinct approaches, a blocking LRP1 antibody as well as use of an LRP1 antagonist RAP, known to have a strong affinity for cluster II, III and IV regions of the LRP1 receptor.[347] Additionally, while RAP is a non-specific inhibitor known to target a number of low density lipoproteins, including very low density lipoprotein receptor (VLDLR), a direct and specific VWF-LRP1 interaction was further confirmed by proximity ligation assay, which could also be inhibited upon the addition of RAP.[349,385]

Interestingly, RAP treatment of LRP1 expressing MDA-MB-231 cells was previously found to reduce invasion and migration *in vitro*.[349] Congruently, LRP1 has been described to have a pro-invasive role in breast cancer. Using atomic force microscopy, siRNA and shRNA knock-down of breast tumour LRP1 resulted in decreasing the migration of MDA-MB-231 seeded on collagen and to a lesser extent fibronectin.[352] Additionally, LRP1 silencing prevented LRP1 mediated cellular movement and impaired cell speed of MDA-MB-231 cells on collagen. In addition to this enhanced tumour migration role for LRP1, it has been described to increase well known pro-invasive proteases, MMP-2 and MMP-9 in human glioblastoma and MMP-9 in breast cancer 4T1 cells.[348,351,379] Moreover, silencing of LRP1 ligand protease nexin-1 in those 4T1 breast cancer cells severely attenuated lung metastasis in an *in vivo* mouse model. Altogether, these data point to important role for LRP1 in contributing to breast tumour disease progression yet, importantly, the LRP1 ligands and mechanisms underpinning all of these effects have not been fully defined. Thus our observation of VWF as a novel ligand for

breast tumour LRP1 may be of significant interest in understanding key initial endothelial adhesion events in blood-borne metastasis of breast tumour cells.

Separately, but also of relevance to understanding the potential role of VWF in tumour-endothelial tethering, Mojiri *et al*. have described that VWF expressing osteosarcoma SAOS2 and glioma U251 cells display enhanced endothelial adhesion compared to VWF siRNA knock down tumour cells.[143] While the endothelial receptor involved in tumour adhesion was not studied, the effect appears to be at least in part dependent on the presence of platelets, with significant tumour-platelet heteroaggregate formation along the endothelial monolayer under both static and shear stress conditions observed. These data point to a role for VWF, expressed directly by tumour cells, in contributing to enhanced interactions of tumour cells with platelets and endothelial cells *in vitro*. Although, we do not observe VWF expression in our breast cancer cells, the expression of both LRP1 and GPIbα receptors appears to directly promote VWF-breast tumour interactions which contribute to tethering along an activated endothelial layer under shear stress. Collectively, these data may suggest that different tumour types utilise distinct mechanisms to facilitate endothelial adhesion as they disseminate through the vasculature. This may also be influenced by the subsequent colonization tissue or tropism favoured by different tumour types, for example triple negative breast cancers that metastasize to the liver, lung and bone may favour binding to endothelial released VWF multimers.[386] In contrast, gliomas, which have been shown to directly express VWF tend to spread within the brain tissues.[387]

In summary, we have identified through the use of specific truncated VWF domain fragments that VWF adhesion to MDA-MB-231 cells was mediated by multiple domains. However, the predominant VWF domains responsible for triple negative breast cancer cell adhesion to VWF are D'A3, in contrast to the distinct role the VWF C-domains play in melanoma cell adhesion. By characterising specific tumour receptor expression we were able to identify both GPIbα and LRP1 as key receptors in VWF-MDA-MB-231 breast cancer cell adhesion both statically and under shear flow. However, the relative contribution of each of these receptors *in vivo* remains to be examined. Notwithstanding this, we were also able to characterise a partial role for the RGD motif in the C-domains of VWF, indicating a potential role for as of yet unidentified tumour integrins. Altogether, VWF multimers released from the endothelial layer can facilitate stable adhesion of circulating MDA-MB-231 cells along the endothelium through

both breast tumour expressed LRP1 and GPIbα (Figure 4.18). This interaction may serve as a preliminary step to breast cell invasion and eventual colonisation and metastasis of distal tissues.

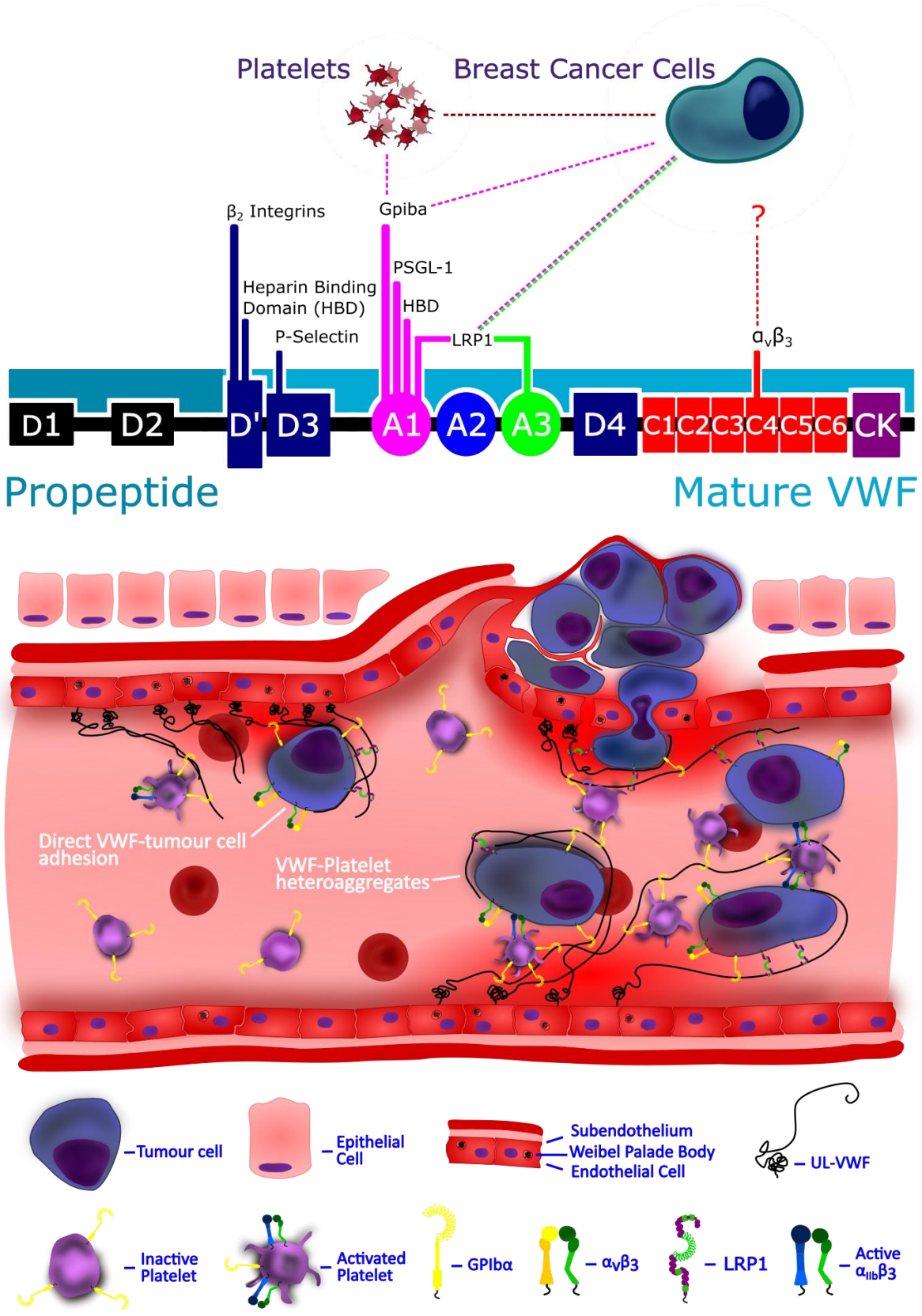
Platelets
Breast Cancer Cells
β2 Integrins
Gpiba
PSGL-1
Heparin Binding Domain (HBD)
HBD
P-Selectin
LRP1
αvβ3
?
D1
D2
D'
D3
A1
A2
A3
D4
C1
C2
C3
C4
C5
C6
CK
Propeptide
Mature VWF
Direct VWF-tumour cell adhesion
VWF-Platelet heteroaggregates
Tumour cell
Epithelial Cell
Subendothelium
Weibel Palade Body
Endothelial Cell
UL-VWF
Inactive Platelet
Activated Platelet
GPIbα
αvβ3
LRP1
Active αIIbβ3

Figure 4.18 Chapter summary - The adhesion profile of breast cancer cells to VWF strings: VWF can adhere to breast cancer cells through indirect platelet adhesion however in addition VWF has now been shown to display direct adhesive to breast cancer cells. Breast cancer cells expressing LRP1 and GPIbα on their surface are capable of interacting with VWF strings both statically and under conditions of shear stress. In the blood VWF release from endothelial cells by tumour cell activation could promote tethering of circulating tumour cells to the endothelium, potentially enhancing the metastatic advancement of the breast cancer cell into a secondary site.

Chapter 5: Investigating a potential role for VWF in breast cancer metastasis

5.0 Introduction

5.0.1 Roles for VWF in promoting metastasis

Metastasis of a tumour cell from a primary tumour mass is determined by a number of molecular alterations within individual tumour cells.[358] These alterations are important for establishing a metastatic niche, remodelling the ECM as well as enhancing immune evasion, tumour cell migration, colonisation, EMT switching and chromosomal instability.[358] *In vitro* assays have been developed that assess the pathological changes in cancer cells as they become more metastatic.[388] A growing body of evidence suggests that VWF may promote metastasis in cancers.

A recent report from our group showed that VWF secreted from endothelial cells can adhere to circulating tumour cells and promote adhesion.[156] In addition osteosarcoma cells expressing VWF demonstrate increased tumour cell adhesion as well as colonisation and migration through the endothelial layer.[143] Furthermore, it was found that VWF was primarily responsible for LLC and B16-BL6 melanoma tumour cell adhesion and transmigration through the endothelial layer in hyperglycaemic conditions.[300] Other studies have implicated VWF in the platelet cloaking of tumour cells to avoid immune cell surveillance.[118,148,187,242] Furthermore, studies using wound healing and transmigration assays have reported pro-migratory roles for VWF in a number of cancers.[3] Cumulatively, these data suggest that VWF has the potential to influence various steps in metastasis.

Interestingly, Karpatkin *et al*. described that inhibition of VWF in CT26 colon cancer cells, B16 melanoma cells and T24 bladder cancer cells injected into mice resulted in a 53-64%, 45% and 46% reduction in pulmonary metastases respectively.[189] In another study, anti-VWF antibody treatment inhibited brain metastasis of JimT1 breast cancer cells from the perivascular niche as determined by multiphoton laser scanning microscopy.[241] Moreover, antibody targeting of the VWF-GPIbα axis in B16F10 melanoma, LLC and 4T1 breast cancer cells also significantly reduced pulmonary metastatic foci.[184]

Concordant with evidence that inhibiting VWF prevents metastasis, VWF expressing tumour cells display pro-metastatic functions. Notably, in NOD/SCID mice, VWF over-expressing BGC823 gastric cancer cells had significantly worse overall survival than the control.[118] Importantly, both siRNA knockdown and direct anti-VWF antibody treatment of the VWF

over-expressing BGC823 gastric cancer enhanced overall survival. Congruently, 4T1 breast cancer cells shown to express VWF were linked with increased pulmonary metastatic node formation in an *in vivo* mouse model compared to VWF knockdown cells.[141]

5.0.2 The anti-metastatic effect of VWF in cancer

Despite the evidence that VWF may enhance tumour metastasis, *in vivo* studies have reported some apparently paradoxical findings. Terraube *et al*. showed increased pulmonary metastasis in VWF-deficient mice tail vein injection of B16-BL6 melanoma cells and LLC cells.[190] Of note, treatment with recombinant VWF corrected metastasis levels to those of wild-type controls. While VWF treatment had no effect on migration and invasion of B16-BL6 melanoma cells, it did enhance cell death.[255] Notably, Mochizuki *et al*. reported another apoptotic role for VWF in a specific subset of cancer cells that did not express the VWF cleaving protease ADAM28.[101] Interestingly, knock down of ADAM28 expressed on PC-9 lung and MDA-MB-231 breast cancer cells not only induced susceptibility to VWF mediated apoptosis, but also reduced tumour growth and metastasis *in vivo*.

More recently, a study reported increased apoptosis in ADAM28 knockdown SGC7901 gastric cancer cells that could be ablated through siRNA knockdown of VWF.[144] Mochizuki *et al*. also determined that ADAM28 promoted metastasis *in vivo* by cleaving insulin growth factor binding protein-3 (IGFB-3) to release proliferative molecule insulin growth factor (IGF).[389] Furthermore, in BGC823 and SGC7901 gastric cancer cells ADAM28 over-expression promoted gastric cancer cell proliferation and migration.[144] Although VWF is described to have a pro-apoptotic effect in ADAM28 knockdown cells, it is unclear to what extent VWF cleavage contributes to the metastatic pathogenesis associated with ADAM28 inhibition.

Importantly, ADAMTS13-deficient mice have also been assessed for pulmonary metastasis following B16-BL6 melanoma tail vein injection.[181] Metastatic foci were increased in ADAMTS13-deficient mice where luminal VWF fibres were correlated with greater levels of pulmonary metastasis. Therefore, a paradox exists where VWF-deficiency and elevated luminal VWF are both pro-metastatic, but conversely VWF has also been found to be a pro-apoptotic factor.

5.0.3 VWF and angiogenesis

Angiogenic regulation is a key process in tumour growth with early carcinomas limited by the diffusion limit from the nearest capillary.[390] As tumour cells develop vascular and lymphatic systems there is an increased propensity for tumour cells to spread.[390] Following tumour cell dissemination, neovascularisation is again required to colonise the secondary site. Tumour cells induce angiogenesis through a sequence of steps including release of growth factors (VEGF, FGF) where endothelial cells then remodel the ECM before they can begin to generate sprouting tips towards the stimulant.[390] Through migration and proliferation, a new vessel is formed allowing blood to perfuse into the new vasculature.

Recent data suggests that VWF may play a role in regulating angiogenesis. In a stroke mouse model, both VWF-deficiency and VWF-targeted antibody neutralisation promoted vascular remodelling after stroke.[391] Interestingly, VWF-deficient HUVEC displayed significantly higher tube formation than wild-type cells.[73] Furthermore, addition of exogenous VWF reduced HUVEC tube length.[73] VWF-deficient mice were also found to have increased angiogenesis with increased blood vessel density in the vascularised mouse ear. In contrast however, a matrigel angiogenesis assay found reduced tubule formation in endothelial colony-forming cells (ECFC) derived from type-3 VWD patients with near-complete VWF-deficiency compared to control cells. [178]

Starke *et al.* proposed that VWF mediates endothelial cell angiogenesis by regulating Ang-2 storage in endothelial cells.[73] Multiple studies have found that complete loss of VWF in endothelial cells is associated with dysregulated increases in Ang-2 and galectin-3 levels.[73,74,100,178] Neovascularisation and network development at the angiogenic front of retinal vasculature was associated with a decrease in WPB density within endothelial cells.[74] Furthermore, release of WPB through VEGF-VEGFR signalling was responsible for Ang-2 mediated pericyte migration.[74] Cumulatively, these data indicate that the pro-angiogenic effects seen in VWF-deficient endothelial cells may be due to WPB depletion and dysregulation of Ang-2.

In contrast to its role as an inhibitor of angiogenesis, a novel role as a growth factor reservoir has also been suggested for VWF.[100] A range of growth factors have been demonstrated to adhere to VWF through the A1-domain including VEGF-A, FGF-2, FGF-7, TGF-β1, NT-3, PIGF-2, PDGF-AA, PDGF-BB and PDGF-DD.[100] VWF-deficiency in mice caused defective wound

healing and reduced levels of growth factors. Similarly, in a hind limb ischemia model it was found that blood recovery was impaired in VWF-deficient mice.[179]

5.0.4 A role for VWF in promoting angiogenesis in cancer

In patients with glioblastoma magnetic resonance imaging found a correlation between VWF:Ag levels >248IU/dL and angiogenic parameters linked with increased permeability and blood flow.[392] Interestingly, 4T1 breast cancer cells expressing VWF exhibited increased CD34 expression in tumour sections compared to VWF knockdown cells, suggesting that blood vessel formation was enhanced by VWF in this model.[141] Furthermore, the conditioned media from VWF over-expressing MDA-MB-231 and MCF-7 breast cancer cells was shown to induce angiogenesis in HUVEC.[141]

Assessment of vascular angiogenesis in a melanoma mouse model found that greater vessel size positively correlated with increased luminal VWF fibres.[181] Cossutta *et al*. found in a tumour angiogenesis model that VWF depletion from endothelial cells upregulated Ang-2 mediated angiogenesis.[74] Increased release of Ang-2 resulted in a 2.4-fold reduction in pericyte coverage of remodelling tumour vessels.[74] It was concluded that WPB exocytosis and Ang-2 secretion are regulated during angiogenesis to limit pericyte coverage of vessels.[74]

Importantly, the conditioned media from breast cancer cells were described to induce endothelial angiogenesis.[141,156] Moreover, in a VEGF-A dependent manner conditioned media from melanoma, breast, gastric and urothelial cancers have been shown to induce VWF release from endothelial cells.[119,148,153,156,181] Collectively, in addition to endothelial WPB exocytosis promoting angiogenesis in a tumour setting, released luminal VWF has also been described to promote angiogenesis. It is likely that the angiogenic effects of VWF seen in tumour cells are a result of two mechanisms. Firstly, tumour cell secretions induce WPB and VWF release and indirectly dysregulate Ang-2 secretion from endothelial cells. Secondly, increased luminal VWF can directly induce angiogenesis through growth factor retention.[100]

5.0.5 VWF as a metastatic agent

Aside from articles reporting absolute VWF:Ag levels in patients with metastasis, clinical data on VWF levels and their link with cancer are very limited. Notably, a retrospective study that tracked 106 cancers in 92 Italian patients with VWD found that no patients with type 3 VWD displayed metastasis. [393,394] However, the data remains inconclusive due to the size of the

study. To date no study has been attempted to track the epidemiological onset of cancer and metastasis in VWD patients at a large enough scale to derive meaningful results.

Another consideration is the role of blood groups in the onset of cancer. VWF and FVIII levels are known to be up to 25% higher in non-O blood group subjects.[395] In a non-small cell lung cancer cohort, VWF and FVIII were the only haemostatic parameters significantly upregulated between O and non-O blood groups in patients with lung cancer. [396] Correspondingly, non-O blood groups have been attributed with increased risk for diverse cancers.[396–401] It is possible that VWF is a confounding factor for the increase of cancers in non-O blood groups.

5.1 VWF induced wound closure in breast cells

5.1.1 Assessing the effects of VWF on wound closure for non-neoplastic breast cell lines

In the previous chapter we showed VWF can adhere to and promote breast cancer cell tethering to the endothelial layer. Subsequently, we wanted to assess whether VWF could promote migration and cell motility in breast cancer cells and whether the functional differences were distinct from non-neoplastic breast cell lines. In a scratch wound assay, siRNA knock down of VWF in HUVEC resulted in increased migration and reduced directionality suggesting that VWF may play a role in non-cancerous cell migration.[73] Furthermore, endothelial VWF has been shown to enhance osteosarcoma cell metastasis by triggering known pro-migratory EMT switches through upregulation of transcription factor TWIST.[161]

We first investigated the migratory effect of VWF in a scratch wound assay. As a preliminary step we studied whether VWF induced motility of non-cancerous primary breast cells (HMEC). We determined that VWF treatment had no significant difference on migration compared to the negative control (AUC: 3152 (CI: 2967 – 3336) vs 2942 (CI: 2702 – 3183), p = 0.647, Figure 5.1 A+B). Similarly, VWF had no significant effect on non-neoplastic MCF-10A (AUC 2084 (CI: 1913-2255) vs 2267 (CI: 2045 -2489), p = 0.695, Figure 5.1 C+D). 10% FCS was used as a positive control.

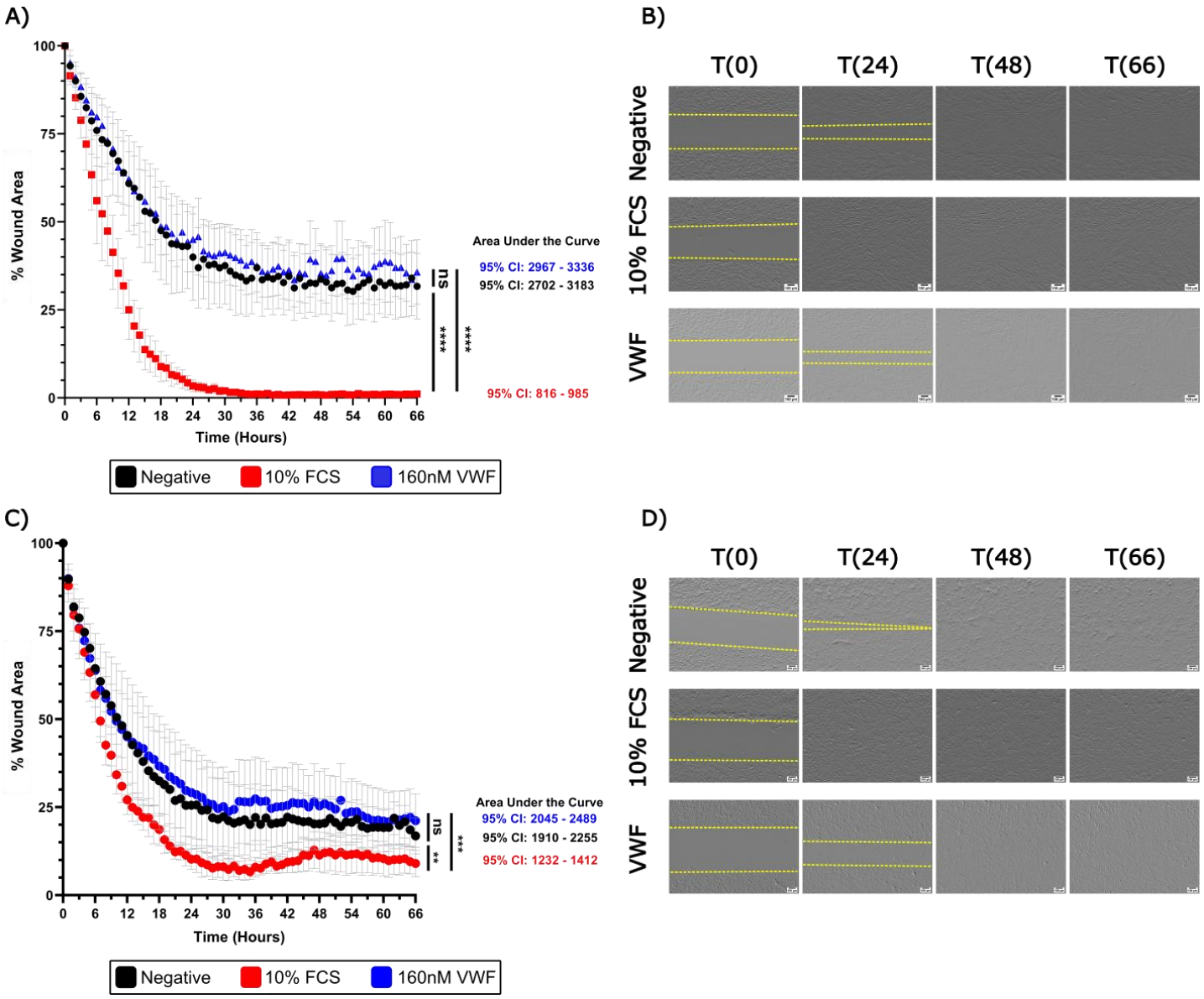

Figure 5.1 VWF does not influence wound closure in non-neoplastic MCF-10A or HMEC breast cells: MCF-10A (N=3) and HMEC (N=3) cells were seeded into silicon inserts and consistent scratches were made after cells had reached confluence. Cells were then treated ± 10% FCS or pd-VWF and left in serum free media. Wound closure was live imaged every hour over 66h in the cell discoverer 6 microscope at 10x magnification at 37°C. **A-D)** Images were quantified by measuring total remaining available space (pixels) over total possible space (pixels) as determined by an average from the first unstimulated control image. AUC was generated from the graph and values compared through ordinary one way ANOVA, significance was determined using Tukeys multiple comparisons test, **p ≤ 0.01, **** p ≤ 0.0001.

5.1.2 Assessing the effects of VWF on wound closure for breast cancer cell lines

Despite VWF being unable to alter cell migration and motility in the non-neoplastic breast cell lines, HMEC and MCF-10A there are reports of VWF mediated scratch wound migration in malignant cell lines.[140–142] For example, in two hepatocellular carcinoma cell lines HEPG2 and BEL7402 shown to express VWF, when VWF expression was knocked down with siRNA it resulted in a 57-65% and 46-60% decrease in wound closure respectively.[140] Furthermore, siRNA knockdown of VWF also reduced wound healing in 95D lung adenocarcinoma cells,[142] as well as in MDA-MB-231 and MCF-7 breast cancer cells.[141] Therefore we addressed the effect of VWF on cellular migration in malignant MCF-7 and MDA-MB-231 breast cancer cell lines.

We found that VWF treatment of MCF-7 cells significantly increased wound closure compared to the negative control (AUC: 4401 (CI: 4291 – 4510) vs 5635 (CI: 5551 – 5719), $p \leq 0.0001$) (Figure 5.2 A). Consistent with these data, MDA-MB-231 cellular motility was also significantly increased in a dose-dependent manner by VWF. Wound closure was enhanced compared to the negative control at every concentration tested (40nM - 320nM). For example, VWF migration was enhanced compared to the negative control at 160nM (AUC: 3869 (CI: 3688 – 4050) vs 5336 (CI: 5145 – 5528) $p \leq 0.0001$, Figure 5.2 B), which is a concentration similar to the plasma VWF:Ag levels we observed in the patients with breast cancer.

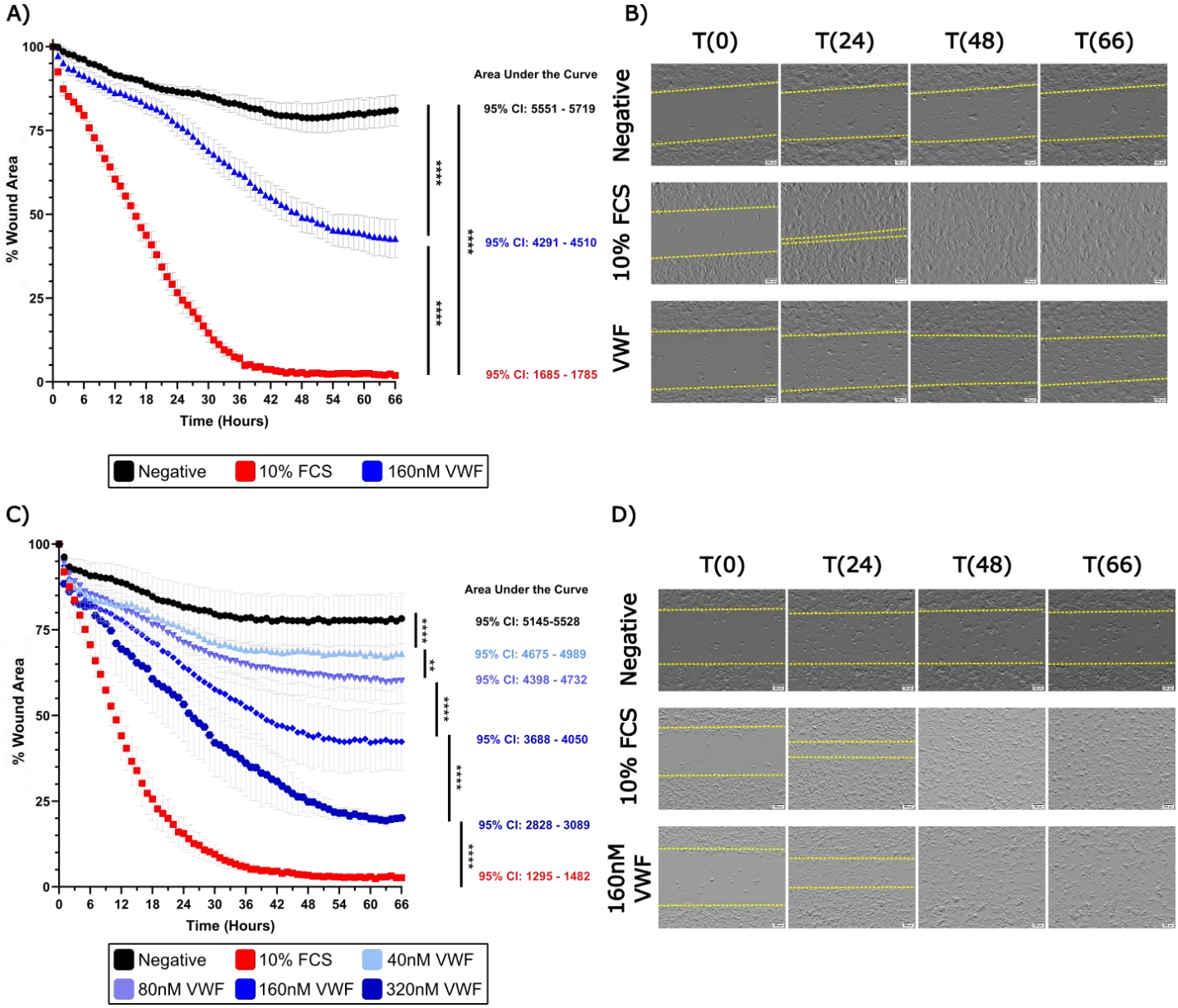

Figure 5.2 VWF enhances wound closure in MCF-7 and MDA-MB-231 breast cancer cells: MCF-7 (N=4) or MDA-MB-231 (N=4) cells were seeded into silicon inserts and consistent scratches were made by removing the inserts after cells had reached confluence. Cells were then treated ± 10% FCS or pd-VWF and left in serum free media. Wound closure was live imaged every hour over 66h in the cell discoverer 6 microscope at 10x magnification at 37°C. **A-B)** Images were quantified by measuring total remaining available space (pixels) over total possible space (pixels) as determined by an average from the first unstimulated control image. AUC was generated from the graph and values compared through ordinary one way ANOVA, significance was determined using Tukeys multiple comparisons test, **** $p \leq 0.0001$.

5.2 The effect of VWF on breast cancer cell line viability

5.2.1 Assessing the effect of VWF on cellular viability of breast cell lines.

VWF is reported to induce proliferation through the retention and delivery of growth factors like VEGF-A165 and PDGF-BB in smooth muscle cells *in vivo*.[100] However, to date the effects of VWF on tumour cell proliferation and viability are poorly understood with contradictory reports.[138,255] For example, up to 72h post VWF-treatment there was no significant effect on the proliferation of B16-Bl6 mouse melanoma cells.[255] Conversely, in TPC-1 papillary thyroid carcinoma cells knockdown of expressed VWF with siRNA reduced proliferation versus a normal control.[138]

Therefore, we next investigated the effects of VWF in cell viability assays. MCF-10A, MCF-7 and MDA-MB-231 breast cell proliferation and cell death were quantified at 24, 48 and 72h in the presence and absence of increasing VWF doses. Collectively, we found that during a 72h period VWF stimulation could not induce significant proliferation, or cell death in MCF-10A, MCF-7 or MDA-MB-231 breast cell lines at all doses tested (20nM-160nM) (Figure 5.3 A-C). Therefore, VWF had no effect on the cell viability of the breast cell lines tested.

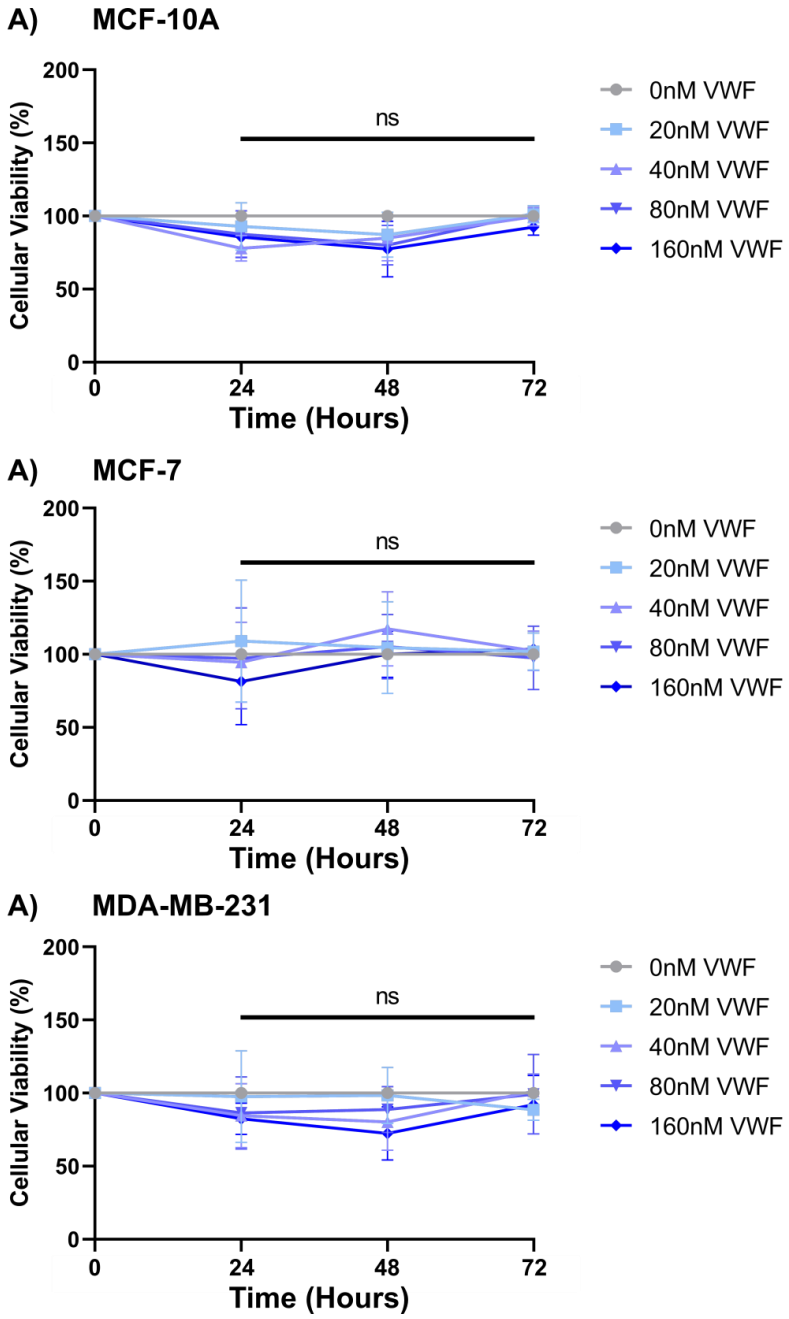

Figure 5.3 VWF does not affect cellular viability of breast cells over 72h: MCF-10A (N=3), MCF-7 (N=3) and MDA-MB-231 (N=3) cells were seeded at 5000 cells per well and left to grow overnight. Cells were then treated ± pd-VWF for the desired time points (24, 48 or 72h) before being treated with MTS tetrazolium. Results were graphed for each cell line **A)** MCF-10A **B)** MCF-7 **C)** MDA-MB-231 with each dose of VWF compared against untreated conditions set to 100% cellular viability. Distribution of the data was determined by Shapiro-Wilks normality test where normal data is presented as mean ± SD. Significance was determined through an ordinary one way ANOVA using the Dunnett's multiple comparisons test, * $p \leq 0.05$.

5.3 Assessing VWF induced apoptosis in breast cell lines

5.3.1 The apoptotic effect of VWF on MCF-10A breast cells over 72h

VWF has been described to have pro-apoptotic role in a number of cancer cells.[101,255] Mochizuki *et al*. described an apoptotic role for VWF in neoplastic cell lines that did not express proposed VWF cleaving protease ADAM28.[101] Interestingly, VWF treatment of ADAM28-deficient cancer cell lines MCF-7, 769P and HEPG2 displayed increased DNA fragmentation, a marker of apoptosis.[101]

Consequently we investigated if VWF could induce apoptosis in breast cell lines MCF-10A, MCF-7 and MDA-MB-231 (Figure 5.4, 5.5 and 5.6). Similar to previous reports, we showed that VWF treatment of non-neoplastic cell line MCF-10A had no significant apoptotic effect (Figure 5.4). Additionally, MDA-MB-231 breast cancer cell lines had no susceptibility to VWF-mediated apoptosis (Figure 5.6). In contrast to Mochizuki *et al*, VWF had no apoptotic effect on cancer cell line MCF-7 versus unstimulated controls across each time point, for example at 24h (8.36 ± 1.05 vs 10.45 ± 1.35, p=0.96).[101]

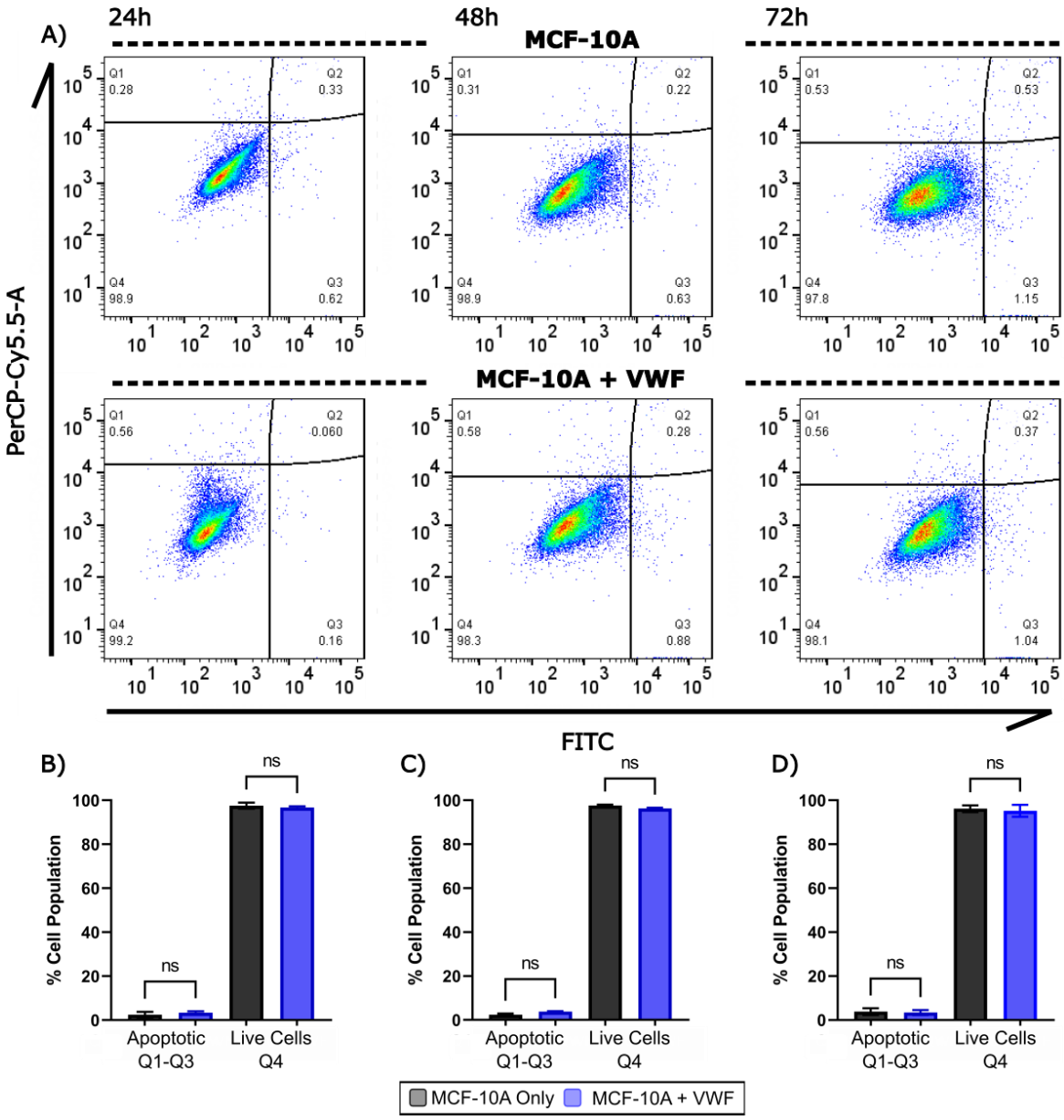

Figure 5.4 VWF does not induce apoptosis in MCF-10A breast cells over 72h: MCF-10A (N=3) cells were grown in a 24-well plate and treated ± pd-VWF (24, 48 or 72h). Cells were measured for apoptotic markers annexin V and DNA marker propidium iodide using flow cytometry **A)** where representative flow cytometry quadrants were derived for each time point. Graphs were generated for each time point **B)** 24h ± VWF treatment **C)** 48h ± VWF treatment **D)** 72h ± VWF treatment where both the apoptotic effect and total live population were depicted. All experiments were conducted with a positive control for cell death. Distribution was determined through Shapiro-Wilks test for normality. Normal values were then graphed as mean ± SD, significance was calculated by student t-test, ** $p \leq 0.01$.

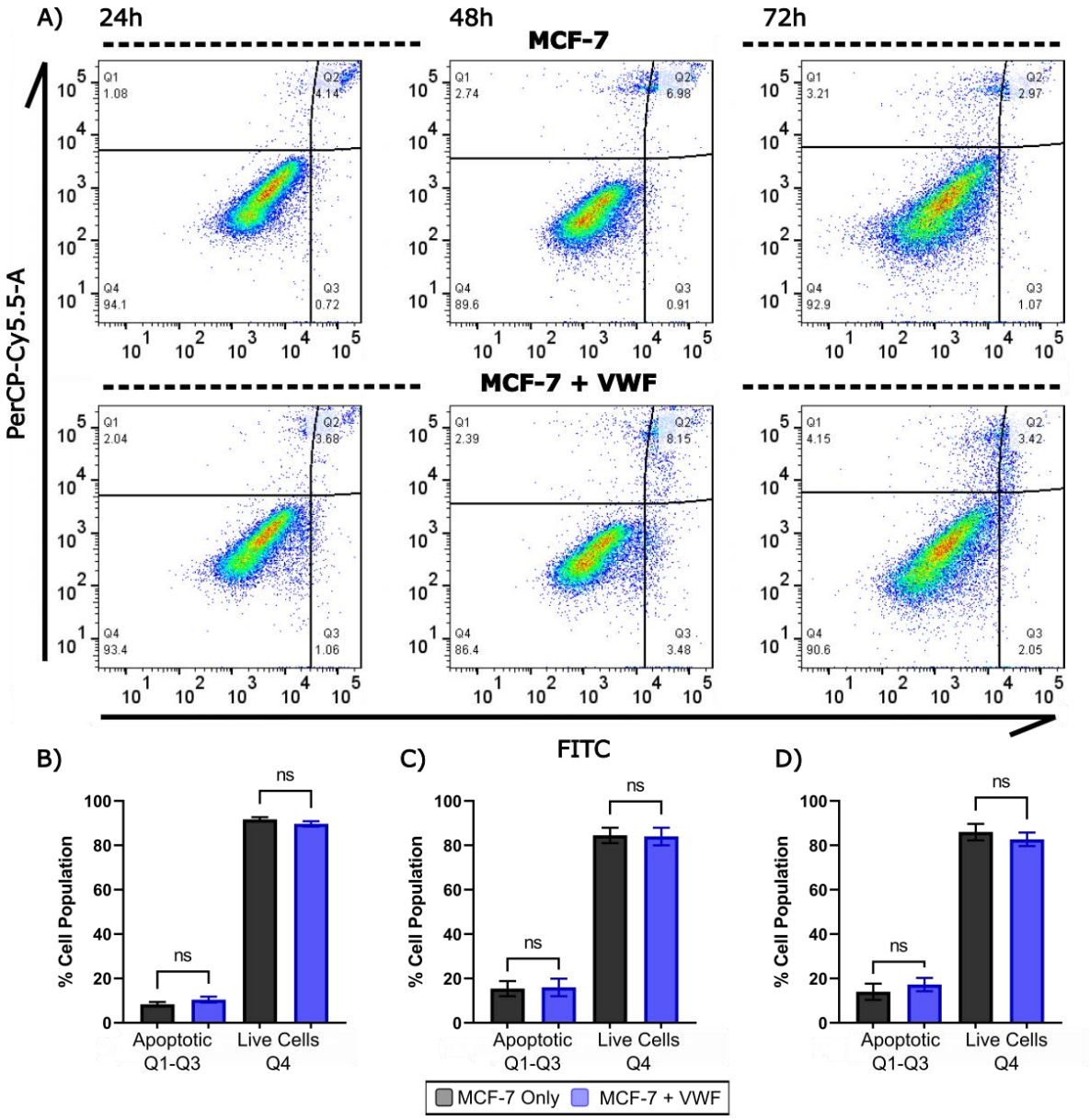

Figure 5.5 VWF does not induce apoptosis in MCF-7 breast cancer cells: MCF-7 (N=4) cells were grown in a 24-well plate and treated ± pd-VWF (24, 48 or 72h). Cells were measured for apoptotic markers annexin V and DNA marker propidium iodide using flow cytometry **A)** where representative flow cytometry quadrants were derived for each time point. Graphs were generated for each time point **B)** 24h ± VWF treatment **C)** 48h ± VWF treatment **D)** 72h ± VWF treatment where both the apoptotic effect and total live population were depicted. All experiments were conducted with a positive control for cell death. Distribution was determined through Shapiro-Wilks test for normality. Normal values were then graphed as mean ± SD, significance was calculated by student t-test, * $p \leq 0.05$.

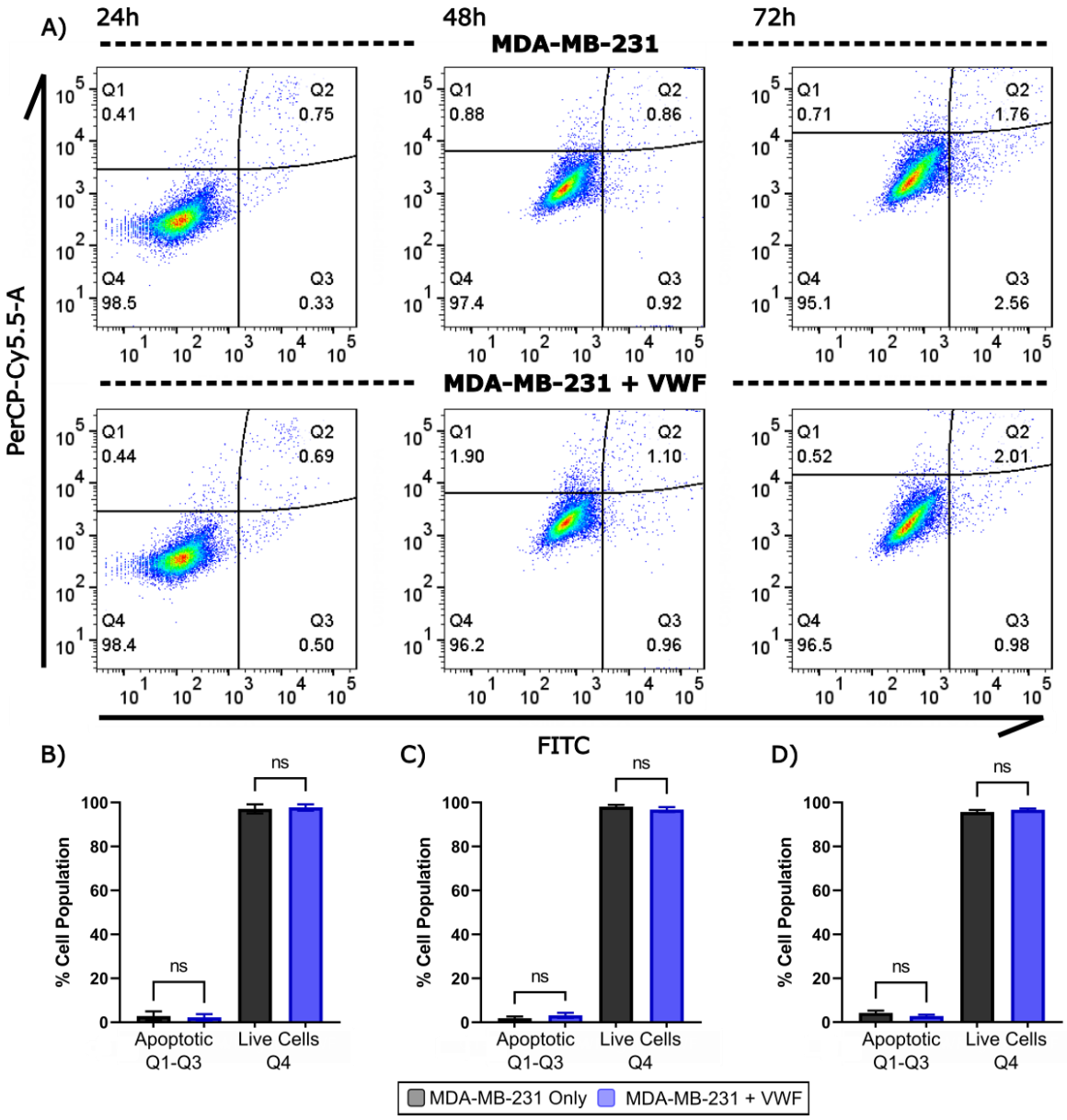

Figure 5.6 VWF does not induce apoptosis in MDA-MB-231 breast cancer cells:
MDA-MB-231 (N=4) cells were grown in a 24-well plate and treated ± pd-VWF (24, 48 or 72h). Cells were measured for apoptotic markers annexin V and DNA marker propidium iodide using flow cytometry **A)** where representative flow cytometry quadrants were derived for each time point. Graphs were generated for each time point **B)** 24h ± VWF treatment **C)** 48h ± VWF treatment **D)** 72h ± VWF treatment where both the apoptotic effect and total live population were depicted. All experiments were conducted with a positive control for cell death. Distribution was determined through Shapiro-Wilks test for normality. Normal values were then graphed as mean ± SD, significance was calculated by student t-test, * $p \leq 0.05$.

5.4 The migratory effect of VWF on breast cells

5.4.1 Assessing VWF induced transmigration of breast cells

In the scratch wound assays, we identified that both MCF-7 and MDA-MB-231 cells exhibited increased migration upon VWF stimulation. Besides collective migration, cells can also migrate as individual cells through amoeboid- or mesenchymal–type movement.[402] VWF has been shown to induce EMT changes in osteosarcoma cells as well as increase filapodial extensions in MDA-MB-231.[161,188] Correspondingly, In TPC-1 papillary thyroid carcinoma cells knockdown of VWF expressed in these cells was able to suppress migration and invasion.

Notably, metastatic cells are more likely to chemotactically polarise towards blood vessels than non-metastatic cells in an EGF dependent manner.[403,404] Of note, VWF has been found to act as a reservoir for growth factors including VEGF and EGF and VWF:Ag levels are increased in a variety of cancers (Table 1.1).[100] We hypothesized that VWF may be able to chemotactically direct tumour cell migration. Therefore we next assessed the ability of VWF to direct individual breast cancer cell migration in breast cancer cells.

Using transmigration assays we quantified the effect of VWF in promoting migration of breast cells MCF-10A, MCF-7 and MDA-MB-231. Consistent with the scratch wound assay, VWF was unable to induce cellular migration of MCF-10A cells through the transwell insert (34 ± 9.67 vs 29.6 ± 27.93 cells migrated, p=0.9935) (Figure 5.7 A). Subsequently, we assessed MCF-7 cells that while of metastatic origin are poorly invasive. [216] Accordingly, we found that the addition of VWF to the bottom well of the Boyden chamber transmigration assay was unable to induce cellular movement of MCF-7 cells compared to untreated conditions (1 ± 1.67 vs 1 ± 0.89 average cells migrated, p>0.99) (Figure 5.7 B). Following the dose dependent migratory effects seen in the scratch wound assay we assessed the chemotactic properties of VWF on MDA-MB-231 cells. Addition of VWF significantly enhanced migration of MDA-MB-231 to the bottom well compared to untreated control (114.5 ± 36.7 vs 6.3 ± 6.14 average migrated cells, $p \leq 0.0001$) (Figure 5.7 C) in levels comparable to the 10% FCS positive control.

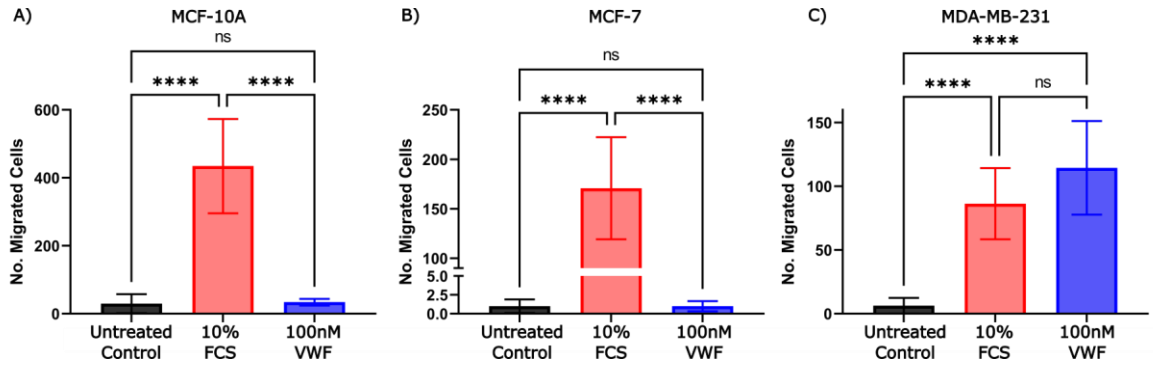

Figure 5.7 VWF induced migration of breast cells: MCF-10A (N=3), MCF-7 (N=3) and MDA-MB-231 (N=5) cells were seeded at $4x10^5$ cells/mL into an 8µm transwell insert where they were added into a 24 well plate with serum-free media ± treatment conditions: pd-VWF or 10% FCS. Cells were allowed to migrate for 24h before they were fluorescently tagged and imaged at 4x magnification. **A)** Representative images of each treatment condition were taken. Live migrated cell numbers for each well were counted. Data distribution was determined through Shapiro-Wilks normality test where normal distributions were graphed as mean values ± SD. **B)** Number of migrated cells were plotted for each treatment condition. Significance was determined by ordinary one way ANOVA using Tukeys multiple comparison test, **** $p \leq 0.0001$.

5.4.2 Assessing VWF induced invasion of MDA-MB-231 breast cancer cells

In addition to cellular migration in haematogenous metastasis tumour cells can modify their structure and induce the release of factors capable of promoting vascular permeability and the breakdown of the ECM.[402,405] Endothelial VWF and VWF derived from tumour cells have both been shown to enhance the invasion of tumour cells to a secondary site. In an *ex ovo* chorioallontoic membrane assay, VWF expression in SAOS2 and U251 cells corresponded with intravascular extravasation through the endothelium while VWF shRNA knockdown cells were trapped within the vessels.[143]

In view of the migratory effect of VWF on MDA-MB-231 cells in both scratch wound and Boyden chamber transmigration assays we next investigated whether VWF influenced MDA-MB-231 cells invasion through an ECM layer. By adding VWF in the bottom well of the assay we assessed the chemotactic properties of VWF on MDA-MB-231 cells. We found that with increasing doses of VWF there was a dose dependent increase in the cellular invasion of MDA-MB-231 cells through the ECM (2.96 ± 0.7 vs 1.0 ± 0.14, $p \leq 0.001$) (Figure 5.8).

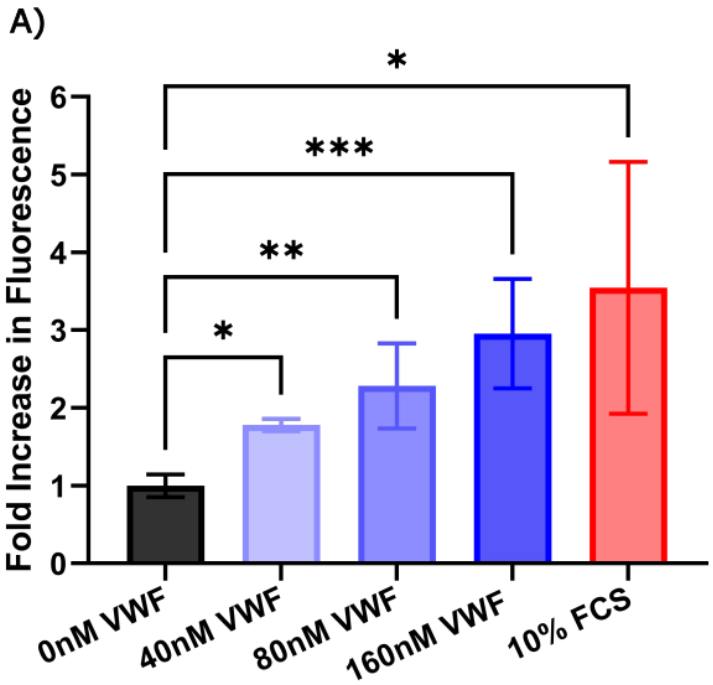

Figure 5.8 VWF induces MDA-MB-231 invasion through an extracellular matrix layer: MDA-MB-231 cells were seeded at $1x10^6$ cells/mL into an 8µm transmigration insert with an ECM layer in a 24 well plate with serum-free media ± treatment conditions: pd-VWF or 10% FCS (N=6). Cells were allowed to invade for 72h before being lysed. Lysed migrated cells were tagged with a CyQUANT™ green dye and measured by fluorometer. Distribution was determined through Shapiro-Wilks normality test and graphed as mean values ± SD. **A)** Number of migrated cells were plotted for each treatment condition. Significance was determined by ordinary one way ANOVA using Dunnett's multiple comparison test, * $p \leq 0.05$, ** $p \leq 0.01$, *** $p \leq 0.001$.

5.4.3 Assessing the molecular effects of VWF stimulation on MDA-MB-231 breast cancer cells

Having established that VWF enhances the invasive properties of MDA-MB-231 cells we next investigated the effects of VWF using a selected cytokine array that detected 104 proteins including chemokines, growth factors and cytokines involved in inflammation, angiogenesis and invasion (Figure 5.9). Following VWF stimulation of MDA-MB-231 cells, significant effects on a number of secreted proteins were seen including adiponectin (105 fold) (Figure 5.9 B). Furthermore, platelet endothelial cell adhesion molecule-1 (Pecam-1/CD31) and apoliprotein A-I (ApoA-I) were increased upon VWF stimulation. Of particular interest, MMP-9 known to breakdown the ECM layer was also increased following VWF stimulation (32 fold). Increases in IL-17A, IL-1α and Ang-2 levels were also observed.

A)

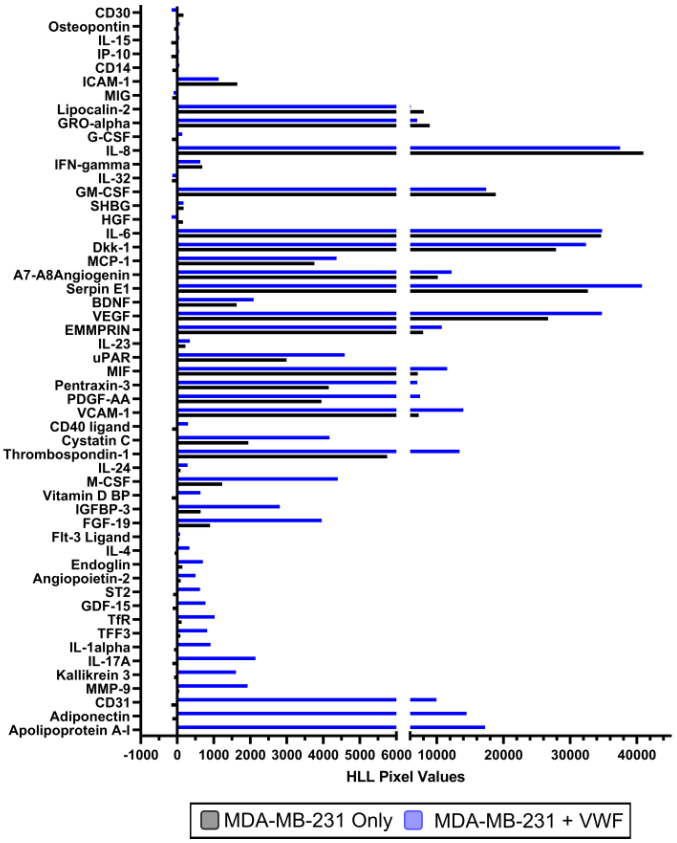

B)

Gene ID	Name	Proposed function	Fold Change
335	Apolipoprotein A-I	Proliferation	18312.57
9370	Adiponectin	Proliferation	105.6802
5175	CD31	Adhesion Receptor	59.29667
4318	MMP-9	Invasion	32.49802
3605	IL-17A	Migration	15.66662
285	Angiopoietin-2	Angiogenesis	5.235217
4353	Myeloperoxidase	Inflammation	-16.7025

C)

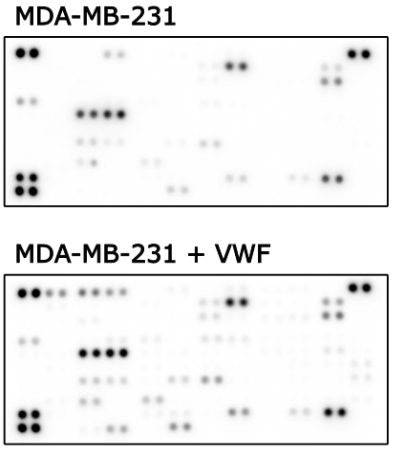

Figure 5.9 VWF treatment influences MDA-MB-231 secretome: MDA-MB-231 cells were grown in a 6-well plate and stimulated ± 100nM pd-VWF for 24h, the supernatant was collected and incubated on a pre-coated cytokine array membrane. Values of each protein were quantified by densitometry and normalised. **A)** VWF treated and untreated MDA-MB-231 secretomes for each protein were graphed against each other based on pixel density from the membrane. **B)** Fold changes were derived by normalising VWF treated samples against unstimulated controls **C)** representative images of the membrane following the supernatant of VWF treated and untreated MDA-MB-231 cells are depicted for visual comparison.

5.4.4 Measuring VWF induced MMP-9 release in MDA-MB-231 cells

From the cytokine array, VWF treatment upregulates the release of MMP-9. MMPs have been described to remodel the ECM through their potential to cleave a variety ECM proteins like collagen IV, perlecan and laminins.[406,407] In healthy breast tissue MMP-9 expression is low, however in different molecular subtypes of breast cancer over expression of MMP-9 was found to be a clear feature of TNBC.[408]

MMPs play important roles in the metastatic process as they can aid tumour neo-vascularisation, invasion and ECM remodelling.[407] Therefore we quantified the secreted levels of MMP-9 after VWF stimulation of MDA-MB-231 cells. Consistent with the cytokine array, data VWF stimulation promoted increased levels of secreted MMP-9 in the supernatant of MDA-MB-231 cells (32.95 ± 5.4pg/mL vs 14.93 ± 4.5pg/mL, $p \leq 0.05$)(Figure 5.10).

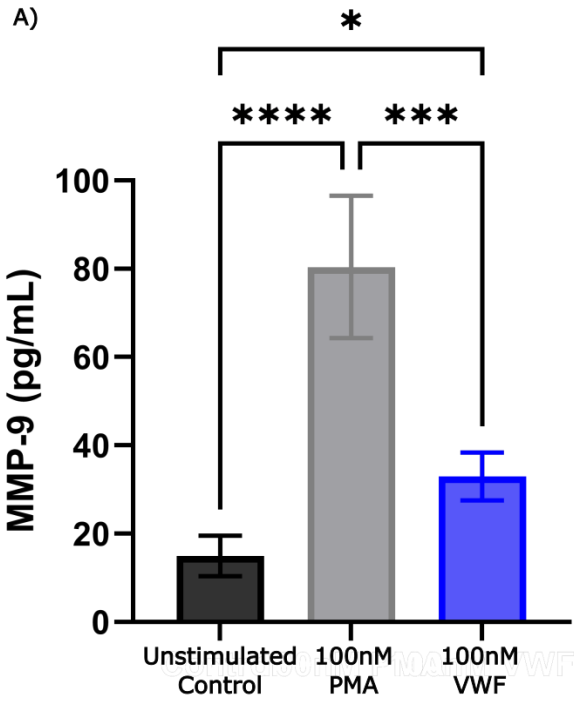

Figure 5.10 VWF stimulation induces MMP-9 release in MDA-MB-231 cells: MDA-MB-231 cells were grown in a 6-well plate and stimulated for 24h ± pd-VWF (N=3). Supernatants from the cells was collected and secreted MMP-9 levels were quantified by ELISA. **A)** Data distribution was determined through Shapiro-Wilks test for normality with normal data represented as mean values ± SD. Statistical significance was calculated by one way ANOVA using Tukeys multiple comparisons test, * $p \leq 0.05$, *** $p \leq 0.001$, **** $p \leq 0.0001$.

5.5 The angiogenic effect of VWF on MDA-MB-231 breast cancer cells

5.5.1 Assessing VWF induced gene expression of angiogenic factors in MDA-MB-231 breast cancer cells

As discussed, VWF is an established regulator of endothelial angiogenesis. However, the mechanisms through which VWF induces angiogenesis in cancer are not fully known. Conditioned media of VWF overexpressing MDA-MB-231 and MCF-7 cells has been shown to induce angiogenesis with VWF knockdown in these cells correcting endothelial angiogenesis levels.[141] Considering the link between VWF and angiogenesis in cancer, we sought to characterise the angiogenic potential of VWF in breast cancer.

We therefore conducted a series of qPCR assays to determine whether VWF influenced expression of angiogenesis related genes (Figure 5.11). After stimulating MDA-MB-231 cells with VWF, we found a number of upregulated genes, including *Ang-2* (2.56 ± 1.2 fold increase, $p \leq 0.01$), *EGF* (2.74 ± 1.4 fold increase, $p \leq 0.01$), and *EGFR* (2.44 ± 0.91 fold increase, $p \leq 0.01$). Critically, VWF treatment resulted in no significant change of VEGF expression (-0.18 ± 0.85 fold, $p=0.97$).

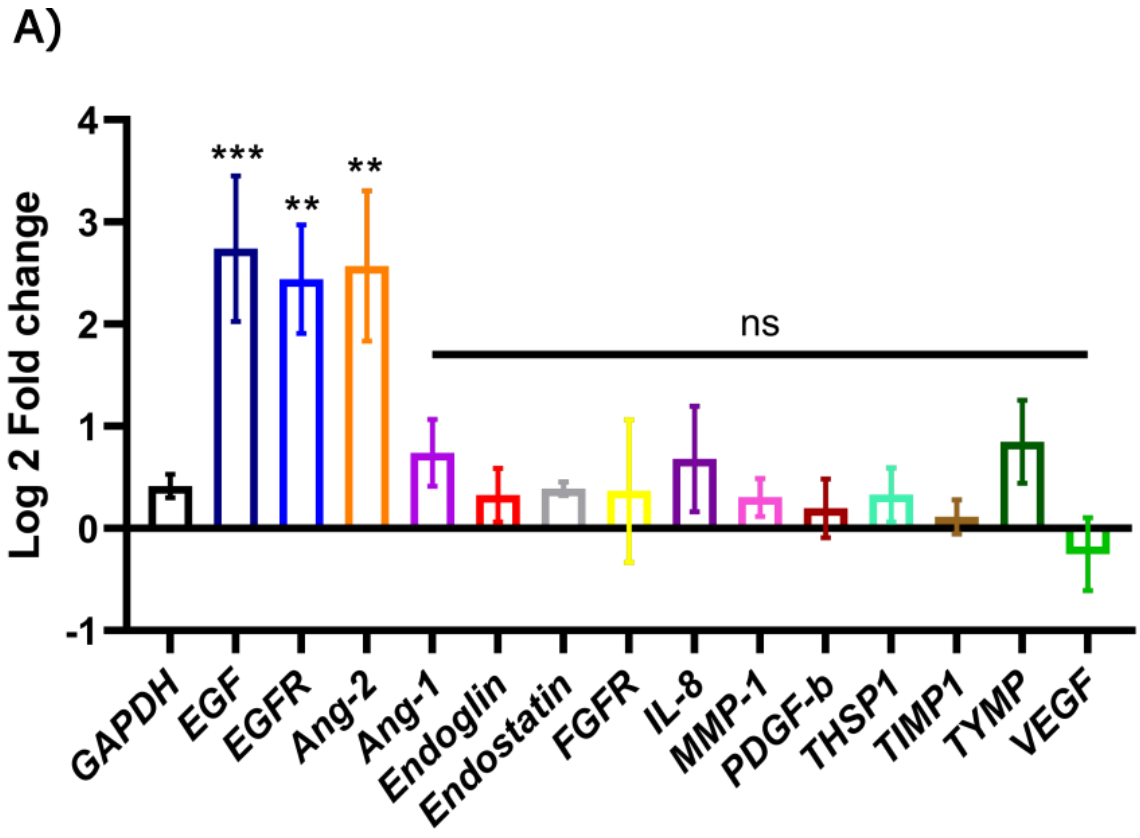

Figure 5.11 VWF enhances EGF and EGFR mRNA expression in MDA-MB-231 cells: Angiogenesis-related genes were assessed via qPCR for mRNA expression levels in MDA-MB-231 cells following 24h stimulation ± 200nM recombinant VWF (N=3). **A)** Expression levels were denoted by Log-fold change standardised against housekeeping gene *18S*. Data distribution was determined through Shapiro-Wilks test for normality, normal values were drawn as mean values ± SD and statistics derived from a second housekeeper gene *GAPDH*. Statistical analysis was performed through ordinary one way ANOVA using Dunnett's multiple comparison test, * $p \leq 0.05$, ** $p \leq 0.01$.

5.5.2 Assessing the angiogenic molecular changes of VWF stimulation in MDA-MB-231 breast cancer cells

Using an angiogenesis array, we next investigated changes from a profile of secreted angiogenic factors released from MDA-MB-231 cells in response to VWF treatment. VWF stimulation of MDA-MB-231 cells had some effects on the angiogenic secretome. Upon VWF stimulation, we found only small increases in VEGF (1.27 fold) and platelet factor 4 (1.61 fold) (Figure 5.12 A-C).

Several reports have shown a link between VEGF and VWF in cancer. [119,148,153,156,181] VEGF-A released from a transgenic Ret melanoma cell line was associated with luminal VWF release from endothelial cells.[148] Moreover, a report from our group found HUVEC angiogenesis induced by MDA-MB-231 and MCF-7 cells was inhibited by anti-VEGF antibody, bevacizumab.[156] After identifying VWF enhanced VEGF secretion within our angiogenesis assay we next investigated absolute secreted values of VEGF from MDA-MB-231 after VWF treatment by ELISA. Following VWF stimulation no significant change in VEGF secretion was observed compared to controls (1334 ± 27.3 vs 1365 ± 56.16pg/mL, p=0.43) (Figure 5.12 D).

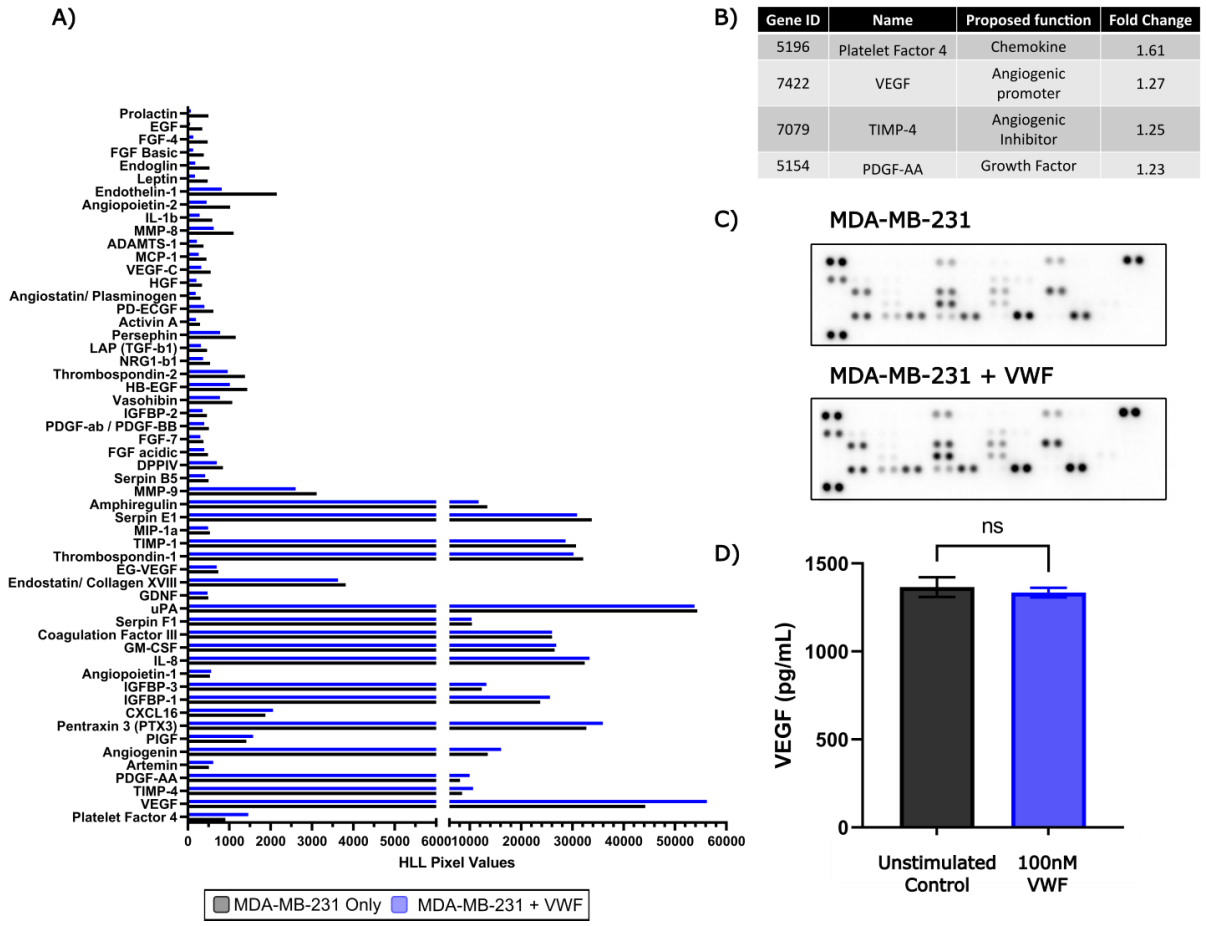

Gene ID	Name	Proposed function	Fold Change
5196	Platelet Factor 4	Chemokine	1.61
7422	VEGF	Angiogenic promoter	1.27
7079	TIMP-4	Angiogenic Inhibitor	1.25
5154	PDGF-AA	Growth Factor	1.23

Figure 5.12 VWF stimulation shows small changes in angiogenic markers in MDA-MB-231 cells: MDA-MB-231 cells were grown in a 6-well plate and stimulated ± 200nM recombinant VWF for 24h, the supernatant was collected and incubated on a pre-coated angiogenesis array membrane. Values of each protein were quantified by densitometry and normalised. **A)** VWF treated and untreated MDA-MB-231 angiogenic secretomes for each protein were graphed against each other based on pixel density from the membrane. **B)** Fold changes were derived by normalising VWF treated samples against unstimulated controls, angiogenic proteins of interest were displayed as a table **C)** representative images of the membrane following the supernatant of VWF treated and untreated MDA-MB-231 cells are depicted for visual comparison. **D)** MDA-MB-231 cells were stimulated for 24h ± 100nM VWF (N=3). Supernatants from the cells was collected and secreted VEGF levels were quantified by ELISA. Data distribution was determined by Shapiro-Wilks normality test, normal data was graphed as mean values ± SD. Statistical significance was calculated by student-t test, * $p \leq 0.05$.

5.5.3 Assessing VWF induced vasculogenic mimicry in MDA-MB-231 breast cancer cells

We next investigated the role of VWF on alternative angiogenic pathway, vasculogenic mimicry (VM). VM has been proposed to be a major feature in the early stages of tumour growth in metastatic cells.[409] Invasive tumour cells organise into pseudo-vasculature structures for nutrient supply before more robust endothelial networks are established. The formation of VM is independent of endothelial cells and is associated with high tumour grade, invasion and metastasis.[410,411]

Interestingly, VM is highly regulated by EMT pathways. Known EMT transcription factors TWIST, ZEB and SNAI1, shown to downregulate E-cadherin have been implicated in VM.[409] Notably, in osteosarcoma cells dose dependent increases in VWF showed corresponding increases in EMT marker TWIST1 and proportional downregulation of E-cadherin.[161] Accordingly, higher VWF expression in osteosarcoma tissues was associated with metastatic tumours whereas low VWF expression was attributed to non-cancerous tissues. As such, we stimulated MDA-MB-231 cells with VWF to assess whether VWF could induce pro-invasive VM changes in the breast cancer cell line.

In an angiogenesis assay we found that VWF stimulation significantly enhanced vasculogenic features in the MDA-MB-231 cells (Figure 5.13). Using the same concentration of VWF as in the qPCR assay stimulation of MDA-MB-231 cells resulted in a nearly 2-fold increase in cell-cell joining events (nodes) compared to the unstimulated controls (1.88 ± 0.92, $p \leq 0.05$, Figure 5.13 B). Furthermore, the number of connected branches (junctions) in MDA-MB-231 cells were also significantly elevated after VWF stimulation (1.88 ± 0.7, $p \leq 0.01$, Figure 5.13 C). Finally, the number of complete luminal loops (meshes) formed were also significantly increased in VWF stimulated cells (2.63 ± 1.1, $p \leq 0.01$, Figure 5.13 D). Altogether VWF stimulation induced morphological changes in MDA-MB-231 cells generating pseudo-vasculature like networks on a matrigel layer.

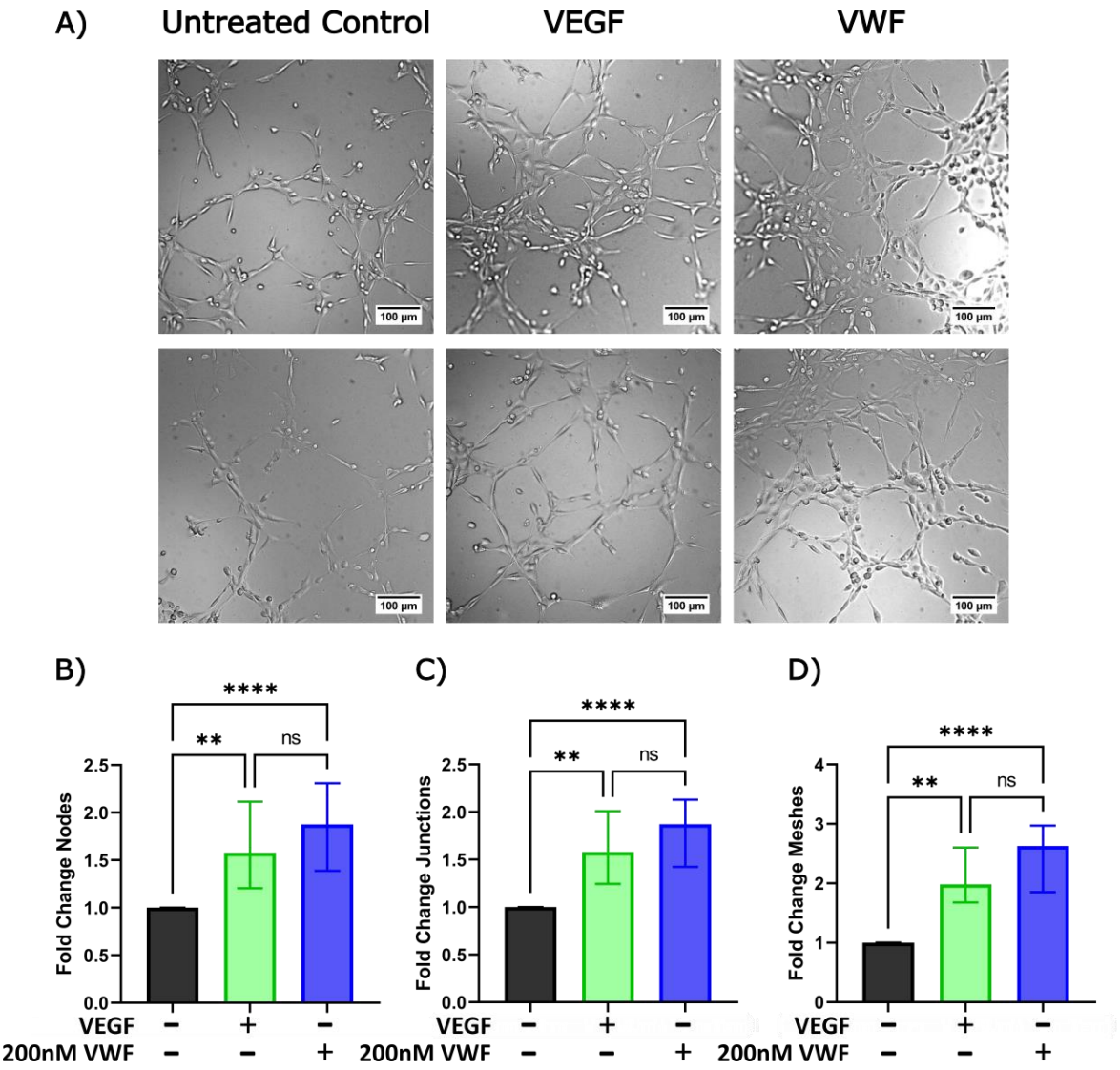

Figure 5.13 VWF promotes an endothelial-like phenotype in MDA-MB-231 cells: MDA-MB-231 cells were seeded on an angiogenesis slide pre-coated with basement membrane (N=6). Cells were stimulated ± 200nM recombinant VWF or VEGF for 6h at 37°C. Images of each well were taken by the Zeiss Axio Vert at 20x magnification, **A)** representative images of each treatment condition were captured. Images of each well were quantified using the ImageJ plug-in angiogenesis analyser. Graphs were generated from the measured angiogenic properties and values normalised against an untreated control **B)** fold change in nodes **C)** fold change in junctions **D)** fold change in meshes. Following Shapiro-Wilks test for normality, non-normal data was presented as a median ± IQR. Significance was determined through ordinary one way ANOVA using Tukeys multiple comparisons test, ** $p \leq 0.01$, **** $p \leq 0.0001$.

5.5.4 Inhibiting VWF mediated vasculogenic mimicry in MDA-MB-231 breast cancer cells with LMWH

In a recent study from our group we determined that conditioned media from MDA-MB-231 and MCF-7 breast cancer cells could induce angiogenesis in HUVEC.[156] However, LMWH inhibited the effects of conditioned media on endothelial angiogenesis. Furthermore, Goertz *et al*. have shown that LMWH ablated tumour cell induced VWF release and vessel occlusion in a mouse model.[181] Additionally, *in vivo* tumour tissues treated with LMWH dramatically decreased intratumoural blood vessel density and size compared to control tumours. Moreover in a matrigel angiogenesis assay LMWH treatment dose dependently inhibited HUVEC angiogenesis.[181]

We therefore investigated the effects of LMWH (tinzaparin) on VWF-mediated VM. LMWH was used at 100IU/mL following previous reports showing anti-angiogenic effects in HUVEC cells at the same concentration.[156,181] Of note, tumour cell conditioned media induced increases in tube length of human macrovascular endothelial cells have been reduced by pharmacological doses of LMWH as low as 0.1IU/mL.[412] We found that LMWH treatment of MDA-MB-231 cells abolished VWF-induced VM (Figure 5.14). LMWH treatment reduced VWF mediated node changes to levels seen in uncoated control cells (0.43 ± 0.59 vs 1.88 ± 0.92 $p \leq 0.0001$)(Figure 5.14 B). Similarly, VWF associated increases in MDA-MB-231 junction and mesh formation were significantly reduced, returning to levels seen in the baseline control conditions (Figure 5.14 C + D). Notably, LMWH treatment alone was unable to significantly alter VM in controls.

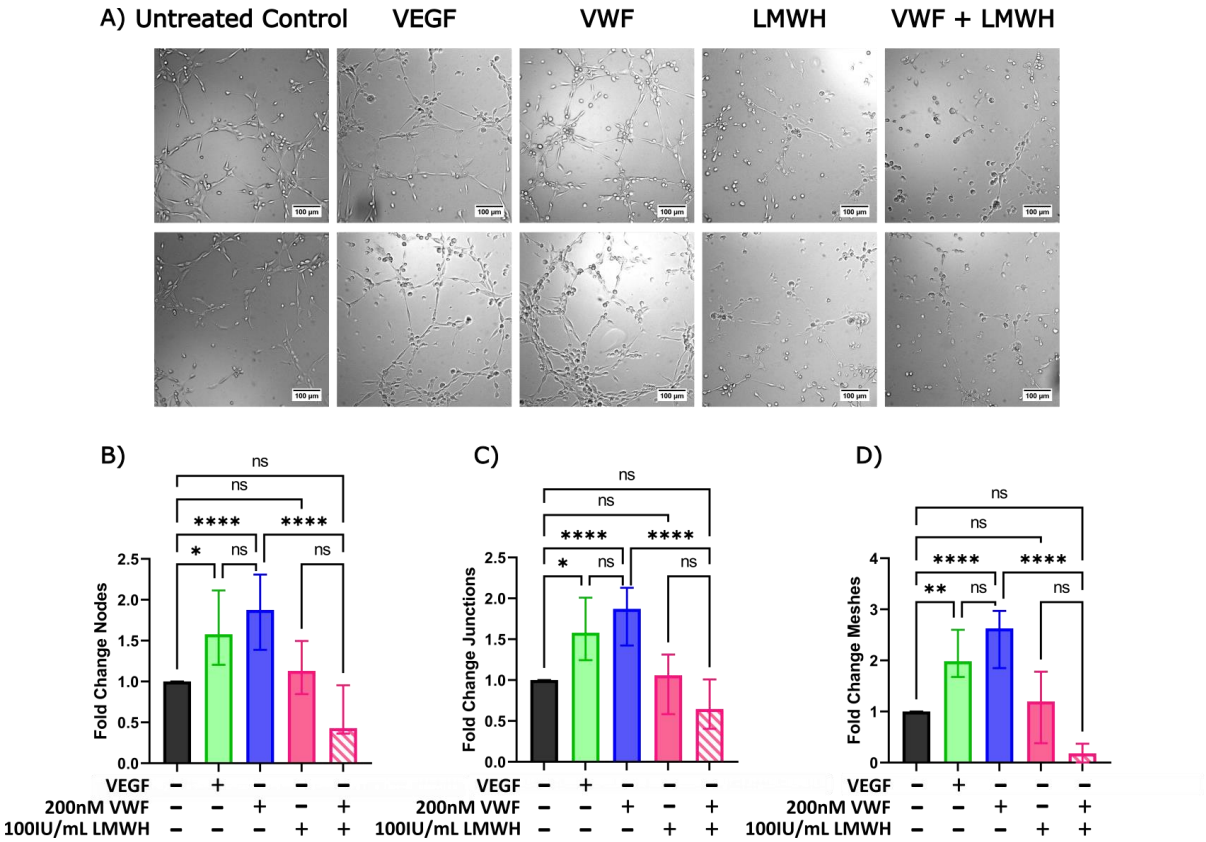

Figure 5.14 LMWH (tinzaparin) treatment of MDA-MB-231 cells inhibits VWF enhanced vasculogenic mimicry: MDA-MB-231 cells were seeded on an angiogenesis slide pre-coated with basement membrane (N=6). Cells were stimulated ± VEGF or recombinant VWF in combination with 100IU/mL LMWH for 6h at 37°C. Images of each well were taken by the Zeiss Axio Vert at 20x magnification, **A)** representative images of each treatment condition. Images of were quantified using the ImageJ plug-in angiogenesis analyser. Graphs were generated from the measured angiogenic properties and values normalised **B)** fold change in nodes **C)** fold change in junctions **D)** fold change in meshes. Following Shapiro-Wilks test for normality, non-normal data was presented as a median ± IQR. Significance was determined through ordinary one way ANOVA using Tukeys multiple comparisons test, * $p \leq 0.05$, ** $p \leq 0.01$, **** $p \leq 0.0001$.

5.5.5 Inhibiting VWF mediated vasculogenic mimicry in MDA-MB-231 breast cancer cells with anti-EGFR and anti-VEGF treatment

VEGF is a potent tumour derived pro-angiogenic factor that can drive pathological angiogenesis and vasculogenesis.[413] In addition VEGF is associated with the development of VM, for example silencing of VEGF in osteosarcoma MG63 cells reduced cell growth and VM development. [414]

Recent reports suggest that in breast cancer, VM may be regulated by EGFR.[415–417] Interestingly, in MDA-MB-231 and BT549 breast cancer cells an anti-EGFR aptamer CL4, inhibited tube formation and also abolished pre-established tumour cell networks.[416] Additionally, anti-EGFR treatment with cetuximab also diminished loop formation in MDA-MB-231 cells. Given the association between VEGF and VWF, as well as the link between EGF and VWF, we wanted to assess which pathway VWF induced VM in MDA-MB-231 cells.

We studied VWF induced VM in the presence and absence of anti-EGFR and anti-VEGF antibodies. Anti-VEGF treatment had no impact on VWF induced MDA-MB-231 VM (Figure 5.15). However, treatment of MDA-MB-231 cells with anti-EGFR ablated VM in VWF stimulated MDA-MB-231 cells with significant decreases in the number of nodes (1.2 ± 0.56 vs 1.77 ± 0.27, $p \leq 0.05$)(Figure 5.15 B), number of junctions (1.2 ± 0.56 vs 1.83 ± 0.3, $p \leq 0.05$)(Figure 5.15 C) and number of meshes (1.26 ± 0.88 vs 2.53 ± 0.72 $p \leq 0.0001$)(Figure 5.15 D) compared to the VWF treated cells. Cumulatively, this indicates that VWF induced VM is mediated through EGFR pathways.

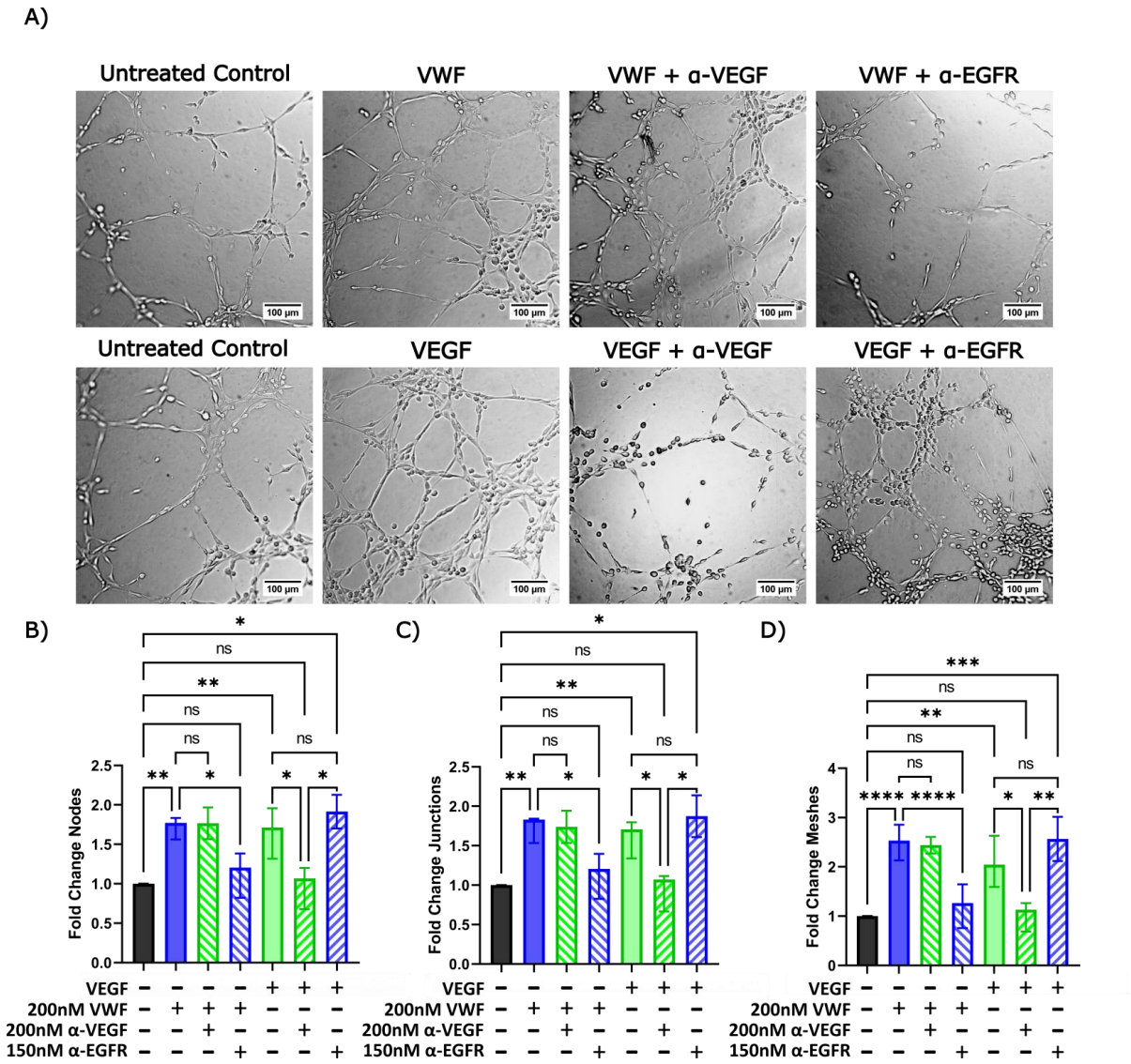

Figure 5.15 Anti-EGFR but not anti-VEGF inhibits VWF enhanced vasculogenic mimicry: MDA-MB-231 cells were seeded on an angiogenesis slide pre-coated with basement membrane (N=6). Cells were stimulated ± recombinant VWF and simultaneously blocked with either anti-EGFR or anti-VEGF antibody treatment for 6h at 37°C with VEGF used as a positive control. Images of each well were taken by the Zeiss Axio Vert at 20x magnification, **A)** representative images of each treatment condition. Images were quantified using the ImageJ plug-in angiogenesis analyser. Graphs were generated from the measured angiogenic properties and values normalised **B)** fold change in nodes **C)** fold change in junctions **D)** fold change in meshes. Following Shapiro-Wilks test for normality, non-normal data was presented as a median ± IQR. Significance was determined through ordinary one way ANOVA using Tukeys multiple comparisons test, * $p \leq 0.05$, ** $p \leq 0.01$, *** $p \leq 0.001$, **** $p \leq 0.0001$.

5.5.6 Assessing the cytotoxic effects of anti-EGFR treatment on MDA-MB-231 cells

Since anti-EGFR treatment abolished VWF-mediated VM in MDA-MB-231 cells we next assessed the cytotoxic effects of the anti-EGFR used (cetuximab) on MDA-MB-231 cells alone or in conjunction with VWF. VM is determined through an increase in tube length and the formation of vasculature-like structures. However, morphological changes are a feature of cell death like apoptosis as cells shrink and round up.[418] When measuring VM, cell rounding reduces tube length, node formation and the ability of cells to form meshes. Therefore, we examined the ability of anti-EGFR treatment to influence cell death in MDA-MB-231. Consistent with the VM angiogenesis assay the cell viability assay was conducted over 6h. Treating MDA-MB-231 cells with increased doses of anti-EGFR had no effect on cytotoxicity either in the presence and absence of 200nM VWF treatment (Figure 5.16).

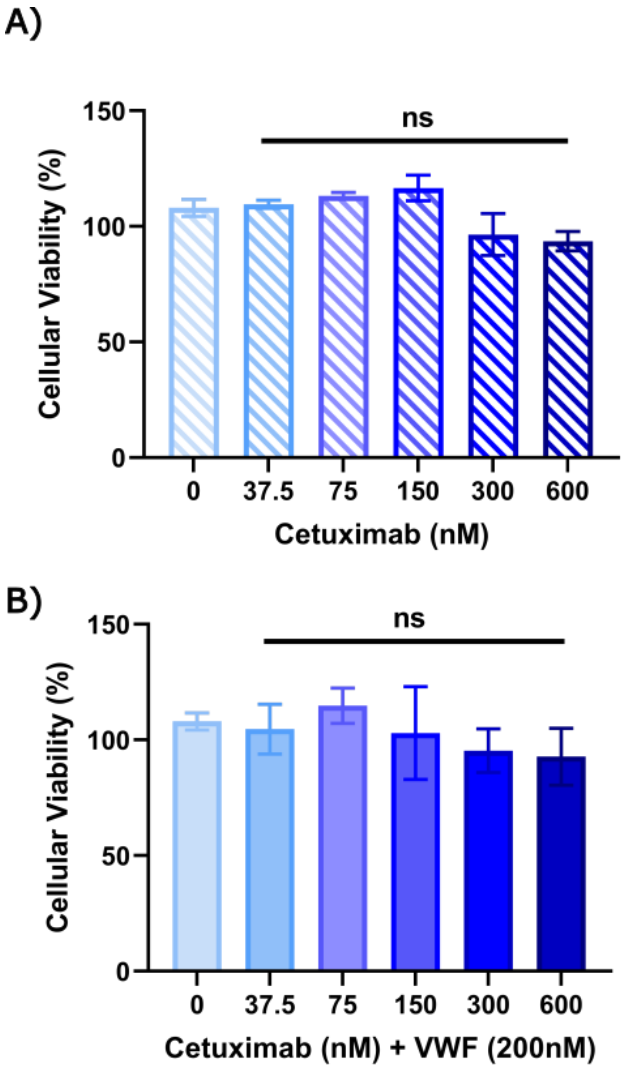

Figure 5.16 Anti-EGFR treatment has no effect on MDA-MB-231 viability: MDA-MB-231 cells were seeded at 5000 cells per well and left to grow overnight (N=3). MDA-MB-231 cells were then treated with increasing doses of anti-EGFR antibody ± 200nM recombinant VWF for 6h before being treated with MTS tetrazolium. Results were graphed for **A)** anti-EGFR treatment alone **B)** anti-EGFR + 200nM VWF compared against an untreated control cell line normalised to 100% cellular viability. Distribution was determined through Shapiro-Wilks test for normality. Normal data is graphed as mean ± SD. Significance was determined through an ordinary one way ANOVA using the Dunnett's multiple comparisons test, * $p \leq 0.05$.

5.6 *In vivo* analysis of anti-VWF treatment in a metastatic breast xenograft mouse model

5.6.1 Assessing the occurrence of metastasis in anti-VWF treated mice

In vitro assays have demonstrated that VWF can influence endothelial angiogenesis, tumour cell migration and invasion.[138,141,143,156,188] *In vivo* studies have also suggested that VWF may influence metastasis of melanoma, colon, Lewis bladder, gastric and breast cancers.[118,141,184,189,241] Our *in vitro* data show that VWF enhances pro-metastatic functions of invasive MDA-MB-231 breast cancer cells. Therefore we sought to identify the effect of VWF inhibition on metastasis in an *in vivo* breast cancer model. We observed that following resection of the primary tumour, twice weekly treatment with anti-VWF antibodies increased the median time to metastasis compared to isotype control treated mice (70 vs 84 days) with a Log-rank hazard ratio of 2.469 (Figure 5.17). Notably, no change in bleeding or wound closure was detected between the two treatment conditions.

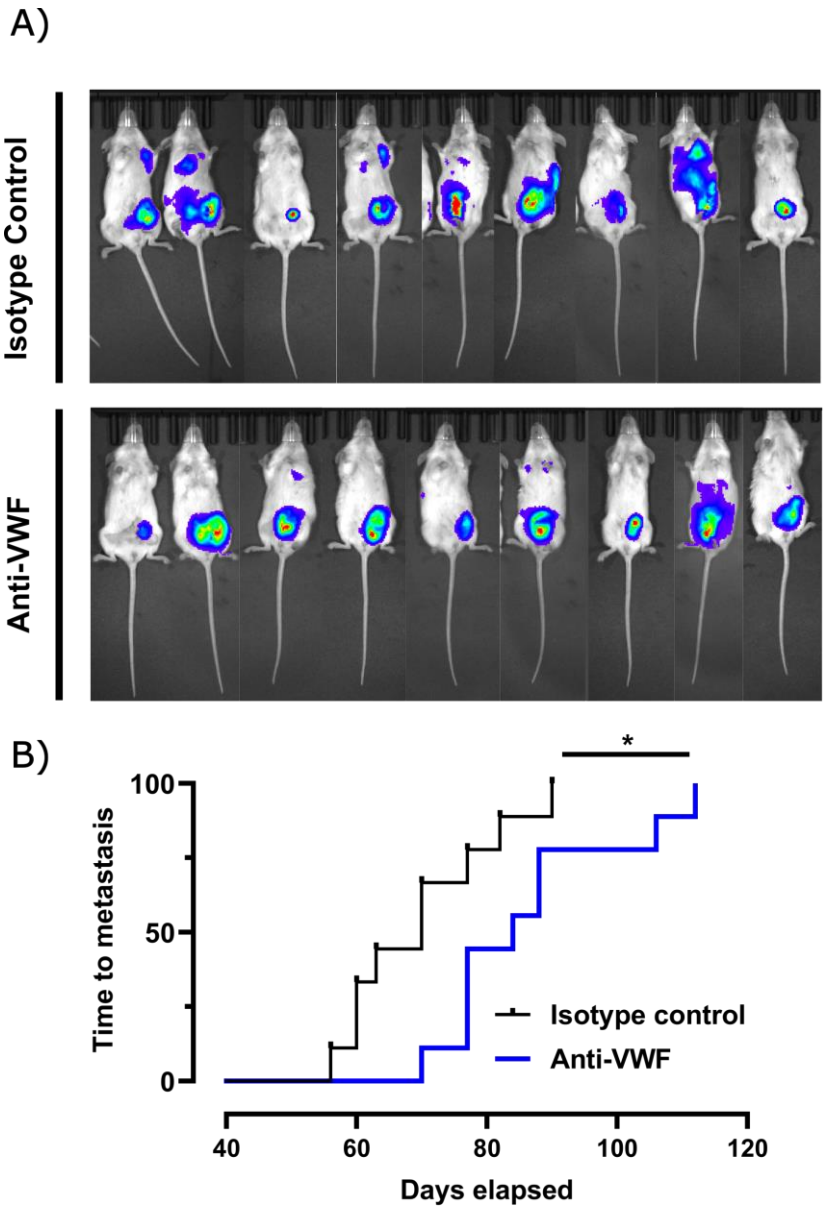

Figure 5.17 Anti-VWF treatment is protective against the onset of metastasis in an in vivo xenograft model: Luciferin tagged MDA-MB-231 cells were injected into the mammary fat pads of SCID mice. Following resection of the primary tumour mice were intravenously injected with a polyclonal anti-VWF (N=9) or isotype control (N=9) antibodies through the tail vein. The onset of metastasis was longitudinally assessed up to 15-weeks through bioluminescent imaging (radiance). **A)** Representative images of mice upon bioluminescent detection of metastases. **B)** The time taken for each mouse to develop metastases was graphed. Survival curve analysis was compared using log-rank (Mantel-Cox) test, * $p \leq 0.05$.

5.6.2 Assessing the metastatic burden in organs of anti-VWF treated mice

VWF is a blood-borne protein. However, VWF can also be expressed in tumour cells.[15,118,137–140,143,144] We wanted to assess the route through which VWF affects metastasis in breast cancer cells. Interestingly, in tumour models with wild-type as well as VWF and ADAMTS13-deficient mice VWF fibre density correlated with lung metastatic node formation.[181] Therefore we quantified metastasis in specific mouse organs to identify the metastatic route MDA-MB-231 breast cancer cells in the presence and absence of anti-VWF treatment (Figure 5.18).

Anti-VWF treatment had differential effects in regulating metastasis to different organ types. Representative images of the complete collection of organs from three mice under each treatment condition anti-VWF and isotype control anti-igG were taken [Appendix II, Figure 7.2]. VWF inhibition had no significant effect on lymphatic metastasis compared to isotype controls ($3.16x10^9 \pm 1.46\ x10^9$ vs $1.51x10^9 \pm 0.99x10^9$ total radiance, p=0.48)(Figure 5.18 C). Similarly, splenic metastasis was not significantly different in anti-VWF treated or isotype control mice ($9.09x10^8 \pm 2.34x10^8$ vs $4.88x10^8 \pm 2.5x10^8$ total radiance, p=0.28)(Figure 5.18 F). There was no change detected in anti-VWF or isotype control treatment in either brain metastasis ($1.62x10^8 \pm 0.56x10^8$ vs $2.04x10^8 \pm 0.65x10^8$ total radiance, p=0.63)(Figure 5.18 B) or kidney ($5.85x10^8 \pm 2.54x10^8$ vs $3.32x10^8 \pm 2.54x10^8$ total radiance, p=0.51)(Figure 5.18 G). Importantly, anti-VWF treatment resulted in a significant attenuation of liver metastasis compared to the control ($0.82x10^9 \pm 0.052x10^9$ vs $1.95x10^9 \pm 0.7x10^9$ total radiance, $p \leq 0.05$)(Figure 5.18 E). Furthermore, inhibition of VWF also reduced lung metastasis ($0.49x10^{10} \pm 0.32x10^{10}$ vs $2.45x10^{10} \pm 0.97x10^{10}$ total radiance, $p \leq 0.05$)(Figure 5.18 D).

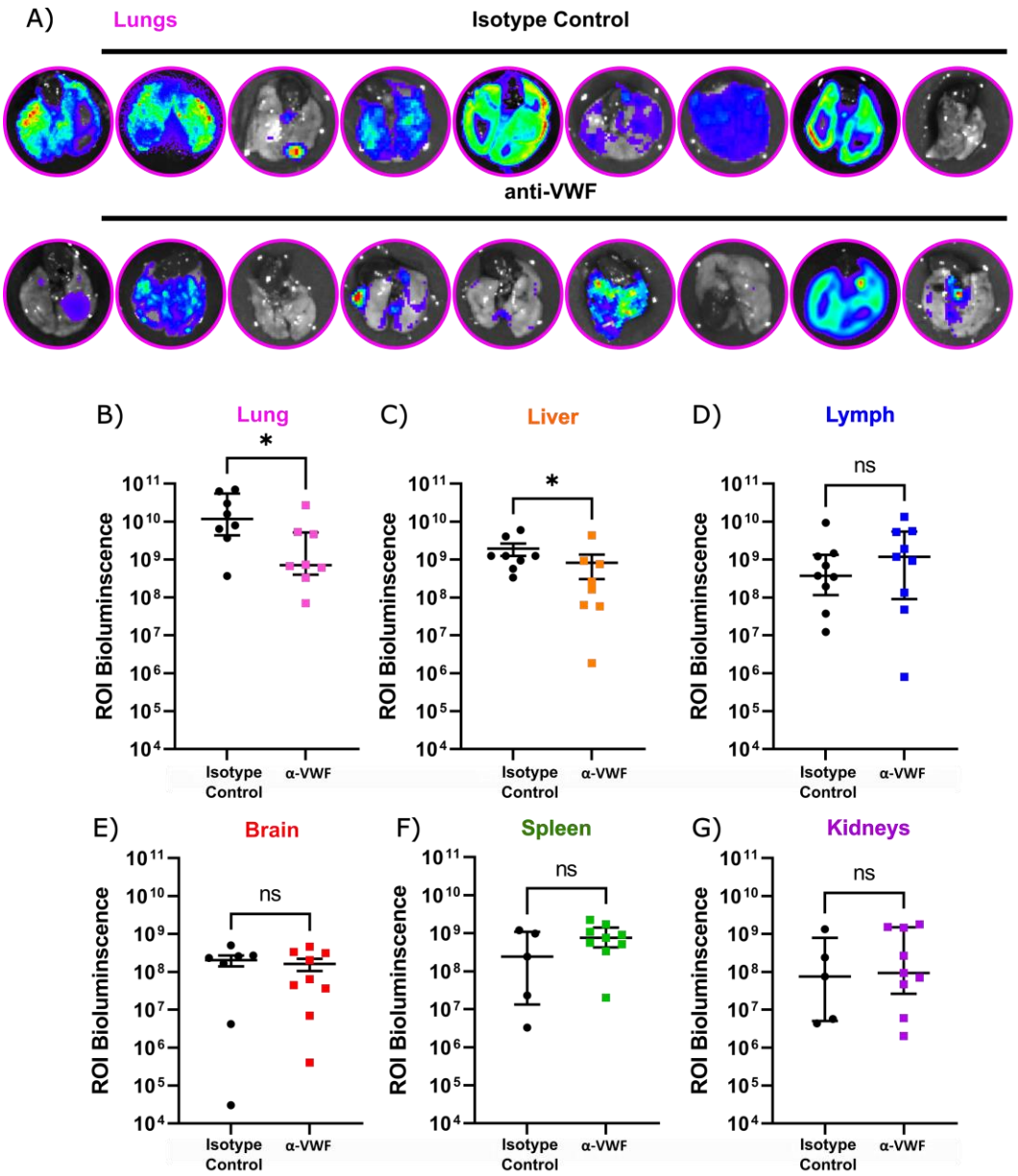

Figure 5.18 Anti-VWF treatment reduces lung and liver tumour burden in metastatic breast cancer model: Anti-VWF and isotype control treated mice with detectable metastases were euthanized following the experimental end point. Lung, liver, lymph, brain, spleen and kidney tissues were harvested and infused with luciferase where they were assessed for bioluminescent radiance signals from invaded luciferin tagged MDA-MB-231 cells. **A)** Representative images of bioluminescent signalling from the lungs of all the isotype controls and anti-VWF treated mice were taken for comparison. Total bioluminescent radiance readouts for **B)** lung **C)** liver **D)** lymph **E)** brain **F)** spleen **G)** kidneys were graphed with anti-VWF treatment and isotype controls ± interquartile range for non-parametric or SEM for parametric data sets. Data was assessed for normality where significance was then determined with parametric or non-parametric student t-test, * $p \leq 0.05$.

5.7 Discussion

5.7.1 Characterising the effect of VWF on breast cancer viability

Reports have shown that VWF can cause proliferation in smooth muscle cells through the LRP4/$\alpha_v\beta_3$ receptor axis. [100,268,419] Therefore we assessed whether VWF could induce cell proliferation in breast cells. Interestingly, VWF treatment had no significant effect on cell proliferation in MCF-10A, MCF-7 or MDA-MB-231 breast cells. Furthermore, VWF treatment also had no effect on cell death. These data are consistent with a previous report that found exogenous VWF treatment of B16/BL6 melanoma cells had no effect on viability.[255]

VWF has been shown to induce apoptosis through DNA fragmentation and annexin V exposure.[101,144,255] Interestingly, resistance to these VWF-mediated apoptotic pathways was found in metastatic cells expressing metalloproteinase ADAM28.[101] Notably, ADAM28, which is purported to induce VWF-mediated apoptotic resistance in MDA-MB-231 was not expressed in our hands [Appendix III, Table 7.1].

While ADAM28 was found to be responsible for cancer cell protection from VWF, Mochizuki *et al* found that non-neoplastic cell lines not expressing ADAM28 exhibited no susceptibility to VWF-induced apoptosis.[101] Accordingly, our data found that VWF treatment of non-neoplastic MCF-10A cells had no apoptotic effect. Additionally, MDA-MB-231 cells were not susceptible to VWF-mediated apoptosis despite not expressing *ADAM28* [Appendix III, Table 7.1]. Interestingly, MCF-7 breast cancer cells have previously been described to undergo apoptosis in the presence of VWF. However, in our hands, MCF-7 cells exhibited no susceptibility to VWF-mediated apoptosis over 72h. This is in contrast to reports that show ADAM28-deficient cancer cells are susceptible to VWF-mediated apoptosis, however, we used higher doses of VWF (160nM) representative of those seen in patients with metastasis. Furthermore, we assessed the apoptotic effect for longer time points than those used in previous reports.[101,144,389]

5.7.3 Characterising the migratory effects of VWF on breast cells

Enhanced motility of cancer cells is a fundamental step in the metastatic cascade, as tumour cells migrate in order to reposition within the tissues for increased access to nutrients.[402] Our scratch wound assays demonstrated that VWF was unable to alter the migratory capacity of non-neoplastic breast cells MCF-10A or HMEC. However, both breast cancer cell lines (MDA-

MB-231 and MCF-7) displayed enhanced migration following VWF treatment. Following our findings that VWF does not influence cell viability in breast cancer cells, it is likely that the enhanced wound closure seen in VWF treated MDA-MB-231 and MCF-7 cells is a result of migration and proliferation.[420] These results align with a number of reports in various cancer cell lines that have revealed a pro-migratory role for VWF in scratch wound assays.[140–142] Interestingly, previous reports focussed on VWF expressed by tumour cells. [3,119,149,158] Despite the prevalence of VWF within the stroma of cancer tissues, application of exogenous VWF to cancer cells was not assessed in any previous scratch wound assays.

Our transmigration assay determined that, similar to the scratch wound assay, VWF had no migratory effect on non-neoplastic MCF-10A migration. Furthermore, while poorly metastatic MCF-7 cells migrated collectively in the scratch wound assay, they were unable to migrate as individual cells, with VWF unable to induce transmigration across the transwell insert. However, VWF influenced chemotactic migration of the invasive MDA-MB-231 breast cancer cell line. Congruently, VWF not only directed the invasive MDA-MB-231 cell migration but also induced ECM breakdown in response to increasing concentrations of VWF. The chemotactic properties of VWF correspond with a report from Goertz *et al*. that proposed tumour cells are able to pre-emptively induce VWF in sites for metastasis.[181] It was found that injection of ret melanoma cells increased endothelial cell activation at distal sites, leading to an at least two fold increase in VWF fibres in metastasis-free organs (lung, liver and brain) compared to corresponding organs in healthy controls.[181] In addition, injection of an A3-collagen binding domain of VWF into mice has been shown to localise at tumour sites.[160] Taken together, perhaps elevated systemic VWF:Ag levels seen in metastatic cancers are able to induce invasion and migration of tumour cells following accumulation at tumour sites and distant organs through chemotaxis (Table 1.1).

Considering the invasive properties of VWF on the MDA-MB-231 cell line, our cytokine array highlighted a number of proteins that were differentially regulated upon VWF stimulation including MMP-9, IL-17A, CD31 and ApoA-I. Through ELISA we determined that secreted MMP-9 levels were upregulated by VWF in MDA-MB-231 cells. MMPs are known to contribute to the dynamic remodelling of the ECM, as well as facilitating metastasis and angiogenesis in tumours.[407] Interestingly, in HT29 colorectal cancer spheroids the addition of MMP-9 was able to release VEGF from the tumour cells dose-dependently which lead to

increased endothelial sprouting in an angiogenesis assay.[421] IL-17A, another protein upregulated by VWF in the cytokine array was found to be associated not only with MMP-9 but also intratumoural microvessel density (CD31) and VEGF in B16 mouse melanoma and MC38 colon carcinoma tumour sections.[422] Cumulatively, this highlights VWF may induce the release of an interconnected milieu of factors from MDA-MB-231 cells that promote invasive properties.

5.7.4 Characterising the angiogenic effect of VWF on breast cancer cells

Angiogenesis is a critical step in the metastatic process. VWF has been suggested as a pro-angiogenic factor. Therefore, it is interesting that VWF stimulation of MDA-MB-231 cells displayed no alteration in angiogenic factor secretion profile, including VEGF, which was unchanged following ELISA quantification. Previous studies have found that VWF and VEGF are closely associated in cancer, Yang *et al*. showed in late stage cancers immunohistochemistry samples with high VWF expression associated and co-localised with high VEGF and VEGFR2 levels.[119] Altogether, our data demonstrates that VWF does not directly induce the release of classical angiogenic factors like VEGF from breast cancer cells.

We elucidated for the first time that VWF can induce non-classical angiogenic pathway VM in cancer cells. VWF stimulation of MDA-MB-231 breast cancer cells enhanced morphological VM features quantified through number of nodes, junctions and complete mesh formation. Tumour cells utilise VM as an endothelial cell independent mechanism to incorporate into the vasculature.[423] These pseudo-vasculature like networks provide tumour cells with direct access to nutrients as well as making them readily permissible for tumour dissemination.[423] After assessing angiogenic primers through QPCR at both 100 and 200nM we saw significant upregulation of these factors at the higher dose. To keep our results consistent we performed our VM and other angiogenic assays at 200nM. Importantly, we did see small increases in VM at lower doses of VWF (not shown), however, they did not reach statistical significance.

LMWH, which we have described to block VWF adhesion to MDA-MB-231 cells also inhibited VWF mediated VM. This reflects the anti-angiogenic role for LMWH seen by inhibiting VWF fibre accumulation in mouse melanoma tissues.[148] LMWH was found to reduce VWF fibre formation within the tumour microvasculature and also mediated the inhibition of skin tumour vascularisation and subsequent metastasis.[148] It is possible that lower concentrations of LMWH may also be able to induce these reductions in VM.[412]

Following our findings that VWF upregulates *EGFR* mRNA levels in MDA-MB-231 cells we discerned that inhibition of VWF-mediated VM with anti-EGFR antibodies abolished VM node, junction and mesh formation. Anti-EGFR treatment alone and in conjunction with VWF had no significant effect on cell death. Altogether, this data shows that VWF acts through EGFR to induce VM. Correspondingly, while VM is regulated by EMT pathways that involve the downregulation of cell junction proteins like E-cadherin, notably within breast cancer these processes are regulated by EGFR.[415–417,423] Consistent with the link between EGFR and EMT in breast cancer MDA-MB-231 inhibition of EGFR signalling by oestrogen receptor beta (ERβ1) reduced EMT by diminishing the phosphorylation of ERK1/2.[424] Moreover, the overexpression of EGFR in these cells further downregulated EMT marker E-Cadherin. It is possible that VWF interacts directly with the EGFR receptor to induce EMT signalling. Further study is warranted to assess VWF-EGFR signalling in breast cancer cells.

5.7.5 Characterising the metastatic effects of VWF *in vivo*

We showed *in vivo* that antibody treatment targeted against VWF not only reduced the time to metastasis in MDA-MB-231 breast cancer cells but also specifically reduced lung and liver metastasis. Interestingly, no change in metastatic burden was detected in the kidneys or brain. Of note, in a cohort of 197 female patients who died of metastatic breast cancer the most prevalent metastatic sites were lungs/pleura (80% of all metastatic cases), bone (74% of all metastatic cases), liver (71% of all metastatic cases) as well as axillary lymph nodes (55% of all metastatic cases).[425] Interestingly, VWF inhibition in our breast metastasis mouse model significantly ablated metastasis in two of the most frequent metastatic sites in breast cancer.

As a blood-borne protein VWF will have most contact with tumour cells undergoing haematogenous metastasis. In agreement with this, our data found that blocking VWF levels *in vivo* had no impact on lymph node metastasis, one of the most prevalent metastatic sites in breast cancer.[425] Similarly, no effect was seen when lymph nodes were subdivided into left and right sides nor in related lymphatic organ the spleen [Appendix IV, Figure 7.3]. Interestingly, it has been shown that VWF fibre density correlated with pulmonary metastatic node formation but had no effect on lymphatic metastasis.[181] Correspondingly, in a study assessing brain metastasis and clot formation, VWF was found to co-localise with tumour cells caught in clots within the brain microvasculature.[241] It was found that anti-VWF treatment

before perivascular colonisation inhibited metastasis while treatment administered after perivascular niche colonisation was unable to prevent metastasis.

Altogether our data has shown that VWF enhances a series of pro-metastatic functions in the MDA-MB-231 breast cancer cells including tumour motility, migration and invasion (Figure 5.19). While VWF was unable to alter breast cancer cell proliferation we also showed that it was unable to induce apoptosis in breast cancer cells. The chemotactic properties of VWF may be able to induce breakdown of the ECM through MMP-9 protease activity. High VWF: Ag levels associated with metastatic breast cancer patients could influence metastasis by mediating intravasation of the primary tumour into the vasculature where it can begin to circulate through the bloodstream. Additionally, we have identified for the first time that VWF can induce VM in cancer cells, a process that can help tumour cells undergo blood-borne metastasis. Finally, by targeting VWF with antibodies in an *in vivo* system we could inhibit haematogenous metastatic routes, reaffirming our data that VWF was pro-invasive in breast cancer cells as well as highlighting a potential therapeutic target in metastatic development.

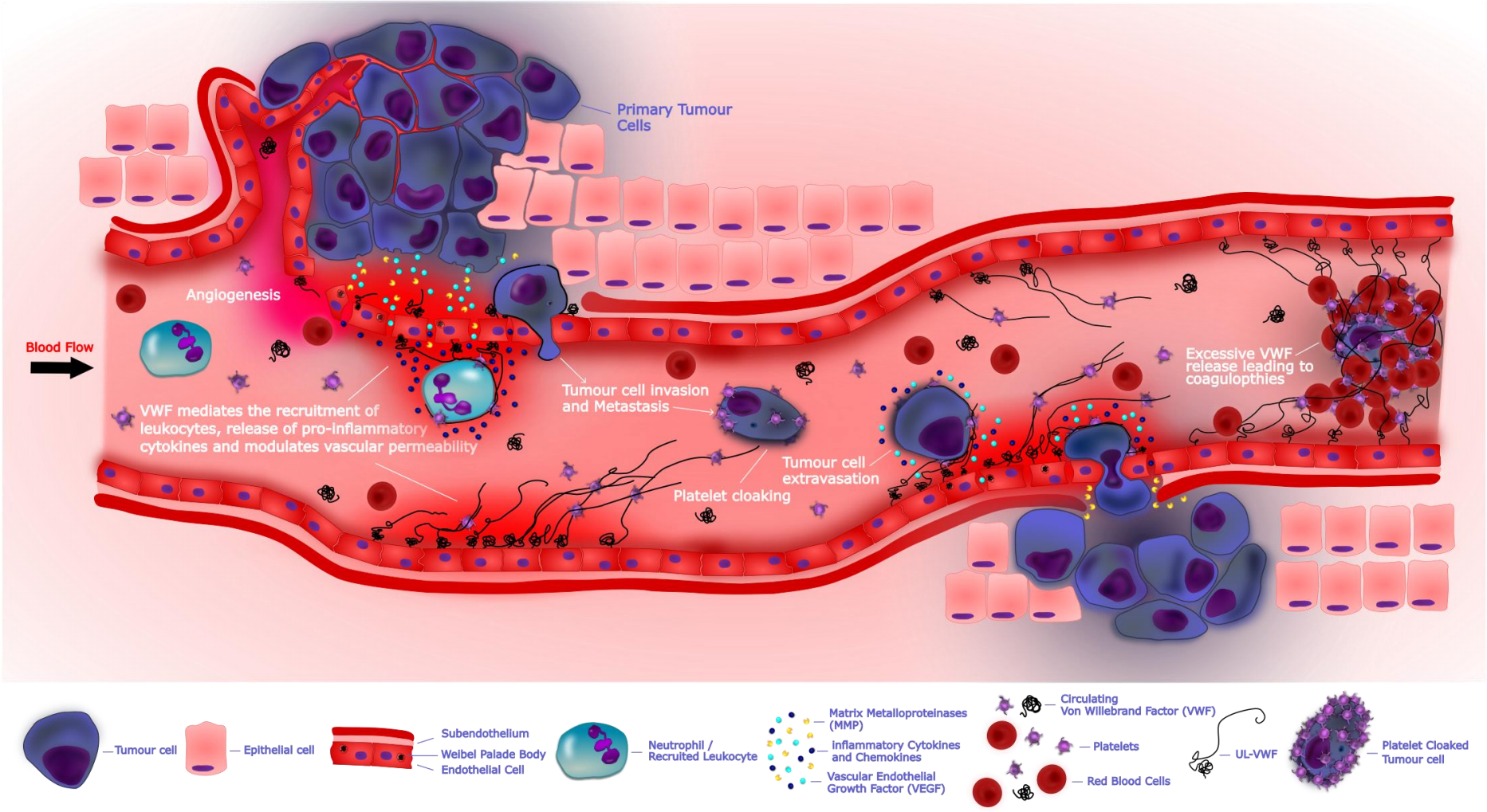
Primary Tumour Cells
Angiogenesis
Blood Flow
VWF mediates the recruitment of leukocytes, release of pro-inflammatory cytokines and modulates vascular permeability
Tumour cell invasion and Metastasis
Platelet cloaking
Tumour cell extravasation
Excessive VWF release leading to coagulopthies
Tumour cell
Epithelial cell
Subendothelium
Weibel Palade Body
Endothelial Cell
Neutrophil / Recruited Leukocyte
Matrix Metalloproteinases (MMP)
Inflammatory Cytokines and Chemokines
Vascular Endothelial Growth Factor (VEGF)
Circulating Von Willebrand Factor (VWF)
Platelets
Red Blood Cells
UL-VWF
Platelet Cloaked Tumour cell

Figure 5.19 The role of VWF in metastasis: A proposed summary image of the metastatic functions of VWF. VWF is released from the endothelium following stimulation from a primary tumour mass. Increasing stromal and plasma levels of VWF induce pseudo-vasculature features in the metastasizing cells as they integrate into the endothelial network. Elevated plasma VWF levels through chemoattraction enable tumour cells to intravasate into the blood vessels through the breakdown of the ECM via MMP-9. Deposits of VWF accumulate at distant metastatic sites where they can prepare a niche that breast cancer cells can migrate and adhere before extravasation into a secondary site. Further induction of VWF will enable breast cancer cells to form vascular-like structures and initiate tumour growth and proliferation before the metastatic process is repeated.

6: Future Directions

6.0 Future Directions

6.1 Assessing VWF deposition in breast cancer

- Depending on the metastatic route of cancer dissemination, differing systemic levels of VWF may be observed, it would be interesting to assess whether VWF:Ag levels vary between different metastatic sites.
- Localised levels of VWF have not been measured as part of a longitudinal study. Measuring how VWF:Ag levels change at primary and secondary sites could help to inform how cancer cells use VWF deposits.

6.2 Investigating the role of VWF multimers in breast cancer

- The multimeric length of VWF is critical for its haemostatic function. ADAMTS13 levels have previously been shown to be dysregulated in a number of cancer types. However, it is unknown whether multimeric length is important for VWF-mediated effects on breast cancer metastasis.
- Determining the multimeric composition of VWF from patients with early and late stage breast cancer through multimer gels would provide insight into the haemostatic capabilities of VWF in cancer patients.
- Future work measuring ADAMTS13 levels from patients with early and late stage breast cancer would allow correlations between ADAMTS13 and overall survival. Using our VWF:Ag levels we could also calculate the VWF:Ag/ADAMTS13 ratio for each patient and assess the predictive power of the VWF:Ag/ADAMTS13 ratio in determining overall survival in breast cancer patients.
- In addition to our *in vivo* data showing a role for anti-VWF treatment in preventing metastasis *in vivo*, it would be interesting to assess the role of VWF multimers in metastatic development. Using the same *in vivo* breast cancer model we could study the effects of recombinant ADAMTS13 on metastasis formation.

6.3 Assessing the role of platelet heteroaggregation

- Endothelial adhesion of breast cancer cells is increased in the presence of platelets. Furthermore, platelet-VWF-tumour heteroaggregates promote survival of tumour cells as they undergo haematogenous metastasis. However, the receptors involved in this process are not fully elucidated.

- We found that VWF adhered to MDA-MB-231 breast cancer cells through LRP1 and GPIbα. Using platelet-tumour cell co-culture assays it would be of interest to determine whether platelet co-culture upregulates the expression of VWF-adhering receptors in breast cancer cells, like LRP1, GPIbα and $\alpha_v\beta_3$.
- Additionally, it has been shown that within whole blood tumour cells accumulate plasma VWF on their cell surface. Future work studying endothelial adhesion could assess the adhesive properties of tumour cells with pre-bound plasma VWF on their surface. Furthermore, in a perfusion assay the ability of pre-bound tumour cells in the presence and absence of platelets to adhere to the endothelial layer would provide insight into the role of platelet-VWF-tumour heteroaggregates in endothelial adhesion under shear stress.

6.4 Mechanistic roles of VWF in cancer

- We have shown that VWF adheres to LRP1 on the surface of MDA-MB-231 breast cancer cells. Multiple reports have linked LRP1 with increased motility and a pro-invasive phenotype in cancer cells. Moreover, LRP1 expression in varied malignant cells has been associated with MMP-9 regulation. Through siRNA knockdown of LRP1 we could assess the link between VWF induced invasion and migration and the regulation of invasive factors like MMP-9.
- Following our work that found a novel link between VWF and EGFR in VM, further assessment is required to follow the downstream signalling pathway of VWF-EGFR signalling. Potentially, using siRNA to knockdown $\alpha_v\beta_3$, a known receptor of VWF, which has been shown to associate with EGFR in order to induce VM in breast cancer. Additionally, further study is required to elucidate whether VWF and EGFR directly interact with each other as a receptor-ligand pair in breast cancer cells.
- Immunohistochemistry slides from our anti-VWF metastasis *in vivo* experiment will be assessed for tumour burden within lungs, liver, brain, kidney, lymph nodes and spleen. In addition, metastatic nodes will be assessed for patterned or tubular VM features using periodic acid-Schiff and CD34 stains.

References

1. Kirwan, C. C., Descamps, T. & Castle, J. Circulating tumour cells and hypercoagulability: a lethal relationship in metastatic breast cancer. *Clinical and Translational Oncology* **22**, 870–877 (2020).

2. Shaker, H. *et al.* Breast cancer stromal clotting activation (Tissue Factor and thrombin): A pre-invasive phenomena that is prognostic in invasion. *Cancer Med* **9**, 1768–1778 (2020).

3. Patmore, S., Dhami, S. P. S. & O'Sullivan, J. M. Von Willebrand factor and cancer; metastasis and coagulopathies. *J Thromb Haemost* **18**, 2444–2456 (2020).

4. Kuwano, A. *et al.* Precise chromosomal locations of the genes for dentatorubral-pallidoluysian atrophy (DRPLA), von Willebrand factor (F8vWF) and parathyroid hormone-like hormone (PTHLH) in human chromosome 12p by deletion mapping. *Hum Genet* **97**, 95–98 (1996).

5. Ginsburg, D. *et al.* Human von Willebrand factor (vWF): isolation of complementary DNA (cDNA) clones and chromosomal localization. *Science* **228**, 1401–1406 (1985).

6. Mancuso, D. J. *et al.* Structure of the gene for human von Willebrand factor. *Journal of Biological Chemistry* **264**, 19514–19527 (1989).

7. Bonthron, D. T. *et al.* Structure of pre-pro-von Willebrand factor and its expression in heterologous cells. *Nature* **324**, 270–273 (1986).

8. Mancuso, D. J. *et al.* Human von Willebrand factor gene and pseudogene: structural analysis and differentiation by polymerase chain reaction. *Biochemistry* **30**, 253–269 (1991).

9. Lenting, P. J., Christophe, O. D. & Denis, C. v. von Willebrand factor biosynthesis, secretion, and clearance: connecting the far ends. *Blood* **125**, 2019–28 (2015).

10. Yamamoto, K., de Waard, V., Fearns, C. & Loskutoff, D. J. Tissue Distribution and Regulation of Murine von Willebrand Factor Gene Expression In Vivo. *Blood* **92**, 2791–2801 (1998).

11. Pusztaszeri, M. P., Seelentag, W. & Bosman, F. T. Immunohistochemical expression of endothelial markers CD31, CD34, von Willebrand factor, and Fli-1 in normal human tissues. *J Histochem Cytochem* **54**, 385–395 (2006).

12. Pannekoek, H. & Voorberg, J. Molecular cloning, expression and assembly of multimeric von Willebrand factor. *Baillieres Clin Haematol* **2**, 879–896 (1989).

13. Sadler, J. E. Biochemistry and genetics of von Willebrand factor. *Annu Rev Biochem* **67**, 395–424 (1998).

14. Zhou, Y.-F. *et al.* Sequence and structure relationships within von Willebrand factor. *Blood* **120**, 449–58 (2012).

15. Springer, T. A. von Willebrand factor, Jedi knight of the bloodstream. *Blood* **124**, 1412–1425 (2014).

16. Foster, P. A., Fulcher, C. A., Marti, T., Titani, K. & Zimmerman, T. S. A major factor VIII binding domain resides within the amino-terminal 272 amino acid residues of von Willebrand factor. *Journal of Biological Chemistry* **262**, 8443–8446 (1987).

17. Lynch, C. J., Lane, D. A. & Luken, B. M. Control of VWF A2 domain stability and ADAMTS13 access to the scissile bond of full-length VWF. *Blood* **123**, 2585–2592 (2014).

18. Fu, H. *et al.* Flow-induced elongation of von Willebrand factor precedes tension-dependent activation. *Nat Commun* **8**, (2017).

19. Li, F., Li, C. Q., Moake, J. L., López, J. A. & McIntire, L. v. Shear stress-induced binding of large and unusually large von Willebrand factor to human platelet glycoprotein Ibalpha. *Ann Biomed Eng* **32**, 961–9 (2004).

20. Arce, N. A. *et al.* Activation of von Willebrand factor via mechanical unfolding of its discontinuous autoinhibitory module. *Nature Communications 2021 12:1* **12**, 1–14 (2021).

21. Federici, A. B. *et al.* Clinical and molecular predictors of thrombocytopenia and risk of bleeding in patients with von Willebrand disease type 2B: a cohort study of 67 patients. *Blood* **113**, 526–534 (2009).

22. Deng, W. *et al.* A discontinuous autoinhibitory module masks the A1 domain of von Willebrand factor. *J Thromb Haemost* **15**, 1867–1877 (2017).

23. Mohri, H. *et al.* Structure of the von Willebrand factor domain interacting with glycoprotein Ib. *J Biol Chem* **263**, (1988).

24. Howard, M. A. & Firkin, B. G. Ristocetin--a new tool in the investigation of platelet aggregation. *Thromb Diath Haemorrh* **26**, (1971).

25. Read, M. S., Shermer, R. W. & Brinkhous, K. M. Venom coagglutinin: an activator of platelet aggregation dependent on von Willebrand factor. *Proc Natl Acad Sci U S A* **75**, 4514–4518 (1978).

26. Zhang, X., Halvorsen, K., Zhang, C. Z., Wong, W. P. & Springer, T. A. Mechanoenzymatic cleavage of the ultralarge vascular protein von Willebrand factor. *Science* **324**, 1330–1334 (2009).

27. Romijn, R. A. *et al.* Mapping the collagen-binding site in the von Willebrand factor-A3 domain. *J Biol Chem* **278**, 15035–15039 (2003).

28. Brondijk, T. H. C., Bihan, D., Farndale, R. W. & Huizinga, E. G. Implications for collagen I chain registry from the structure of the collagen von Willebrand factor A3 domain complex. *Proc Natl Acad Sci U S A* **109**, 5253–5258 (2012).

29. Huizinga, E. G., van der Plas, R. M., Kroon, J., Sixma, J. J. & Gros, P. Crystal structure of the A3 domain of human von Willebrand factor: implications for collagen binding. *Structure* **5**, 1147–1156 (1997).

30. Nishida, N. *et al.* Collagen-binding mode of vWF-A3 domain determined by a transferred cross-saturation experiment. *Nat Struct Biol* **10**, 53–58 (2003).

31. Pareti, F. I., Niiya, K., McPherson, J. M. & Ruggeri, Z. M. Isolation and characterization of two domains of human von Willebrand factor that interact with fibrillar collagen types I and III. *Journal of Biological Chemistry* **262**, 13835–13841 (1987).

32. Zhou, Y. F. *et al.* A pH-regulated dimeric bouquet in the structure of von Willebrand factor. *EMBO J* **30**, 4098 (2011).

33. Beacham, D. A., Wise, R. J., Turci, S. M. & Handin, R. I. Selective inactivation of the Arg-Gly-Asp-Ser (RGDS) binding site in von Willebrand factor by site-directed mutagenesis. *Journal of Biological Chemistry* **267**, 3409–3415 (1992).

34. Denis, C., Williams, J. A., Lu, X., Meyer, D. & Baruch, D. Solid-Phase von Willebrand Factor Contains a Conformationally Active RGD Motif That Mediates Endothelial Cell Adhesion Through the αvβ3 Receptor. *Blood* **82**, 3622–3630 (1993).

35. Wagner, D. D. & Marder, V. J. Biosynthesis of von Willebrand protein by human endothelial cells. Identification of a large precursor polypeptide chain. *Journal of Biological Chemistry* **258**, 2065–2067 (1983).

36. Sporn, L. A., Chavin, S. I., Marder, V. J. & Wagner, D. D. Biosynthesis of von Willebrand protein by human megakaryocytes. *J Clin Invest* **76**, 1102–1106 (1985).

37. Wagner, D. D. & Marder, V. J. Biosynthesis of von Willebrand protein by human endothelial cells: Processing steps and their intracellular localization. *Journal of Cell Biology* **99**, 2123–2130 (1984).

38. Vischer, U. M. & Wagner, D. D. von Willebrand Factor Proteolytic Processing and Multimerization Precede the Formation of Weibel-Palade Bodies. *Blood* **83**, 3536–3544 (1994).

39. McGrath, R. T. *et al.* Expression of terminal α2-6–linked sialic acid on von Willebrand factor specifically enhances proteolysis by ADAMTS13. *Blood* **115**, 2666–2673 (2010).

40. Preston, R. J. S., Rawley, O., Gleeson, E. M. & O'Donnell, J. S. Elucidating the role of carbohydrate determinants in regulating hemostasis: insights and opportunities. *Blood* **121**, 3801–3810 (2013).

41. Aguila, S. *et al.* Increased galactose expression and enhanced clearance in patients with low von Willebrand factor. *Blood* **133**, 1585–1596 (2019).

42. Ellies, L. G. *et al.* Sialyltransferase ST3Gal-IV operates as a dominant modifier of hemostasis by concealing asialoglycoprotein receptor ligands. *Proc Natl Acad Sci U S A* **99**, 10042–10047 (2002).

43. Kornfeld, R. & Kornfeld, S. Assembly of asparagine-linked oligosaccharides. *Annu Rev Biochem* **54**, 631–664 (1985).

44. Samor, B. *et al.* Primary structure of a new tetraantennary glycan of the N-acetyllactosaminic type isolated from human factor VIII/von Willebrand factor. *Eur J Biochem* **158**, 295–298 (1986).

45. Canis, K. *et al.* Mapping the N-glycome of human von Willebrand factor. *Biochem J* **447**, 217–228 (2012).

46. Schwarz, F. & Aebi, M. Mechanisms and principles of N-linked protein glycosylation. *Curr Opin Struct Biol* **21**, 576–582 (2011).

47. Samor, B. *et al.* Primary structure of the major O-glycosidically linked carbohydrate unit of human von Willebrand factor. *Glycoconj J* **6**, 263–270 (1989).

48. Canis, K. *et al.* The plasma von Willebrand factor O-glycome comprises a surprising variety of structures including ABH antigens and disialosyl motifs. *J Thromb Haemost* **8**, 137–145 (2010).

49. Solecka, B. A., Weise, C., Laffan, M. A. & Kannicht, C. Site-specific analysis of von Willebrand factor O-glycosylation. *J Thromb Haemost* **14**, 733–746 (2016).

50. van den Steen, P., Rudd, P. M., Dwek, R. A. & Opdenakker, G. Concepts and principles of O-linked glycosylation. *Crit Rev Biochem Mol Biol* **33**, 151–208 (1998).

51. Matsui, T., Titani, K. & Mizuochi, T. Structures of the asparagine-linked oligosaccharide chains of human von Willebrand factor. Occurrence of blood group A, B, and H(O) structures. *Journal of Biological Chemistry* **267**, 8723–8731 (1992).

52. Gashash, E. A. *et al.* An Insight into Glyco-Microheterogeneity of Plasma von Willebrand Factor by Mass Spectrometry. *J Proteome Res* **16**, 3348–3362 (2017).

53. O'Donnell, J. S., McKinnon, T. A. J., Crawley, J. T. B., Lane, D. A. & Laffan, M. A. Bombay phenotype is associated with reduced plasma-VWF levels and an increased susceptibility to ADAMTS13 proteolysis. *Blood* **106**, 1988–1991 (2005).

54. Ledford-Kraemer, M. R. Analysis of von Willebrand factor structure by multimer analysis. *Am J Hematol* **85**, 510–514 (2010).

55. Shapiro, S. E. *et al.* The von Willebrand factor predicted unpaired cysteines are essential for secretion. *J Thromb Haemost* **12**, 246–254 (2014).

56. Marti, T., Rosselet, S. J., Titani, K. & Walsh, K. A. Identification of disulfide-bridged substructures within human von Willebrand factor. *Biochemistry* **26**, 8099–8109 (1987).

57. Voorberg, J. *et al.* Assembly and routing of von Willebrand factor variants: the requirements for disulfide-linked dimerization reside within the carboxy-terminal 151 amino acids. *J Cell Biol* **113**, 195–205 (1991).

58. Katsumi, A., Tuley, E. A., Bodo, I. & Sadler, J. E. Localization of disulfide bonds in the cystine knot domain of human von Willebrand factor. *J Biol Chem* **275**, 25585–25594 (2000).

59. Schneppenheim, R. *et al.* Defective dimerization of von Willebrand factor subunits due to a Cys-> Arg mutation in type IID von Willebrand disease. *Proc Natl Acad Sci U S A* **93**, 3581–3586 (1996).

60. Huang, R. H. *et al.* Assembly of Weibel-Palade body-like tubules from N-terminal domains of von Willebrand factor. *Proc Natl Acad Sci U S A* **105**, 482–487 (2008).

61. Mayadas, T. N. & Wagner, D. D. In vitro multimerization of von Willebrand factor is triggered by low pH. Importance of the propolypeptide and free sulfhydryls. *J Biol Chem* **264**, (1989).

62. Fowler, W. E., Fretto, L. J., Hamilton, K. K., Erickson, H. P. & McKee, P. A. Substructure of human von Willebrand factor. *J Clin Invest* **76**, 1491–500 (1985).

63. Rehemtulla, A. & Kaufman, R. J. Protein processing within the secretory pathway. *Curr Opin Biotechnol* **3**, 560–565 (1992).

64. Haberichter, S. L., Fahs, S. A. & Montgomery, R. R. Von Willebrand factor storage and multimerization: 2 independent intracellular processes: Presented in abstract form at the 41st Annual Meeting of the American Society of Hematology, New Orleans, LA, December 3-7, 1999. *Blood* **96**, 1808–1815 (2000).

65. Bendetowicz, A. V., Morris, J. A., Wise, R. J., Gilbert, G. E. & Kaufman, R. J. Binding of Factor VIII to von Willebrand Factor Is Enabled by Cleavage of the von Willebrand Factor Propeptide and Enhanced by Formation of Disulfide-Linked Multimers. *Blood* **92**, 529–538 (1998).

66. Ferraro, F. *et al.* A two-tier Golgi-based control of organelle size underpins the functional plasticity of endothelial cells. *Dev Cell* **29**, 292–304 (2014).

67. Weibel, E. R. & Palade, G. E. New cytoplasmic components in arterial endothelia. *J Cell Biol* **23**, 101–112 (1964).

68. Metcalf, D. J., Nightingale, T. D., Zenner, H. L., Lui-Roberts, W. W. & Cutler, D. F. Formation and function of Weibel-Palade bodies. *J Cell Sci* **121**, 19–27 (2008).

69. Wolff, B., Burns, A. R., Middleton, J. & Rot, A. Endothelial cell 'memory' of inflammatory stimulation: human venular endothelial cells store interleukin 8 in Weibel-Palade bodies. *J Exp Med* **188**, 1757–1762 (1998).

70. Zannettino, A. C. W. *et al.* Osteoprotegerin (OPG) is localized to the Weibel-Palade bodies of human vascular endothelial cells and is physically associated with von Willebrand factor. *J Cell Physiol* **204**, 714–723 (2005).

71. Denis, C. v., André, P., Saffaripour, S. & Wagner, D. D. Defect in regulated secretion of P-selectin affects leukocyte recruitment in von Willebrand factor-deficient mice. *Proc Natl Acad Sci U S A* **98**, 4072–4077 (2001).

72. Fiedler, U. *et al.* Angiopoietin-2 sensitizes endothelial cells to TNF-alpha and has a crucial role in the induction of inflammation. *Nat Med* **12**, 235–239 (2006).

73. Starke, R. D. *et al.* Endothelial von Willebrand factor regulates angiogenesis. *Blood* **117**, 1071 (2011).

74. Cossutta, M. *et al.* Weibel-Palade Bodies Orchestrate Pericytes During Angiogenesis. *Arterioscler Thromb Vasc Biol* **39**, 1843–1858 (2019).

75. Cramer, E., Meyer, D., le Menn, R. & Breton-Gorius, J. Eccentric Localization of von Willebrand Factor in an Internal Structure of Platelet α-Granule Resembling That of Weibel-Palade Bodies. *Blood* **66**, 710–713 (1985).

76. da Silva, M. L. & Cutler, D. F. Von Willebrand factor multimerization and the polarity of secretory pathways in endothelial cells. *Blood* **128**, 277–285 (2016).

77. Sporn, L. A., Marder, V. J. & Wagner, D. D. Inducible secretion of large, biologically potent von Willebrand factor multimers. *Cell* **46**, 185–190 (1986).

78. Bierings, R. & Voorberg, J. Up or out: polarity of VWF release. *Blood* **128**, 154–155 (2016).

79. Giblin, J. P., Hewlett, L. J. & Hannah, M. J. Basal secretion of von Willebrand factor from human endothelial cells. *Blood* **112**, 957–964 (2008).

80. Nightingale, T. & Cutler, D. The secretion of von Willebrand factor from endothelial cells; an increasingly complicated story. *J Thromb Haemost* **11 Suppl 1**, 192–201 (2013).

81. de Wit, T. R., Rondaij, M. G., Hordijk, P. L., Voorberg, J. & van Mourik, J. A. Real-time imaging of the dynamics and secretory behavior of Weibel-Palade bodies. *Arterioscler Thromb Vasc Biol* **23**, 755–761 (2003).

82. Dong, J. fei *et al.* ADAMTS-13 rapidly cleaves newly secreted ultralarge von Willebrand factor multimers on the endothelial surface under flowing conditions. *Blood* **100**, 4033–4039 (2002).

83. André, P. *et al.* Platelets adhere to and translocate on von Willebrand factor presented by endothelium in stimulated veins. *Blood* **96**, 3322–3328 (2000).

84. Kaufmann, J. E. *et al.* Vasopressin-induced von Willebrand factor secretion from endothelial cells involves V2 receptors and cAMP. *J Clin Invest* **106**, 107–116 (2000).

85. Leebeek, F. W. G. & Eikenboom, J. C. J. Von Willebrand's Disease. *N Engl J Med* **375**, 2067–2080 (2016).

86. Savage, B., Sixma, J. J. & Ruggeri, Z. M. Functional self-association of von Willebrand factor during platelet adhesion under flow. *Proc Natl Acad Sci U S A* **99**, 425–430 (2002).

87. Blenner, M. A., Dong, X. & Springer, T. A. Structural Basis of Regulation of von Willebrand Factor Binding to Glycoprotein Ib. *J Biol Chem* **289**, 5565 (2014).

88. Fullard, J. The role of the platelet glycoprotein IIb/IIIa in thrombosis and haemostasis. *Curr Pharm Des* **10**, 1567–1576 (2004).

89. de Ceunynck, K., de Meyer, S. F. & Vanhoorelbeke, K. Unwinding the von Willebrand factor strings puzzle. *Blood* **121**, 270–277 (2013).

90. Zheng, X. L. ADAMTS13 and von Willebrand factor in thrombotic thrombocytopenic purpura. *Annu Rev Med* **66**, 211–225 (2015).

91. Interlandi, G., Ling, M., Tu, A. Y., Chung, D. W. & Thomas, W. E. Structural Basis of Type 2A von Willebrand Disease Investigated by Molecular Dynamics Simulations and Experiments. *PLoS One* **7**, e45207 (2012).

92. Yee, A. *et al.* A von Willebrand factor fragment containing the D'D3 domains is sufficient to stabilize coagulation factor VIII in mice. *Blood* **124**, 445–452 (2014).

93. Weiss, H. J., Sussman, I. I. & Hoyer, L. W. Stabilization of factor VIII in plasma by the von Willebrand factor. Studies on posttransfusion and dissociated factor VIII and in patients with von Willebrand's disease. *J Clin Invest* **60**, 390–404 (1977).

94. Vlot, A. J., Koppelman, S. J., van den Berg, M. H., Bouma, B. N. & Sixma, J. J. The Affinity and Stoichiometry of Binding of Human Factor VIII to von Willebrand Factor. *Blood* **85**, 3150–3157 (1995).

95. Casonato, A., Galletta, E., Sarolo, L. & Daidone, V. Type 2N von Willebrand disease: Characterization and diagnostic difficulties. *Haemophilia* **24**, 134–140 (2018).

96. Nossent, A. Y. *et al.* von Willebrand factor and its propeptide: the influence of secretion and clearance on protein levels and the risk of venous thrombosis. *Journal of Thrombosis and Haemostasis* **4**, 2556–2562 (2006).

97. Rietveld, I. M. *et al.* High levels of coagulation factors and venous thrombosis risk: strongest association for factor VIII and von Willebrand factor. *Journal of Thrombosis and Haemostasis* **17**, 99–109 (2019).

98. Khorana, A. A., Francis, C. W., Culakova, E., Kuderer, N. M. & Lyman, G. H. Thromboembolism is a leading cause of death in cancer patients receiving outpatient chemotherapy. *J Thromb Haemost* **5**, 632–634 (2007).

99. Palacios-Acedo, A. L. *et al.* Platelets, Thrombo-Inflammation, and Cancer: Collaborating With the Enemy. *Front Immunol* **10**, 1805 (2019).

100. Ishihara, J. *et al.* The heparin binding domain of von Willebrand factor binds to growth factors and promotes angiogenesis in wound healing. *Blood* **133**, 2559–2569 (2019).

101. Mochizuki, S. *et al.* Effect of ADAM28 on carcinoma cell metastasis by cleavage of von willebrand factor. *J Natl Cancer Inst* **104**, 906–922 (2012).

102. Wang, W. S. *et al.* Plasma von Willebrand factor level as a prognostic indicator of patients with metastatic colorectal carcinoma. *World Journal of Gastroenterology : WJG* **11**, 2166 (2005).

103. Koh, S. C. L. *et al.* The association with age, human tissue kallikreins 6 and 10 and hemostatic markers for survival outcome from epithelial ovarian cancer. *Arch Gynecol Obstet* **284**, 183–190 (2011).

104. Guo, R., Yang, J., Liu, X., Wu, J. & Chen, Y. Increased von Willebrand factor over decreased ADAMTS-13 activity is associated with poor prognosis in patients with advanced non-small-cell lung cancer. *J Clin Lab Anal* **32**, (2018).

105. Marfia, G. *et al.* Prognostic value of preoperative von Willebrand factor plasma levels in patients with Glioblastoma. *Cancer Med* **5**, 1783–1790 (2016).

106. Rho, J. H. *et al.* Protein and glycomic plasma markers for early detection of adenoma and colon cancer. *Gut* **67**, 473–484 (2018).

107. Takaya, H. *et al.* VWF/ADAMTS13 ratio as a potential biomarker for early detection of hepatocellular carcinoma. *BMC Gastroenterol* **19**, (2019).

108. Mannucci, P. M., Karimi, M., Mosalaei, A., Canciani, M. T. & Peyvandi, F. Patients with localized and disseminated tumors have reduced but measurable levels of ADAMTS-13 (von Willebrand factor cleaving protease). *Haematologica* **88**, (2003).

109. Pépin, M. *et al.* ADAMTS-13 and von Willebrand factor predict venous thromboembolism in patients with cancer. *Journal of Thrombosis and Haemostasis* **14**, 306–315 (2016).

110. Morena Barrio, P. de la. Análisis del sistema hemostático en neoplasias avanzadas. *Proyecto de investigación:* (2017).

111. Röhsig, L. M. *et al. von Willebrand factor antigen levels in plasma of patients with malignant breast disease*. *von Willebrand in breast disease Brazilian Journal of Medical and Biological Research* vol. 34 (2001).

112. Yigit, E. *et al.* Relation between hemostatic parameters and prognostic/predictive factors in breast cancer. *Eur J Intern Med* **19**, 602–607 (2008).

113. Blann, A. D. *et al.* Increased soluble P-selectin in patients with haematological and breast cancer: a comparison with fibrinogen, plasminogen activator inhibitor and von Willebrand factor. *Blood Coagul Fibrinolysis* **12**, 43–50 (2001).

114. Weiss, D. R. *et al.* The structure of the von Willebrand factor is not altered in patients with colorectal carcinoma. *Colorectal Disease* **14**, 1500–1506 (2012).

115. Damin, D. C. *et al.* Von Willebrand factor in colorectal cancer. *Int J Colorectal Dis* **17**, 42–45 (2002).

116. Gil-Bazo, I. *et al.* Impact of surgery and chemotherapy on von Willebrand factor and vascular endothelial growth factor levels in colorectal cancer. *Clin Transl Oncol* **7**, 150–5 (2005).

117. Martini, F. *et al.* Plasma von Willebrand factor antigen levels in non-small cell lung cancer patients. *Anticancer Res* **25**, 403–7 (2005).

118. Yang, A. J. *et al.* Cancer cell-derived von Willebrand factor enhanced metastasis of gastric adenocarcinoma. *Oncogenesis* **7**, (2018).

119. Yang, X. *et al.* Gastric cancer-associated enhancement of von Willebrand factor is regulated by vascular endothelial growth factor and related to disease severity. *BMC Cancer* **15**, (2015).

120. Ziętek, Z., Iwan-Ziętek, I., Paczulski, R., Kotschy, M. & Wolski, Z. von Willebrand factor antigen in blood plasma of patients with urinary bladder carcinoma. *Thromb Res* **83**, 399–402 (1996).

121. Gadducci, A. *et al.* Pretreatment plasma levels of fibrinopeptide-A (FPA), D-dimer (DD), and von Willebrand factor (vWF) in patients with ovarian carcinoma. *Gynecol Oncol* **53**, 352–6 (1994).

122. Blann, A. D., Balakrishnan, B., Shantsila, E., Ryan, P. & Lip, G. Y. H. Endothelial progenitor cells and circulating endothelial cells in early prostate cancer: A comparison with plasma vascular markers. *Prostate* **71**, 1047–1053 (2011).

123. Ablin, R. J., Bartkus, J. M. & Gonder, M. J. Immunoquantitation of factor VIII-related antigen (von Willebrand factor antigen) in prostate cancer. *Cancer Lett* **40**, 283–9 (1988).

124. Navone, S. E. *et al.* Significance and Prognostic Value of The Coagulation Profile in Patients with Glioblastoma: Implications for Personalized Therapy. *World Neurosurg* **121**, e621–e629 (2019).

125. Burley, K. *et al.* Evaluation of coagulopathy before and during induction chemotherapy for acute lymphoblastic leukaemia, including assessment of global clotting tests. *Blood Cancer J* **7**, e574 (2017).

126. Hagag, A. A. E., Abdel-Lateef, A. E. & Aly, R. Prognostic value of plasma levels of thrombomodulin and von Willebrand factor in Egyptian children with acute lymphoblastic leukemia. *Journal of Oncology Pharmacy Practice* **20**, 356–361 (2014).

127. Sherif, N. H. K. el, Narouz, M. F. G., Elkerdany, T. A. & Habashy, S. A. el. *Von Willebrand Factor and Factor VIII Levels in Egyptian Children With Newly Diagnosed Acute Lymphoblastic Leukemia in Relation to Peripheral Blast Cells and Steroid Therapy*. www.jpho-online.com (2014).

128. Athale, U. *et al.* Von Willebrand factor and thrombin activation in children with newly diagnosed acute lymphoblastic leukemia: An impact of peripheral blasts. *Pediatr Blood Cancer* **54**, 963–969 (2010).

129. Hatzipantelis, E. S. *et al.* Thrombomodulin and von Willebrand factor: Relation to endothelial dysfunction and disease outcome in children with acute lymphoblastic leukemia. *Acta Haematol* **125**, 130–135 (2011).

130. Giordano, P. *et al.* Prospective study of hemostatic alterations in children with acute lymphoblastic leukemia. *Am J Hematol* **85**, 325–330 (2010).

131. Auwerda, J. J. A., Sonneveld, P., de Maat, M. P. M. & Leebeek, F. W. G. Prothrombotic coagulation abnormalities in patients with newly diagnosed multiple myeloma. *Haematologica* **92**, 279–280 (2007).

132. van Marion, A. M. W. *et al.* Prospective evaluation of coagulopathy in multiple myeloma patients before, during and after various chemotherapeutic regimens. *Leuk Res* **32**, 1078–1084 (2008).

133. Robak, M., Treliński, J. & Chojnowski, K. Hemostatic changes after 1 month of thalidomide and dexamethasone therapy in patients with multiple myeloma. *Medical Oncology* **29**, 3574–3580 (2012).

134. Tiong, I. S., Rodgers, S. E., Lee, C. H. S. & McRae, S. J. Baseline and treatment-related changes in thrombin generation in patients with multiple myeloma. *Leuk Lymphoma* **58**, 941–949 (2017).

135. Larkin, D. *et al.* Severe Plasmodium falciparum malaria is associated with circulating ultra-large von willebrand multimers and ADAMTS13 inhibition. *PLoS Pathog* **5**, (2009).

136. Peetermans, M. *et al.* Von Willebrand factor and ADAMTS13 impact on the outcome of Staphylococcus aureus sepsis. *Journal of Thrombosis and Haemostasis* **18**, 722–731 (2020).

137. Eppert, K., Wunder, J. S., Aneliunas, V., Kandel, R. & Andrulis, I. L. Von Willebrand factor expression in osteosarcoma metastasis. *Modern Pathology* **18**, 388–397 (2005).

138. Kong, Q. F. *et al.* Association of von Willebrand factor (vWF) expression with lymph node metastasis and hemodynamics in papillary thyroid carcinoma. *Eur Rev Med Pharmacol Sci* **24**, 2564–2571 (2020).

139. Liu, G. & Ren, Y. [Effect of von Willebrand factor on the biological characteristics of colorectal cancer cells]. *Zhonghua Wei Chang Wai Ke Za Zhi* **13**, (2010).

140. Liu, Y. *et al.* The role of von Willebrand factor as a biomarker of tumor development in hepatitis B virus-associated human hepatocellular carcinoma: a quantitative proteomic based study. *J Proteomics* **106**, 99–112 (2014).

141. Tao, Q. *et al.* Breast cancer cells-derived Von Willebrand Factor promotes VEGF-A-related angiogenesis through PI3K/Akt-miR-205-5p signaling pathway. *Toxicol Appl Pharmacol* **440**, (2022).

142. Gu, J. *et al.* Lung adenocarcinoma–derived vWF promotes tumor metastasis by regulating PHKG1-mediated glycogen metabolism. *Cancer Sci* **113**, 1362 (2022).

143. Mojiri, A. *et al.* Functional assessment of von Willebrand factor expression by cancer cells of non-endothelial origin. *Oncotarget* **8**, 13015–13029 (2017).

144. Yin, Q. *et al.* ADAM28 from both endothelium and gastric cancer cleaves von Willebrand Factor to eliminate von Willebrand Factor-induced apoptosis of gastric cancer cells. *Eur J Pharmacol* **898**, 173994 (2021).

145. McGrath, R. T. *et al.* Altered glycosylation of platelet-derived von Willebrand factor confers resistance to ADAMTS13 proteolysis. *Blood* **122**, 4107–10 (2013).

146. Verhenne, S. *et al.* Platelet-derived VWF is not essential for normal thrombosis and hemostasis but fosters ischemic stroke injury in mice. *Blood* **126**, 1715–1722 (2015).

147. Bernardo, A., Ball, C., Nolasco, L., Moake, J. F. & Dong, J. F. Effects of inflammatory cytokines on the release and cleavage of the endothelial cell-derived ultralarge von Willebrand-factor multimers under flow. *Blood* **104**, 100–106 (2004).

148. Bauer, A. T. *et al.* von Willebrand factor fibers promote cancer-associated platelet aggregation in malignant melanoma of mice and humans. *Blood* **125**, 3153–3163 (2015).

149. Xu, Y. *et al.* GATA3-induced vWF upregulation in the lung adenocarcinoma vasculature. *Oncotarget* **8**, 110517–110529 (2017).

150. Karagiannis, G. S., Saraon, P., Jarvi, K. A. & Diamandis, E. P. Proteomic signatures of angiogenesis in androgen-independent prostate cancer. *Prostate* **74**, 260–272 (2014).

151. Kerk, N., Strozyk, E. A., Pöppelmann, B. & Schneider, S. W. The mechanism of melanoma-associated thrombin activity and von willebrand factor release from endothelial cells. *Journal of Investigative Dermatology* **130**, 2259–2268 (2010).

152. Desch, A. *et al.* Highly invasive melanoma cells activate the vascular endothelium via an MMP-2/integrin αvβ5-induced secretion of VEGF-A. *American Journal of Pathology* **181**, 693–705 (2012).

153. John, A. *et al.* Urothelial carcinoma of the bladder induces endothelial cell activation and hypercoagulation. *Molecular Cancer Research* **18**, 1099–1109 (2020).

154. Goerge, T. *et al.* Microfluidic reveals generation of platelet-strings on tumor-activated endothelium. *Thromb Haemost* **98**, 283–286 (2007).

155. Robador, J. R. *et al.* Involvement of platelet-derived VWF in metastatic growth of melanoma in the brain. *Neurooncol Adv* **3**, (2021).

156. Dhami, S. P. S. *et al.* Breast cancer cells mediate endothelial cell activation, promoting von Willebrand factor release, tumor adhesion, and transendothelial migration. *J Thromb Haemost* **20**, 2350–2365 (2022).

157. Goerge, T. *et al.* Tumor-derived matrix metalloproteinase-1 targets endothelial proteinase-activated receptor 1 promoting endothelial cell activation. *Cancer Res* **66**, 7766–7774 (2006).

158. Ohtani, H. & Sasano, N. Characterization of microvasculature in the stroma of human colorectal carcinoma: an immunoelectron microscopic study on factor VIII/von Willebrand factor. *J Electron Microsc (Tokyo)* **36**, 204–12 (1987).

159. Cahlin, C., Lönnroth, C., Arvidsson, A., Nordgren, S. & Lundholm, K. Growth associated proteins in tumor cells and stroma related to disease progression of colon cancer accounting for tumor tissue PGE2 content. *Int J Oncol* **32**, 909–918 (2008).

160. Ishihara, J. *et al.* Targeted antibody and cytokine cancer immunotherapies through collagen affinity. *Sci Transl Med* **11**, (2019).

161. Ling, J. *et al.* Feedback modulation of endothelial cells promotes epithelial-mesenchymal transition and metastasis of osteosarcoma cells by Von Willebrand Factor release. *J Cell Biochem* **120**, 15971–15979 (2019).

162. Coussens, L. M. & Werb, Z. Inflammation and cancer. *Nature* **420**, 860–7 (2002).

163. Balkwill, F. & Mantovani, A. Inflammation and cancer: back to Virchow? *Lancet* **357**, 539–545 (2001).

164. Müller, A. *et al.* Involvement of chemokine receptors in breast cancer metastasis. *Nature* **410**, 50–6 (2001).

165. Kawecki, C., Lenting, P. J. & Denis, C. v. von Willebrand factor and inflammation. *Journal of Thrombosis and Haemostasis* **15**, 1285–1294 (2017).

166. Bernardo, A. *et al.* Platelets adhered to endothelial cell-bound ultra-large von Willebrand factor strings support leukocyte tethering and rolling under high shear stress. *J Thromb Haemost* **3**, 562–570 (2005).

167. Popa, M. *et al.* Role of CD40 and ADAMTS13 in von Willebrand factor-mediated endothelial cell-platelet-monocyte interaction. *Proc Natl Acad Sci U S A* **115**, E5556–E5565 (2018).

168. Morganti, M. *et al.* Von Willebrand's factor mediates the adherence of human tumoral cells to human endothelial cells and ticlopidine interferes with this effect. *Biomed Pharmacother* **54**, 431–436 (2000).

169. Gomes, N., Legrand, C. & Fauvel-Lafève, F. Shear stress induced release of von Willebrand factor and thrombospondin-1 in HUVEC extracellular matrix enhances breast tumour cell adhesion. *Clin Exp Metastasis* **22**, 215–223 (2005).

170. Nome, M. E. *et al.* Serum levels of inflammation-related markers and metabolites predict response to neoadjuvant chemotherapy with and without bevacizumab in breast cancers. *Int J Cancer* **146**, 223–235 (2020).

171. Hillgruber, C. *et al.* Blocking Von Willebrand Factor for Treatment of Cutaneous Inflammation. *Journal of Investigative Dermatology* **134**, 77–86 (2014).

172. Petri, B. *et al.* von Willebrand factor promotes leukocyte extravasation. *Blood* **116**, 4712–9 (2010).

173. Aymé, G. *et al.* A Novel Single-Domain Antibody Against von Willebrand Factor A1 Domain Resolves Leukocyte Recruitment and Vascular Leakage during Inflammation - Brief Report. *Arterioscler Thromb Vasc Biol* **37**, 1736–1740 (2017).

174. Drakeford, C. *et al.* von Willebrand factor links primary hemostasis to innate immunity. *Nat Commun* **13**, 6320 (2022).

175. Suidan, G. L. *et al.* Endothelial von willebrand factor promotes blood-brain barrier flexibility and provides protection from hypoxia and seizures in mice. *Arterioscler Thromb Vasc Biol* **33**, 2112–2120 (2013).

176. Zhu, X. *et al.* Von Willebrand factor contributes to poor outcome in a mouse model of intracerebral haemorrhage. *Sci Rep* **6**, (2016).

177. Ferrara, N. VEGF and the quest for tumour angiogenesis factors. *Nature Reviews Cancer 2002 2:10* **2**, 795–803 (2002).

178. Selvam, S. N. *et al.* Abnormal angiogenesis in blood outgrowth endothelial cells derived from von Willebrand disease patients. *Blood Coagul Fibrinolysis* **28**, 521 (2017).

179. de Vries, M. R., Peters, E. A. B., Quax, P. H. A. & Nossent, A. Y. von Willebrand factor deficiency leads to impaired blood flow recovery after ischaemia in mice. *Thromb Haemost* **117**, 1412–1419 (2017).

180. Zanetta, L. *et al.* Expression of Von Willebrand factor, an endothelial cell marker, is up-regulated by angiogenesis factors: a potential method for objective assessment of tumor angiogenesis. *Int J Cancer* **85**, 281–8 (2000).

181. Goertz, L. *et al. Heparins that block VEGF-A-mediated von Willebrand factor fiber generation are potent inhibitors of hematogenous but not lymphatic metastasis*. vol. 7 www.impactjournals.com/oncotarget (2016).

182. Gasic, G. J., Gasic, T. B. & Stewart, C. C. Antimetastatic effects associated with platelet reduction. *Proc Natl Acad Sci U S A* **61**, 46–52 (1968).

183. McCarty, O. J. T., Mousa, S. A., Bray, P. F. & Konstantopoulos, K. Immobilized platelets support human colon carcinoma cell tethering, rolling, and firm adhesion under dynamic flow conditions. *Blood* **96**, 1789–1797 (2000).

184. Qi, Y. *et al.* Novel antibodies against GPIbα inhibit pulmonary metastasis by affecting vWF-GPIbα interaction. *J Hematol Oncol* **11**, (2018).

185. Jain, S. *et al.* Platelet glycoprotein Ibα supports experimental lung metastasis. *Proc Natl Acad Sci U S A* **104**, 9024 (2007).

186. O'Sullivan, J. M., Preston, R. J. S., Robson, T. & O'Donnell, J. S. Emerging Roles for von Willebrand Factor in Cancer Cell Biology. *Semin Thromb Hemost* **44**, 159–166 (2018).

187. Oleksowicz, L., Dutcher, J. P., Deleon-Fernandez, M., Paietta, E. & Etkind, P. Human breast carcinoma cells synthesize a protein immunorelated to platelet glycoprotein-Ib alpha with different functional properties. *J Lab Clin Med* **129**, 337–46 (1997).

188. Suter, C. M., Hogg, P. J., Price, J. T., Chong, B. H. & Ward, R. L. Identification and characterisation of a platelet GPIb/V/IX-like complex on human breast cancers: Implications for the metastatic process. *Japanese Journal of Cancer Research* **92**, 1082–1092 (2001).

189. Karpatkin, S., Pearlstein, E., Ambrogio, C. & Coller, B. S. Role of adhesive proteins in platelet tumor interaction in vitro and metastasis formation in vivo. *J Clin Invest* **81**, 1012–9 (1988).

190. Terraube, V. *et al.* Increased metastatic potential of tumor cells in von Willebrand factor-deficient mice. *Journal of Thrombosis and Haemostasis* **4**, 519–526 (2006).

191. Wun, T. & White, R. H. Epidemiology of cancer-related venous thromboembolism. *Best Pract Res Clin Haematol* **22**, 9–23 (2009).

192. Sørensen, H. T., Mellemkjær, L., Olsen, J. H. & Baron, J. A. Prognosis of cancers associated with venous thromboembolism. *N Engl J Med* **343**, 1846–1850 (2000).

193. Kakkar, A. K. *et al.* Low molecular weight heparin, therapy with dalteparin, and survival in advanced cancer: The fragmin advanced malignancy outcome study (FAMOUS). *Journal of Clinical Oncology* **22**, 1944–1948 (2004).

194. Klerk, C. P. W. *et al.* The effect of low molecular weight heparin on survival in patients with advanced malignancy. *Journal of Clinical Oncology* **23**, 2130–2135 (2005).

195. Auer, R. C. *et al.* Efficacy and safety of extended duration to perioperative thromboprophylaxis with low molecular weight heparin on disease-free survival after surgical resection of colorectal cancer (PERIOP-01): multicentre, open label, randomised controlled trial. *BMJ* **378**, (2022).

196. Meyer, G. *et al.* Anti-tumour effect of low molecular weight heparin in localised lung cancer: a phase III clinical trial. *European Respiratory Journal* **52**, 1801220 (2018).

197. Macbeth, F. *et al.* Randomized phase III trial of standard therapy plus low molecular weight heparin in patients with lung cancer: FRAGMATIC trial. *Journal of Clinical Oncology* **34**, 488–494 (2016).

198. Becattini, C., Verso, M., Muňoz, A. & Agnelli, G. Updated meta-analysis on prevention of venous thromboembolism in ambulatory cancer patients. *Haematologica* **105**, (2020).

199. Fuentes, H. E. *et al.* Meta-analysis on anticoagulation and prevention of thrombosis and mortality among patients with lung cancer. *Thromb Res* **154**, (2017).

200. Lee, A. Y. Y. When can we stop anticoagulation in patients with cancer-associated thrombosis? *Hematology Am Soc Hematol Educ Program* **2017**, (2017).

201. Lee, A. Y. Y. *et al.* CATCH: a randomised clinical trial comparing long-term tinzaparin versus warfarin for treatment of acute venous thromboembolism in cancer patients. *BMC Cancer* **13**, (2013).

202. Lee, A. Y. Y. *et al.* Randomized comparison of low molecular weight heparin and coumarin derivatives on the survival of patients with cancer and venous thromboembolism. *Journal of Clinical Oncology* **23**, 2123–2129 (2005).

203. Obermeier, H. L. *et al.* The role of ADAMTS-13 and von Willebrand factor in cancer patients: Results from the Vienna Cancer and Thrombosis Study. *Res Pract Thromb Haemost* **3**, 503–514 (2019).

204. Oleksowicz, L., Bhagwati, N. & DeLeon-Fernandez, M. Deficient activity of von Willebrand's factor-cleaving protease in patients with disseminated malignancies. *Cancer Res* **59**, 2244–50 (1999).

205. Sobel, M. *et al.* Heparin inhibition of von Willebrand factor-dependent platelet function in vitro and in vivo. *J Clin Invest* **87**, 1787–93 (1991).

206. Győrffy, B. Survival analysis across the entire transcriptome identifies biomarkers with the highest prognostic power in breast cancer. *Comput Struct Biotechnol J* **19**, 4101–4109 (2021).

207. Ősz, Á., Lánczky, A. & Győrffy, B. Survival analysis in breast cancer using proteomic data from four independent datasets. *Sci Rep* **11**, 16787 (2021).

208. Tang, W. *et al.* Integrated proteotranscriptomics of breast cancer reveals globally increased protein-mRNA concordance associated with subtypes and survival. *Genome Med* **10**, (2018).

209. Boersma, B. J. *et al.* Association of breast cancer outcome with status of p53 and MDM2 SNP309. *J Natl Cancer Inst* **98**, (2006).

210. Terunuma, A. *et al.* MYC-driven accumulation of 2-hydroxyglutarate is associated with breast cancer prognosis. *J Clin Invest* **124**, (2014).

211. McShane, L. M. *et al.* REporting recommendations for tumour MARKer prognostic studies (REMARK). *Br J Cancer* **93**, (2005).

212. Ward, S. E. *et al.* ADAMTS13 regulation of VWF multimer distribution in severe COVID-19. *Journal of Thrombosis and Haemostasis* **19**, 1914–1921 (2021).

213. Cailleau,', R., Olive, M. & Cruciger, Q. V. J. *LONG-TERM HUMAN BREAST CARCINOMA CELL LINES OF METASTATIC ORIGIN: PRELIMINARY CHARACTERIZATION*. *IN VITRO* vol. 14 (1978).

214. Holliday, D. L. & Speirs, V. Choosing the right cell line for breast cancer research. *Breast Cancer Res* **13**, 215 (2011).

215. Chavez, K. J., Garimella, S. v & Lipkowitz, S. Triple negative breast cancer cell lines: one tool in the search for better treatment of triple negative breast cancer. *Breast Dis* **32**, 35–48 (2010).

216. Comşa, Ş., Cîmpean, A. M. & Raica, M. The Story of MCF-7 Breast Cancer Cell Line: 40 years of Experience in Research. *Anticancer Res* **35**, 3147–54 (2015).

217. Qu, Y. *et al.* Evaluation of MCF10A as a Reliable Model for Normal Human Mammary Epithelial Cells. *PLoS One* **10**, (2015).

218. Soule, H. D. *et al.* Isolation and characterization of a spontaneously immortalized human breast epithelial cell line, MCF-10. *Cancer Res* **50**, 6075–6086 (1990).

219. Joshi, P. S., Modur, V., Cheng, J. M., Robinson, K. & Rao, K. Characterization of immortalized human mammary epithelial cell line HMEC 2.6. *Tumor Biology* **39**, 1–12 (2017).

220. Miller, I. S. *et al.* Durability of cell line xenograft resection models to interrogate tumor micro-environment targeting agents. *Sci Rep* **9**, (2019).

221. McKinnon, T. A. J., Chion, A. C. K., Millington, A. J., Lane, D. A. & Laffan, M. A. N-linked glycosylation of VWF modulates its interaction with ADAMTS13. *Blood* **111**, 3042–3049 (2008).

222. Chion, A. *et al.* N-linked glycans within the A2 domain of von Willebrand factor modulate macrophage-mediated clearance. *Blood* **128**, 1959–1968 (2016).

223. Smith, P. K. *et al.* Measurement of protein using bicinchoninic acid. *Anal Biochem* **150**, 76–85 (1985).

224. Carpentier, G. *et al.* Angiogenesis Analyzer for ImageJ — A comparative morphometric analysis of “Endothelial Tube Formation Assay” and “Fibrin Bead Assay”. *Scientific Reports 2020 10:1* **10**, 1–13 (2020).

225. Jones, L. J., Gray, M., Yue, S. T., Haugland, R. P. & Singer, V. L. Sensitive determination of cell number using the CyQUANT cell proliferation assay. *J Immunol Methods* **254**, 85–98 (2001).

226. Berridge, M. v. & Tan, A. S. Characterization of the Cellular Reduction of 3-(4,5-dimethylthiazol-2-yl)-2,5-diphenyltetrazolium bromide (MTT): Subcellular Localization, Substrate Dependence, and Involvement of Mitochondrial Electron Transport in MTT Reduction. *Arch Biochem Biophys* **303**, 474–482 (1993).

227. Metharom, P., Falasca, M. & Berndt, M. C. cancers The History of Armand Trousseau and Cancer-Associated Thrombosis. doi:10.3390/cancers11020158.

228. Trousseau A. Clinique Médicale de L'hôtel-dieu de Paris. Phlegmatia alba dolens. . in vol. Volume 3 654–712 (J.-B. Baillière et fils;, 1865).

229. Fernandes, C. J. *et al.* Cancer-associated thrombosis: the when, how and why. *Eur Respir Rev* **28**, (2019).

230. Lal, I., Dittus, K. & Holmes, C. E. Platelets, coagulation and fibrinolysis in breast cancer progression. *Breast Cancer Research* **15**, 1–11 (2013).

231. Lima, L. G. & Monteiro, R. Q. Activation of blood coagulation in cancer: implications for tumour progression. doi:10.1042/BSR20130057.

232. Koizume, S. & Miyagi, Y. Breast cancer phenotypes regulated by tissue factor-factor VII pathway: Possible therapeutic targets. *World J Clin Oncol* **5**, 908 (2014).

233. Ohshiro, K. *et al.* Thrombin stimulation of inflammatory breast cancer cells leads to aggressiveness via EGFR-PARI-PAK1 pathway. *Int J Biol Markers* **27**, e305 (2012).

234. Mandoj, C. *et al.* Observational study of coagulation activation in early breast cancer: Development of a prognostic model based on data from the real world setting. *J Transl Med* **16**, 1–9 (2018).

235. Giaccherini, C. *et al.* Thrombotic biomarkers for risk prediction of malignant disease recurrence in patients with early stage breast cancer. *Haematologica* **105**, 1704 (2020).

236. Marchetti, M. *et al.* Thrombin generation predicts early recurrence in breast cancer patients. *Journal of Thrombosis and Haemostasis* **18**, 2220–2231 (2020).

237. Tsai, A. W. *et al. Coagulation Factors, Inflammation Markers, and Venous Thromboembolism: The Longitudinal Investigation of Thromboembolism Etiology (LITE)*.

238. Kim, K. J. *et al.* STAT3 activation in endothelial cells is important for tumor metastasis via increased cell adhesion molecule expression. *Oncogene* **36**, 5445–5459 (2017).

239. Pilch, J. & Habermann, R. Unique ability of integrin α vβ 3 to support tumor cell arrest under dynamic flow conditions. *Journal of Biological Chemistry* **277**, 21930–21938 (2002).

240. Wang, Y. *et al.* Heparan sulfate dependent binding of plasmatic von Willebrand factor to blood circulating melanoma cells attenuates metastasis. *Matrix Biology* **111**, 76–94 (2022).

241. Feinauer, M. J. *et al.* Local blood coagulation drives cancer cell arrest and brain metastasis in a mouse model. *Blood* **137**, 1219–1232 (2021).

242. Gay, L. J. & Felding-Habermann, B. Contribution of platelets to tumour metastasis. *Nat Rev Cancer* **11**, 123–34 (2011).

243. Mojiri, A. *et al. Functional assessment of von Willebrand factor expression by cancer cells of non-endothelial origin*. *Oncotarget* vol. 8 www.impactjournals.com/oncotarget/ (2017).

244. Kirwan, C. C., McDowell, G., McCollum, C. N., Kumar, S. & Byrne, G. J. Early changes in the haemostatic and procoagulant systems after chemotherapy for breast cancer. *Br J Cancer* **99**, 1000 (2008).

245. Jiang, H. G. *et al.* Value of fibrinogen and D-dimer in predicting recurrence and metastasis after radical surgery for non-small cell lung cancer. *Medical Oncology* **31**, 1–9 (2014).

246. Yamashita, H., Kitayama, J., Kanno, N., Yatomi, Y. & Nagawa, H. Hyperfibrinogenemia is associated with lymphatic as well as hematogenous metastasis and worse clinical outcome in T2 gastric cancer. (2006) doi:10.1186/1471-2407-6-147.

247. Cantrell, R. & Palumbo, J. S. The thrombin-inflammation axis in cancer progression. *Thromb Res* **191 Suppl 1**, S117–S122 (2020).

248. Olson, J. D. D-dimer: An Overview of Hemostasis and Fibrinolysis, Assays, and Clinical Applications. *Adv Clin Chem* **69**, 1–46 (2015).

249. Dai, H. *et al.* D-dimer as a potential clinical marker for predicting metastasis and progression in cancer. *Biomed Rep* **9**, 453 (2018).

250. Ay, C. *et al.* High D-dimer levels are associated with poor prognosis in cancer patients. *Haematologica* **97**, 1158–1164 (2012).

251. Gray, E., Marti, J., Brewster, D. H., Wyatt, J. C. & Hall, P. S. Independent validation of the PREDICT breast cancer prognosis prediction tool in 45,789 patients using Scottish Cancer Registry data. *British Journal of Cancer 2018 119:7* **119**, 808–814 (2018).

252. Cleris, L., Daidone, M. G., Fina, E. & Cappelletti, V. The Detection and Morphological Analysis of Circulating Tumor and Host Cells in Breast Cancer Xenograft Models. (2019) doi:10.3390/cells8070683.

253. Zarà, M. *et al.* Release of Prometastatic Platelet-Derived Microparticles Induced by Breast Cancer Cells: A Novel Positive Feedback Mechanism for Metastasis. *TH Open* **1**, e155 (2017).

254. de Luca, M. *et al.* Structure and function of the von Willebrand factor A1 domain: analysis with monoclonal antibodies reveals distinct binding sites involved in recognition of the platelet membrane glycoprotein Ib-IX-V complex and ristocetin-dependent activation. *Blood* **95**, 164–172 (2000).

255. Terraube, V., Marx, I. & Denis, C. v. Role of von Willebrand factor in tumor metastasis. *Thromb Res* **120**, (2007).

256. Chen, J., Ling, M., Fu, X., López, J. A. & Chung, D. W. Simultaneous exposure of sites in von willebrand factor for glycoprotein ib binding and ADAMTS13 cleavage studies with ristocetin. *Arterioscler Thromb Vasc Biol* **32**, 2625–2630 (2012).

257. Fujimura, Y. *et al.* A heparin-binding domain of human von Willebrand factor. Characterization and localization to a tryptic fragment extending from amino acid residue Val-449 to Lys-728. *Journal of Biological Chemistry* **262**, 1734–1739 (1987).

258. Grässle, S. *et al.* Von willebrand factor directly interacts with DNA from neutrophil extracellular traps. *Arterioscler Thromb Vasc Biol* **34**, 1382–1389 (2014).

259. Reymond, N., Borda, B. & Ridley, A. J. Crossing the endothelial barrier during metastasis. *Nature Publishing Group* (2013) doi:10.1038/nrc3628.

260. de Ceunynck, K. *et al.* Local Elongation of Endothelial Cell-anchored von Willebrand Factor Strings Precedes ADAMTS13 Protein-mediated Proteolysis. *Journal of Biological Chemistry* **286**, 36361–36367 (2011).

261. Pendu, R. *et al.* P-selectin glycoprotein ligand 1 and β2-integrins cooperate in the adhesion of leukocytes to von Willebrand factor. *Blood* **108**, 3746–3752 (2006).

262. Huang, J., Roth, R., Heuser, J. E. & Sadler, J. E. Integrin alpha(v)beta(3) on human endothelial cells binds von Willebrand factor strings under fluid shear stress. *Blood* **113**, 1589–97 (2009).

263. McCarty, O. J., Mousa, S. A., Bray, P. F. & Konstantopoulos, K. Immobilized platelets support human colon carcinoma cell tethering, rolling, and firm adhesion under dynamic flow conditions. *Blood* **96**, 1789–97 (2000).

264. Tim Goodnough, L., Saito, H., Manni, A., Jones, P. K. & Pearson, O. H. Increased Incidence of Thromboembolism in Stage IV Breast Cancer Patients Treated With a Five-Drug Chemotherapy Regimen A Study of 159 Patients. doi:10.1002/1097-0142.

265. Walker, A. J. *et al.* When are breast cancer patients at highest risk of venous thromboembolism? A cohort study using English health care data. *Blood* **127**, 849 (2016).

266. Chew, H. K., Wun, T., Harvey, D. J., Zhou, H. & White, R. H. Incidence of venous thromboembolism and the impact on survival in breast cancer patients. *J Clin Oncol* **25**, 70–76 (2007).

267. Hanahan, D. Hallmarks of Cancer: New Dimensions. *Cancer Discov* **12**, 31–46 (2022).

268. Lagrange, J. *et al.* The VWF/LRP4/αVβ3-axis represents a novel pathway regulating proliferation of human vascular smooth muscle cells. *Cardiovasc Res* **118**, 622–637 (2022).

269. Wu, Y. *et al.* von Willebrand factor enhances microvesicle-induced vascular leakage and coagulopathy in mice with traumatic brain injury. *Blood* **132**, 1075–1084 (2018).

270. Tsai, A. W. *et al.* Coagulation factors, inflammation markers, and venous thromboembolism: the longitudinal investigation of thromboembolism etiology (LITE). *Am J Med* **113**, 636–642 (2002).

271. Lehrer, S., Green, S., Dembitzer, F. R., Rheinstein, P. H. & Rosenzweig, K. E. Increased RNA Expression of von Willebrand Factor Gene Is Associated With Infiltrating Lobular Breast Cancer and Normal PAM50 Subtype. *Cancer Genomics Proteomics* **16**, 147–153 (2019).

272. Liu, Y. *et al.* The role of von Willebrand factor as a biomarker of tumor development in hepatitis B virus-associated human hepatocellular carcinoma: A quantitative proteomic based study. *J Proteomics* **106**, 99–112 (2014).

273. Breast cancer statistics | Cancer Research UK. https://www.cancerresearchuk.org/health-professional/cancer-statistics/statistics-by-cancer-type/breast-cancer.

274. Rhone, P., Zarychta, E., Bielawski, K. & Ruszkowska-Ciastek, B. Pre-surgical level of von Willebrand factor as an evident indicator of breast cancer recurrence. *Cancer Biomarkers* **29**, 359–372 (2020).

275. O'Donnell, J. S. & Lavin, M. Perioperative management of patients with von Willebrand disease. *Hematology Am Soc Hematol Educ Program* **2019**, (2019).

276. Alexander, E. T. & Gilmour, S. K. Immunomodulatory role of thrombin in cancer progression. *Mol Carcinog* **61**, 527–536 (2022).

277. Reddel, C. J., Tan, C. W. & Chen, V. M. Thrombin Generation and Cancer: Contributors and Consequences. *Cancers (Basel)* **11**, (2019).

278. Lip, G. Y. H. & Blann, A. von Willebrand factor: a marker of endothelial dysfunction in vascular disorders? *Cardiovasc Res* **34**, 255–265 (1997).

279. Pieters, M. & Wolberg, A. S. Fibrinogen and fibrin: An illustrated review. *Res Pract Thromb Haemost* **3**, 161–172 (2019).

280. Mei, Y. *et al.* Plasma fibrinogen level may be a possible marker for the clinical response and prognosis of patients with breast cancer receiving neoadjuvant chemotherapy. *Tumor Biology* **39**, (2017).

281. Fu, S. *et al.* Cancer antigen 15-3, platelet distribution width, and fibrinogen in combination to distinguish breast cancer from benign breast disease in non-conclusive mammography patients. *Oncotarget* **8**, 67829–67836 (2017).

282. Yu, X. *et al.* Serum fibrinogen levels are positively correlated with advanced tumor stage and poor survival in patients with gastric cancer undergoing gastrectomy: a large cohort retrospective study. *BMC Cancer* **16**, (2016).

283. Im, J. H. *et al.* Coagulation Facilitates Tumor Cell Spreading in the Pulmonary Vasculature during Early Metastatic Colony Formation. *Cancer Res* **64**, 8613–8619 (2004).

284. Palumbo, J. S. *et al.* Platelets and fibrin(ogen) increase metastatic potential by impeding natural killer cell-mediated elimination of tumor cells. (2005) doi:10.1182/blood-2004-06.

285. Rayner, S. G. *et al.* Endothelial-derived von Willebrand factor accelerates fibrin clotting within engineered microvessels. *Journal of Thrombosis and Haemostasis* **20**, 1627–1637 (2022).

286. Ma, Y., Qian, Y. & Lv, W. The correlation between plasma fibrinogen levels and the clinical features of patients with ovarian carcinoma. *J Int Med Res* **35**, 678–684 (2007).

287. Sheng, L. *et al.* Serum fibrinogen is an independent prognostic factor in operable nonsmall cell lung cancer. *Int J Cancer* **133**, 2720–2725 (2013).

288. Zhang, X. & Long, Q. Elevated serum plasma fibrinogen is associated with advanced tumor stage and poor survival in hepatocellular carcinoma patients. *Medicine* **96**, (2017).

289. Adam, S. S., Key, N. S. & Greenberg, C. S. D-dimer antigen: current concepts and future prospects. *Blood* **113**, 2878–2887 (2009).

290. Dong, J. F. *et al.* Ristocetin-dependent, but not botrocetin-dependent, binding of von Willebrand factor to the platelet glycoprotein Ib-IX-V complex correlates with shear-dependent interactions. *Blood* **97**, 162–168 (2001).

291. Carlson, P. *et al.* Targeting the perivascular niche sensitizes disseminated tumour cells to chemotherapy. *Nat Cell Biol* **21**, 238–250 (2019).

292. Nierodzik, M. L., Plotkin, A., Kajumo, F. & Karpatkin, S. Thrombin stimulates tumor-platelet adhesion in vitro and metastasis in vivo. *Journal of Clinical Investigation* **87**, 229 (1991).

293. Yee, J. Hypercalcemia. *xPharm: The Comprehensive Pharmacology Reference* 1–6 (2007) doi:10.1016/B978-008055232-3.60633-6.

294. Tiwari, S., Askari, J. A., Humphries, M. J. & Bulleid, N. J. Divalent cations regulate the folding and activation status of integrins during their intracellular trafficking. *J Cell Sci* **124**, 1672 (2011).

295. Rastegar-Lari, G. *et al.* Two clusters of charged residues located in the electropositive face of the von Willebrand factor A1 domain are essential for heparin binding. *Biochemistry* **41**, 6668–78 (2002).

296. Dhami, S. P. S., Patmore, S., O'Sullivan, J. M. & O'Sullivan, J. M. Advances in the Management of Cancer-Associated Thrombosis. *Semin Thromb Hemost* **47**, 139–149 (2021).

297. Harvey, J. R. *et al.* Inhibition of CXCR4-mediated breast cancer metastasis: A potential role for heparinoids? *Clinical Cancer Research* **13**, 1562–1570 (2007).

298. Mellor, P. *et al.* Modulatory effects of heparin and short-length oligosaccharides of heparin on the metastasis and growth of LMD MDA-MB 231 breast cancer cells in vivo. *Br J Cancer* **97**, 761–768 (2007).

299. Borsig, L. Antimetastatic activities of heparins and modified heparins. Experimental evidence. *Thromb Res* **125**, S66–S71 (2010).

300. Jeong, H.-S. *et al.* Hyperglycemia-induced oxidative stress promotes tumor metastasis by upregulating vWF expression in endothelial cells through the transcription factor GATA1. *Oncogene* **41**, 1634–1646 (2022).

301. Dayananda, K. M., Singh, I., Mondal, N. & Neelamegham, S. von Willebrand factor self-association on platelet GpIbalpha under hydrodynamic shear: effect on shear-induced platelet activation. *Blood* **116**, 3990–3998 (2010).

302. Nicolay, J. P. *et al.* Cellular stress induces erythrocyte assembly on intravascular von Willebrand factor strings and promotes microangiopathy. *Sci Rep* **8**, (2018).

303. Arisz, R. A., de Vries, J. J., Schols, S. E. M., Eikenboom, J. C. J. & de Maat, M. P. M. Interaction of von Willebrand factor with blood cells in flow models: a systematic review. *Blood Adv* **6**, 3979–3990 (2022).

304. Glinsky, V. v *et al.* The role of Thomsen-Friedenreich antigen in adhesion of human breast and prostate cancer cells to the endothelium. *Cancer Res* **61**, (2001).

305. Glinskii, O. v. *et al.* Endothelial integrin α3β1 stabilizes carbohydrate-mediated tumor/endothelial cell adhesion and induces macromolecular signaling complex formation at the endothelial cell membrane. *Oncotarget* **5**, 1382 (2014).

306. Saint-Lu, N. *et al.* Identification of galectin-1 and galectin-3 as novel partners for von Willebrand factor. *Arterioscler Thromb Vasc Biol* **32**, 894–901 (2012).

307. Padilla, A. *et al.* P-selectin anchors newly released ultralarge von Willebrand factor multimers to the endothelial cell surface. *Blood* **103**, 2150–2156 (2004).

308. Denis, C., Williams, J. A., Lu, X., Meyer, D. & Baruch, D. Solid-Phase von Willebrand Factor Contains a Conformationally Active RGD Motif That Mediates Endothelial Cell Adhesion Through the αvβ3 Receptor. *Blood* **82**, 3622–3630 (1993).

309. Cruz, M. A., Diacovo, T. G., Emsley, J., Liddington, R. & Handin, R. I. Mapping the glycoprotein Ib-binding site in the von willebrand factor A1 domain. *J Biol Chem* **275**, 19098–19105 (2000).

310. Schneider, S. W. *et al.* Shear-induced unfolding triggers adhesion of von Willebrand factor fibers. *Proc Natl Acad Sci U S A* **104**, 7899 (2007).

311. Schneider, S. W. *et al.* Shear-induced unfolding triggers adhesion of von Willebrand factor fibers. *Proc Natl Acad Sci U S A* **104**, 7899–7903 (2007).

312. Siedlecki, C. A. *et al.* Shear-Dependent Changes in the Three-Dimensional Structure of Human von Willebrand Factor. *Blood* **88**, 2939–2950 (1996).

313. Shim, K., Anderson, P. J., Tuley, E. A., Wiswall, E. & Sadler, J. E. Platelet-VWF complexes are preferred substrates of ADAMTS13 under fluid shear stress. *Blood* **111**, 651–657 (2008).

314. Rastegarlari, G. *et al.* Macrophage LRP1 contributes to the clearance of von Willebrand factor. *Blood* **119**, 2126–2134 (2012).

315. Koivunen, E. *et al.* Inhibition of β2Integrin–Mediated Leukocyte Cell Adhesion by Leucine–Leucine–Glycine Motif–Containing Peptides. *Journal of Cell Biology* **153**, 905–916 (2001).

316. Xu, E. R. *et al.* Structure and dynamics of the platelet integrin-binding C4 domain of von Willebrand factor. *Blood* **133**, 366 (2019).

317. Frenette, P. S. P-selectin and VWF tie the knot. *Blood* **103**, 1979–1980 (2004).

318. Smeets, M. W. J. *et al.* Platelet-independent adhesion of calcium-loaded erythrocytes to von Willebrand factor. *PLoS One* **12**, e0173077 (2017).

319. Constantinescu-Bercu, A. *et al.* Activated αiibβ3 on platelets mediates flow-dependent netosis via slc44a2. *Elife* **9**, (2020).

320. Goh, C. Y. *et al.* The role of von Willebrand factor in breast cancer metastasis. *Transl Oncol* **14**, 101033 (2021).

321. Suter, C. M., Morgan, G., Hanby, A., Hawkins, N. J. & Ward, R. L. Clinicopathological correlates of GpIbalpha expression in human breast cancers. *Anticancer Res* **22**, 1251–1256 (2002).

322. Grossi, I. M. *et al. Role of tumor cell glycoproteins immunologically related to glycoproteins Tb and Jib/lila in tumor cell-platelet and tumor cell-matrix interactions*.

323. Jurasz, P. *et al.* Role of von Willebrand factor in tumour cell-induced platelet aggregation: differential regulation by NO and prostacyclin. *Br J Pharmacol* **134**, 1104 (2001).

324. Felding-Habermann, B. *et al. Integrin activation controls metastasis in human breast cancer*. www.pnas.org.

325. Bridges, D. J. *et al.* Rapid activation of endothelial cells enables Plasmodium falciparum adhesion to platelet-decorated von Willebrand factor strings. *Blood* **115**, 1472–1474 (2010).

326. Michaux, G., Pullen, T. J., Haberichter, S. L. & Cutler, D. F. P-selectin binds to the D'-D3 domains of von Willebrand factor in Weibel-Palade bodies. *Blood* **107**, 3922–3924 (2006).

327. Cheresh, D. A. Human endothelial cells synthesize and express an Arg-Gly-Asp-directed adhesion receptor involved in attachment to fibrinogen and von Willebrand factor. *Proc Natl Acad Sci U S A* **84**, 6471–6475 (1987).

328. Ikeda, Y. *et al.* The role of von Willebrand factor and fibrinogen in platelet aggregation under varying shear stress. *Journal of Clinical Investigation* **87**, 1234 (1991).

329. Huizinga, E. G. *et al.* Structures of glycoprotein Ibalpha and its complex with von Willebrand factor A1 domain. *Science* **297**, 1176–1179 (2002).

330. Dumas, J. J. *et al.* Crystal structure of the wild-type von Willebrand factor A1-glycoprotein Ibα complex reveals conformation differences with a complex bearing von Willebrand disease mutations. *Journal of Biological Chemistry* **279**, 23327–23334 (2004).

331. Moestrup, S. K., Gliemann, J. & Pallesen, G. Distribution of the alpha 2-macroglobulin receptor/low density lipoprotein receptor-related protein in human tissues. *Cell Tissue Res* **269**, 375–382 (1992).

332. Zheng, G. *et al.* Organ distribution in rats of two members of the low-density lipoprotein receptor gene family, gp330 and LRP/alpha 2MR, and the receptor-associated protein (RAP). *J Histochem Cytochem* **42**, 531–542 (1994).

333. Li, Y., Wood, N., Grimsley, P., Yellowlees, D. & Donnelly, P. K. In vitro invasiveness of human breast cancer cells is promoted by low density lipoprotein receptor-related protein. *Invasion Metastasis* **18**, 240–251 (1998).

334. Strickland, D. K., Au, D. T., Cunfer, P. & Muratoglu, S. C. Low-density lipoprotein receptor-related protein-1: role in the regulation of vascular integrity. *Arterioscler Thromb Vasc Biol* **34**, 487–498 (2014).

335. Lillis, A. P., van Duyn, L. B., Murphy-Ullrich, J. E. & Strickland, D. K. LDL receptor-related protein 1: unique tissue-specific functions revealed by selective gene knockout studies. *Physiol Rev* **88**, 887–918 (2008).

336. Schulz, S. *et al.* The LDL receptor-related protein (LRP1/A2MR) and coronary atherosclerosis--novel genomic variants and functional consequences. *Hum Mutat* **20**, 404 (2002).

337. Young, P. A., Migliorini, M. & Strickland, D. K. Evidence That Factor VIII Forms a Bivalent Complex with the Low Density Lipoprotein (LDL) Receptor-related Protein 1 (LRP1): IDENTIFICATION OF CLUSTER IV ON LRP1 AS THE MAJOR BINDING SITE*. *J Biol Chem* **291**, 26035 (2016).

338. Fazavana, J. *et al.* Investigating the clearance of VWF A-domains using site-directed PEGylation and novel N-linked glycosylation. *J Thromb Haemost* **18**, 1278 (2020).

339. Snapp, K. R. *et al.* A Novel P-Selectin Glycoprotein Ligand-1 Monoclonal Antibody Recognizes an Epitope Within the Tyrosine Sulfate Motif of Human PSGL-1 and Blocks Recognition of Both P- and L-Selectin. *Blood* **91**, 154–164 (1998).

340. Peyvandi, F., Garagiola, I. & Baronciani, L. Role of von Willebrand factor in the haemostasis. *Blood Transfusion* **9**, s3 (2011).

341. Quach, M. E. & Li, R. Structure-function of platelet glycoprotein Ib-IX. *J Thromb Haemost* **18**, 3131 (2020).

342. Wohner, N. *et al.* Shear stress-independent binding of von Willebrand factor-type 2B mutants p.R1306Q & p.V1316M to LRP1 explains their increased clearance. *J Thromb Haemost* **13**, 815–820 (2015).

343. Xing, P. *et al.* Roles of low-density lipoprotein receptor-related protein 1 in tumors. *Chin J Cancer* **35**, 6 (2016).

344. Le, C. C. *et al.* LRP-1 Promotes Colon Cancer Cell Proliferation in 3D Collagen Matrices by Mediating DDR1 Endocytosis. *Front Cell Dev Biol* **8**, 412 (2020).

345. Boyé, K. *et al.* The role of CXCR3/LRP1 cross-talk in the invasion of primary brain tumors. *Nature Communications 2017 8:1* **8**, 1–20 (2017).

346. A. Chion *et al.* VWFA1 Interacts with Scavenger Receptor LRP1 via Lysine 1408. ISTH Academy. Chion A. Jul 9 2019; 273980. https://academy.isth.org/isth/2019/melbourne/273980/alain.chion.vwfa1.interacts.with.scavenger.receptor.lrp1.via.lysine.1408.html?f=listing%3D0%2Abrowseby%3D8%2Asortby%3D2%2Atopic%3D21508 (2019).

347. Bu, G. & Rennke, S. Receptor-associated Protein Is a Folding Chaperone for Low Density Lipoprotein Receptor-related Protein. *Journal of Biological Chemistry* **271**, 22218–22224 (1996).

348. Song, H., Li, Y., Lee, J., Schwartz, A. L. & Bu, G. Low-density lipoprotein receptor-related protein 1 promotes cancer cell migration and invasion by inducing the expression of matrix metalloproteinases 2 and 9. *Cancer Res* **69**, 879–886 (2009).

349. Li, Y., Wood, N., Grimsley, P., Yellowlees, D. & Donnelly, P. K. In vitro invasiveness of human breast cancer cells is promoted by low density lipoprotein receptor-related protein. *Invasion Metastasis* **18**, 240–51 (2000).

350. Campion, O. *et al.* Contribution of the Low-Density Lipoprotein Receptor Family to Breast Cancer Progression. *Front Oncol* **10**, 882 (2020).

351. Catasus, L. *et al.* Low-density lipoprotein receptor–related protein 1 is associated with proliferation and invasiveness in Her-2/neu and triple-negative breast carcinomas. *Hum Pathol* **42**, 1581–1588 (2011).

352. Berquand, A. *et al.* A gentle approach to investigate the influence of LRP-1 silencing on the migratory behavior of breast cancer cells by atomic force microscopy and dynamic cell studies. *Nanomedicine* **18**, 359–370 (2019).

353. Wong, S. Y. & Hynes, R. O. Lymphatic or Hematogenous Dissemination: How Does a Metastatic Tumor Cell Decide? *Cell Cycle* **5**, 812 (2006).

354. Bubendorf, L. *et al.* Metastatic patterns of prostate cancer: An autopsy study of 1,589 patients. *Hum Pathol* **31**, 578–583 (2000).

355. Coste, A. *et al.* Hematogenous Dissemination of Breast Cancer Cells From Lymph Nodes Is Mediated by Tumor MicroEnvironment of Metastasis Doorways. *Front Oncol* **10**, 571100 (2020).

356. Sugino, T. *et al.* An Invasion-Independent Pathway of Blood-Borne Metastasis : A New Murine Mammary Tumor Model. *Am J Pathol* **160**, 1973 (2002).

357. Luzzi, K. J. *et al.* Multistep Nature of Metastatic Inefficiency : Dormancy of Solitary Cells after Successful Extravasation and Limited Survival of Early Micrometastases. *Am J Pathol* **153**, 865 (1998).

358. Fares, J., Fares, M. Y., Khachfe, H. H., Salhab, H. A. & Fares, Y. Molecular principles of metastasis: a hallmark of cancer revisited. *Signal Transduction and Targeted Therapy 2020 5:1* **5**, 1–17 (2020).

359. Fidler, I. J. Metastasis: quantitative analysis of distribution and fate of tumor emboli labeled with 125 I-5-iodo-2'-deoxyuridine. *J Natl Cancer Inst* **45**, (1970).

360. Mierke, C. T. Role of the Endothelium during Tumor Cell Metastasis: Is the Endothelium a Barrier or a Promoter for Cell Invasion and Metastasis? *Journal of Biophysics* **2008**, 1–13 (2008).

361. Laferrière, J., Houle, F., Taher, M. M., Valerie, K. & Huot, J. Transendothelial Migration of Colon Carcinoma Cells Requires Expression of E-selectin by Endothelial Cells and Activation of Stress-activated Protein Kinase-2 (SAPK2/p38) in the Tumor Cells. *Journal of Biological Chemistry* **276**, 33762–33772 (2001).

362. Weis, S., Cui, J., Barnes, L. & Cheresh, D. Endothelial barrier disruption by VEGF-mediated Src activity potentiates tumor cell extravasation and metastasis. *J Cell Biol* **167**, 223 (2004).

363. Jin, Y. *et al.* Tissue factor potentiates adherence of breast cancer cells to human umbilical vein endothelial cells under static and flow conditions. *Cell Adh Migr* **15**, 74–83 (2021).

364. Osmani, N. *et al.* Metastatic Tumor Cells Exploit Their Adhesion Repertoire to Counteract Shear Forces during Intravascular Arrest. *Cell Rep* **28**, 2491-2500.e5 (2019).

365. Tischer, A., Cruz, M. A. & Auton, M. The linker between the D3 and A1 domains of vWF suppresses A1-GPIbα catch bonds by site-specific binding to the A1 domain. *Protein Sci* **22**, 1049 (2013).

366. Gritsch, H. *et al.* Structure and Function of Recombinant versus Plasma-Derived von Willebrand Factor and Impact on Multimer Pharmacokinetics in von Willebrand Disease. *J Blood Med* **13**, 649–662 (2022).

367. Reymond, N., D'Água, B. B. & Ridley, A. J. Crossing the endothelial barrier during metastasis. *Nat Rev Cancer* **13**, 858–870 (2013).

368. Labelle, M. & Hynes, R. O. The initial hours of metastasis: the importance of cooperative host-tumor cell interactions during hematogenous dissemination. *Cancer Discov* **2**, 1091 (2012).

369. Laferrière, J., Houle, F. & Huot, J. Adhesion of HT-29 colon carcinoma cells to endothelial cells requires sequential events involving E-selectin and integrin beta4. *Clin Exp Metastasis* **21**, 257–265 (2004).

370. Barthel, S. R. *et al.* Definition of molecular determinants of prostate cancer cell bone extravasation. *Cancer Res* **73**, 942–952 (2013).

371. Bauer, K., Mierke, C. & Behrens, J. Expression profiling reveals genes associated with transendothelial migration of tumor cells: A functional role for αvβ3 integrin. *Int J Cancer* **121**, 1910–1918 (2007).

372. Placke, T. *et al.* Platelet-derived MHC class I confers a pseudonormal phenotype to cancer cells that subverts the antitumor reactivity of natural killer immune cells. *Cancer Res* **72**, 440–448 (2012).

373. Aceto, N. *et al.* Circulating Tumor Cell Clusters are Oligoclonal Precursors of Breast Cancer Metastasis. *Cell* **158**, 1110 (2014).

374. Boulagnon-Rombi, C. *et al.* LRP1 expression in colon cancer predicts clinical outcome. *Oncotarget* **9**, 8849 (2018).

375. Gilardoni, M. B. *et al.* Decreased Expression of the Low-density Lipoprotein Receptor-related Protein-1 (LRP-1) in Rats with Prostate Cancer. *Journal of Histochemistry and Cytochemistry* **51**, 1575–1580 (2003).

376. de Vries, T. J. *et al.* Decreased expression of both the low-density lipoprotein receptor-related protein/α2-macroglobulin receptor and its receptor-associated protein in late stages of cutaneous melanocytic tumor progression. *Cancer Res* **56**, 1432–1439 (1996).

377. van Gool, B., Dedieu, S., Emonard, H. & Roebroek, A. J. M. The Matricellular Receptor LRP1 Forms an Interface for Signaling and Endocytosis in Modulation of the Extracellular Tumor Environment. *Front Pharmacol* **6**, (2015).

378. Huang, X. Y. *et al.* Low Level of Low-Density Lipoprotein Receptor-Related Protein 1 Predicts an Unfavorable Prognosis of Hepatocellular Carcinoma after Curative Resection. *PLoS One* **7**, e32775 (2012).

379. Fayard, B. *et al.* The serine protease inhibitor protease nexin-1 controls mammary cancer metastasis through LRP-1-mediated MMP-9 expression. *Cancer Res* **69**, 5690–5698 (2009).

380. Chang, C. *et al.* LRP-1 receptor combines EGFR signalling and eHsp90α autocrine to support constitutive breast cancer cell motility in absence of blood supply. *Scientific Reports 2022 12:1* **12**, 1–12 (2022).

381. Taheri, M., Motalebzadeh, J. & Mahjoubi, F. Expression of LRP Gene in Breast Cancer Patients Correlated with MRP1 as Two Independent Predictive Biomarkers in Breast Cancer. *Asian Pac J Cancer Prev* **19**, 3111 (2018).

382. Chen, H. *et al.* Association of LRP1B mutation with tumor mutation burden and outcomes in melanoma and non-small cell lung cancer patients treated with immune check-point blockades. *Front Immunol* **10**, 1113 (2019).

383. Beroukhim, R. *et al.* The landscape of somatic copy-number alteration across human cancers. *Nature* **463**, 899 (2010).

384. Asano, Y. *et al.* Nuclear localization of LDL receptor-related protein 1B in mammary gland carcinogenesis. *J Mol Med (Berl)* **97**, 257–268 (2019).

385. Argraves, K. M. *et al.* The Very Low Density Lipoprotein Receptor Mediates the Cellular Catabolism of Lipoprotein Lipase and Urokinase-Plasminogen Activator Inhibitor Type I Complexes. *Journal of Biological Chemistry* **270**, 26550–26557 (1995).

386. Li, Y. *et al.* Impact of histotypes on preferential organ-specific metastasis in triple-negative breast cancer. *Cancer Med* **9**, 872 (2020).

387. Larjavaara, S. *et al.* Incidence of gliomas by anatomic location. *Neuro Oncol* **9**, 319 (2007).

388. Pouliot, N., Pearson, H. & Burrows A. Investigating Metastasis Using In Vitro Platforms. *Madame Curie Bioscience Database. Austin (TX): Landes Bioscience;* (2013).

389. Mochizuki, S. *et al.* Selective inhibition of ADAM28 suppresses lung carcinoma cell growth and metastasis. *Mol Cancer Ther* **17**, 2427–2438 (2018).

390. Bielenberg, D. R. & Zetter, B. R. The Contribution of Angiogenesis to the Process of Metastasis. *Cancer J* **21**, 267 (2015).

391. Xu, H. *et al.* ADAMTS13 controls vascular remodeling by modifying VWF reactivity during stroke recovery. *Blood* **130**, 11–22 (2017).

392. Navone, S. E. *et al.* Correlation of Preoperative Von Willebrand Factor with Magnetic Resonance Imaging Perfusion and Permeability Parameters as Predictors of Prognosis in Glioblastoma. *World Neurosurg* **122**, e226–e234 (2019).

393. Franchini, M. Response to Parathyroid Adenoma in a Young Girl with Type 3 von Willebrand Disease. *Semin Thromb Hemost* **48**, 627 (2022).

394. Franchini, M. *et al.* Cancers in Patients with von Willebrand Disease: A Survey from the Italian Association of Haemophilia Centres. *Semin Thromb Hemost* **42**, 36–41 (2015).

395. Jenkins, P. V. & O'Donnell, J. S. ABO blood group determines plasma von Willebrand factor levels: a biologic function after all? *Transfusion (Paris)* **46**, 1836–1844 (2006).

396. Liu, X., Chen, X., Yang, J. & Guo, R. Association of ABO blood groups with von Willebrand factor, factor VIII and ADAMTS-13 in patients with lung cancer. *Oncol Lett* **14**, 3787–3794 (2017).

397. Edgren, G. *et al.* Risk of gastric cancer and peptic ulcers in relation to ABO blood type: a cohort study. *Am J Epidemiol* **172**, 1280–1285 (2010).

398. Wang, Z. *et al.* ABO blood group system and gastric cancer: a case-control study and meta-analysis. *Int J Mol Sci* **13**, 13308–13321 (2012).

399. Song, Q., Wu, J. Z., Wang, S. & Chen, Z. B. The ABO Blood Group is an Independent Prognostic Factor in Patients with Ovarian Cancer. *J Cancer* **10**, 6754–6760 (2019).

400. Hsiao, L. T., Liu, N. J., You, S. L. & Hwang, L. C. ABO blood group and the risk of cancer among middle-aged people in Taiwan. *Asia Pac J Clin Oncol* **11**, e31–e36 (2015).

401. Stakišaitis, D. *et al.* Abo blood group polymorphism has an impact on prostate, kidney and bladder cancer in association with longevity. *Oncol Lett* **16**, 1321–1331 (2018).

402. Friedl, P. & Wolf, K. Tumour-cell invasion and migration: diversity and escape mechanisms. *Nature Reviews Cancer 2003 3:5* **3**, 362–374 (2003).

403. Wyckoff, J. B., Jones, J. G., Condeelis, J. S. & Segall, J. E. A critical step in metastasis: in vivo analysis of intravasation at the primary tumor. *Cancer Res* **60**, (2000).

404. Wang, W. *et al.* Single cell behavior in metastatic primary mammary tumors correlated with gene expression patterns revealed by molecular profiling. *Cancer Res* **62**, (2002).

405. Martin TA, Andrew LY, Sanders J, Lane J & Jiang WG. *Cancer invasion and metastasis: molecular and cellular perspective.* (2013).

406. Mott, J. D. & Werb, Z. Regulation of matrix biology by matrix metalloproteinases. *Curr Opin Cell Biol* **16**, 558–564 (2004).

407. Quintero-Fabián, S. *et al.* Role of Matrix Metalloproteinases in Angiogenesis and Cancer. *Front Oncol* **9**, 1370 (2019).

408. Yousef, E. M., Tahir, M. R., St-Pierre, Y. & Gaboury, L. A. MMP-9 expression varies according to molecular subtypes of breast cancer. *BMC Cancer* **14**, (2014).

409. Liu, Q. *et al.* The relationship between vasculogenic mimicry and epithelial-mesenchymal transitions. *J Cell Mol Med* **20**, 1761 (2016).

410. Maniotis, A. J. *et al.* Vascular Channel Formation by Human Melanoma Cells in Vivo and in Vitro: Vasculogenic Mimicry. *Am J Pathol* **155**, 739 (1999).

411. Luo, Q. *et al.* Vasculogenic mimicry in carcinogenesis and clinical applications. *Journal of Hematology & Oncology 2020 13:1* **13**, 1–15 (2020).

412. Marchetti, M. *et al.* Endothelial capillary tube formation and cell proliferation induced by tumor cells are affected by low molecular weight heparins and unfractionated heparin. *Thromb Res* **121**, 637–45 (2008).

413. Niu, G. & Chen, X. Vascular Endothelial Growth Factor as an Anti-angiogenic Target for Cancer Therapy. *Curr Drug Targets* **11**, 1000 (2010).

414. Mei, J. *et al.* VEGF-siRNA silencing induces apoptosis, inhibits proliferation and suppresses vasculogenic mimicry in osteosarcoma in vitro. *Exp Oncol* **30**, 29–34 (2008).

415. Lee, C. H. *et al.* Epidermal growth factor/heat shock protein 27 pathway regulates vasculogenic mimicry activity of breast cancer stem/progenitor cells. *Biochimie* **104**, 117–126 (2014).

416. Camorani, S. *et al.* Aptamer-mediated impairment of EGFR-integrin αvβ3 complex inhibits vasculogenic mimicry and growth of triple-negative breast cancers. *Sci Rep* **7**, (2017).

417. Shin, S. U. *et al.* Inhibition of vasculogenic mimicry and angiogenesis by an anti-egfr igg1-human endostatin-p125a fusion protein reduces triple negative breast cancer metastases. *Cells* **10**, 2904 (2021).

418. Taatjes, D. J., Sobel, B. E. & Budd, R. C. Morphological and cytochemical determination of cell death by apoptosis. *Histochem Cell Biol* **129**, 33–43 (2008).

419. Qin, F., Impeduglia, T., Schaffer, P. & Dardik, H. Overexpression of von Willebrand factor is an independent risk factor for pathogenesis of intimal hyperplasia: Preliminary studies. *J Vasc Surg* **37**, 433–439 (2003).

420. Molinie, N. & Gautreau, A. Directional Collective Migration in Wound Healing Assays. *Methods Mol Biol* **1749**, 11–19 (2018).

421. Hawinkels, L. J. A. C. *et al.* VEGF release by MMP-9 mediated heparan sulphate cleavage induces colorectal cancer angiogenesis. *Eur J Cancer* **44**, 1904–1913 (2008).

422. Hayata, K. *et al.* Inhibition of IL-17A in Tumor Microenvironment Augments Cytotoxicity of Tumor-Infiltrating Lymphocytes in Tumor-Bearing Mice. *PLoS One* **8**, e53131 (2013).

423. Andonegui-Elguera, M. A. *et al.* An Overview of Vasculogenic Mimicry in Breast Cancer. *Front Oncol* **10**, 220 (2020).

424. Thomas, C. *et al.* ERβ1 represses basal-like breast cancer epithelial to mesenchymal transition by destabilizing EGFR. *Breast Cancer Research* **14**, 1–15 (2012).

425. Cummings, M. C. *et al.* Metastatic progression of breast cancer: insights from 50 years of autopsies. *J Pathol* **232**, 23 (2014).

7: Appendices

7.1 Appendix I

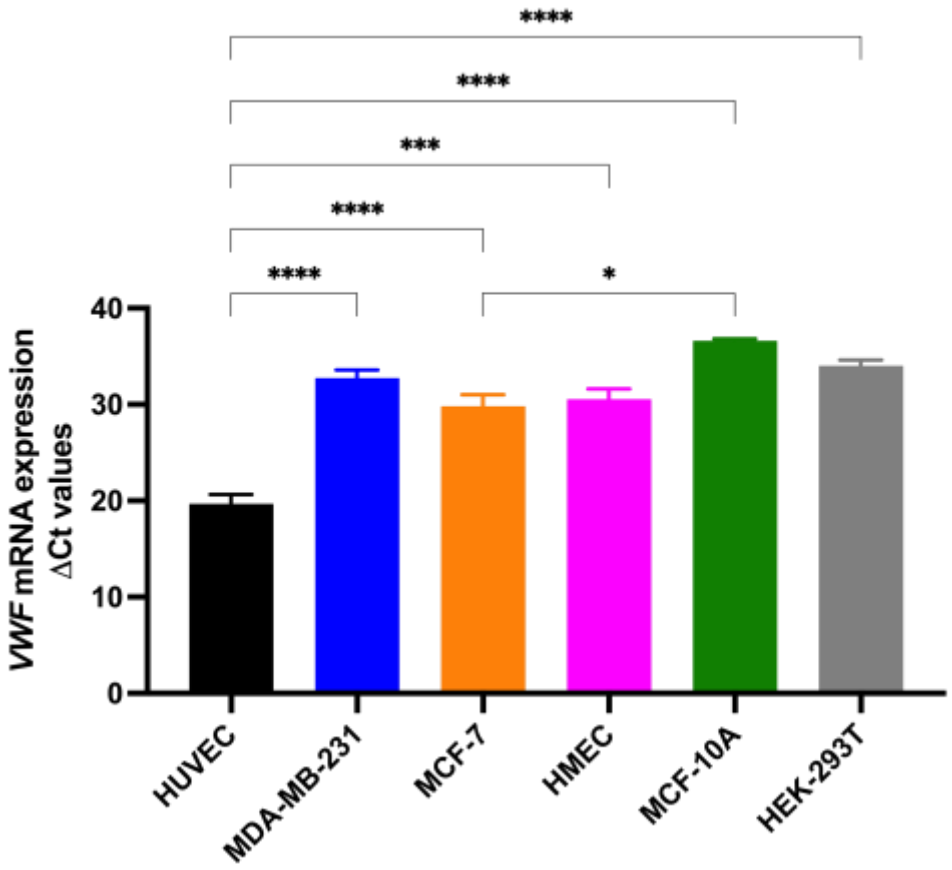

Figure 7.1 VWF mRNA expression in different cell lines: Baseline mRNA levels of VWF were measured against in a number of cell lines including breast cancer cells MDA-MB-231 and MCF-7, breast cells MCF-10A and HMEC, and negative control kidney cell line HEK293T against the predominant source of VWF in the body endothelial cells, represented through HUVEC. Each cell line was grown to confluence where they were lysed and processed to isolate their RNA before being converted into cDNA and subsequently assessed through qPCR. Unsurprisingly, VWF expression is several orders of magnitude higher in HUVEC compared to all other cell lines tested. Furthermore, each of the other cell lines tested exhibited very low or no *VWF* expression at the 30 cycles cut off range with MCF-7 displaying significant increase in ΔCt value compared to breast cell line MCF-10A but not primary breast cells HMEC. All significant values were represented with stars and non-significant changes were left blank. Statistical significance was determined with one way ANOVA through Tukeys multiple comparisons test, * $p \leq 0.05$, *** $p \leq 0.001$, **** $p \leq 0.0001$.

7.3 Appendix II

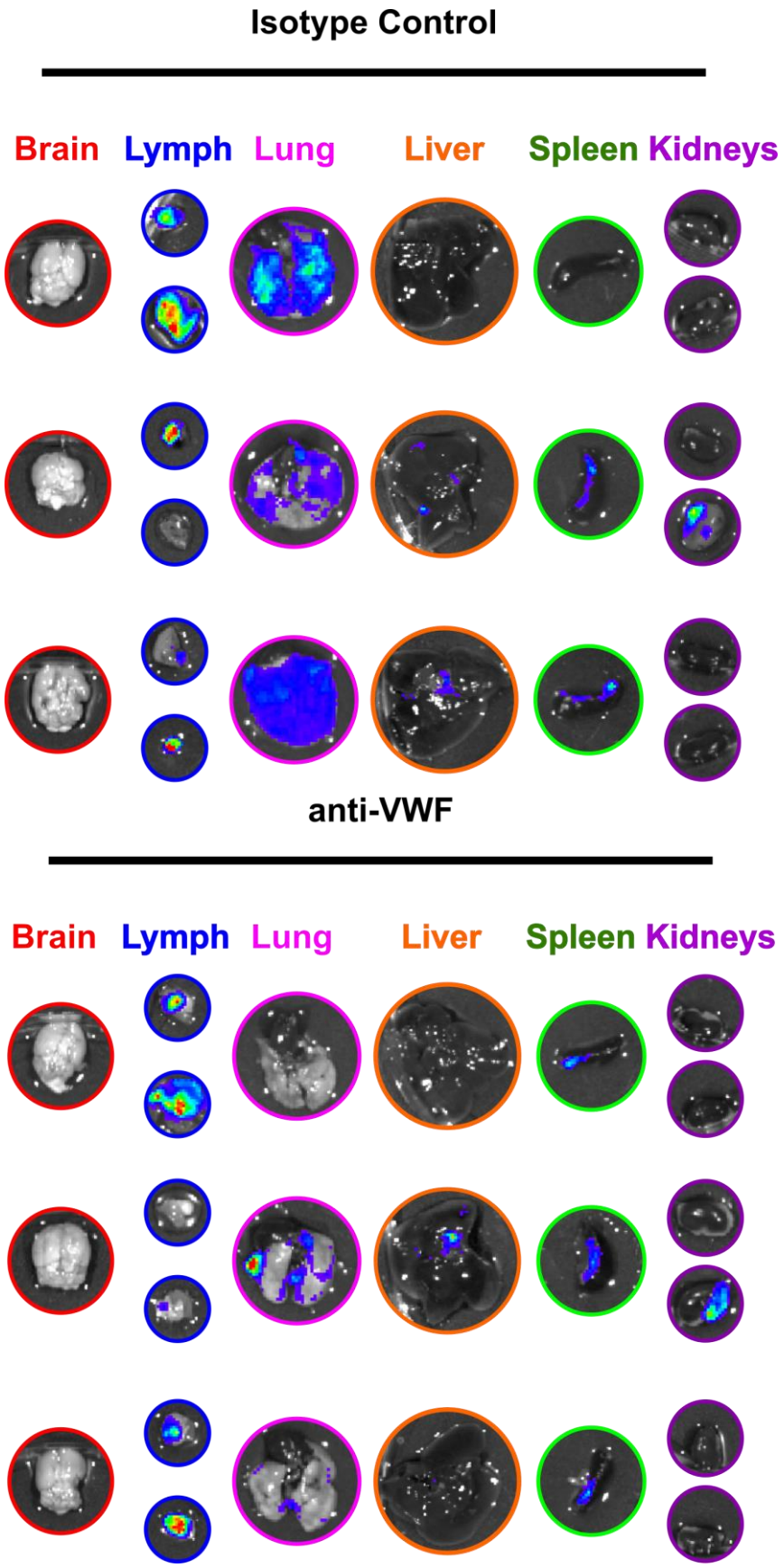

Figure 7.2 Representative bioluminescent signalling of harvested organs from xenograft breast cancer model: Images of the organs harvested from each mice were taken following infusion of luciferin substrate. Bioluminescent signalling indicated the presence of luciferin tagged MDA-MB-231 in secondary sites. Representative images of three mice with anti-VWF treatment and three mice with respective anti-isotype treatment are shown for each organ including brain, lymph, lung, liver, spleen and kidneys.

7.2 Appendix III

Table 7. 1 The mRNA levels of VWF cleaving proteases in MDA-MB-231 cells

MDA			MDA+VWF		
Gene: ADAM28s ΔCt value					
23.84328	23.69131	23.59254	23.37196	24.11203	23.01199
Undetermined	Undetermined	Undetermined	Undetermined	Undetermined	Undetermined
Undetermined	Undetermined	Undetermined	Undetermined	Undetermined	Undetermined
Gene: ADAM28m ΔCt value					
30.74996	31.65179	31.63875	29.40792	29.93728	29.38442
Undetermined	Undetermined	Undetermined	30.02926	Undetermined	Undetermined
Undetermined	Undetermined	Undetermined	Undetermined	Undetermined	Undetermined
Gene: ADAMTS13 ΔCt value					
33.12775	33.74465	35.29318	33.06566	31.94412	33.15189
36.72644	36.04867	36.06213	36.10327	33.75483	34.08622
35.38012	35.7202	35.17457	35.38221	35.07543	34.83956

Secreted ADAM28 and membrane associated ADAM28 expression was assessed through qPCR in MDA-MB-231 cells along with other VWF cleaving protease ADAMTS13 as a comparison. MDA-MB-231 cells were grown to confluence before RNA isolation, cDNA conversion and subsequent assessment of mRNA values through qPCR. Undetermined values are defined by genes unable to show significant amplification during the qPCR beyond the threshold within 40 cycles.

7.4 Appendix IV

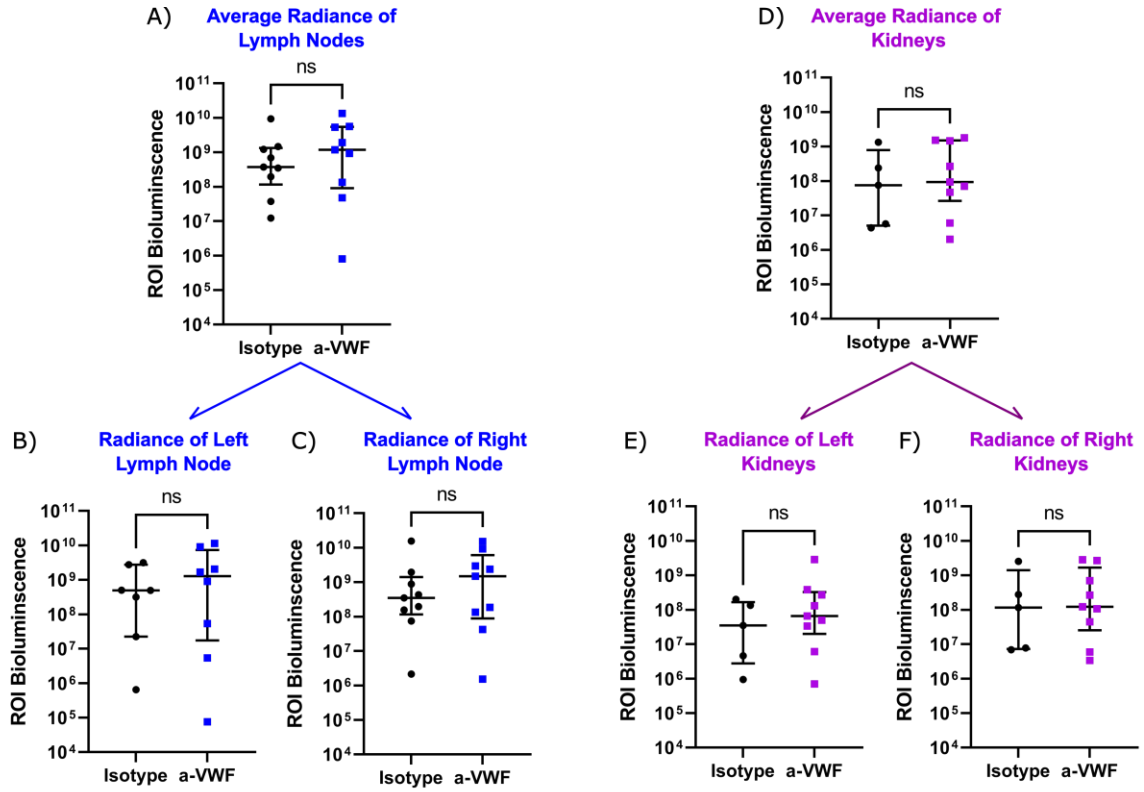

Figure 7.3 Metastatic tumour burden in left and right lymph nodes and kidneys in a xenograft breast cancer model: Following the termination of the metastatic breast cancer mouse *in vivo* model kidneys and lymph nodes were harvested and the tumour burden assessed through measuring bioluminescent radiance signalling. Both kidneys and lymph nodes were represented as an average bioluminescent radiance of left and right organs following anti-VWF or isotype control treatment. However, the organs were further subdivided into left and right, where the difference between treatment groups was quantified. Due to the injection of luciferin tagged MDA-MB-231 in the right mammary pads it is possible the right hand organs may display more metastatic tumour burden. **A-C)** kidneys exhibited no significant difference between left and right organs under the different treatment conditions **D-F)** Lymph nodes also displayed no significant difference between left and right organs under the different treatment conditions. Statistical significance was determined with one way ANOVA through Tukeys multiple comparisons test, * $p \leq 0.05$.

7.5 Appendix V

Publications